Rôle neurovasculaire de l'activateur tissulaire du plasminogène

Mervé Yetim

Normandie Université

THÈSE

Pour obtenir le diplôme de doctorat

Spécialité SCIENCES DE LA VIE ET DE LA SANTE

Préparée au sein de l'Université de Caen Normandie

Rôle neurovasculaire de l'activateur tissulaire du plasminogène

Présentée et soutenue par
MERVE YETIM

Thèse soutenue le 07/12/2021 devant le jury composé de		
M. BRUNO CAULI	Directeur de recherche au CNRS, Sorbonne Université	Rapporteur du jury
M. ZSOLT LENKEI	Directeur de recherche, Université Paris 5 Descartes	Rapporteur du jury
M. OMAR TOUZANI	Professeur des universités, Université Caen Normandie	Membre du jury
MME ZE ZHENG	assistant professeur, Wayne State University	Membre du jury
MME CARINE ALI	Professeur des universités, Université Caen Normandie	Président du jury
M. DENIS VIVIEN	Professeur des universités PraticienHosp, Université Caen Normandie	Directeur de thèse

Thèse dirigée par DENIS VIVIEN, Physiopathologie et imagerie des troubles neurologiques

UNIVERSITÉ CAEN NORMANDIE

ED 497 NBISE
Normande de Biologie Intégrative, Santé, Environnement

Inserm
La science pour la santé
From science to health

« Nous qui incarnons les yeux, les oreilles,

les pensées et les sentiments cosmiques.

Commençons enfin à nous interroger sur nos origines.

Poussières d'étoiles contemplant les étoiles. »

Carl Sagan

Remerciements

Je tiens tout d'abord à remercier Denis Vivien pour m'avoir accueilli au sein de son laboratoire dès mon Master 1, de m'avoir permis de réaliser ce sujet de thèse, tout en ayant fait confiance à mes capacités à pouvoir diriger mes propres travaux. Merci d'avoir suivi de très près l'évolution de ce projet et d'avoir pu développer une belle histoire comme tu le dis.

Je souhaite sincèrement remercier les rapporteurs de cette thèse, le Dr. Bruno Cauli et le Dr. Zsolt Lenkei pour avoir accepté et pris le temps d'évaluer mon travail. Je remercie également le Dr. Ze Zheng, le Pr. Carine Ali et le Pr. Omar Touzani d'avoir accepté de faire partie de mon jury de thèse.

Je voudrais également remercier le Dr. Martinez de Lizarrondo, Yannick, Laurent et le Pr. Maubert pour m'avoir donné des outils et des conseils afin de m'aider à réaliser ce projet.

Merci à toutes les personnes du bureau C047, Fanny, Jojo, Paul, Eloise et Sylvaine ; les anciens du bureau, Sara, Camille, Michou et Audrey ; les voisins de bureau, Quentin, Florent, Damien et Thomas (Bonnasse). Je vous remercie pour votre soutien et tous les moments de détente que l'on a pu passer ensemble, ainsi que les parties de Nerf.

Merci à tous les membres de l'équipe PhIND avec qui j'ai pu échanger, pour vos encouragements, votre aide et vos conseils. C'était un plaisir de travailler dans une telle ambiance.

Je tiens à remercier spécialement Jojo et Quentin pour ces grands moments de rigolade, je tiens à vous dire que l'ambiance du labo ne sera pas la même sans vous. Merci à toi Jojo pour avoir participé à mon projet ainsi que pour les centaines de litres de cafés bus ensemble et les différentes batailles que l'on a pu mener (ressortis avec des ecchymoses ou non).

Grand merci à Fanny, mon éponge, qui a été là pour me soutenir pendant les pires périodes comme les meilleures. Et tous les moments que l'on a pu passer ensemble, gros courage à toi pour la soutenance, on va en venir à bout !

Enorme merci à père Florent, pour m'avoir raconté tant de bobards, d'avoir saboté mes studies (et inversement), les bagarres (je sens que le lecteur commence à avoir peur de moi…), et tes leçons de judo/boxe, j'ai hâte de pouvoir réessayer les techniques que tu m'as enseigné sur toi (quand j'aurai récupéré une jambe en titane). Merci pour toutes ces heures auxquelles on a pu geeker ensemble, surtout Rocket League. Et un grand merci pour ton soutien !

Je remercie ce rocher à Etretat, pour m'avoir aidé à arracher mon LCA du genou. Sans toi, je n'aurai pas pu vivre les six derniers mois de ma thèse en enfer. Mais je ne t'en veux pas, j'ai pu rédiger tranquillement ce manuscrit au lit.

Enfin, je remercie ma famille, mon frère et ma sœur pour m'avoir changé les idées. Mon oncle, pour m'avoir soutenu dans tous mes états. Et mes parents, pour tout, pour avoir fait de votre mieux pour m'instruire, c'est grâce à vous si j'en suis ici aujourd'hui.

Je vous souhaite une bonne lecture…

Résumé

La régulation du débit sanguin cérébral (DSC) implique des mécanismes complexes ayant des influences directes sur les fonctionnements et les dysfonctionnements du cerveau. Parmi ces mécanismes, il a été proposé que l'activateur tissulaire du plasminogène (tPA) de la famille des sérines protéases, pourrait jouer un rôle dans la modulation du couplage neurovasculaire (CNV) induit par la stimulation des vibrisses chez le rongeur, par son mécanisme d'action sur les récepteurs N-Méthyl-D-Aspartate (NMDA). Dans cette étude, via l'utilisation de souris tPA^{Null}, des délétions conditionnelles du tPA endothélial ou de la sous-unité GluN1 des récepteurs NMDA endothéliaux, des parabioses entre des souris tPA^{WT} et tPA^{Null}, des délétions induites par des transfections hydrodynamiques du tPA hépatique, une hépatectomie partielle et des approches pharmacologiques chez la souris, nous avons pu dévoiler ce mécanisme. Nous démontrons ainsi que les concentrations physiologiques de tPA vasculaire, principalement produit et libéré par les cellules endothéliales hépatiques de manière dépendante des récepteurs de la bradykinine de type 2, favorisent le CNV, par un mécanisme dépendant des récepteurs NMDA endothéliaux du cerveau. Ces données mettent en évidence un nouveau mécanisme de régulation du CNV, impliquant à la fois les récepteurs NMDA et le tPA endothéliaux.

Mots clés : tPA, récepteur NMDA, CNV, bradykinine, cellule endothéliale, hepatocyte, cerveau, foie.

Abstract

Regulation of the cerebral blood flow (CBF) involves complex mechanisms with direct influences on brain functions and dysfunctions. Among these mechanisms it was proposed that the serine protease tissue-type plasminogen activator (tPA) could play a role in the control of neurovascular coupling (NVC) induced by whiskers stimulation in rodents through its action on N-methyl-D-Aspartate receptors (NMDARs). In the present study, using tPA^{Null} mice, conditional deletions of either endothelial tPA or endothelial NMDARs, parabioses between wild-type and tPA^{Null} mice, hydrodynamic

transfections-induced deletion of hepatic tPA, hepatectomy and pharmacological approaches in mice, we have unveiled this mechanism in detail. We thus demonstrate, that physiological concentrations of vascular tPA, mainly produced and released by the liver endothelial cells in a bradykinin type 2 receptors-dependent manner, promotes NVC, by a mechanism dependent of brain endothelial NMDA receptors. These data highlight a new mechanism of the regulation of NVC involving both endothelial tPA and NMDA receptors.

Key words: tPA, NMDA receptor, NVC, bradykinin, endothelial cell, hepatocyte, brain, liver.

Sommaire

Index des figures

Liste des abréviations

7-CIKA	*7-chlorokynurenic acid*
AA	Acide Arachidonique
ABD	*Agonist-Binding Domain* - Domaine de liaison de l'agoniste
ACE	*Angiotensin Converting Enzyme* - Enzyme de conversion de l'angiotensine
ACh	Acéthylcholine
ACM	Artère Cérébrale Moyenne
ADNc	ADN complémentaire
AGT	Angiotensinogène
AMPA	α-amino-3-hydroxy-5-méthylisoazol-4-propionate
Ang	Angiotensine
AP5	Acide 2-amino-5-phosphonopentanoique
APA	Aminopeptidase A
APN	Aminopeptidase N
ARNm	ARN messager
a-SMA	*α-Smooth Muscle Actin*
ATF6	*Activating transcription factor 6* – Activateur de facteur de transcription
ATP	Adénosine Triphosphate
AVC	Accident Vasculaire Cérébrale
BHE	Barrière Hémato-Encéphalique
BK	Bradykinine
BOLD	*Blood Oxygen Level Dependent*
CDK2	*Cyclin-Dependant Kinase 2*
CNV	Couplage neurovasculaire
COX-2	Cyclooxygénase 2
DACH1	Gène Dachshund
DSC	Débit Sanguin Cérébral
EET	Acide époxyeicosatriénoique
EGF	*Epidermal Growth Factor*
EGFR	*Epidermal Growth Factor Receptor*
eNOS	NO Synthase endothéliale

EPSC	*Excitatory Postsynaptic Currents*
FDP	Produits de dégradation de la fibrine
GPCR	Récepteur couple aux protéines G
HK	Kininogène de haut poids moléculaire
IEC	Inhibiteurs de l'enzyme de conversion
iGluR	Récepteurs ionotropes du glutamate
iNOS	NO synthase inductible
IP3	*Inositol-1,4,5-triphosphate*
IRM	Imagerie par Résonance Magnétique
IRMf	Imagerie par Résonance Magnétique fonctionnelle
K2	Kringle 2
K_{Ca}	Canaux potassiques calcium dépendant
KD	Kallidine
K_{IR}	Canaux potassiques rectifiant entrant
KO	*Knockout*
LBS	*Lysine Binding Site*
LDL	*Low Density Lipoprotein*
LK	Kininogène de bas poids moléculaire
LRP	*Low Density Lipoprotein Receptor-related Protein*
LTD	*Long Term Depression* - Dépression à long terme
LTP	*Long Term Potentiation* - Potentialisation à long terme
mGluR	Récepteurs métabotropes du glutamate
MMP	*Matrix metalloproteinase*
NMDA	N-Méthyl-D-Aspartate
nNOS	NO synthase neuronale
NO	Monoxyde d'azote
NS	Neuroserpine
PAI-1	*Plasminogen Activator Inhibitor-1* - Inhibiteur de type 1 du plasminogène
PDGF-CC	*Platelet-Derived Growth Factor CC*
PDGFR-α	*Platelet-Derived Growth Factor Receptor α*
PGE_2	Prostaglandines E2
PKA	Protéine Kinase A
PKC	Protéine Kinase C

PLA_2	Phospholipases A2
PLAT	*Plasminogen Activator Tissue type*
ROS	*Reactive Oxygen Species* - Espèces réactives de l'oxygène
rtPA	tPA recombinant
sc-tPA	*single-chain tPA* – tPA simple chaine
Serpine	*SERine Protease INhibitor*
SKK	Système kinine-kallicréine
SNC	Système Nerveux Central
SRA	Système rénine-angiotensine
tc-tPA	*two-chain tPA* – tPA double chaine
TEP	Tomographie par Emission de Positrons
tPA	*tissue-type Plasminogen Activator* - activateur tissulaire du plasminogène
uPA	*Urokinase plasminogen activator*
uPAR	*Urokinase plasminogen activator receptor*
WT	*Wild-type*

Introduction

1. L'activateur tissulaire du plasminogène

L'activateur tissulaire du plasminogène (*tissue-type Plasminogen Activator*, tPA) est une sérine protéase capable de cliver le plasminogène en plasmine, permettant ainsi la dégradation de la fibrine, un des constituants majeurs des caillots sanguins. Par sa capacité de fibrinolyse, le tPA est à ce jour le seul traitement pharmacologique utilisé pour la phase aigüe des accidents vasculaires cérébraux (AVC) ischémiques. Cette protéase retrouvée principalement dans la circulation sanguine est également exprimée dans le système nerveux central (SNC) et joue différents rôles physio-pathologiques.

1.1. Historique

Dès la Grèce antique, Hippocrate avait observé que le sang des personnes décédées ne coagulait pas et cette observation a été corroborée par Morgani en 1761 (Morgani, 1761). Ironiquement, Morgani a fait ses observations sur des patients atteints d'apoplexie (terme médical historique désignant l'accident vasculaire cérébral), ignorant que deux cents ans plus tard, c'est en partie grâce à ses observations que naitra un traitement capable de solubiliser les caillots sanguins dans le cas des AVC. En 1843, Andral constate que le sang coagulé peut se liquéfier à nouveau, apportant ainsi les premiers fondements de la compréhension de la fibrinolyse (Andral, 1843). Denys, Marbaix et Dastre déterminent l'existence d'une enzyme fibrinolytique responsable de ce mécanisme, ils nommeront cette activité protéolytique la fibrinolyse (Dastre, 1893 ; Denys & de Marbaix, 1889). Hedin réussit à identifier plus tard le plasminogène, précurseur de la plasmine qui est responsable de la dégradation de la fibrine (Hedin, 1903). Cependant, l'origine de l'activation de ce précurseur en conditions physiologiques était encore confuse.

C'est en 1952 que la fibrinokinase, ancien nom du tPA, a été isolée pour la première fois (Astrup & Stage, 1952). Elle fut ensuite caractérisée dans la circulation sanguine en 1979 (Binder et al., 1978), puis dans l'utérus où l'enzyme a été purifiée à

partir de surnageants de cultures cellulaires de mélanome humain. La protéine fut renommée par la suite activateur tissulaire du plasminogène (Rijken & Collen, 1981).

La première administration du tPA chez l'Homme a été réalisée en 1981, pour traiter des patients atteints de thrombose de la veine rénale à la suite d'une transplantation (Weimar et al., 1981). Par la suite, le gène du tPA a été cloné puis produit sous forme recombinante par des bactéries *E.coli* (Pennica et al., 1983). Cela a permis de réaliser les premières études cliniques sur des patients souffrant d'infarctus du myocarde ; l'injection intraveineuse du tPA a permis une recanalisation complète des artères coronaires (van de Werf et al., 1986). A la suite de ces avancées et désormais le tPA est utilisé comme agent thrombolytique lors d'un AVC ischémique (National Institute of Neurological Disorders and Stroke rt-PA Stroke Study Group, 1995), et reste le seul agent pharmacologique autorisé lors de la phase aigüe d'un AVC ischémique.

1.2. Structure

Le tPA est une glycoprotéine de 70 kDa qui appartient à la famille des sérines protéases. Composée de 527 acides aminés (Pennica et al., 1983), cette protéase est encodée par le gène *Plasminogen Activator Tissue type* (PLAT) situé sur le chromosome 8 chez l'Homme (Yang-Feng et al., 1986).

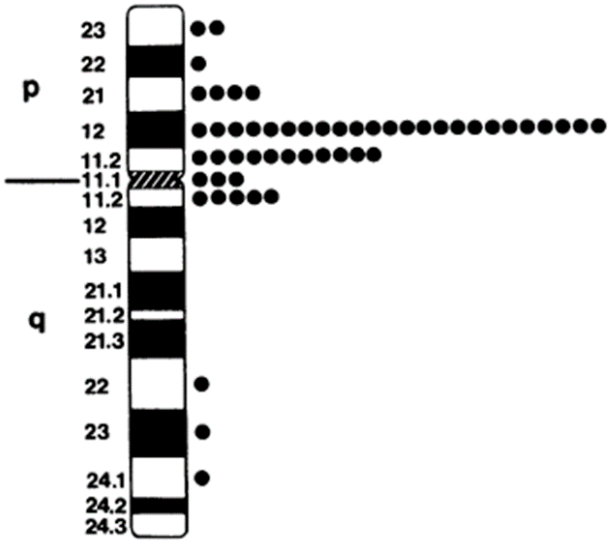

Figure 1 : La distribution de grains d'argent autoradiographiques représentant la localisation de l'ADNc du tPA sur le chromosome 8. La majorité des sondes (81%) sont fixées entre les bandes 8p12 et 8q11.2, correspondant au gène du tPA (Yang-Feng et al., 1986)

Sécrété dans l'organisme sous forme de polypeptide simple chaine (*single-chain tPA*, sc-tPA), il est rapidement transformé en polypeptide double chaine (*two-chain tPA*, tc-tPA ; Rijken & Collen, 1981), une forme plus active catalytiquement. La conversion en tc-tPA se produit via le clivage de la forme sc-tPA, au niveau de la liaison entre l'Arginine^{275} et l'Isoleucine^{276}. Cette liaison peptidique est hydrolysée par d'autres protéases comme la plasmine ou les kallicréines (Tachias & Madison, 1997). La chaine légère du tc-tPA a ainsi un poids moléculaire de 33 kD contenant 252 acides aminés, la chaine lourde quant à elle fait 39 kD pour 275 acides aminés (Pennica et al., 1983). Malgré l'hydrolyse du sc-tPA, les deux chaines restent quand même connectées via la formation d'un pont disulfure entre deux Cystéines (Cys^{299} et Cys^{430}) et un pont électrolytique localisé entre une Arginine^{302} et une Glutamine^{430} (Lamba et al., 1996). Comme vu plus haut, la forme double chaine du tPA est plus active que la forme simple chaine, mais les deux formes possèdent la même activité fibrinolytique en présence de fibrine (Rijken et al., 1982).

Morphologiquement, le tPA possède cinq domaines possédant différentes fonctions sur ses chaines, répartis comme suit :

La chaine lourde :

- **Le domaine finger**, possédant une similitude avec le site de la fibronectine. Il permet la liaison du tPA à la fibrine (Kagitani et al., 2878), aux récepteurs aux lipoprotéines de faible densité (*Low Density Lipoprotein Receptor-related Protein*, LRP), responsables de l'endocytose du tPA par les cellules hépatiques (Vivien et al., 2011), ainsi qu'à l'annexine II, impliqué dans l'activation microgliale, la fibrinolyse et la néoangiogénèse (Ling et al., 2004 ; Siao & Tsirka, 2002).

- **Le domaine EGF** est capable d'activer les récepteurs au facteur de croissance épidermique (*Epidermal Growth Factor Receptor*, EGFR ; Correa et al., 2011) et ainsi d'améliorer la recapture du tPA par les hépatocytes après sa glycolisation (Hajjar & Reynolds, 1994).

- **Le domaine kringle 1** contient un site Asn^{117}, permet la clairance du tPA grâce à la glycosylation de celui-ci et augmente ainsi l'affinité aux récepteurs du mannose, bordant les cellules hépatiques (Kuiper et al., 1988).

- **Le domaine kringle 2** a une plus faible affinité avec la fibrine que le domaine finger, mais permet de stabiliser le complexe tPA-plasminogène-fibrine (van Zonneveld et al., 1986). Il active le facteur de croissance dérivé des plaquettes *(Platelet-Derived Growth Factor-CC*, PDGF-CC ; Su et al., 2017) stimulant ainsi la croissance tissulaire. Le domaine interagit également avec la sous-unité GluN1 des récepteurs N-Méthyl-D-Aspartate (NMDA ; Lopez-Atalaya et al., 2008).

La chaine légère :

- Le domaine sérine protéase dans laquelle la fonction catalytique est ancrée, permet ainsi de convertir le plasminogène en plasmine (Macdonald et al., 1986). C'est également le site de liaison de l'inhibiteur le plus courant du tPA, l'inhibiteur de type 1 du plasminogène (*Plasminogen Activator Inhibitor-1*, PAI-1 ; Andreasen et al., 1986).

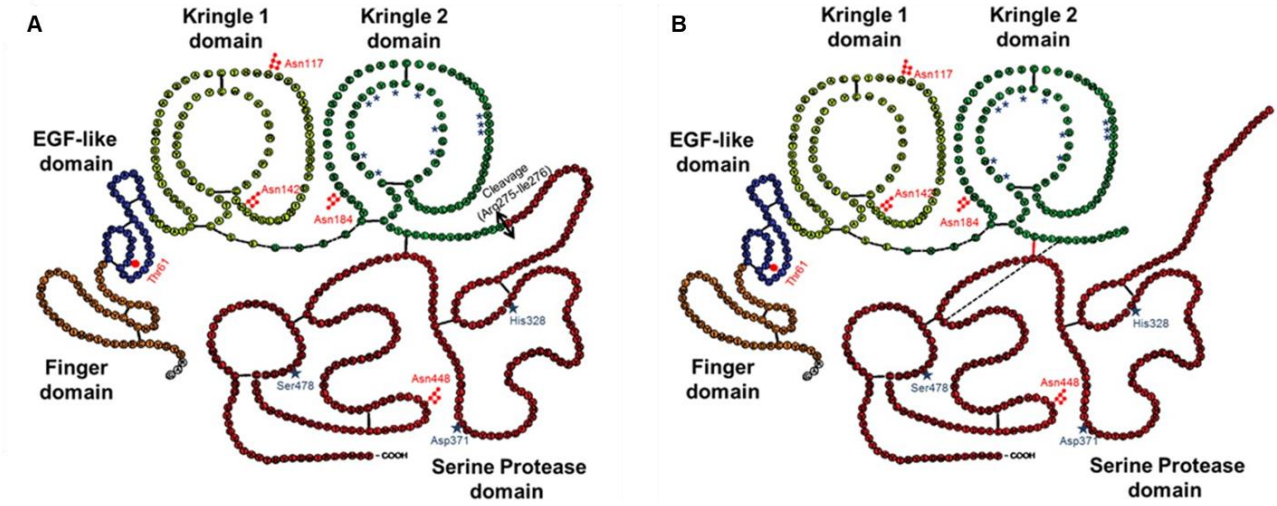

Figure 2 : Structure de l'activateur tissulaire du plasminogène (tPA) simple et double chaine. Représentation schématique du tPA sous la forme simple (**A**) et double chaine (**B**), composé de cinq domaines bien distincts. Les ponts disulfures sont représentés par des barres noires, en rouge les différents sites de glycosylation et le pont électrolytique en pointillés noirs (Chevilley et al., 2015)

1.3. Expression du tPA

1.3.1. Expression et distribution du tPA circulant

Le tPA est principalement exprimé dans le compartiment sanguin, à une concentration d'environ 70 pM (Binder et al., 1978). Il est synthétisé et libéré essentiellement par les cellules endothéliales vasculaire (Levin & Loskutofft, 1982). Son stockage dans ces cellules reste incertain. Des études suggèrent que le tPA serait situé au sein des corps de Weibel-Palade, dont la principale protéine stockée est le facteur de von Willebrand (Huber et al., 2002 ; Sadler, 1998). Dans d'autres études plus récentes, il a été observé que le tPA serait stocké dans de petits granules distincts des corps de Weibel-Palade car ils sont dépourvus de facteurs de von Willebrand (Emeis et al., 1997 ; Knipe et al., 2010 ; Knop et al., 2004). Le tPA peut alors être libéré par deux voies de sécrétions différentes : la voie constitutive et la voie contrôlé.

- La sécrétion constitutive :

L'exocytose du tPA via la voie constitutive permet une protection de la surface des cellules endothéliales vasculaire. En effet, la surface interne des vaisseaux sanguins étant une niche propice à la formation de fibrine. Le tPA libéré peut ainsi exercer son activité fibrinolytique et maintenir une perméabilité vasculaire adéquate. Cette activité fibrinolytique est modulée par la présence de l'inhibiteur de l'activateur du plasminogène de type 1 (*Plasminogen Activator Inhibitor-1*, PAI-1). Il est présent en plus grande quantité que le tPA dans le compartiment vasculaire, et limite ainsi l'activité du tPA avec une demi-vie d'environ cinq minutes (Suzuki et al., 2009).

- La sécrétion contrôlée :

Le tPA peut être libéré en supplément de la voie constitutive, via différents facteurs. Pour que les cellules endothéliales puissent fournir le tPA selon les demandes, celui-ci est stocké dans des vésicules comme décrit plus haut. A la suite d'un stimulus, via une voie de signalisation encore mal connue, impliquant une activation de protéines-G et une augmentation de calcium intracellulaire, le tPA peut être libéré dans la circulation (Knop & Gerke, 2002 ; van den Eijnden-Schrauwen et al., 1997).

Il existe différents facteurs permettant d'activer cette voie, pouvant être d'origine pharmacologique comme la desmopressine (Allen et al., 1985) ou la bradykinine (Brown et al., 1997), ainsi que certains agonistes issus de la cascade de coagulation (Emeis et al., 1997). D'autres facteurs d'origine hémodynamique peuvent également stimuler la libération de tPA ; en effet des études observent une augmentation de tPA plasmatique à la suite d'une occlusion veineuse d'un membre (Keber, 1988 ; Petäjä, 1989).

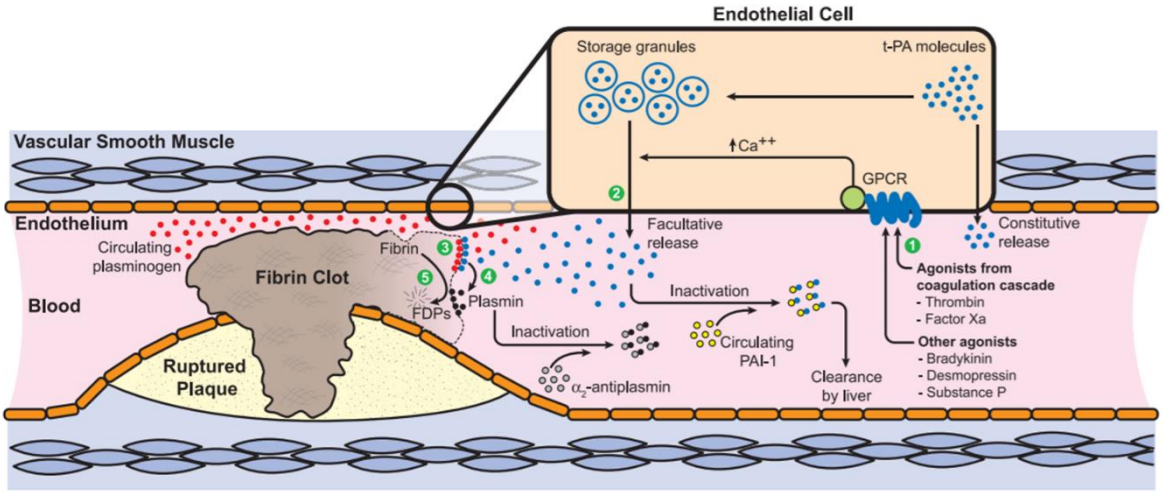

Figure 3 : La cascade de libération et d'activation du tPA à la fibrinolyse d'un thrombus vasculaire. Les agents pharmacologiques interagissent avec les récepteurs couplés aux protéines G (GPCR) à la surface des cellules endothéliales. L'augmentation de calcium intracellulaire stimule la libération du tPA stocké dans des granules vers la circulation. Le tPA converti le plasminogène contenu dans le caillot en plasmine pour que lui-même à son tour puisse dégrader la fibrine insoluble en produits de dégradations de la fibrine soluble (FDP). Ce processus est inhibé par l'inactivation du tPA par le PAI-1 et la plasmine par l'intermédiaire de l'α_2-antiplasmine. (Oliver et al., 2005).

La capacité de synthèse du tPA par les cellules endothéliales peut varier en fonction du diamètre des vaisseaux ainsi que sa localisation dans l'organisme. Chez l'Homme, le tPA serait localisé en partie dans les cellules endothéliales tapissant les artères thoraciques internes, coronaires, la veine saphène ainsi que l'aorte (Padró et al., 1995 ; Salame et al., 2000 ; Steins et al., 1999). Les vaisseaux sanguins des membres supérieurs sont également plus sujets à libérer du tPA que les membres inférieurs (Keber, 1988).

Même si depuis des décennies, il est apparent que la majeure source de tPA circulant provient des cellules endothéliales, une étude à récemment observé une autre source de production du tPA circulant. En effet, les hépatocytes présents dans le foie, joueraient un rôle important dans le niveau basal de tPA plasmatique. Le gène Dachshund (DACH1), codant pour un corépresseur transcriptionnel et jouant un rôle dans la différentiation cellulaire durant le développement (Popov et al., 2010), réprime

également un activateur de facteur de transcription (*Activating transcription factor 6* ; ATF6) présent dans les hépatocytes (Ozcan et al., 2016). ATF6 serait responsable de l'expression du gène PLAT codant pour le tPA. Une délétion conditionnelle de DACH1 dans les hépatocytes se traduirait par une surexpression du gène PLAT, visible via une augmentation de la concentration et de l'activité du tPA plasmatique (Zheng et al., 2019).

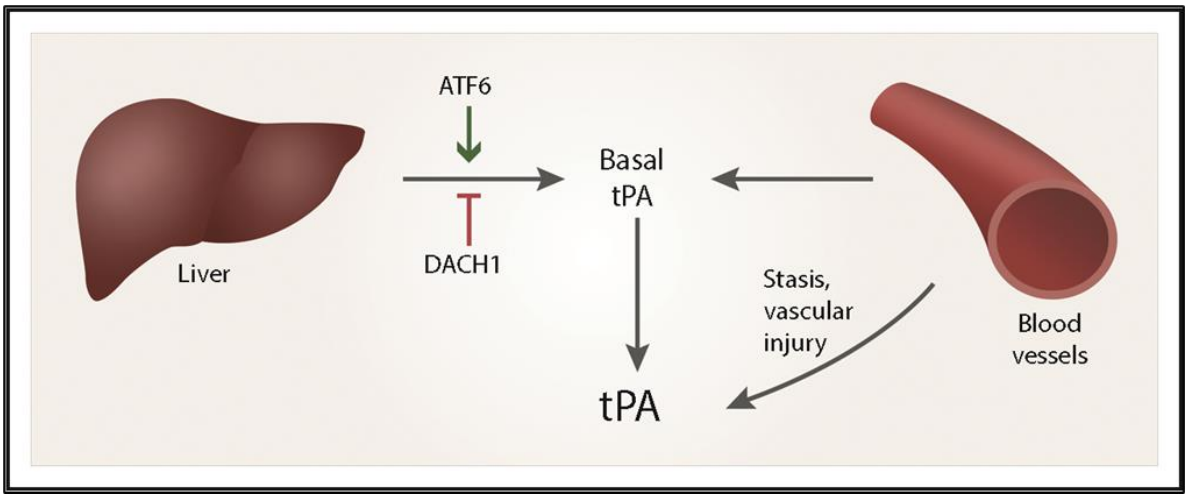

Figure 4 : Le foie et les cellules endothéliales contribuent au taux basal de tPA plasmatique. Les cellules endothéliales participent à la libération du tPA via les voies d'exocytoses constitutives et contrôlées. Le foie exprime le tPA via l'activateur de facteur de transcription 6 (ATF6) et régulé par le corépresseur transcriptionnel DACH1. (Gonias, 2019)

1.3.2. Expression et distribution du tPA périphérique

Le présence du tPA et de son ARN messager (ARNm) est observable dans différents organes tels que les reins, la prostate, les poumons, les muscles ou le cœur (Rouf et al., 1996). La présence du tPA est souvent associée à un remodelage tissulaire, par exemple, son expression dans l'utérus favorise la mise en place de l'endomètre, l'implantation de l'embryon et le déclanchement des menstruations (Lockwood & Schatz, 1996).

Tissue	Activity (units/g fresh tissue)	Tissue	Activity (units/g fresh tissue)
Uterus	720	Pituitary	140
Adrenal	410	Kidney	119
Lymph node	378	Muscle	110
Prostate	334	Heart	82
Thyroid	325	Brain	35
Lung	223	Testis	25
Ovary	210	Liver	0

Figure 5 : Activité du tPA périphérique. L'activité du tPA est mesurée sur différents échantillons de tissus humains en unité internationale (UI) par gramme de tissu frais. (Rouf et al., 1996).

1.3.3. Expression et distribution du tPA dans le système nerveux central

Soreq et Miskin ont été les premiers à observer l'expression du tPA dans le SNC (Soreq & Miskin, 1983), plus précisément au niveau des cellules endothéliales cérébrales mais également dans les neurones chez le rongeur. Par la suite, son niveau d'expression et sa distribution dans différentes structures cérébrales ont été décrits, plus précisément au sein du cervelet, de l'hippocampe, du néocortex et du striatum (Sappino et al., 1993). Ces régions dans lesquelles l'expression du tPA est élevée sont des régions qui subissent de nombreux remodelages synaptiques, associés notamment aux phénomènes d'apprentissage et de mémoire.

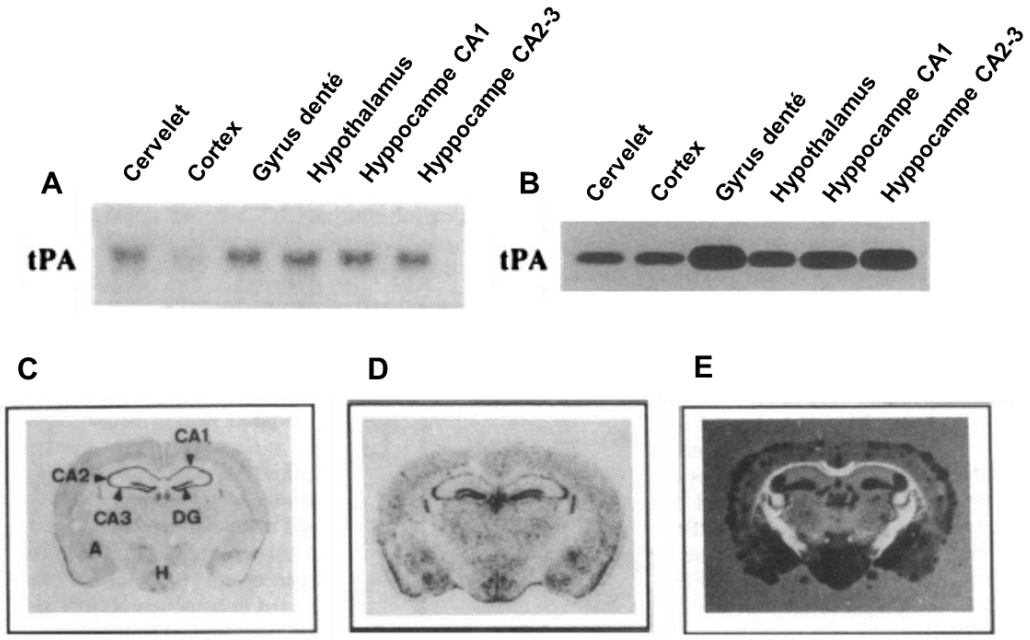

Figure 6 : Localisation du tPA dans le SNC chez la souris. A : Localisation des ARNm du tPA par Northern Blot au niveau de différentes régions cérébrales. **B** : Activité protéolytique du tPA détectée par zymographie *in situ* dans différentes régions cérébrales. **C** : Coupe coronale d'un cerveau de souris coloré au crésyl violet mettant en évidence les régions de protéolyse catalysée par le tPA : A = Amygdale, H = Hypothalamus, DG = Gyrus Denté, CA = Corne d'Ammon. **D** : ARNm du tPA révélé par hybridation *in situ* sur une coupe coronale d'un cerveau de souris. **E** : Activité protéolytique du tPA détectée par zymographie in situ sur une coupe coronale de cerveau de souris. (Adaptée de (Sappino et al., 1993)).

A l'échelle cellulaire, le tPA est exprimé par la majorité des types cellulaires du SNC.

- Dans les **neurones** : le tPA est synthétisé en conditions basales et stocké dans des vésicules présynaptiques et au niveau des dendrites (Parmer et al., 1997 ; Shin et al., 2004). Lors d'une activité neuronale, la dépolarisation libère le tPA via une exocytose dépendante du calcium dans l'espace extracellulaire (Pittman, 1985). L'expression neuronale du tPA est cependant restreinte, en effet, il serait synthétisé au niveau des neurones glutamatergiques excitateurs pyramidaux (Louessard et al., 2016).

- Dans les **astrocytes** : ces derniers sont capables de synthétiser et libérer du tPA ainsi que l'un de ses inhibiteurs, le PAI-1 (Kimura et al., 2000). Une fois le tPA libéré dans la fente synaptique par les neurones, les astrocytes peuvent recapturer le tPA via la fixation du domaine finger du tPA avec les récepteurs LRP (Cassé et al., 2012). Ainsi, les astrocytes sont capables de réguler la quantité de tPA présent dans la fente synaptique et de moduler la neurotransmission en limitant les interactions tPA-NMDAR.

- Dans les **oligodendrocytes** : l'expression du tPA dans les oligodendrocytes matures a été mise en évidence au niveau du corps calleux. Par ailleurs, son expression tant à diminuer avec l'âge (Correa et al., 2011)

- Dans la **microglie** : la production du tPA a été observée au niveau des cellules microgliales de l'hippocampe (Rogove et al., 1999 ; Tsirka et al., 1995). Sa libération entraine l'activation microgliale, impliquée dans des processus inflammatoires et neurodégénératifs (Siao et al., 2003).

Le tPA a également été localisé au sein des mastocytes et des épendymocytes (Louessard et al., 2016).

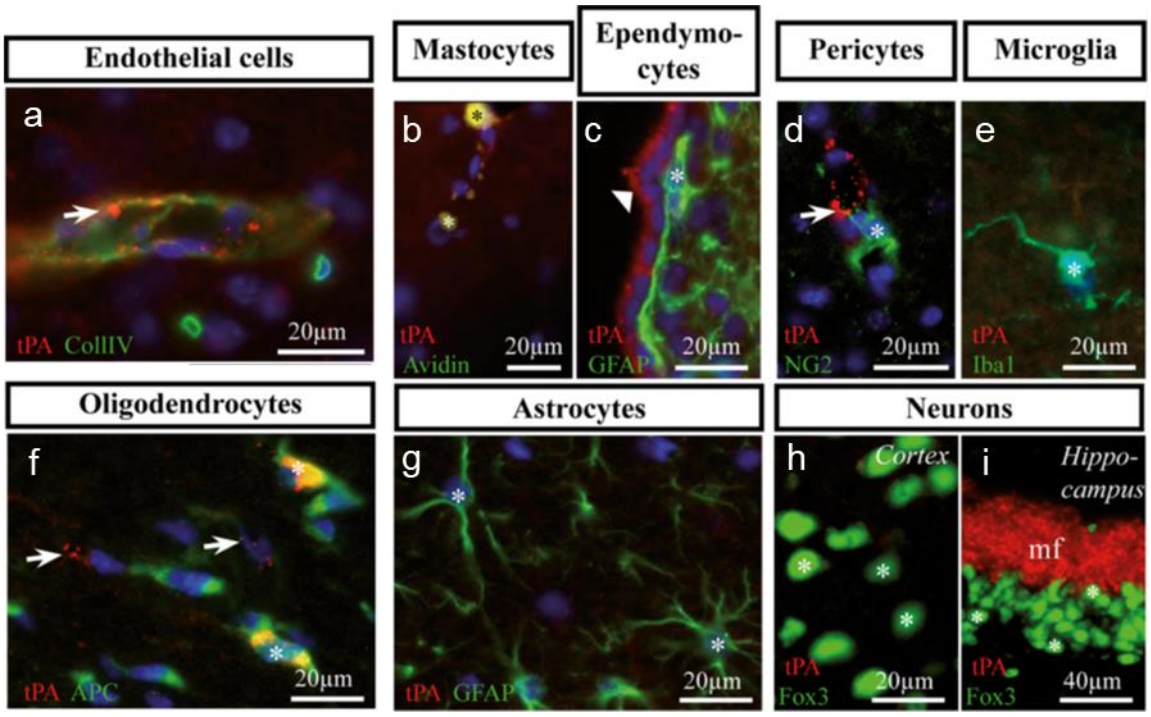

Figure 7 : Expression du tPA au sein de différents types cellulaires du SNC chez la souris adulte. Le tPA a été marqué en rouge afin de le localiser dans les cellules du SNC. Les flèches blanches indiquent les amas de tPA présents dans les cellules. (Adaptée de (Louessard et al., 2016)).

1.4. Fonctions du tPA

1.4.1. Fonctions vasculaires du tPA

1.4.1.1. Fibrinolyse

La fibrinolyse correspond à un mécanisme permettant la dissolution des caillots composés de fibrine, empêchant ainsi l'obstruction des vaisseaux sanguins. L'enzyme clé de ce processus est la plasmine, qui possède deux fonctions physiologiques principales : la dégradation de la fibrine incrustée sur la paroi interne des vaisseaux en produits de dégradation de la fibrine soluble (FDP), et la dégradation de matrices extracellulaires facilitant le remodelage tissulaire et la migration cellulaire (Lin et al., 2020). La plasmine est sécrétée par le foie sous la forme d'une pro-enzyme inactive : le plasminogène. Elle peut être activée par deux activateurs du plasminogène, l'activateur tissulaire du plasminogène (tPA) et l'activateur du plasminogène de type urokinase (uPA ; Collen & Lijnen, 1991). Une fois activée, la plasmine est rapidement

régulée par un inhibiteur spécifique, l'α2-antiplasmine et un inactivateur de protéase non spécifique, l'α2-macroglobuline (Holmes et al., 1987).

En absence de cofacteurs, le tPA possède une faible activité sur le plasminogène. C'est par le biais des domaines finger et kringle 2 que le tPA possède une forte affinité pour la fibrine, la formation du complexe ternaire tPA-fibrine-plasminogène va aboutir à une augmentation de son activité catalytique qui sera multiplié par 100 (Hoylaerts et al., 1982). Cette spécificité fait que le tPA ne peut agir qu'à proximité du thrombus et ainsi épargner le plasminogène circulant.

En revanche, la genèse de plasmine par l'uPA se produit principalement à proximité de cellules endothéliales présentant à leur surface le récepteur à l'uPA (uPAR). L'uPA en se fixant sur son récepteur va pouvoir activer le plasminogène en plasmine se trouvant à proximité, ce dernier pourra donc dégrader la matrice extracellulaire.

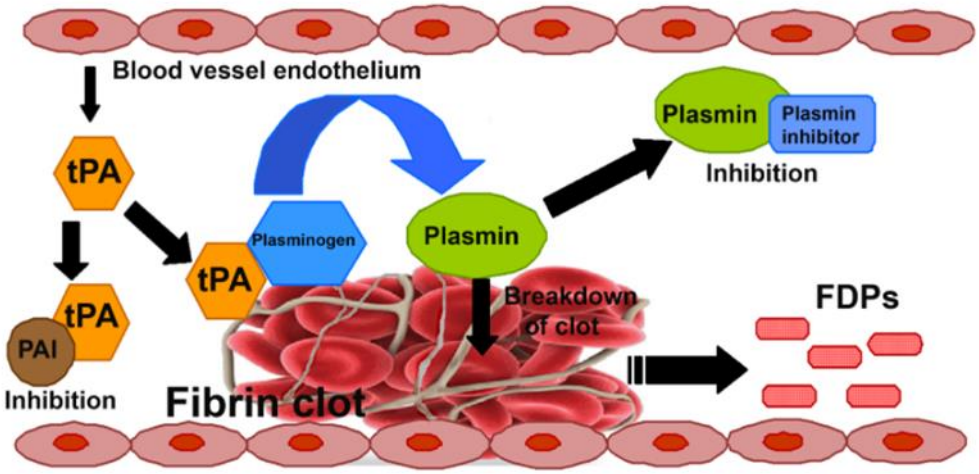

Figure 8 : Le système fibrinolytique. Le tPA sécrété par les cellules endothéliales va convertir le plasminogène en plasmine à proximité du caillot, permettant la dégradation des dépôts de fibrine en produits de dégradation de la fibrine (FDP). Ce système peut être régulé par l'inhibition du tPA par PAI-1, ou par l'inhibition de la plasmine par l'α_2-antiplasmine. (D'après (Bhattacharjee & Bhattacharyy, 2014)).

Une dérégulation du système fibrinolytique peut entrainer un emballement de la fibrinolyse, appelée l'hyperfibrinolyse, augmentant considérablement le risque

d'hémorragie ainsi qu'une altération de la barrière hémato-encéphalique (BHE ; Marcos-Contreras et al., 2016). Afin d'éviter l'hyperfibrinolyse, deux principaux inhibiteurs vont réguler le système, l'α_2-antiplasmine, comme vu plus haut, va inhiber directement la plasmine, et le PAI-1 qui inactivera le tPA.

1.4.1.2. Rôle dans la perméabilité de la barrière hémato-encéphalique

La barrière hémato-encéphalique (BHE) est une structure qui protège le parenchyme cérébral de l'entrée de substances potentiellement nocives présentes dans la circulation sanguine et maintient l'homéostasie du SNC. Présente au niveau des capillaires, elle est formée par les cellules endothéliales cérébrales reliées entre elles par des jonctions serrées et adhérentes, limitant ainsi la quantité de flux paracellulaire (Rubin & Staddon, 1999). Ces cellules endothéliales sont soutenues structurellement et fonctionnellement par des péricytes, une lame basale et par des astrocytes (Abbott et al., 2006).

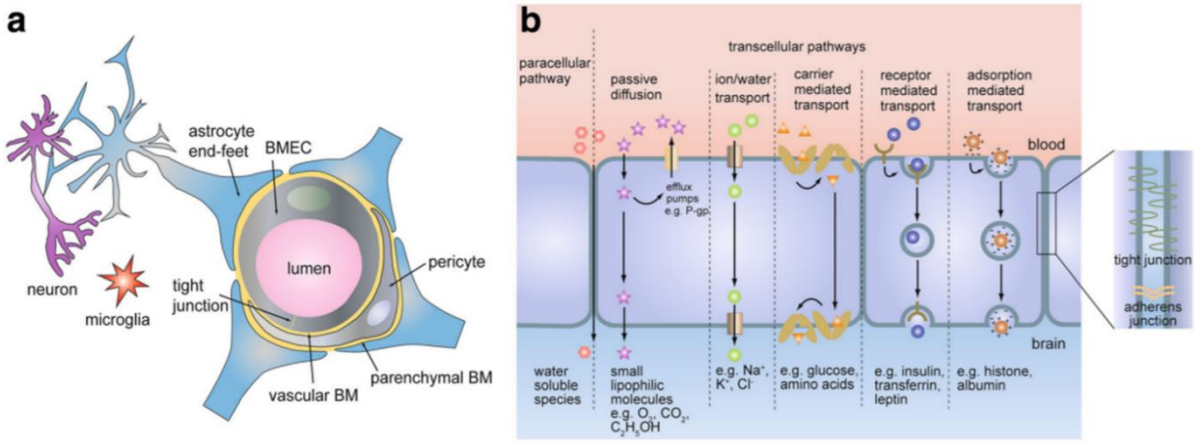

Figure 9 : Structure et fonction de la BHE. La BHE est constituée par les cellules endothéliales reliées par des jonctions serrées, la lame basale, les péricytes et les astrocytes (**a**). Représentation schématique des différentes voies de transport moléculaire paracellulaire et transcellulaire ce faisant à travers la BHE (**b**). (Jamieson et al., 2017).

Dans un contexte d'AVC ischémique, le tPA est le seul traitement pharmacologique utilisé en clinique pour ses capacités pro-fibrinolytiques. Cependant, dans certaines études, le tPA exogène utilisé pour le traitement des AVC ischémiques a été retrouvé dans le parenchyme cérébral (Wang et al., 1998). La seule possibilité expliquant ce phénomène est que le tPA circulant exogène peut traverser la BHE en conditions pathologiques. En effet, le tPA peut induire une perméabilisation ou une rupture de la BHE (Wardlaw et al., 2013), par son interaction avec les récepteurs LRP situés à la surface des cellules endothéliales, augmentant par la même occasion le risque hémorragique (Yepes et al., 2003).

Le facteur de croissance plaquettaire (*Platelet-Derived Growth Factor CC*, PDGF-CC) peut également être activé par le tPA via son domaine kringle 2 et son domaine catalytique. PDGF-CC va provoquer à son tour l'activation des récepteurs α du facteur de croissance plaquettaire (*Platelet-Derived Growth Factor Receptor α*, PDGFR-α) situés sur les astrocytes et les péricytes et induire une ouverture de la BHE (Fredriksson et al., 2004 ; Su et al., 2008).

Par ailleurs, le tPA est capable d'activer des métalloprotéinases matricielles (*matrix metalloproteinase*, MMP), comme les MMP2, 3 et 9. L'activation de ces MMPs peut favoriser l'ouverture de la BHE par la dégradation de la matrice extracellulaire, fragilisant les jonctions serrées des cellules endothéliales (Lijnen, 2001 ; Wang et al., 2003).

Dans des conditions physiologiques, le tPA est également capable de traverser la BHE via les récepteurs LRP (Benchenane et al., 2007). L'augmentation de l'expression des récepteurs LRP après le début d'une ischémie pourrait expliquer l'augmentation du risque hémorragique (Suzuki et al., 2009).

1.4.2. Fonctions du tPA dans le système nerveux central

1.4.2.1. La modulation glutamatergique

Le glutamate est le neurotransmetteur excitateur le plus important du SNC et agit sur trois principaux récepteurs ionotropes : les récepteurs NMDA, kaïnate et α-amino-3-hydroxy-5-méthylisoazol-4-propionate (AMPA). Un potentiel d'action engendré par les neurones va favoriser l'exocytose du glutamate dans la fente synaptiquequi pourra activer récepteurs NMDA, largement répandus dans le SNC. Cette activation va jouer un rôle dans la plasticité synaptique que nous détaillerons ci-après.

Le tPA peut agir comme neuromodulateur glutamatergique par sa capacité à cliver la sous-unité GluN1 des récepteurs NMDA, et potentialiser la neurotransmission glutamatergique (Fernández-Monreal et al., 2004 ; Nicole et al., 2001). Cette interaction entre le tPA et le récepteur NMDA s'effectue au niveau du domaine kringle 2 et du domaine catalytique pour le tPA et du domaine N-terminal au niveau de l'arginine^{260} pour la sous-unité GluN1 du récepteur NMDA, formant un complexe ternaire (Lopez-Atalaya et al., 2008).

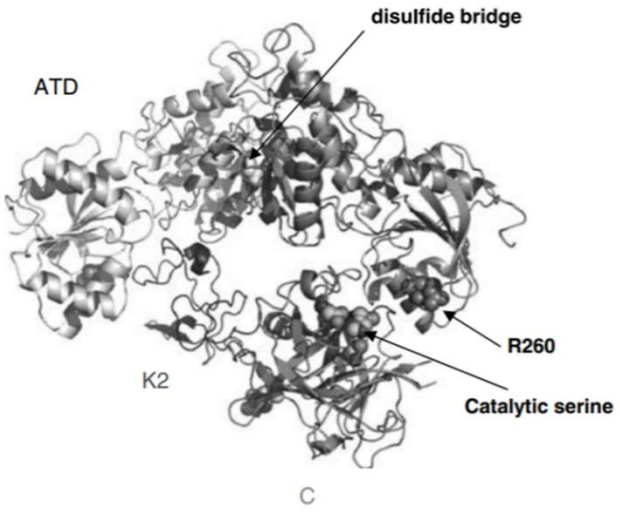

Figure 10 : Représentation tridimensionnelle de l'interaction entre le tPA et la sous-unité GluN1 des récepteurs NMDA. Le domaine kringle 2 (K2) du tPA se lie avec le domaine N-terminal (ATD) de la sous-unité. Le domaine catalytique (C) interagit au niveau de l'arginine^{260} (R260) de la sous-unité GluN1 du récepteur NMDA. (Adaptée de (Lopez-Atalaya et al., 2008)).

De plus, le tPA présent dans la fente synaptique à un rôle de gliotransmetteur. En effet, les astrocytes sont capables de recapturer le tPA par le biais des récepteurs LRP, puis de le relarguer de manière régulée dans la synapse (Cassé et al., 2012).

1.4.2.2. Développement et migration cellulaire

Au cours du développement du SNC, les neurones immatures migrant depuis les zones germinatives vers leur destination finale, vont suivre toute une étape de différenciation, prolifération cellulaire avant de mettre en place les connexions neuronales (Hatten, 1999). Ces processus sont très importants pour un bon fonctionnement cérébral ; un défaut de régulation pourra engendrer des dysfonctionnements (Rakic, 1988). Les premières traces de tPA impliquées au cours du développement ont été découvertes par Krystosek et Seeds. En effet, les cellules granulaires du cervelet peuvent sécréter le tPA le long de leurs prolongements (Krystosek & Seeds, 1981). L'absence de tPA provoque une accumulation des cellules

en grain dans la couche moléculaire du cervelet, qui reflète une diminution de la vitesse de migration neuronale vers la couche granulaire (Seeds et al., 1999).

De plus, le tPA joue un rôle dans la migration des progéniteurs d'oligodendrocytes, via un processus dépendant des récepteurs à l'EGF (Leonetti et al., 2017).

Au cours de la corticogenèse, le tPA agit sur la mise en place, la maturation et l'orientation des cellules de la glie radiaire ainsi que la migration des neurones pyramidaux, via l'interaction du domaine kringle 2 du tPA sur les récepteurs NMDA, localisés sur la glie radiaire (**Figure 11** ; (Pasquet et al., 2019)).

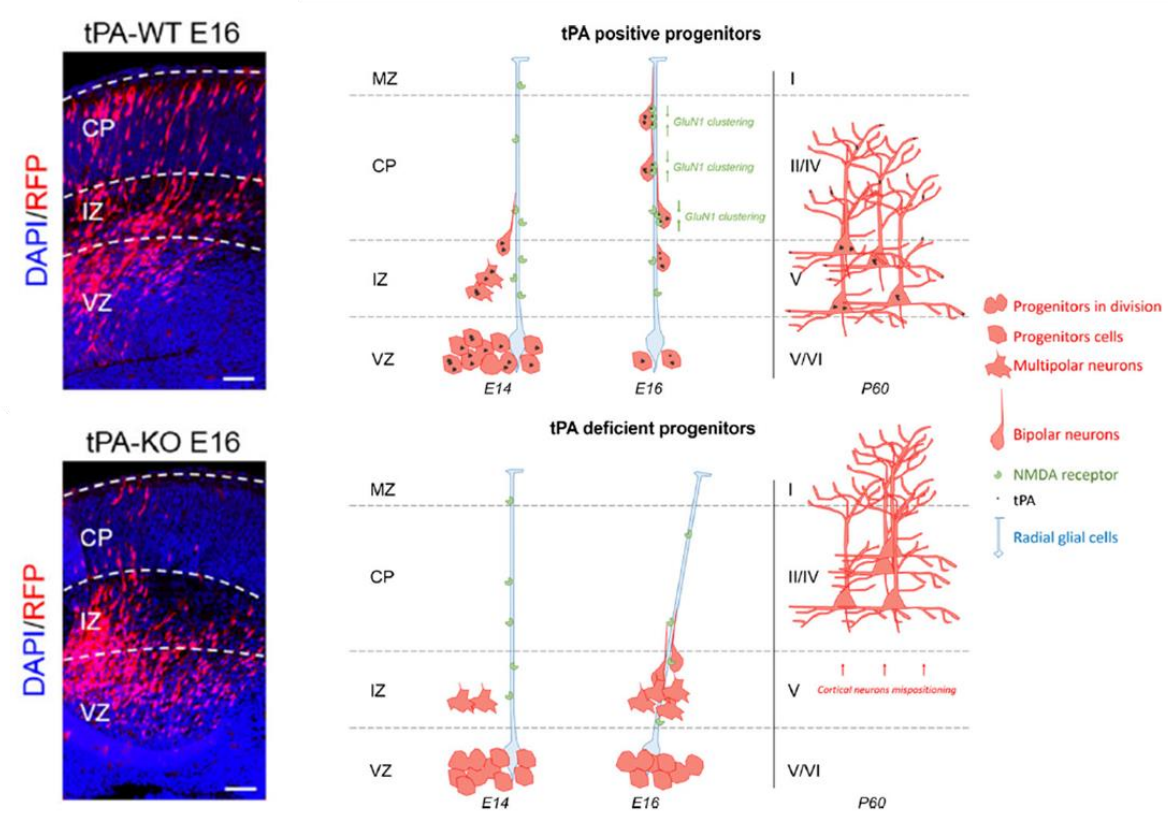

Figure 11 : Influence du tPA sur la migration neuronale lors de la corticogenèse. A gauche, la distribution des neurones marqués au RFP dans le cortex chez des souris tPA WT et KO à E16. Représentation schématique de la corticogenèse. Le tPA libéré par les progéniteurs neuronaux favorise la maturation des cellules de la glie radiaire par l'activation des récepteurs NMDA présents à leur surface. L'absence de tPA affecte l'orientation de la glie radiaire sans impacter la fixation des pieds sur la surface piale. En résumé, l'absence de tPA à E14 retarde la migration neuronale à E16, se traduisant par une altération de la stratification des couches corticales II, IV et V chez l'adulte (Adaptée de (Pasquet et al., 2019)).

Les neurones immatures commencent à établir des connexions entre eux en émettant un prolongement appelé cône de croissance, qui deviendra par la suite l'axone. La sécrétion de tPA au niveau du cône de croissance favorise la dégradation de la matrice extracellulaire, via l'activation du plasminogène et des MMP, facilitant la progression du cône de croissance (Garcia-Rocha et al., 1994).

1.4.2.3. Plasticité synaptique

Une des facultés du cerveau est de pouvoir enregistrer des informations et de garder celles qui sont utiles, on retrouve cela dans l'apprentissage ou la mémoire. Les neurones ont la capacité à moduler leur activité électrique via l'efficacité de la transmission synaptique, c'est la potentialisation à long terme (*Long Term Potentiation*, LTP). Ce phénomène a été observé pour la première fois dans l'hippocampe (Bliss & Lomo, 1973), puis a été retrouvé également dans le cortex, l'amygdale ou le striatum (Iriki et al., 1988 ; Uno & Ozawa, 1991). Une avancée majeure dans la compréhension de la LTP a été la mise en évidence sur l'implication des récepteurs ionotropes du glutamate, les récepteurs NMDA et AMPA (Morishita et al., 2005). Une stimulation à haute fréquence va induire la libération de glutamate en grande quantité par les neurones dans la fente synaptique. Le glutamate va dans un premier temps activer les récepteurs AMPA, induisant une dépolarisation du neurone post-synaptique et provoquant l'expulsion des ions magnésiums bloquant les récepteurs NMDA. Le glutamate peut activer dans un second temps les récepteurs NMDA et permettre l'entrée du calcium dans le neurone post-synaptique. Cette entrée de calcium va engendrer d'autres cascades moléculaires conduisant à la plasticité synaptique.

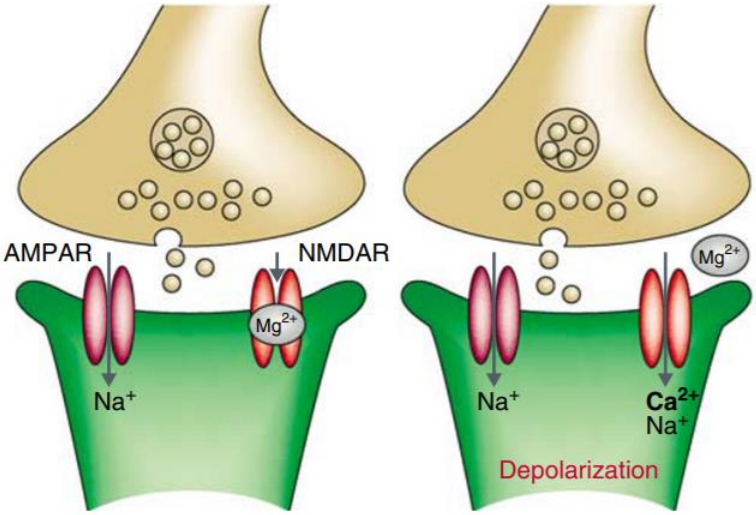

Figure 12 : Représentation de la transmission synaptique au cours d'une LTP. Lors d'une activité neuronale, le glutamate libéré dans la fente synaptique va se lier aux récepteurs AMPA et NMDA. Une activation des récepteurs AMPA à lieu mais ce n'est pas le cas pour les récepteurs NMDA, les ions magnésium bloquant ce récepteur. La dépolarisation induite par l'entrée de ions sodium dans l'élément post-synaptique induit l'évacuation de l'ion magnésium bloquant le récepteur NMDA. L'entrée de calcium dans l'épine dendritique va assurer le maintien de la plasticité synaptique (Adaptée de (Citri & Malenka, 2008)).

Le tPA, localisé dans l'hippocampe, le cortex, l'amygdale et le cervelet, est impliqué dans les processus d'apprentissage et de mémoire (Pawlak et al., 2002 ; Teesalu et al., 2004). En effet, une augmentation de la synthèse des ARNm du tPA a été observée à la suite d'une activation neuronale induite par stimulation électrique (Qian et al., 1993 ; **Figure 13**).

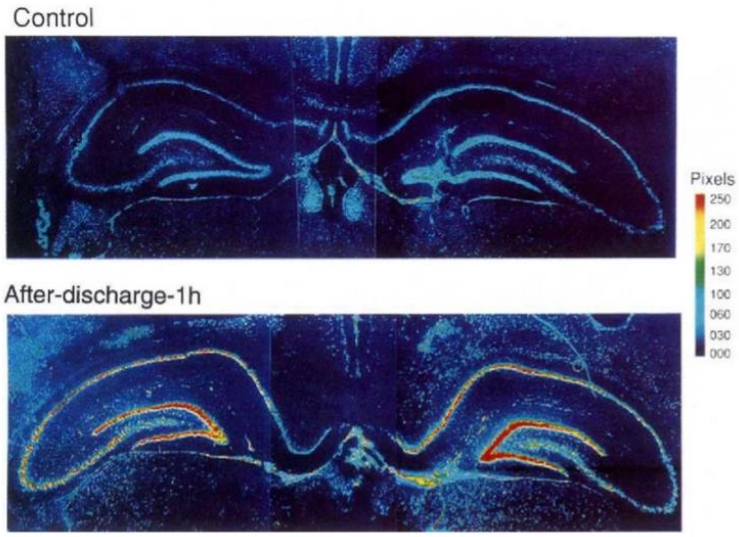

Figure 13 : Synthèse d'ARNm du tPA suite à une activation neuronale. Hybridation *in situ* des ARNm de tPA dans l'hippocampe de rat en conditions normales et 1h après une stimulation électrique dans le gyrus denté. (Qian et al., 1993).

L'influence du tPA dans le processus de LTP peut être expliqué par son interaction avec les récepteurs NMDA et a pu être confirmé par différents modèles d'approches pharmacologiques et d'utilisation d'animaux transgéniques (Baranes et al., 1998 ; Madani et al., 1999 ; Pawlak et al., 2005). Également, la fixation du tPA sur les récepteurs LRP contribue à l'établissement de la phase tardive de la LTP en activant des voies de signalisations dépendantes des protéines kinase A (PKA ; Zhuo et al., 2000). Enfin, le domaine EGF du tPA peut cliver la reeline, une protéine intervenant dans la régulation de l'activité synaptique (Trotter et al., 2014).

1.4.2.4. Cognition

Les processus de mémoire et d'apprentissage sont importants pour s'adapter à différentes situations au cours de la vie. La mémoire permet de se souvenir d'expériences passées tandis que l'apprentissage va modifier le comportement suite à un évènement vécu. A une échelle plus microscopique, les neurones vont former

des réseaux entre eux, connectant différentes aires cérébrales pour pouvoir stocker et se rappeler d'un souvenir.

Nous avons vu dans le paragraphe précédent que le tPA jouait un rôle dans la plasticité synaptique, qui constitue la base de la mémoire et de l'apprentissage. Lors d'une exposition au stress, il a été observé que le tPA était surexprimé au niveau de l'amygdale, une région impliquée à la réponse au stress, l'anxiété ainsi que la peur (Matys et al., 2004 ; Pawlak et al., 2003). En effet, des souris déficientes au tPA présentent un comportement moins anxieux que des souris sauvages. Le tPA est aussi impliqué dans l'apprentissage spatial, les souris n'exprimant plus de tPA montrent des déficits dans la reconnaissance d'objets et l'exploration (Calabresi et al., 2000). Les mêmes déficits sont observés chez des souris sauvages immunisées contre la sous-unité GluN1 des récepteurs NMDA (Benchenane et al., 2007), laissant penser que l'interaction du tPA avec les récepteurs NMDA serait impliquée dans le processus de mémoire spatiale.

1.4.2.5. Excitotoxicité

L'excitotoxicité correspond à une souffrance des cellules neuronales provoquée par un excès de glutamate, résultant d'une activation excessive des récepteurs ionotropes. L'accumulation de calcium dans les neurones va entrainer une production de radicaux libres, impliqués dans la mort cellulaire. Cette excitotoxicité est retrouvée dans certaines pathologies comme les AVC, la sclérose en plaques ou encore la maladie d'Alzheimer (Mehta et al., 2013).

L'implication du tPA dans l'excitotoxicité a été mise en évidence par Tsirka en 1995. Les souris déficientes en tPA sont plus résistantes au processus de dégénérescence neuronale induite par l'injection d'agonistes glutamatergiques (Tsirka et al., 1995).

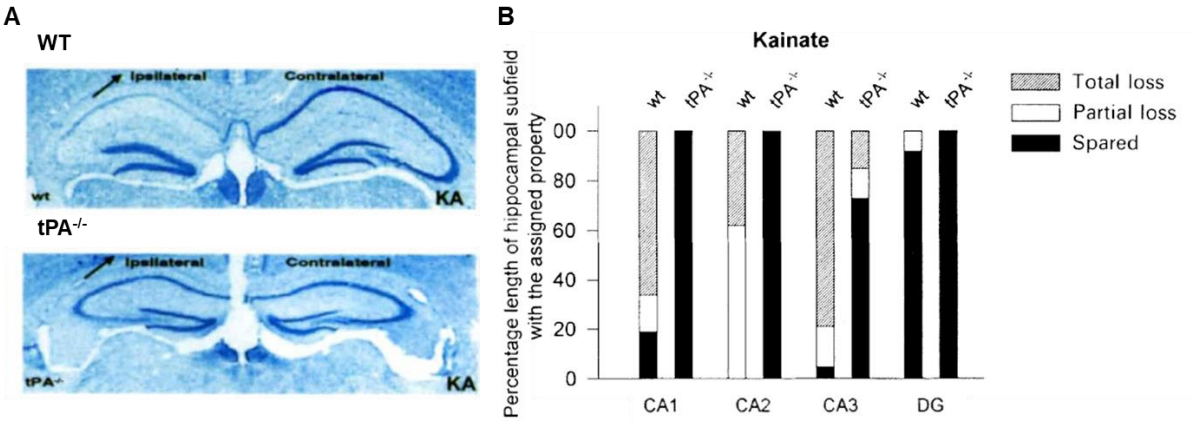

Figure 14 : Le tPA potentialise la mort neuronale excitotoxique dans l'hippocampe. A : L'injection d'un agoniste du glutamate (kaïnate) dans la région intra-hippocampique ipsilatérale chez des souris tPA$^{-/-}$ n'entraine pas de mort neuronale contrairement aux souris WT. **B** : Les souris déficientes en tPA présentent une perte neuronale plus réduite selon différentes régions de l'hippocampe (CA1, 2, 3 et gyrus denté) comparée aux souris WT (Adaptée de (Tsirka et al., 1995)).

C'est plus tard qu'il a été mis en évidence que l'interaction tPA-NMDA jouait un rôle dans l'excitotoxicité. En effet, le tPA est capable de cliver la sous-unité GluN1 des récepteurs NMDA, induisant une augmentation de l'influx calcique et une dégénérescence neuronale (Nicole et al., 2001). Le tPA se fixe sur la Lysine^{178} de la sous-unité GluN1, par ce mécanisme, le tPA favorise l'influx calcique NMDA-dépendant ainsi que la mort neuronale, à la fois *in vitro* et *in vivo* (Lesept et al., 2016). Concernant la composition et la distribution des récepteurs NMDA intervenant dans l'effet pro-excitotoxique, la présence de la sous-unité GluN2D sur les récepteurs NMDA favoriserait cet effet. En effet, le blocage des récepteurs NMDA par du PPDA (un bloqueur spécifique de la sous unité GluN2D) prévient l'effet pro-neurotoxique du tPA induite par les récepteurs NMDA. Par ailleurs, les neurones de la région hippocampique ne possèdent pas de sous-unité GluN2D contrairement aux neurones corticaux, les rendant plus résistant à l'effet délétère du tPA sur la mort neuronale induite par le récepteur NMDA (Baron et al., 2010 ; Jullienne et al., 2011).

Dans le cas d'un AVC ischémique, bien que le tPA ait des effets bénéfiques concernant la lyse du thrombus et la restauration de la circulation sanguine grâce à

son activité fibrinolytique, il peut également avoir des effets délétères en potentialisant la mort neuronale de type excitotoxique. Des travaux ont montré que le volume de lésion était réduit d'environ 50% sur des souris déficientes en tPA, après occlusion de l'artère cérébrale moyenne à l'aide d'un filament. De plus, l'injection intraveineuse de tPA sur ces souris provoque une augmentation du volume de lésion cérébrale (Wang et al., 1998). Des stratégies ont été élaborées afin d'empêcher l'effet excitotoxique du tPA tout en conservant l'effet fibrinolytique. En effet, l'utilisation d'un anticorps dirigé contre le domaine N-terminal de la sous-unité GluN1, le Glunomab®, bloque la fixation du tPA sur cette sous-unité, limitant les effets délétères du tPA (Macrez et al., 2011). Il a également été mis au point un tPA dans lequel le domaine kringle 2 a été modifié, plus précisément au niveau du site de liaison à la lysine (*Lysine Binding Site*, LBS). Ce tPA-K2* ne pouvant pas interagir avec les récepteurs NMDA, cela réduit l'effet excitotoxique du tPA (Parcq et al., 2013).

1.4.2.6. Apoptose

L'apoptose, ou mort cellulaire programmée, est caractérisée par une autodestruction cellulaire finement régulée, jouant un rôle majeur dans l'élimination des cellules endommagées ou inutilisées. Une dérégulation de ce système engendre des dommages considérables dans l'organisme, une absence d'apoptose peut entrainer l'apparition de cellules cancéreuses, alors qu'un excès peut entrainer le développement de maladies neurodégénératives.

Bien que les premières études suggèrent que le tPA a un effet pro-apoptotique sur les cellules endothéliales et les neurones corticaux (Liu et al., 2004), d'autres études lui ont trouvé un effet plutôt anti-apoptotique sur les neurones et les oligodendrocytes. En effet, le tPA peut réduire la mort apoptotique des neurones corticaux induite par privation de sérum, ce mécanisme est indépendant de l'activité protéolytique du tPA et des récepteurs LRP (Liot et al., 2006). Cet effet passe par la réduction de l'activation des caspases 3, des protéines majeures de la cascade apoptotique. Cela impliquerait les voies PI3K/Akt, AMPK ou mTor-HIF-1alpha (Correa et al., 2011 ; Wu et al., 2013).

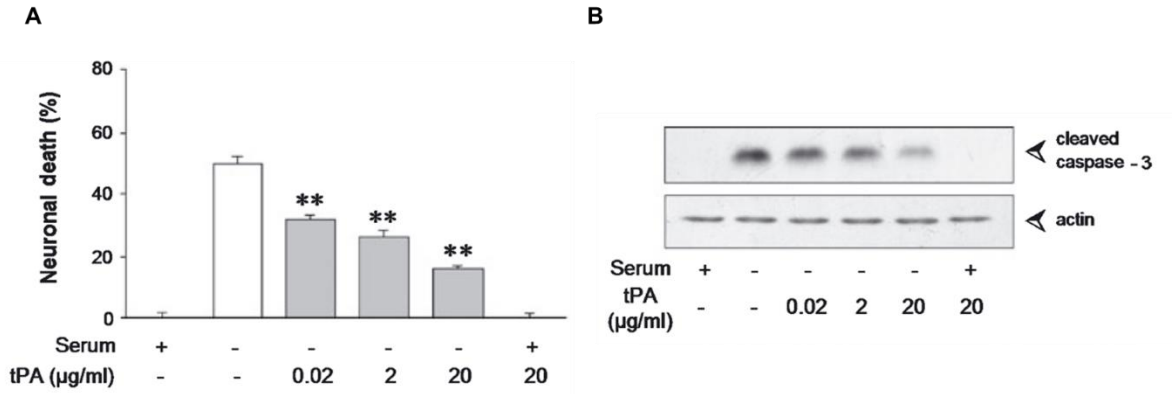

Figure 15 : Le tPA protège les neurones de l'apoptose induite par une privation de sérum. A : Quantification de la mort neuronale après 24h de privation de sérum. La mort neuronale diminue avec la quantité de tPA. **B** : Western Blot montrant que le tPA induit une diminution dose dépendante du clivage de la caspase 3 (Liot et al., 2006).

Les récepteurs à l'origine de l'effet du tPA sur l'apoptose ne sont pas encore parfaitement connus. Certains rapportent une activation des récepteurs à l'annexine II (Lee et al., 2007 ; Siao & Tsirka, 2002) ou une activation des récepteurs à l'EGF (Correa et al., 2011 ; Henry et al., 2013 ; Lemarchand et al., 2016).

1.4.2.7. Inflammation

L'inflammation est une réaction du système immunitaire à la suite d'une agression externe ou interne. Elle a pour but d'éliminer les éléments nuisibles et nettoyer la zone atteinte par diverses réparations tissulaires. L'inflammation est impliquée dans de nombreuses pathologies neurodégénératives comme l'AVC, la maladie d'Alzheimer ou la maladie de Parkinson.

Le tPA peut moduler la réponse inflammatoire en jouant un rôle dans l'activation microgliale. En conditions d'excitotoxicité, des animaux déficients en tPA ont une activation microgliale nettement réduite (Rogove et al., 1999). En effet, la liaison du

domaine finger du tPA sur les récepteurs à l'annexine II serait à l'origine de l'activation microgliale (Siao & Tsirka, 2002). L'interaction du tPA avec les récepteurs LRP1 microgliaux favorise l'activation microgliale lors d'une ischémie cérébrale. En effet, des souris déficientes en récepteurs LRP microgliaux ont un œdème cérébral réduit et un taux de MMP9 plus faible. Par ailleurs, l'administration exogène de tPA augmente l'activation microgliale chez les souris déficientes en tPA mais pas chez les souris déficientes en récepteurs LRP microgliaux (Zhang et al., 2009).

1.5. Régulation du tPA

1.5.1. Inhibiteurs du tPA

Après sa libération, le tPA circulant est majoritairement inactif, sa demi-vie ne dépassant pas les 5 minutes (Korninger et al., 1981). Plusieurs mécanismes sont impliqués dans la clairance du tPA et son inhibition par une famille de protéines, les serpines (SERine Protease INhibitor). Actuellement, les serpines capables d'inhiber le tPA dans le SNC sont le PAI-1, la neuroserpine (NS) et la nexine-1.

1.5.1.1. Le PAI-1

PAI-1 est une glycoprotéine de 50 kDa qui comporte 379 acides aminés, c'est l'inhibiteur principal du tPA et de l'uPA. Il est produit par les cellules endothéliales, les hépatocytes et les plaquettes et se trouve principalement dans la circulation sanguine où il est présent en excès par rapport au tPA (Brogren et al., 2004 ; Sprengers & Kluft, 1987). Comme vu un peu plus haut, le tPA est majoritairement inactif car complexé à PAI-1 de manière très stable (Zhou et al., 2001), et ce aussi bien sous sa forme simple chaine que double chaine (Rijken & Lijnen, 2009). La formation du complexe se fait tout d'abord au niveau du site catalytique du tPA, puis au niveau des domaines finger et kringle 2, bloquant l'interaction entre le tPA et la fibrine (Kaneko et al., 1992). De plus, le complexe tPA-PAI-1 ne gêne en aucun cas son élimination, en effet la clairance du tPA par le foie peut se faire aussi bien sous sa forme libre que complexée (Nagaoka et al., 2002).

1.5.1.2. La neuroserpine

La NS est une serpine de 54-60 kDa composée de 410 acides aminés. Elle est exprimée majoritairement dans les neurones mais aussi par les astrocytes, ainsi la NS n'a pas d'influence sur le tPA vasculaire (Docagne et al., 1999 ; Osterwalder et al., 1996). La NS se caractérise comme un inhibiteur transitoire car le complexe NS-tPA est très peu stable, le tPA peut hydrolyser la boucle réactive de la NS afin de se libérer et reprendre son activité (Carlson et al., 2016). La demi-vie du complexe NS-tPA est d'une dizaine de minutes du fait de l'instabilité de ce complexe, contrairement au complexe tPA-PAI-1 qui a une demi-vie de plusieurs semaines (Ricagno et al., 2009).

1.5.1.3. La nexine-1

La nexine-1 est une molécule de 378 acides aminés, pour un poids moléculaire de 45-50 kDa. Exprimée par les plaquettes, sa quantité reste très faible dans le compartiment vasculaire (Bouton et al., 2012). Son niveau d'expression va varier en fonction de la quantité de plaquettes présentes dans la circulation sanguine. De ce fait, la nexine-1 est impliqué dans la régulation du tPA lors de la fibrinolyse (Boulaftali et al., 2010).

1.5.2. Dégradation du tPA

Le foie est l'organe principal dans lequel la clairance du tPA a lieu. La dégradation du tPA peut se faire par plusieurs voies différentes. Tout d'abord, les récepteurs du mannose sont exprimés au niveau des hépatocytes, des cellules endothéliales hépatiques et des cellules de Kupffer, où ils peuvent se lier au tPA par son domaine kringle 1 (Kuiper et al., 1988 ; Rijken et al., 1990). Les récepteurs LRP peuvent aussi lier le tPA par son domaine finger et EGF (Orth et al., 1994). Ces derniers récepteurs peuvent recapturer le tPA sous sa forme libre mais aussi

complexée avec PAI-1. Les galectines quant à elles participent à la dégradation du tPA, elle-même régulée par l'inhibition de la recapture du tPA par les β-galactosides (Nagaoka et al., 2002).

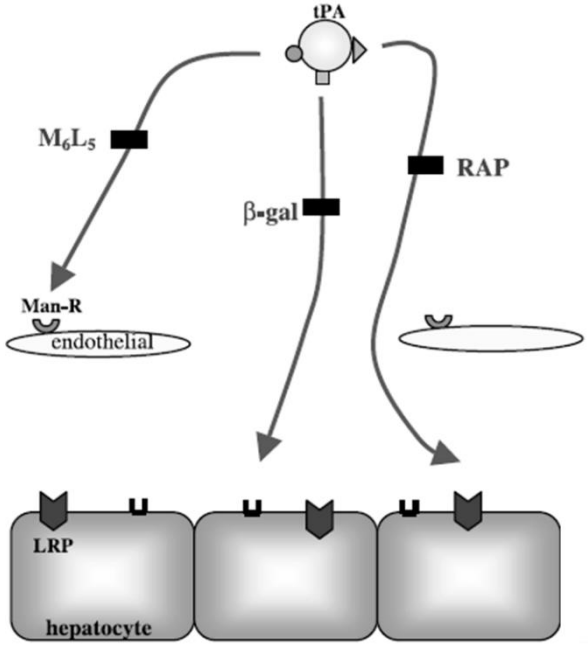

Figure 16 : Mécanismes de dégradation du tPA par le foie. Il existe trois voies de recapture du tPA vasculaire : une voie dépendant des récepteurs du mannose à la surface des récepteurs endothéliaux hépatiques, cette voie est inhibée par des mannosides (M_6L_5), une voie dépendante des récepteurs LRP, régulée par des protéines associées au récepteur (RAP), et une voie dépendante des galectines bloquée par les β-galactosides, ces deux derniers récepteurs se trouvent à la surface des hépatocytes (Adaptée de (Nagaoka et al., 2002)).

Pour résumer, le tPA est une sérine protéase présente principalement dans le système vasculaire et cérébral.

Le tPA est capable d'exercer diverses fonctions :

- **Dans le compartiment sanguin, le tPA est capable de convertir le plasminogène en plasmine, responsable de la dégradation des caillots riche en fibrine. Le tPA joue également un rôle dans l'altération de la BHE.**
- **Dans le compartiment cérébral, le tPA est impliqué dans le développement cérébral et cognitif, mais aussi dans l'inflammation et l'excitotoxicité.**

Le tPA agit comme modulateur de la neurotransmission glutamatergique par son interaction avec les récepteurs NMDA, mais peut également se lier à d'autres types de récepteurs grâce à ses domaines variés.

To summarize, tPA is a serine protease localized especially in the vascular system and brain.

tPA can play a role in various functions:

- **In bloodstream, tPA is able to convert plasminogen into plasmin, which is responsible for the degradation of fibrin clots. tPA also plays a role in the alteration of the BBB.**
- **In central nervous system, tPA is involved in brain and cognitive development, but also in inflammation and excitotoxicity.**

tPA acts as a modulator of glutamatergic neurotransmission through its interaction with NMDA receptors, but can also bind to other types of receptors through its various domains.

2. Le récepteur NMDA

La neurotransmission excitatrice glutamatergique est l'un des mécanismes crucial et vital du SNC. Ceci est particulièrement vrai pour les récepteurs NMDA, un des récepteurs ionotropes du glutamate, jouant un rôle central dans la plasticité synaptique du SNC. Nous allons développer dans les parties suivantes les caractéristiques de ce récepteur ainsi que ses fonctions au sein du SNC.

2.1. Historique

Les premières observations du fonctionnement du glutamate dans le SNC ont été faites en 1936, décrivant le glutamate comme un carburant dans le métabolisme cérébral. Il a été utilisé comme traitement dans les troubles mentaux et épileptiques. En 1954, Hayashi observa les effets du glutamate sur l'activité neuronale ; l'injection de glutamate dans le cortex chez le chien provoque une activité neuronale plus importante que la normale, et à fortes doses, le glutamate conduit à des convulsions (Hayashi, 1954). Dans les années 60, Curtis et Watkins montrèrent les effets de la dépolarisation lorsque du glutamate est appliqué sur une moelle épinière de crapaud. En effet, un phénomène d'excitation puis de dépression des neurones a été observé lors de l'application du glutamate. De plus, l'effet dépolarisant du glutamate, lorsque celui-ci est suffisamment important, conduit à une inactivation de l'activité neuronale (Curtis et al., 1961 ; Curtis & Watkins, 1960). C'est dans les années 70 que le glutamate a été reconnu par la communauté scientifique comme étant un neurotransmetteur, grâce aux observations qui ont montré que lors d'une dépolarisation induite par stimulation électrique ou par le potassium, la libération de glutamate au niveau des synapses était dépendante du calcium (Watkins, 1972). Des agonistes du glutamate sont découverts par la suite comme l'acide kaïnique (Shinozaki & Konishi, 1970) ou l'AMPA (Krogsgaard-Larsen et al., 1980).

En parallèle, des études concernant les effets toxiques du glutamate se sont développés. Les concentrations élevées du glutamate et ses analogues conduisent à

la mort neuronale, les corrélant aux lésions cérébrales retrouvés dans les ischémies cérébrales (Olney, 1978).

Par la suite, McLennan a comparé du glutamate avec un de ses analogues dans différentes régions du thalamus, et a observé des différences de puissance relative de ces deux molécules, suggérant la possibilité d'avoir plusieurs types de récepteurs au glutamate (McLennan et al., 1968). D'autres travaux menant à la même conclusion ont été réalisée en comparant les différences de puissance relative entre un analogue du glutamate et un analogue de l'aspartate au sein d'un même type cellulaire (Mcculloch et al., 1974).

Il a été relevé que dans un milieu contenant du magnésium, les dépolarisations étaient amoindries selon l'analogue du glutamate utilisé sur des moelles épinières de crapaud, classant ainsi les dépolarisations produites par les analogues selon deux types : les analogues au glutamate sensible au magnésium et insensibles au magnésium. Par ailleurs, la diminution de l'activité synaptique est liée à la capacité du magnésium à bloquer l'excitation induite par les analogues sur les récepteurs NMDA (Evans et al., 1979), proposant alors deux types de récepteurs : les récepteurs NMDA et non-NMDA.

L'implication des récepteurs NMDA et non-NMDA a alors été étudiée dans des processus fonctionnels tel que la LTP. En effet, il a été rapporté qu'après une première faible réponse excitatrice des cellules de la région CA1 de l'hippocampe, s'en suit une activation additionnelle des récepteurs NMDA permettant de générer une LTP (Collingridge et al., 1983a). Une caractéristique supplémentaire du récepteur NMDA est qu'il a besoin d'un co-agoniste avec le glutamate, la glycine ou la D-sérine, pour être activé (Johnson & Ascher, 1987).

La classification des récepteurs glutamatergiques a été proposée dans les années 90. Deux grandes familles de récepteurs ont été décrits : les récepteurs qui dépendent de l'ouverture de canaux ioniques pour induire une réponse à un signal,

appelées récepteurs ionotropes du glutamate (iGluR), incluant les récepteurs NMDA, AMPA et kaïnate, et les récepteurs associés à des changements biochimiques, les récepteurs métabotropes du glutamate (mGluR ; Schoepp et al., 1999).

2.2. Structure des récepteurs NMDA

2.2.1. Les différentes sous-unités des récepteurs NMDA

Une variété de sous-unités des récepteurs NMDA a été identifiée par clonage. Elles sont catégorisées en trois grandes familles : les sous-unités GluN1, GluN2 et GluN3, anciennement appelées NR1, NR2 et NR3 (Mori & Mishina, 1995 ; Paoletti, 2011).

- La sous-unité **GluN1** : Elle est codée par un seul gène mais possède trois sites d'épissage alternatifs, un positionné à l'extrémité N-terminale et deux à l'extrémité C-terminale. Ces sites d'épissages permettent de générer 8 isoformes fonctionnelles de la sous-unité GluN1 (GluN1-1a, 2a, 3a, 4a et GluN1-1b, 2b, 3b, 4b ; Yamazaki et al., 1992). Cette sous-unité est ubiquitaire sur les récepteurs NMDA, et est nécessaire au fonctionnement du récepteur. On retrouve l'expression de cette sous-unité principalement au sein du SNC, mais aussi au niveau du cœur, des reins, du pancréas, des cellules immunitaires et des cellules endothéliales (Inagaki et al., 1995 ; Leung et al., 2002 ; Mashkina et al., 2010 ; Sharp et al., 2003).

- La sous-unité **GluN2** : Elle est codée par 4 gènes différents, donnant 4 isoformes (GluN2A, GluN2B, GluN2C et GluN2D ; Ikeda et al., 1992 ; Monyer et al., 1992). Les sous-unités GluN2 ne sont pas exprimées de la même façon, à la fois dans l'espace (d'une région cérébrale à une autre) et dans le temps (au cours du développement). Dans le SNC des embryons chez le rongeur, seuls les sous-unités GluN2B et 2D sont exprimées ; GluN2B a une distribution très étendue alors que GluN2D se trouve principalement dans le diencéphale et le tronc cérébral. L'expression de la sous-unité GluN2A augmente après la

naissance pour au final être exprimée dans tout le cerveau à l'âge adulte. Les sous-unités GluN2C apparaissent plus tard dans le développement et sont exprimées dans le cervelet et les bulbes olfactifs (Paoletti, 2011).

- La sous-unité **GluN3** : Elle existe sous deux isoformes différents (GluN3A et GluN3B), codées par deux gènes distincts. L'expression de la sous-unité GluN3A est faible avant la naissance, elle atteint un pic d'expression juste après la naissance, puis baisse de nouveau jusqu'à l'âge adulte. Au contraire, GluN3B est faiblement exprimé après la naissance, puis augmente avec l'âge, distribué de façon ubiquitaire dans le SNC (Low & Wee, 2010).

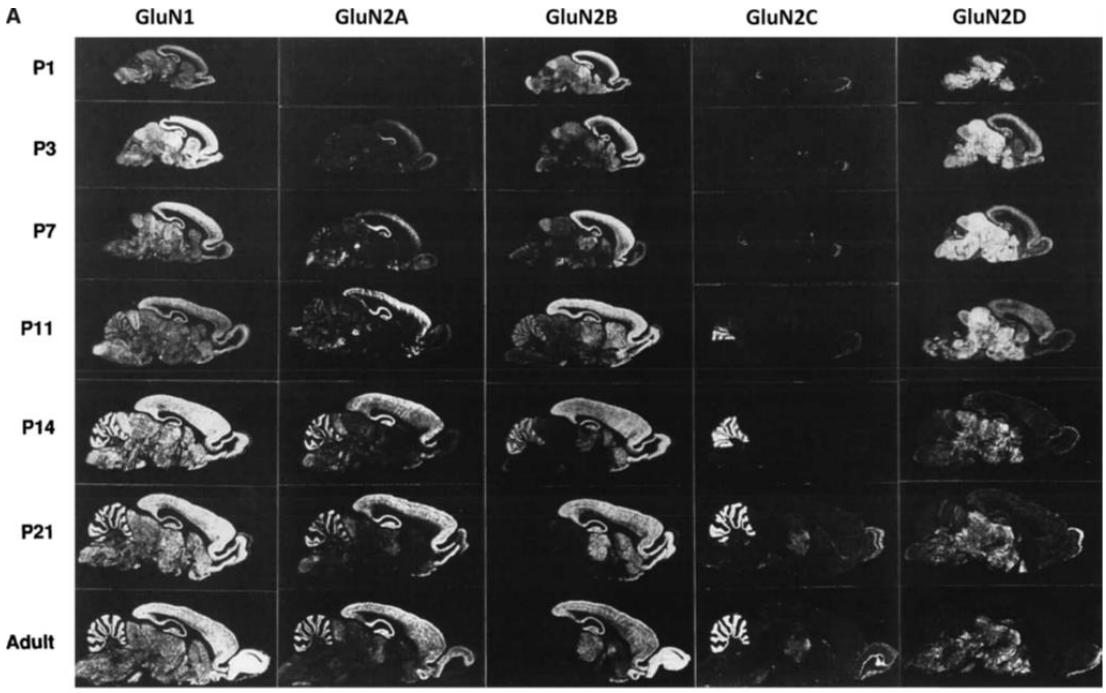

Figure 17 : Distribution des ARNm des différentes sous-unités des récepteurs NMDA dans le cerveau. Les changements d'expression des sous-unités GluN1 et GluN2A, 2B, 2C et 2D au cours du développement post-natal sont visibles en Hybridation *in situ* sur des coupes sagittales de cerveau de rat (Akazawa et al., 1994).

Chaque sous-unité est constituée de 4 domaines distincts (Mayer, 2006 ; Paoletti & Neyton, 2007) :

- Le domaine N-terminal qui englobe les 380 premiers acides aminés de la sous-unité, permet l'assemblage des sous-unités entre elles.
- Le domaine de liaison de l'agoniste (*Agonist-Binding Domain*, ABD), constitué d'environ 300 acides aminés, il permet à l'agoniste de se fixer à son ligand (la glycine et la D-sérine pour les sous-unités GluN1 et GluN3 et le glutamate pour la sous-unité GluN2).
- Le domaine transmembranaire constitué de trois segments et d'une courte boucle réentrante qui forme le canal ionique.
- Le domaine C-terminal dont la longueur dépend de la sous-unité, impliqué dans le trafic des récepteurs, l'ancrage et l'interaction à différents complexes de signalisation.

2.2.2. Composition des sous-unités NMDA

Le récepteur NMDA est composé de quatre sous-unités formant un complexe tétramérique. Il doit contenir obligatoirement deux sous-unités GluN1 et deux autres sous-unités, issues des familles GluN2 ou GluN3 (Furukawa et al., 2005). La forme la plus commune de ces récepteurs est composée de deux sous-unités GluN1 et deux sous-unités GluN2, ces hétérodimères pouvant être assemblés de différentes façons (Ulbrich & Isacoff, 2008). La composition des récepteurs NMDA en sous-unités varie selon sa localisation dans le cerveau, affectant par la même occasion ses propriétés pharmacologiques.

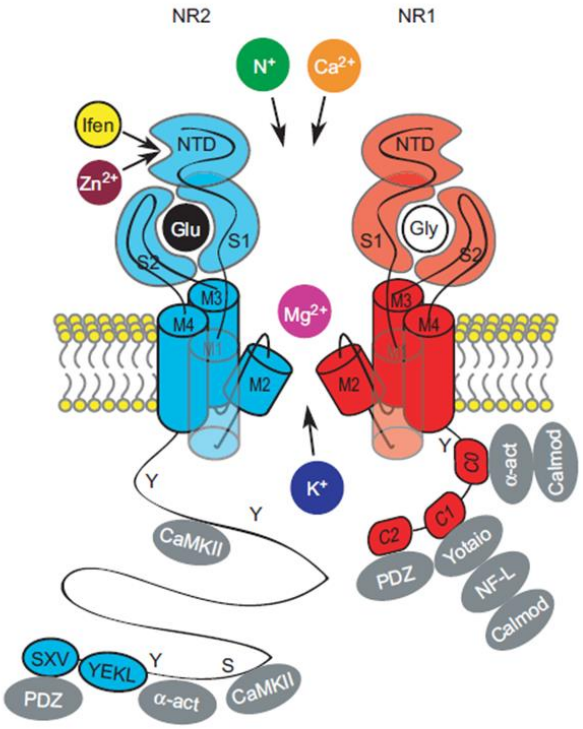

Figure 18 : Architecture du récepteur NMDA. Les sous-unités GluN1 (NR1) et GluN2 (NR2) sont composés de plusieurs domaines. La partie extracellulaire comprend les domaines N-terminaux qui contiennent les sites de modulations par le zinc (Zn^{2+}) ou l'ifenprodil (Ifen). Les domaines S1 et S2 sur la sous-unité GluN2 forment le site de liaison au glutamate et la glycine pour la sous-unité GluN1. Le domaine transmembranaire formé des domaines M1, M2, M3 et M4 forment un canal perméable aux ions sodium, potassium et calcium grâce à la partie M2 formant une boucle. Le magnésium induit un blocage voltage-dépendant en se liant à l'intérieur du canal. Le domaine C-terminal des sous-unités GluN1 et GluN2 se lie à des kinases synaptiques ainsi que des protéine structurelles (Cull-Candy & Leszkiewicz, 2004).

2.3. Fonctionnement des récepteurs NMDA

L'activation du récepteur NMDA requiert la liaison de deux molécules de glutamate, qui se fixeront sur la sous-unité GluN2, et de deux co-agonistes (glycine ou D-sérine) qui se fixeront sur les domaines ABD des sous-unités GluN1 (Johnson & Ascher, 1987 ; Kleckner & Dingledine, 1988). La dépolarisation cellulaire va libérer le magnésium qui obstruait le canal ionique ; ainsi le canal retrouve ainsi sa perméabilité

aux différents ions (Mayer et al., 1984). La perméabilité des récepteurs NMDA au calcium est une des plus élevées parmi les récepteurs ionotropes. Le blocage par le magnésium et la perméabilité au calcium sont influencés par la composition en sous-unités, par exemple, les récepteurs composés en GluN2A et GluN2B sont plus sensibles au blocage du magnésium (Paoletti et al., 2013).

Après l'activation du récepteur, le canal ionique va adopter une conformation fermée malgré la présence des ligands. Cette désactivation est assez lente et peut varier en fonction de la composition des sous-unités (Paoletti et al., 2013).

Enfin, de nombreuses molécules extracellulaires peuvent moduler de manière positive ou négative l'activité des récepteurs NMDA. En effet, les ions hydrogène tendent à inhiber la propagation du potentiel d'action, sans modifier l'affinité pour les agonistes (Tang et al., 1990). L'ion zinc exerce aussi une action inhibitrice dont le site d'action se trouve sur la partie N-terminale des sous-unités (Paoletti et al., 1997). Au contraire, les polyamines modulent positivement l'activité des récepteurs NMDA en augmentant l'affinité des sites ABD pour leur co-agoniste (Paoletti, 2011).

2.4. Localisation cellulaire des récepteurs NMDA

Dans les neurones, les récepteurs NMDA sont localisés au niveau de la synapse, plus précisément sur les éléments pré, péri et post-synaptiques. Le rôle des récepteurs NMDA pré-synaptiques est encore débattu, ils pourraient faciliter la libération du glutamate en augmentant les courants excitateurs postsynaptique spontanés et évoqués (*Excitatory Postsynaptic Currents*, EPSC ; Corlew et al., 2008). Les récepteurs périsynaptiques ne sont activés qu'en cas de forte stimulation glutamatergique, et les récepteurs postsynaptiques vont participer à la signalisation glutamatergique (le Meur et al., 2007).

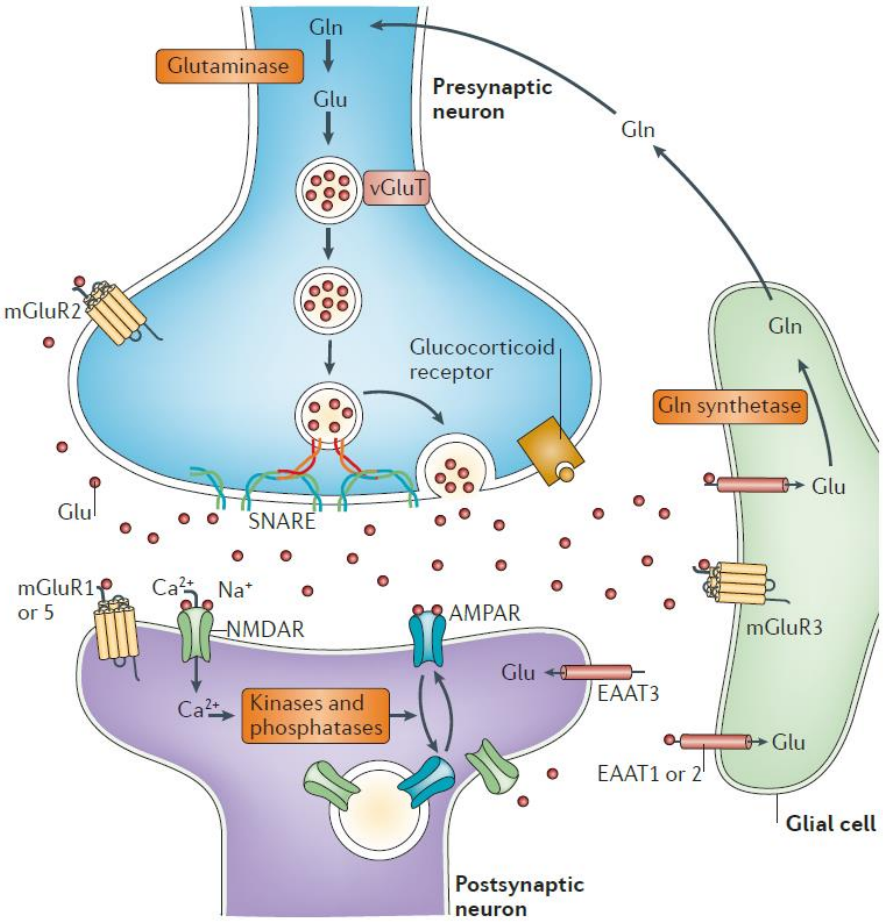

Figure 19 : La synapse glutamatergique. Le glutamate (Glu) neuronal est synthétisé à partir de glutamine (Gln) apportés par les cellules gliales. Le glutamate est stocké dans des vésicules synaptiques par des transporteurs vésiculaire du glutamate (vGluT). Les complexes SNARE (Soluble N-éthylmaleimide-sensitive-factor Attachment protein REceptor) interviennent dans l'interaction et la fusion des vésicules avec la membrane présynaptique. Après la libération du glutamate dans la fente synaptique, le glutamate se lie aux récepteurs AMPA et NMDA et métabotropes (mGluR) présents sur les neurones pré et postsynaptiques ainsi que les cellules gliales. Les récepteurs vont alors initier diverses réponses comme la dépolarisation membranaire, l'activation de cascades de signalisation ou bien la modulation de la synthèse protéique. Le recyclage du glutamate se fait par des transporteurs d'acides aminés excitateurs (*Excitatory Amino Acid Transporters* ; EAAT) au niveau des cellules gliales où le glutamate sera converti en glutamine par la glutamine synthétase, ainsi la boucle est bouclée (Popoli et al., 2012).

Les récepteurs NMDA sont également exprimés à la surface des cellules endothéliales cérébrales, plus précisément au niveau des jonctions serrées (Macrez et al., 2016 ; Reijerkerk et al., 2010).

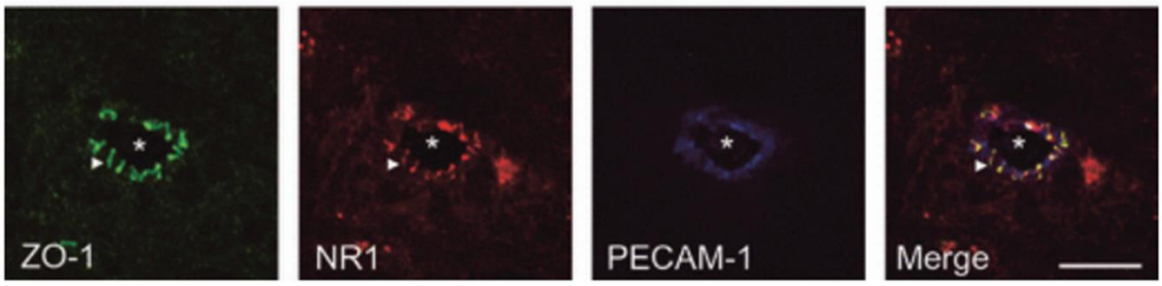

Figure 20 : L'expression de la sous-unité GluN1 dans les cellules endothéliales cérébrales. Immunohistochimie révélant la sous-unité GluN1 des récepteurs NMDA en rouge (NR1), les jonctions serrées en vert (*Zona Occludens-1* ; ZO-1) et les cellules endothéliales en bleu (*Platelet endothelial cell adhesion molecule* ; PECAM-1) sur des cerveaux de souris. Les astérisques représentent la lumière des vaisseaux sanguins, les flèches représentent les colocalisations entre ZO-1 et NR1 (Adaptée de (Reijerkerk et al., 2010a)).

Les récepteurs NMDA peuvent également être présents au sein des astrocytes, des oligodendrocytes, des lymphocytes et des cellules neuro-épithéliales (Káradóttir et al., 2005 ; Krebs et al., 2003 ; Sharp et al., 2003 ; Tuneva et al., 2003).

2.5. Rôles des récepteurs NMDA

2.5.1. Récepteurs NMDA et le développement des projections axonales

Les premières études mettant en évidence que le potentiel postsynaptique joue un rôle dans le développement des projections axonales ont été faites sur des cellules ganglionnaires. En effet, le blocage des récepteurs NMDA avec des antagonistes comme MK-801 (Dizocilpine) ou l'AP5 (acide 2-amino-5-phosphonopentanoique) ont prouvé que les récepteurs NMDA étaient importants pour le maintien des projections axonales des cellules ganglionnaires de la rétine (Cline et al., 1987).

De plus, l'activité des récepteurs NMDA s'est également avérée nécessaire dans le développement et l'orientation des neurones dans le cortex visuel primaire (Ramoa et al., 2001).

D'autres travaux, concernant le développement des projections axonales dans le cortex somatosensoriel des vibrisses, appelé aussi cortex à tonneaux (ou *barrel cortex* en anglais) ont été étudié chez des souris déficientes en sous-unité GluN1 et GluN2B. Le cortex à tonneaux contient une carte somatotopique des vibrisses dans laquelle une vibrisse correspond à une unité en forme de colonne dans la couche IV du cortex. Les neurones sensitifs issus des vibrisses à la base du museau projettent leurs axones au niveau de noyaux trigéminaux du tronc cérébral, qui présentent une organisation somatotopique en barrelettes similaire aux vibrisses. Ceux-ci se projettent à leur tour au niveau des neurones du thalamus tout en préservant une somatotopie en barreloïdes similaire. Les neurones thalamiques se projettent à leur tour dans le cortex somatosensoriel. Les souris déficientes en sous-unités GluN1 et GluN2B présentent des défauts d'arrangement des colonnes au niveau de la carte somatotopique dans de thalamus et le cortex du a un développement exubérant des projections axonales (Iwasato et al., 2000 ; Kutsuwada et al., 1996 ; Lee et al., 2005).

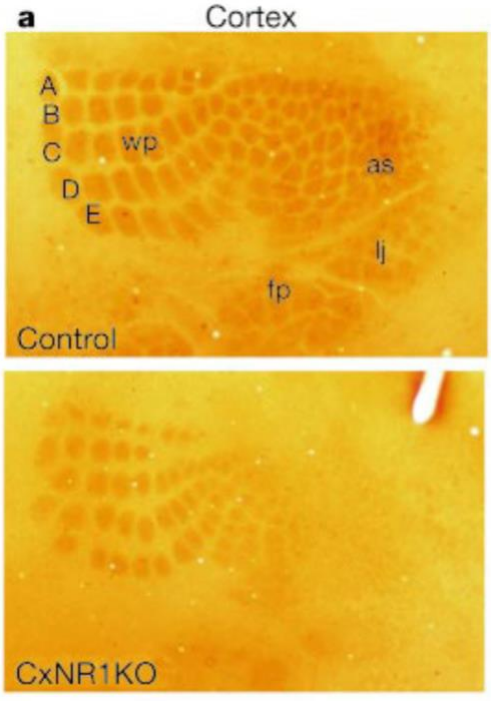

Figure 21 : La carte somatotopique des vibrisses présente un défaut d'arrangement des colonnes chez les souris déficientes en sous-unité GluN1 dans les neurones corticaux excitateurs. Carte corticale comprenant les 5 rangées de barrels (A-E), les barrels sont bien définis chez les souris contrôles mais pas chez les souris CxNR1KO (souris déficientes en sous-unité GluN1 dans les neurones corticaux excitateurs). Wp = babine (*whisker pad*), as= museau antérieur (*anterior snout*), lj= mâchoire inférieure (*lower jaw*), fp= patte avant (*forepaw*). Echelle = 800µm (Iwasato et al., 2000).

2.5.2. La potentialisation à long terme

Comme décrit précédemment (voir la partie « **1.4.2.3. Plasticité synaptique** »), la LTP est un processus important dans la mémoire et l'apprentissage. Le récepteur NMDA est un élément crucial dans la plasticité synaptique, même s'il existe d'autres formes de plasticité indépendantes des récepteurs NMDA (Harris & Cotman, 1986).

En utilisant un antagoniste des récepteurs NMDA (l'AP5), aucun effet n'a été observé sur la réponse synaptique induite par des stimulations à basse fréquence, mais le blocage des récepteurs NMDA empêche l'induction de la LTP dans des tranches d'hippocampe de rats (Collingridge et al., 1983a).

Si le blocage des récepteurs NMDA empêche l'induction de la LTP, nous pouvons supposer que l'activation des récepteurs NMDA serait suffisante pour induire la LTP. Collingridge et collaborateurs se sont focalisés sur l'activation des récepteurs NMDA dendritiques et la LTP n'a pas pu être induite. Mais en prolongeant la durée d'activation, une dépression à long terme a été observée (*Long Term Depression* ; LTD). Donc l'induction d'une LTP nécessite à la fois l'élément déclenchant le potentiel (les récepteurs AMPA) et les récepteurs NMDA (Collingridge, et al., 1983a, 1983b).

2.5.3. La dépression à long terme

Nous avons vu précédemment qu'une activité prolongée des récepteurs NMDA donnait lieu à une LTD lorsque celle-ci est induite par des stimulations à basse fréquence (Dudek & Bear, 1992 ; Nabavi et al., 2013, 2014). Contrairement à une LTP, la LTD ne nécessiterait pas la perméabilité des récepteurs NMDA aux ions calcium, mais impliquerait plutôt une action métabotrope des récepteurs NMDA (Nabavi et al., 2013, 2014). En effet, un antagoniste du site ABD des récepteurs NMDA, le 7-CIKA (*7-chlorokynurenic acid*) bloque l'induction de la LTP mais n'a aucun effet sur l'induction de la LTD (Bashir et al., 1990). Cependant, le 7-CIKA n'étant pas un antagoniste spécifique des sites ABD, l'utilisation d'un antagoniste spécifique des sites ABD des récepteurs NMDA empêche bien l'induction de la LTD (Grimwood et al., 1995). Il a alors été supposé que lors des stimulations à basses fréquences, les co-agonistes libérés prennent le dessus de l'activité de la 7-CIKA, expliquant le maintien de la LTD.

2.5.4. L'excitotoxicité

Comme nous l'avons décrit précédemment (voir la partie « **1.4.2.5. Excitotoxicité »**), l'excitotoxicité correspond à une suractivation des récepteurs du glutamate provoquant une entrée massive de calcium dans le neurone. Cette excitotoxicité conduit à la mort cellulaire prématurée, se caractérisant par un

gonflement de la cellule dû à son milieu hypertonique en calcium, puis à une rupture des membranes nucléaires et cytoplasmiques (Bicknell & Cohen, 1995 ; Dong et al., 1997). Cette entrée de calcium se fait via les récepteurs NMDA (Choi et al., 1988), cela est d'autant plus vrai du fait que les récepteurs NMDA sont les récepteurs ionotropes les plus perméables au calcium (Mayer et al., 1984 ; Tymianski et al., 1993). L'excitotoxicité du glutamate est généralement observée en conditions pathologiques tel que l'ischémie cérébrale. Par ailleurs, des niveaux élevés de glutamate de façon chronique seraient impliqués dans des maladies neurodégénératives comme la maladie d'Alzheimer, de Parkinson ou de Huntington.

2.5.5. L'Apoptose

Comme vu plus haut, l'excitotoxicité induite par le glutamate conduit à une mort cellulaire causée par un important influx de calcium intracellulaire sous-tendu par les récepteurs NMDA. L'activation des récepteurs NMDA extrasynaptiques serait à l'origine d'une mort cellulaire, alors que l'activation des récepteurs NMDA synaptiques favorise la survie neuronale (Hardingham & Bading, 2010). En effet, les récepteurs synaptiques vont moduler l'expression de gènes anti-apoptotiques, contrairement aux récepteurs extrasynaptiques (Hardingham et al., 2002). De plus, ils peuvent moduler l'expression d'une protéine pro-apoptotique, la p53 (Léveillé et al., 2010). Les effets des récepteurs NMDA sur l'apoptose sont surtout marqués lors du développement, moins lors de l'âge adulte (Ikonomidou et al., 1999).

Le récepteur NMDA est un hétérotétramère composé de deux sous-unités GluN1 et d'une association de sous-unités GluN2 et/ou GluN3. Son activation nécessite un agoniste comme le glutamate ou le NMDA, ainsi que d'un co-agoniste, la glycine ou la D-sérine.

Ces sous-unités sont exprimées de manière régulée dans l'espace et dans le temps.

Les récepteurs NMDA sont impliqués dans de nombreuses fonctions physiologiques et pathologiques, telles que la LTP/LTD, la plasticité synaptique, ou bien l'excitotoxicité.

Le tPA peut interagir avec la sous-unité GluN1 des récepteurs NMDA par son domaine kringle 2. Il joue ainsi un rôle de co-agoniste et peut moduler les fonctions du récepteur.

NMDA receptor is a heterotetramer composed of two GluN1 subunits and a combination of GluN2 and/or GluN3 subunits. Its activation requires an agonist such as glutamate or NMDA, as well a co-agonist like glycine or D-serine.

These subunits have a highly regulated expression, in space and time.

NMDA receptors are involved in many physiological and pathological functions, such as LTP/LTD, synaptic plasticity or excitotoxicity.

tPA can interact with GluN1 subunit of NMDA receptors through its kringle 2 domain. It thus plays a role of co-agonist and can modulate the functions of this receptor.

3. Les systèmes kinine-kallicréine et rénine-angiotensine

Le système kinine-kallicréine (SKK) et le système rénine-angiotensine (SRA) jouent de multiples rôles dans des conditions physiologiques comme pathologiques, tels que la régulation de la pression artérielle, la croissance des cellules musculaires lisses et l'inflammation. De plus ces systèmes interagissent entre eux à plusieurs niveaux, par conséquent, des changements d'activité dans un système auront un impact sur l'activité de l'autre.

3.1. Le système kinine-kallicréine

3.1.1. Historique

Le SKK a été découvert en 1909 par l'observation qu'une injection intraveineuse d'urine humaine chez le chien conduisait à une importante chute de la pression artérielle (Abelous & Bardier, 1909). Plus tard, cette substance hypotensive a été isolée à partir d'extraits de pancréas et a été nommé la kallicréine (Kraut et al., 1930). A cette époque, l'hypothèse était que la kallicréine était une hormone synthétisée par le pancréas puis éliminée dans les urines. Cette hypothèse a été abandonnée avec la découverte de la kallicréine plasmatique et tissulaire. En 1949, il a été observé que la mise en contact d'un venin de serpent avec du plasma sanguin induisait une libération d'un peptide hautement hypotenseur, la bradykinine (BK ; Rocha et al., 1949). En 1970, il a été découvert que l'enzyme de conversion de l'angiotensine (*Angiotensin-Converting Enzyme* ; ACE) peut à la fois produire de l'angiotensine II (AngII) vasoconstrictrice et inactiver la BK vasodilatatrice (Yang et al., 1970). Cette découverte a permis d'ouvrir la voie de recherche dans le domaine de l'hypertension avec le développement des inhibiteurs de l'enzyme de conversion (IEC), ainsi le premier inhibiteur compétitif de la BK a pu être synthétisé (Vavrek & Stewart, 1985). En 1980, il a été proposé l'existence de deux types de récepteurs de la BK (Regolit & Barabef, 1980), ces propositions ont été vérifiées lorsque les ADNc de ces deux récepteurs ont pu être clonés (Mceachern et al., 1991 ; Menkes et al., 1994).

3.1.2. Synthèse et dégradation de la bradykinine

La BK est produite grâce à la kallicréine, une sérine protéase dont on peut distinguer deux types : la kallicréine plasmatique faisant 60 kDa, synthétisée par le foie, et la kallicréine tissulaire, protéase de 24-48 kDa synthétisée par de nombreux tissus tels que le pancréas, le rein, l'intestin, le cerveau et les glandes sous-maxillaires et sudoripares. Il existe donc deux grandes voies de synthèses pour produire la BK :

- Synthèse par les **kallicréines tissulaires** : La kallicréine tissulaire est produite de manière intracellulaire à partir de la conversion d'une prokallicréine. La kallicréine tissulaire sécrétée digère le kininogène de bas poids moléculaire (*Low-molecular-weight Kininogen* ; LK) en lys-bradykinine (lys-BK ou kallidine). Des aminopeptidases plasmatiques vont venir cliver la lysine présente en N-terminale de la lys-BK pour donner la BK (Müller-Esterl et al., 1985).

- Synthèse par les **kallicréines plasmatiques** : Le facteur XII de la cascade de coagulation est activé en facteur XIIa. Ce facteur tissulaire peut dégrader deux substrats, la prékallicréine et le facteur XI, qui sont tous les deux complexés avec le kininogène de haut poids moléculaire (*High-molecular-weight Kininogen* ; HK ; Mandle et al., 1976 ; Thompson et al., 1977). Le clivage de ces deux complexes par le facteur XIIa va donner la kallicréine plasmatique et le facteur XIa. La kallicréine plasmatique pourra alors convertir le HK en BK (Kaplan et al., 1998).

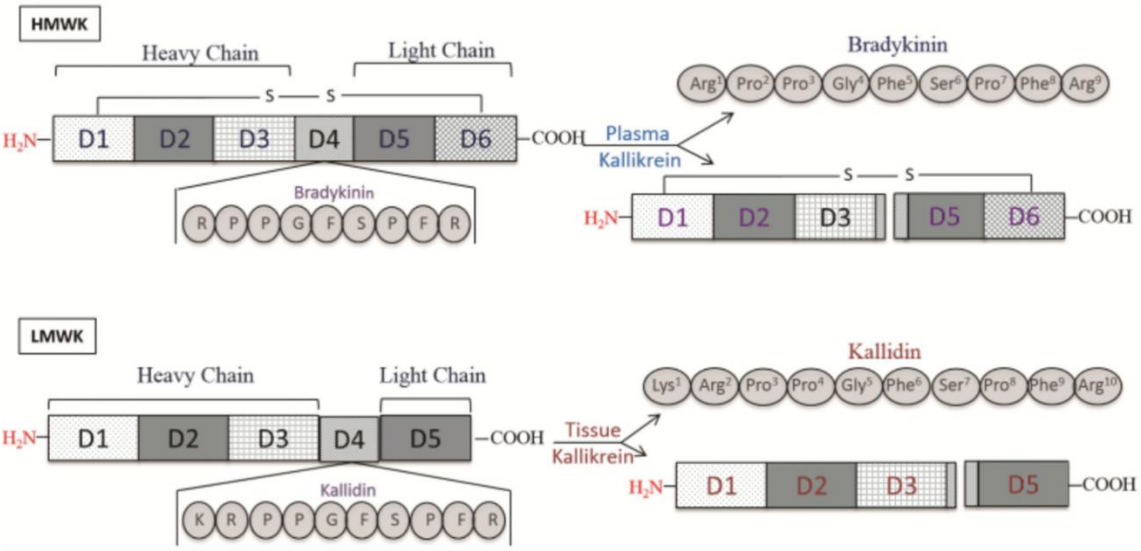

Figure 22 : Représentation schématique des domaines de la LK et HK. Les LK et HK sont identiques au niveau de leur domaine N-terminal, mais diffèrent du côté C-terminal. La HK est une glycoprotéine à simple chaine et est divisée par 6 domaines. Les 3 premiers domaines (D1, D2 et D3) composent la chaine lourde de la HK, les deux derniers domaines (D5 et D6) représentent la chaine légère. La composition de la chaine lourde de la LK est identique à celle de la HK, cependant la chaine légère de la LK ne contient qu'un domaine D5. Lors de la dégradation de la HK par la kallicréine plasmatique, le domaine 4 de la HK va être libéré, ce domaine correspond à la BK. Lors de la dégradation de la LK, c'est la kallidine (KD) qui est libérée (qui était contenu au niveau du domaine 4 de la LK). HMWK, kininogène de haut poids moléculaire, HK ; LMWK, kininogène de bas poids moléculaire, LK (Nokkari et al., 2018).

Il faut noter que les kallicréines tissulaires et plasmatiques clivent le kininogène de façons différentes. En effet, la kallicréine tissulaire a une affinité plus élevée pour cliver le LK mais peut très bien cliver le HK, alors le la kallicréine plasmatique clive exclusivement le HK (Kitamura et al., 1985 ; Müller-Esterl et al., 1985 ; Takagaki et al., 1985).

La demi-vie plasmatique de la BK et de la kallidine (KD) est estimée à environ 30 secondes (Marceau & Regoli, 2004). La dégradation de la BK se fait par l'intermédiaire des kininases. La kininase I va cliver l'arginine se trouvant à l'extrémité C-terminale de la BK ou de la KD pour donner une des-arg^{9}-BK ou une des-arg^{10}-KD (Sheikh & Kaplan, 1986). La kininase II, aussi appelée l'ACE est une dipeptidase qui

va cliver la phénylalanine et l'arginine de l'extrémité C-terminale de la BK pour donner un heptapeptide, qui sera encore clivé par l'ACE pour retirer une sérine et une proline et donner un pentapeptide. Si l'extrémité C-terminale de la BK est d'abord clivée par la kininase I, alors l'ACE va agir comme une tripeptidase et va directement retirer la sérine, proline et la phénylalanine de la des-arg^9-BK pour donner un pentapeptide (Sheikh & Kaplan, 1986, 1989).

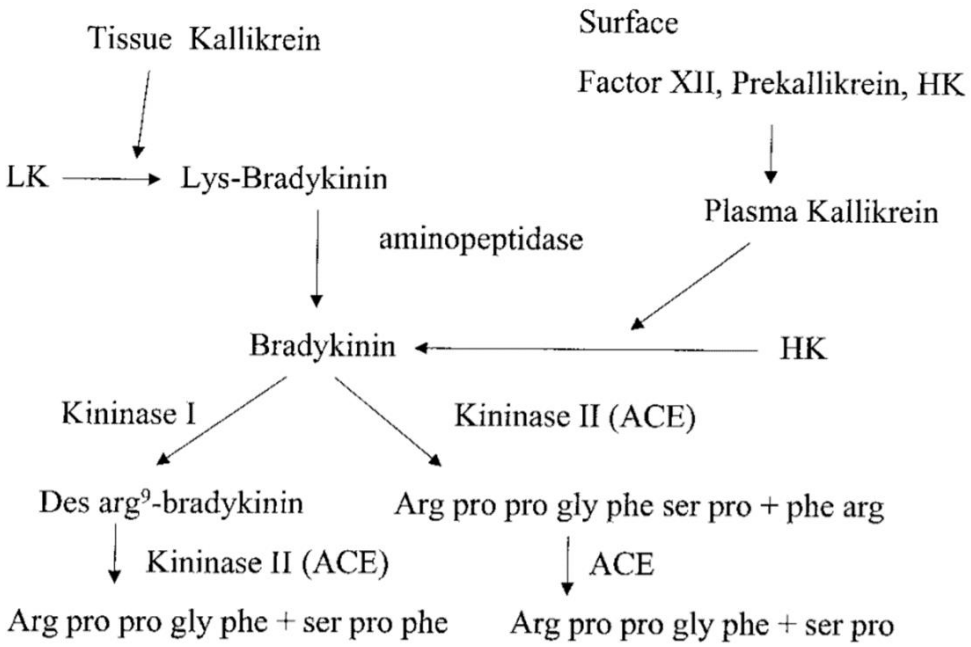

Figure 23 : La voie de synthèse et de dégradation de la bradykinine. Représentation des deux voies de synthèses de la BK par les kallicréines tissulaires et plasmatiques, ainsi que la voie de dégradation médiée par les kininases I et II (Kaplan et al., 2002).

3.1.3. Les récepteurs de la bradykinine

Les kinines (terme qui englobe la BK et la KD) agissent sur deux types de récepteurs, les récepteurs B1 et B2. Faisant partie de la superfamille des récepteurs couplés aux protéines G (Leeb-Lundberg et al., 2005), ces deux récepteurs ont été initialement classés selon leurs propriétés pharmacologiques et en particulier selon leur affinité pour leurs différents ligands (Drouin et al., 1979 ; Regoli et al., 1977, 1978).

Le récepteur B1 est activé par les agonistes des-arg^{9}-BK et des-arg^{10}-KD, les formes résultantes de la dégradation des kinines par la kininase I, il peut être également activé par la BK avec une moindre efficacité. Alors que le récepteur B2 est plutôt activé par les kinines (Leeb-Lundberg et al., 2005).

Le récepteur B2 est exprimé de manière constitutive à la surface de nombreux types cellulaires tels que les cellules endothéliales et musculaires lisses (Raidoo et al., 1997), les fibroblastes, les cellules mésangiales et épithéliales (Bascands et al., 1991 ; Sabatini et al., 2013). Contrairement au récepteur B2, le récepteur B1 est essentiellement inductible et donc généralement impliqué dans les processus inflammatoires (Marceau et al., 1998). En effet, le récepteur B1 est exprimé en cas de lésions tissulaires, d'inflammation et au cours de certaines pathologies comme le diabète (Bozó et al., 2012 ; da Costa et al., 2014 ; Pruneau et al., 2010). L'induction de l'expression des récepteurs B1 implique des cytokines inflammatoires ou des MAP kinases comme la p38 (Ganju et al., 2001 ; Haddad et al., 2000).

La liaison du ligand sur les récepteurs B1 et B2 permet l'activation des voies de signalisation des protéines G, qui induisent l'activation des molécules de signalisation comme la protéine kinase C (PKC) ou les phospholipases ; les cascades de signalisations vont différer selon le type cellulaire. La formation de seconds messagers tels que l'inositol-1,4,5-triphosphate (IP_3) va provoquer une augmentation du calcium intracellulaire qui activera la NO-synthase endothéliale (*endothelial Nitric Oxyde Synthase* ; eNOS). L'activation de phospholipases va également permettre la synthèse de prostaglandines à partir de l'acide arachidonique ainsi recruté. Le monoxyde d'azote (NO) produit par la eNOS et les prostaglandines vont alors diffuser vers les cellules musculaires lisses afin d'induire une vasodilatation (Mathis et al., 1996).

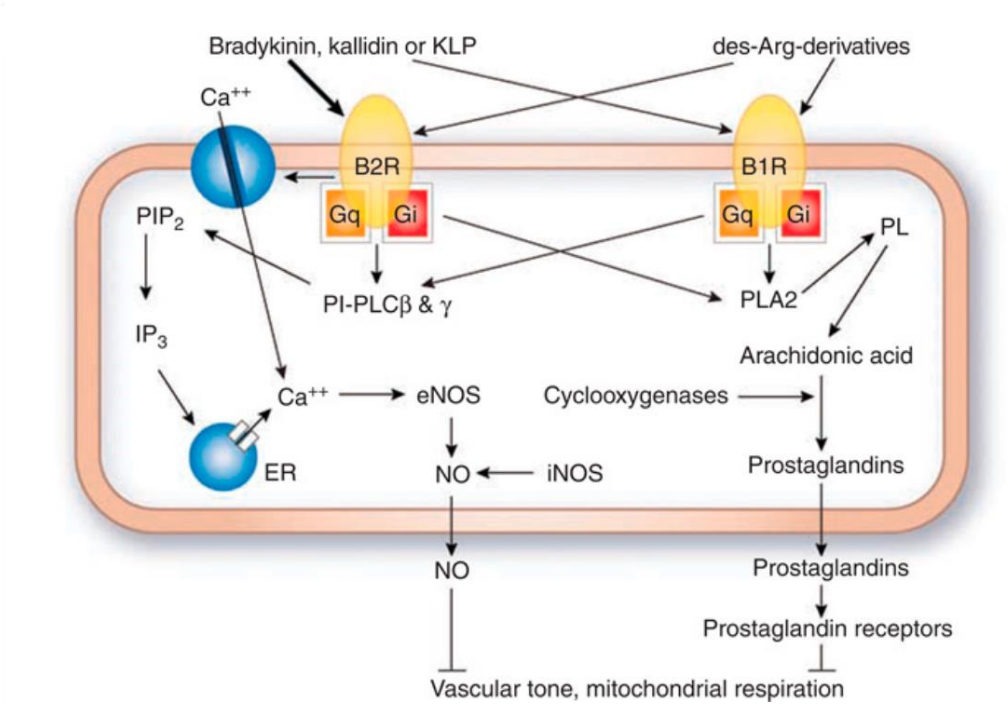

Figure 24 : Les voies de signalisation de la BK à travers les récepteurs B1 et B2. Représentation schématique des voies de signalisation intracellulaire des récepteurs des kinines. PIPL2, phosphatidylinositol-4,5-biphosphate ; PI-PLC, phosphatidylinositol-spécifique phospholipase ; ER, réticulum endoplasmique ; PL, phospholipides ; PLA2, phospholipase A2 ; NO, monoxyde d'azote ; eNOS, NO synthase endothéliale ; iNOS, NO synthase inductible (Lau et al., 2020).

3.1.4. Implications de la bradykinine

3.1.4.1. Implications physiologiques

Les rôles physiologiques des kinines sont nombreux, elles peuvent être impliquées dans la régulation du tonus vasculaire et du flux sanguin local, la coagulation, la fibrinolyse et la balance des électrolytes. Dans le plasma, les quantités de kinines sont très faibles (<50 pg/ml) et ne sont pas suffisantes pour participer à la régulation de la pression artérielle (Mombouli & Vanhoutte, 1995). Cela pourrait s'expliquer par sa courte demi-vie qui n'excède pas les 30 secondes. De plus, la pression artérielle des rats déficients en kininogène reste similaire à ceux des animaux contrôles. Le blocage des récepteurs B2 avec l'antagoniste HOE 140 n'induit pas d'augmentation de la pression artérielle de ces animaux (Rhaleb et al., 2001). Cependant, dans certaines circonstances, un défaut dans le SKK peut contribuer au

développement de l'hypertension. En effet, il a été observé que certains des patients atteints d'hypertension artérielle avaient une faible quantité de kallicréines dans les urines (Elliot et al., 1934 ; Nakahashi et al., 1986). Également, des souris déficientes en récepteur B2 présentent une hypertension vasculaire lorsque celles-ci sont exposées à un régime riche en sodium ou lors du vieillissement (Alfie et al., 1996 ; Emanueli et al., 1999). L'expression des récepteurs B1 semble augmenter chez les souris déficientes en récepteur B2 et l'utilisation d'un antagoniste des récepteurs B1 induit une hypertension, donc le récepteur B1 peut compenser les effets des récepteurs B2 sur la pression artérielle (Duka et al., 2001).

La BK est également présente au sein des terminaisons nerveuses des neurones sensitifs et de petites cellules dans le ganglion spinal dorsal (Steranka et al., 1988). Les récepteurs qui semblent être impliqués dans ce processus sont les récepteurs B2, l'inhibition de ces récepteurs conduit à un blocage de l'activation aigüe des neurones sensitifs (Dray et al., 1992 ; Haley et al., 1989). En effet, la BK induit une dépolarisation immédiate des neurones sensitifs et des fibres nociceptives, via une augmentation de la perméabilité membranaire au sodium (Burgess et al., 1989).

Outre ces rôles, la BK peut être impliquée dans l'unité neurovasculaire comme l'augmentation de la perméabilité de la BHE, la surexpression de cytokines pro-inflammatoires, la libération de glutamate par les astrocytes et l'activation de la microglie (Nokkari et al., 2018).

3.1.4.2. Implications pathologiques

Le dysfonctionnement des cellules endothéliales vasculaires induit l'artériosclérose et d'autres pathologies cardiovasculaires. L'hypercholestérolémie, l'hypertension, le diabète et le vieillissement peuvent être à l'origine de ce dysfonctionnement. Ils induisent progressivement des altérations de la libération de médiateurs vasodilatateurs par les cellules endothéliales, et promeuvent l'accumulation d'agents vasoconstricteurs (Mombouli et al., 1992). En présence de ces

facteurs de risque, la production d'ions superoxides et d'espèces réactives de l'oxygène accélèrent l'oxydation des lipoprotéines à basse densité (*Low Density Lipoprotein* ; LDL), ce qui tend à altérer les vasodilatations induites par les cellules endothéliales et favorise la production plaquettaire et de thrombine (Darley-Usmar et al., 1995 ; Tanner et al., 1991). La reperfusion post-ischémique cause un stress cellulaire et entraine des altérations sur la vasodilatation induite par les cellules endothéliales. L'inhibition des ACE permet de prévenir ces altérations pendant une ischémie, en inhibant l'influence vasoconstrictrice de l'angiotensine II et accroitre l'activité vasodilatatrice des kinines (Piana et al., 1996).

La BK est également impliquée dans des processus inflammatoires et de douleur lorsqu'une surproduction de BK est observée. Le blocage des récepteurs permettrait de réduire l'intensité de la réaction inflammatoire et de la douleur (Boyce et al., 1996 ; Perkins et al., 1993 ; Pesquero et al., 2000). En effet, l'utilisation d'antagonistes pour les récepteurs B1 et B2 réduit les réponses inflammatoires systémiques et aigües induites par les kinines dans un modèle d'arthrite chez le rat (Blais et al., 1997). Les récepteurs B2 sont impliqués dans les phases aigües de l'inflammation, alors que les récepteurs B1 interviennent plutôt dans sa phase chronique (Dray & Perkins, 1993).

3.1.5. tPA et bradykinine

Le mécanisme par lequel la BK est synthétisée par la plasmine est encore discuté. Il a été démontré par électrophorèse que le clivage de la HK varie selon qu'elle soit incubée avec du tPA, du plasminogène, de la plasmine ou une combinaison de tPA et de plasminogène. En effet, la HK reste intacte en présence de tPA ou de plasminogène, alors qu'elle est dégradée de manière importante en présence de plasmine ou de la combinaison tPA et plasminogène, ce qui permet la libération de BK (Marcos-Contreras et al., 2016 ; Molinaro et al., 2002). Bien que la formation de BK à partir de tPA fonctionne *in vitro*, ce mécanisme via l'injection intraveineuse de tPA *in vivo* reste obscur.

Inversement, il a été montré que la BK pouvait libérer du tPA dans la circulation. En effet, l'injection intraveineuse de BK chez des personnes saines induit une augmentation de la concentration de tPA plasmatique (Brown et al., 1999 ; Rahman et al., 2014).

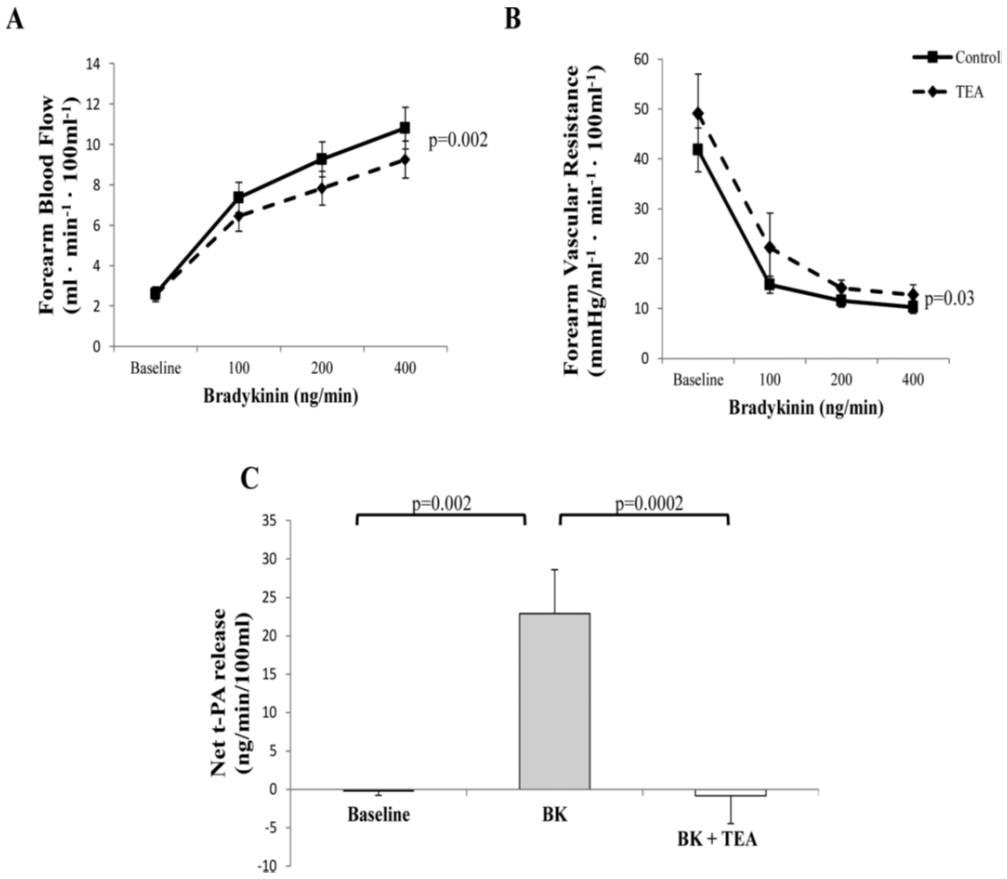

Figure 25 : La BK induit une vasodilatation et une libération de tPA plasmatique. A-B : Mesure du débit sanguin (**A**) et de la résistance vasculaire (**B**) de l'avant-bras en réponse à différentes doses de BK et de TEA (un antagoniste des canaux potassiques calcium dépendant). **C** : Mesure de la concentration de tPA plasmatique en basal, en réponse à une infusion de BK (400 ng/min) ou après injection de TEA puis d'une infusion de BK (400 ng/min ; (Rahman et al., 2014)).

3.2. Le système rénine-angiotensine

3.2.1. Historique

La découverte du SRA remonte à 1898 avec les études de Tigerstedt et Bergman qui ont rapporté l'effet vasopresseur de la rénine obtenu à partir d'extraits rénaux (Robert Tigerstedt & Bergman, 1898). En 1934, Harry Goldblatt a réussi à induire une hypertension persistante chez le chien en clampant une artère rénale (Goldblatt et al., 1934). Quelques années plus tard, un groupe de chercheurs a repris le modèle de Goldblatt et a observé une sécrétion rénale d'un agent vasopresseur similaire à la rénine (Houssay & Fasciolo, 1937). Par la suite, cette substance a été isolée du sang, elle induisait une vasoconstriction très rapide de courte durée, ils ont conclu que la rénine pouvait agir par une voie enzymatique sur une protéine plasmatique pour produire cette nouvelle substance, qu'ils ont nommé l'hypertensine (Braun-Menendez et al., 1940). Plus tard, il a été convenu de renommer l'hypertensine par l'angiotensine, le substrat de la rénine. L'angiotensinogène et les enzymes permettant de métaboliser le peptide ont été renommées les angiotensinases (Braun-Menendez & Page, 1958).

3.2.2. Synthèse et dégradation de l'angiotensine

L'angiotensinogène (AGT) est le seul précurseur de tous les peptides d'angiotensine et est composé de 485 acides aminés. L'AGT est synthétisé et sécrété par le foie et appartient à la superfamille des inhibiteurs des sérines protéases (serpines). Sécrétée par les reins, la rénine clive les 10 acides aminés se trouvant à l'extrémité N-terminale de l'AGT pour donner l'angiotensine I (AngI). L'AngI va alors être la source de toute une cascade de formation de peptides d'angiotensines. Le clivage de l'AGT va laisser un résidu en plus de l'AngI, la des(AngI)AGT dont le devenir et les propriétés de cette protéine ne sont pas encore déterminés (Lu et al., 2016). L'AngI va être par la suite rapidement convertie en AngII par l'ACE, présente en grande quantité à la surface des cellules endothéliales vasculaire et pulmonaire (Coulet et al., 2001).

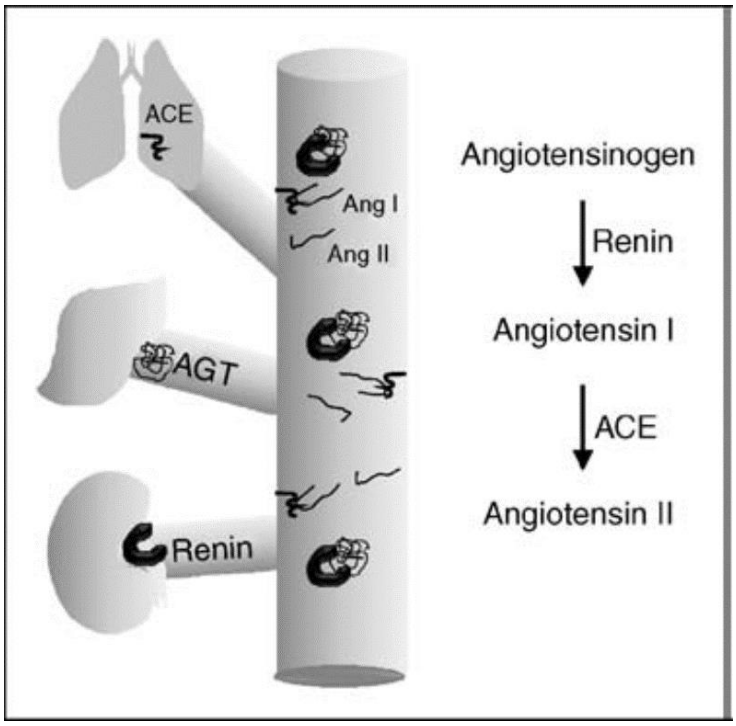

Figure 26 : La voie de synthèse de l'AngII dans la circulation. Dans le SRA, l'angiotensinogène (AGT) libéré par le foie dans la circulation va se faire cliver par la rénine, sécrétée par les reins pour former l'AngI. L'ACE, présente au niveau des cellules endothéliales vasculaire et pulmonaire, convertit l'AngI en AngII (Kumar & Boim, 2009).

La régulation de l'AngII peut se faire à travers plusieurs voies de dégradation :

- Hydrolyse par l'extrémité N-terminale : les enzymes principales dégradant l'AngII par le coté N-terminale sont les aminopeptidases (ou angiotensinases) A et N (APA et APN). L'APA agit sur des peptides ayant un acide aminé acide en N-terminal comme l'AngI ou l'AngII (Wu et al., 1991). Elle convertie l'AngII en des-Asp-AngII, plus connu sous le nom d'angiotensine III (AngIII). Les APA sont exprimées surtout au niveau des glomérules, plus précisément dans les podocytes, mais également dans les cellules mésangiales (Kugler, 1982 ; Troyanovskaya et al., 1996). Les APN agissent sur les peptides ayant un acide aminé neutre en N-terminal. Elles convertissent l'AngIII en un hexapeptide, l'angiotensine IV (AngIV). Les APN se trouvent en grande quantité dans

les tubules proximales du cortex rénal (Kenny & Maroux, 1982 ; Look et al., 1989).

- Hydrolyse par l'extrémité C-terminale : l'enzyme principale dégradant les peptides par l'extrémité C-terminale est l'ACE. Elle peut, comme discuté plus haut, convertir l'AngI en AngII, mais également dégrader la des-Asp-AngI en AngIII. Il existe deux isoformes de l'ACE, une somatique et l'autre germinale (Soubrier et al., 1988). Les ACE somatiques sont localisées dans les cellules endothéliales glomérulaires et à l'extrémité des tubules proximaux, tandis que les ACE germinales sont exprimées dans les cellules germinales (Sibony et al., 1993). Au-delà de sa capacité à convertir l'AngI en AngII, l'ACE peut également cliver la BK. Les chymases appartiennent à la famille des protéases à sérine et existe sous deux isoformes : α que l'on retrouve chez le primate, et β que l'on retrouve chez le rongeur (Caughey et al., 2000). La forme α produit de l'AngII indépendamment de la voie des ACE, contrairement à la forme β qui dégrade l'AngII. La majorité des chymases sont sécrétées au niveau de la matrice extracellulaire dans le cœur. Les prolylendopeptidases de la famille des sérines protéases, clivent à la fois l'AngI et l'AngII pour former une AngII (1-7 ; Odya et al., 1987). Les endopeptidases neutres peuvent dégrader des peptides natriurétiques et des kinines, elles peuvent également hydrolyser l'AngII pour former de l'AngII (1-4 ; Gafford et al., 1983). Elles sont sécrétées par les cellules tubulaires proximales, les podocytes glomérulaires et par les vaisseaux corticaux rénaux. Les carboxypeptidases A sont massivement présentes dans les mastocytes du cœur et peuvent former de l'AngI (1-9 ; Urata et al., 1990).

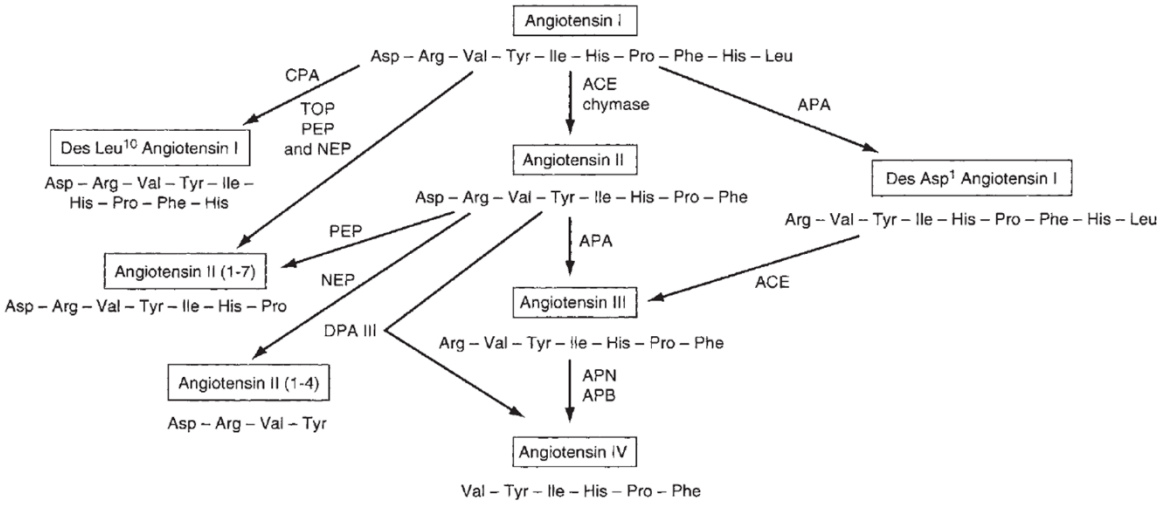

Figure 27 : Les différentes voies enzymatiques de dégradation de l'angiotensine I et II. ACE, enzyme de conversion de l'angiotensine ; APA, aminopeptidase A ; APN, aminopeptidase N ; APB, aminopeptidase B ; PEP, prolylendopeptidase ; NEP, endopeptidase neutre ; DPA III, dipeptidylaminopeptidase III ; TOP, thimet oligopeptidase ; CPA, carboxypeptidase A (Ardaillou & Chansel, 1997).

3.2.3. Les récepteurs de l'angiotensine II

Il existe différents types de récepteurs avec lesquels l'angiotensine peut se lier pour induire ses différents effets.

Les récepteurs à l'angiotensine de type 1 (*type 1 angiotensin receptor*, AT1) sont exprimés dans les vaisseaux sanguins, le cortex surrénal, le foie, le rein, et le SNC. Le récepteur AT1 a une forte affinité pour l'AngII et est un récepteur couplé aux protéines G. Il active une phospholipase C pour produire deux seconds messagers : le diacylglycérol qui active les protéines kinases C, et l'inositol-triphosphate qui libère les stocks de calcium intracellulaire (Hunyady & Catt, 2006). La fonction principale des récepteurs AT1 est de réguler la pression sanguine et l'homéostasie hydrosodée (Audoly et al., 2000).

Les récepteurs à l'angiotensine de type 2 (*type 2 angiotensin receptor*, AT2) sont localisés dans le mésenchyme, les glandes surrénales, l'utérus et les follicules ovariens. Ses fonctions physiologiques et sa signalisation restent incertaines (Porrello et al., 2009). Des premières études ont rapporté que les récepteurs AT2 auraient des effets vasodilatateurs, natriurétiques, antiprolifératifs et pro-apoptotiques (Unger et al., 2000).

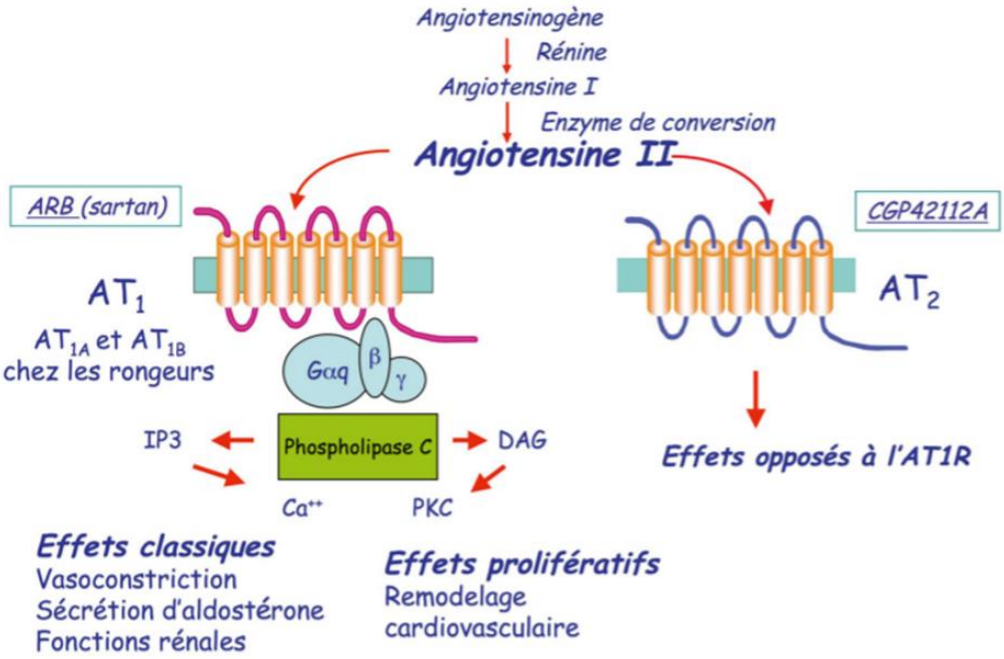

Figure 28 : Structure, pharmacologie, signalisation et fonctions physiologiques des récepteurs AT1 et AT2 de l'AngII. Représentation des récepteurs AT1 et AT2 ayant une forte affinité pour l'AngII ainsi que les effets induits par ces récepteurs et leurs antagonistes : le bloqueur des récepteurs AT1 (*AT1 Receptor Blocker*, ARB) et le CGP42112A (Auzan & Clauser, 2010).

Il a été rapporté l'existence d'un récepteur à l'angiotensine de type 3 (*type 3 angiotensin receptor*, AT3) présentant une pharmacologie unique, cependant aucune confirmation concernant l'existence d'un gène pour ce récepteur chez l'Homme n'a pu être mis en évidence à ce jour (Chaki & Inagami, 1992 ; Inagami et al., 1993).

Les récepteurs à l'angiotensine de type 4 (*type 4 angiotensin receptor*, AT4) sont exprimés principalement dans le SNC, mais également dans le cœur, les reins, les glandes surrénales et les vaisseaux sanguins. Ce type de récepteur a une forte affinité pour l'AngIV et est insensible aux analogues de l'AngII ainsi qu'aux antagonistes des récepteurs AT1 et AT2 (Harding et al., 1992). Ces récepteurs peuvent être exprimés à la surface des cellules via la phosphorylation par des PKC par l'insuline (Albiston et al., 2001).

3.2.4. Implications de l'angiotensine II

3.2.4.1. Implications physiologiques

L'AngII est un élément important dans le système cardiovasculaire, en effet il peut modifier le rythme et la contractilité cardiaques ainsi que la croissance cellulaire. Il a été relevé que l'AngII stimule la contraction de cardiomyocytes ventriculaires isolés de rat (Neyses & Vetter, 1989). De plus, l'AngII peut exercer deux actions opposées sur la fréquence cardiaque : une bradycardie, dû à son action hypertensive et à la stimulation des barorécepteurs (Lumbers et al., 1979), et une tachycardie via divers mécanismes du système sympathoadrénal (Feldberg & Lewis, 1964 ; Knape & van Zwieten, 1988 ; Peach, 1977). Plusieurs études ont rapporté l'implication de l'AngII dans l'hypertrophie cardiaque associée à l'hypertension. En effet, l'administration d'un inhibiteur des ACE permet de réduire l'hypertrophie ventriculaire chez des rats spontanément hypertendus ; au contraire, des agents sympatholytiques ou vasodilatateurs induisent l'effet inverse (Pfeffer et al., 1982 ; Sen et al., 1974).

Une des fonctions principales de l'AngII est de réguler l'homéostasie hydrosodée, c'est-à-dire l'équilibre entre les ions sodium et l'eau, en particulier dans des circonstances de déshydratation et de déplétion volémique (Sparks et al., 2014). L'AngII est capable de stimuler la réabsorption du sel et de l'eau dans le néphron. De plus, l'AngII stimule la sécrétion d'aldostérone afin d'augmenter la rétention d'eau et de sel dans le néphron (Mennuni et al., 2014). L'AngII via les cellules musculaires lisses vasculaires rénales, induit une vasoconstriction, réduisant ainsi le débit sanguin, ce qui favoriserait l'absorption du sodium. En effet, des souris dépourvues de

récepteurs AT1 vasculaires présentent une hypertension dépendante de l'AngII moins importante. Il en résulte par une quantité de sodium plus importante dans les urines (Sparks et al., 2015). De plus, le stress oxydant serait impliqué dans la contraction vasculaire rénale via des espèces réactives de l'oxygène (*Reactive Oxygen Species*, ROS) induites par l'AngII (Lai et al., 2012).

Le SNC possède également des récepteurs AT1 et AT2, et est donc sujet aux effets de l'AngII. Le SRA joue un rôle dans la régulation de la pression artérielle via son interaction avec le système nerveux sympathique. En effet, la délétion des récepteurs AT1 dans les cellules catécholaminergiques supprime les effets hypertenseurs de l'AngII sans altérer la pression artérielle basale et inhibe la stimulation du système nerveux sympathique (Allen et al., 2013). L'organe subfornical est une région produisant de l'AngII et est connue pour induire une polydipsie, une absorption de sodium et de l'hypertension. La surexpression d'AngII dans cette région peut causer une augmentation de la soif chez les souris (Sakai et al., 2007). La présence des récepteurs AT1 dans cette même région permet une élévation de la pression artérielle lors de la survenue d'une hypoxie intermittente, un modèle d'apnée du sommeil (Saxena et al., 2015). Ils sont également impliqués dans la régulation du métabolisme systémique, en effet, la suppression des récepteurs AT1 dans l'organe subfornical diminue la perte de poids induite par la leptine en altérant la thermogenèse des tissus adipeux bruns (Young et al., 2015).

3.2.4.2. Implications pathologiques

L'AngII est un facteur important impliqué dans la croissance et la prolifération cellulaire, entrainant l'hypertrophie des cellules musculaires lisses vasculaires, leur différenciation et l'apoptose (Dzau, 2001). En effet, les cellules musculaires lisses traitées avec de l'AngII voient l'activité de la kinase 2 dépendante des cyclines (*Cyclin-Dependant Kinase 2*, CDK2) supprimée, cette dernière étant une protéine nécessaire dans le cycle cellulaire. L'arrêt dans la phase G1 du cycle cellulaire des cellules musculaires lisses vasculaire, mène à leur hypertrophie (Braun-Dullaeus et al., 1999). La rigidité artérielle conduit au développement de l'hypertension et est associée au

vieillissement. Elle est causée par une fibrose excessive et une élasticité réduite qui sont associées à un dépôt accru de collagène, une dégénérescence des fibres d'élastine ou à une calcification. L'AngII semble être au centre de ces facteurs et est capable d'induire des réponses vasculaires pro-fibrotiques (Harvey et al., 2016). De plus, l'AngII contribue au dysfonctionnement endothélial, au stress oxydant, à l'inflammation ainsi qu'à la thrombose, des phénomènes permettant l'initiation et la progression de l'artériosclérose (Vaccari et al., 2008). Également, l'AngII peut solliciter le recrutement des interleukines et des molécules d'adhésions pour induire une réponse inflammatoire (Ruiz-Ortega et al., 2001 ; Schieffer et al., 2000).

L'hypertension étant l'un des facteurs de risque dans le développement de dysfonctionnement cognitifs, des démences, de la maladie d'Alzheimer et de l'AVC ischémique, l'AngII joue donc un rôle dans le développement de ces maladies. En effet, l'activation continue du SRA sur des souris transgéniques induit l'apparition de troubles cognitifs, et altère la plasticité synaptique (Dai et al., 2016 ; Inaba et al., 2009a). Par ailleurs, l'AngII favorise la production des peptides β-amyloïdes et la délétion des récepteurs AT1, qui inhibent leur formation, ce qui conduit à la formation des plaques amyloïdes (Liu et al., 1997). L'AngII aurait également un rôle dans l'exacerbation du volume de lésion ischémique, en effet, à la suite de l'occlusion de l'artère cérébrale moyenne (ACM), le volume de lésion est plus important chez des souris exprimant les gènes humains de l'angiotensinogène et de la rénine (Inaba et al., 2009b).

3.2.5. PAI-1 et angiotensine II

Comme vu précédemment (voir la partie « **1.5.1.1. Le PAI-1** »), le PAI-1 fait partie de la famille des inhibiteurs des sérines protéases et est l'inhibiteur principal du tPA. Des études suggèrent que l'AngII joue un rôle dans la régulation de l'expression des inhibiteurs de protéases comme le PAI-1, réduisant ainsi l'activité protéolytique du tPA (van Leeuwen et al., 1994 ; Vaughan et al., 1995a). L'inhibiteur de l'ACE et un antagoniste des récepteurs AT1 induisent une diminution de l'expression de PAI-1 dans un modèle de sclérose rénale (Oikawa et al., 1997). De plus, il a été observé

qu'une infusion longue d'AngII par voie intraveineuse chez le rat induit une augmentation de l'expression de PAI-1 dans différents tissus via son interaction avec les récepteurs AT1, et ce, indépendamment de son effet hypertenseur (Nakamura et al., 2000).

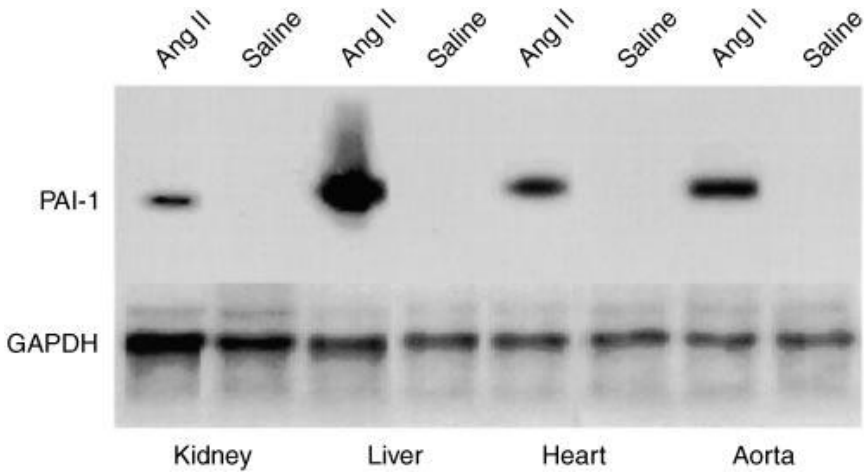

Figure 29 : L'expression des ARNm de PAI-1 augmente après infusion d'AngII dans les tissus. Northern Blot représentant le taux d'ARNm exprimé dans chaque tissu issu de rat (rein, foie, cœur et aorte). En présence d'AngII, le niveau d'expression d'ARNm de PAI-1 augmente par rapport aux conditions salines dans les quatre tissus. (Nakamura et al., 2000).

3.3. Les interactions entre les systèmes kinine-kallicréine et rénine-angiotensine

Le SKK et le SRA peuvent interagir entre eux à différents niveaux. Dans le plasma, la kallicréine est impliquée dans l'activation de la prorénine (Schalekamp & Derkx, 1981). De plus, la kallicréine peut cliver l'angiotensinogène pour générer de l'AngII. Les ACE, en plus de pouvoir convertir l'AngI en AngII, participent également au métabolisme des kinines (Augusto Souza dos Santos et al., 2001). Les inhibiteurs de l'ACE peuvent inhiber le métabolisme de la BK, potentialisant ainsi l'activité de la BK sur ses récepteurs B2 sans altérer le fonctionnement de la BK (Marcic et al., 1992). L'antagoniste des récepteurs B2, le HOE 140 peut prévenir certaines conséquences de l'inhibition des récepteurs AT1, suggérant que la BK peut inhiber certains effets des

récepteurs AT1. En effet, l'activation des récepteurs AT2 pourrait provoquer la formation de la BK, contrebalançant ainsi l'effet vasoconstricteur des récepteurs AT1 (Katada & Majima, 2002 ; Liu et al., 1997).

Le système kinine-kallicréine joue un rôle important dans la pression artérielle, l'inflammation ou la coagulation. Il implique des médiateurs comme la bradykinine, un agent vasodilatateur qui agit sur les récepteurs B2 présents sur de nombreux types cellulaires.

La bradykinine peut également induire une libération de tPA dans la circulation sanguine en sollicitant les cellules endothéliales.

Le système rénine-angiotensine est impliqué dans l'homéostasie hydrosodée, l'hypertension, ainsi que dans de nombreuses pathologies cardiovasculaires. L'angiotensine II est le principal médiateur de ces effets via son interaction avec les récepteurs AT1.

L'angiotensine II peut provoquer la sécrétion de PAI-1 dans la circulation sanguine par les cellules endothéliales.

Kinin-kallikrein system plays an important role in blood pressure regulation, inflammation, or coagulation. It involves mediators like bradykinin, a vasodilator agent that acts on B2 receptors, found on many cell types.

Bradykinin can also induce release of tPA into the bloodstream by stimulating endothelial cells.

Renin-angiotensin system is involved in water and sodium homeostasis, hypertension, or in many cardiovascular pathologies. Angiotensin II is the main mediator of these effects through its interaction with AT1 receptors.

Angiotensin II can secrete PAI-1 into the bloodstream by endothelial cells.

4. Le couplage neurovasculaire

Le cerveau est l'un des organes les plus énergivore du corps humain, consommant 20% de l'énergie produite par l'organisme, même s'il ne représente que 2% de la masse corporelle totale (Raichle & Gusnard, 2002 ; Sokoloff et al., 1955). Le fait que cet organe ait des besoins énergétiques aussi élevés tout en possédant des réserves énergétiques limitées, rend le cerveau fortement dépendant d'un approvisionnement continu et régulé en sang. Un défaut de perfusion cérébrale peut entrainer un défaut de synthèse de protéines cérébrales ou de signalisation pouvant aller jusqu'à l'arrêt de fonctionnement d'une zone du cerveau, et cela pouvant entrainer des dommages irréversibles au SNC (Leker & Shohami, 2002). Pour éviter cela, le cerveau peut mettre en jeu plusieurs mécanismes afin d'optimiser un apport sanguin correct et continu. Le premier mécanisme est la capacité d'arrêter la circulation systémique et de pouvoir réacheminer le sang vers le cerveau en cas de besoin. Le deuxième est l'autorégulation, qui consiste au maintien du débit sanguin cérébral (DSC) à un niveau adéquat lors d'un changement de la pression artérielle sanguine (Lassen, 1959). Le dernier mécanisme correspond à la mise en place d'une cascade de signalisation à la suite à d'une activité neuronale qui permet de garantir un apport d'énergie via l'augmentation du DSC local. Ce phénomène est appelé le couplage neurovasculaire (CNV) ou hyperémie fonctionnelle.

4.1. Historique

Au cours du 18^{e} et 19^{e} siècle, les scientifiques pensaient que le cerveau n'était pas impliqué dans sa propre régulation sanguine, et serait contrôlé exclusivement par la circulation systémique (Friedland & Iadecola, 1991). Ce n'est qu'à la fin du 19^{e} siècle que les premières observations sur les changements de DSC en réponse à une activité cérébrale furent effectuées. En effet, les travaux de Mosso en 1880 sur les malformations crâniennes chez l'Homme, ont permis de découvrir que les stimuli somatiques, mentaux ou émotionnels provoquaient des changements de volume sanguin cérébral (**Figure 30** ; Mosso, 1880).

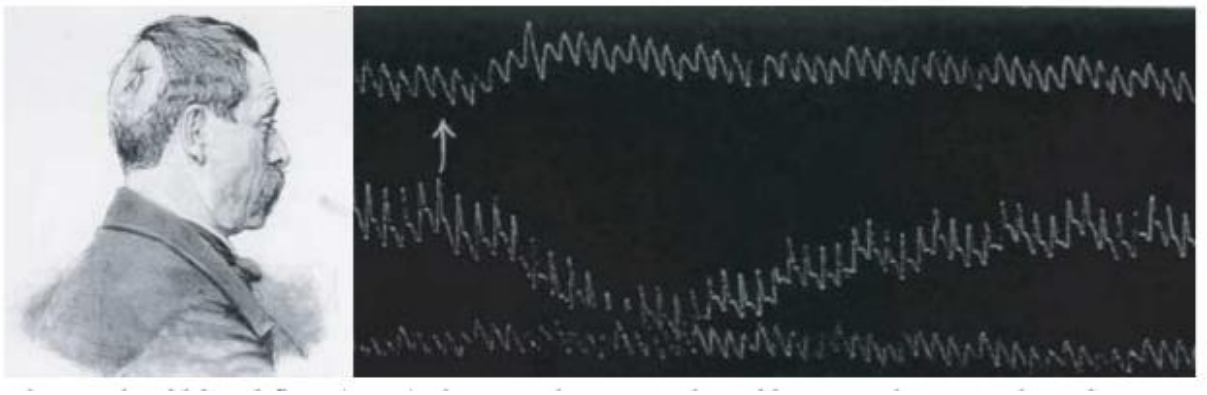

Figure 30 : La variation de volume sanguin cérébral et périphérique à la suite d'un stimulus émotionnel. La mesure du volume sanguin cérébral (tracé du haut) et au niveau d'un pied (tracé du bas) chez un patient ayant une malformation crânienne (photo de L. Cane) est effectuée à la suite d'un stimulus émotionnel (flèche). Mosso raconta que « M. Cane se tenait tranquillement, jusqu'au moment où je lui ai exprimé l'impression que sa femme m'avait faite lorsque je l'ai vue pour la première fois. Cane ne pouvait pas parler, le sang au cerveau a immédiatement augmenté et le volume sanguin des pieds a nettement diminué ». Ces résultats reflètent la capacité vasodilatatrice du cerveau et vasoconstrictrice périphérique causée par une forte émotion (Iadecola, 2004).

Par la suite, Roy et Sherington en 1890 ont suggéré que les métabolites produits par l'activité neuronale pouvaient diffuser dans la circulation sanguine locale pour induire une hausse du DSC dans la région activée (Roy & Sherrington, 1890). Schmidt et Hendrix ont pu démontrer également que l'illumination de l'œil d'un chat provoquait une augmentation de température au niveau du cortex visuel reflétant la perfusion cérébrale lié à l'augmentation du métabolisme (Schmidt & Hendrix, 1938).

La première méthode de mesure quantitative du DSC a été introduite en 1948 via l'utilisation de N_2O comme traceur. En effet, cette méthode a permis de constater que l'hyperactivité cérébrale globale (comme dans le cas de l'anxiété ou l'hyperthyroïdie) pouvait provoquer une augmentation du DSC, et que celui-ci était réduit lors d'une inactivité cérébrale (lors d'un coma par exemple ; Kety, 1950). Cependant, cette méthode permettait de mesurer le DSC pour l'ensemble du cerveau et ne permettait pas d'évaluer les changements de perfusion cérébraux régionaux

induits par une activité neuronale locale. Le développement d'une mesure de DSC régional chez l'Homme via l'injection intracarotidienne d'un traceur radioactif et la détection de celui-ci par une γ-caméra a révolutionné l'imagerie fonctionnelle et a permis par la suite la mise en place de la tomographie par émission de positrons (TEP), toujours utilisée de nos jours (**Figure 31** ; Lassen et al., 1978).

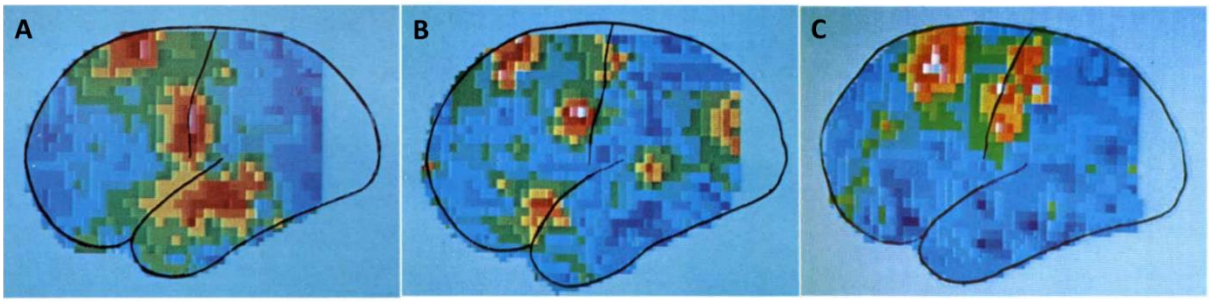

Figure 31 : La mesure des variations locales de DSC au cours de différentes tâches reflète l'activité cérébrale. Représentation de différentes cartes d'activation cérébrale révélées à l'aide d'un isotope radioactif chez l'Homme lors de la prise de parole (**A**), d'une lecture silencieuse (**B**) ou d'un mouvement volontaire (**C**). Les zones présentant une forte augmentation du DSC sont représentées par des couleurs chaudes (Lassen et al., 1978)

La découverte des variations locales de l'oxygénation du sang (appelé également effet BOLD pour *Blood Oxygen Level Dependent*), reflétant la consommation d'oxygène et le DSC à la suite d'une activité cérébrale a permis de développer une technique d'imagerie non invasive via l'imagerie par résonance magnétique (IRM). En effet, la désoxyhémoglobine étant paramagnétique, elle peut être détectée par IRM. Les variations d'oxygénation dans le cerveau au cours d'une activité cérébrale sont ainsi observées en imagerie BOLD (Ogawa et al., 1990). Ainsi, l'IRM basée sur l'effet BOLD est l'une des méthodes les plus puissantes pour la compréhension du fonctionnement du cerveau chez l'Homme.

4.2. L'unité neurovasculaire

L'assemblage de l'unité neurovasculaire varie à travers le réseau cérébrovasculaire. A la base du cerveau, le polygone de Willis va étendre son système vasculaire en différentes branches. Les vaisseaux de la surface cérébrale, au niveau de l'espace sous arachnoïdien, forment des artères pimériennes, un réseau hautement collatéralisé (Blinder et al., 2013). Les artères pimériennes sont formées de plusieurs couches de cellules musculaires lisses, séparées de l'endothélium par une limitante élastique interne (Roggendorf & Cervos-Navarro, 1977). Bien qu'elles ne soient pas en contact direct avec le cerveau, les artères pimériennes sont richement innervées par des fibres nerveuses provenant du système nerveux périphérique (Hamel, 2006). Les artères pimériennes se divisent en plus petites artères, plongeant dans le parenchyme cérébral entouré de l'espace de Virchow-Robin, une extension de l'espace sous-arachnoïdien (Jones, 1970 ; Zhang et al., 1990). Ces artères pénétrantes sont constituées d'une unique couche de cellules musculaires lisses beaucoup plus fine (Roggendorf & Cervos-Navarro, 1977). L'espace de Virchow-Robin contient plusieurs types cellulaires entourant les vaisseaux, comme des macrophages périvasculaires, ou des astrocytes qui viennent former via les pieds astrocytaires une couche continue autours du vaisseau, participant ainsi à la formation de la BHE (Zhang et al., 1990). Au fur et à mesure que les artères pénétrantes entrent dans le parenchyme cérébral, l'espace périvasculaire disparait progressivement et les pieds astrocytaires se resserrent, enfermant le vaisseau via un contact direct avec sa lame basale. Des neurones commencent alors à entrer en contact avec le vaisseau via ses terminaisons axonales, ou ses dendrites (Iadecola, 1993 ; Wang et al., 2005). Enfin, les artérioles vont se diviser en capillaires, les cellules musculaires lisses sont remplacées par des péricytes couvrant les cellules endothéliales. Comme pour les artérioles, les capillaires sont entourés par les pieds astrocytaires et de quelques terminaisons axonales (Armulik et al., 2011 ; Damisah et al., 2017 ; Dahl, 1973).

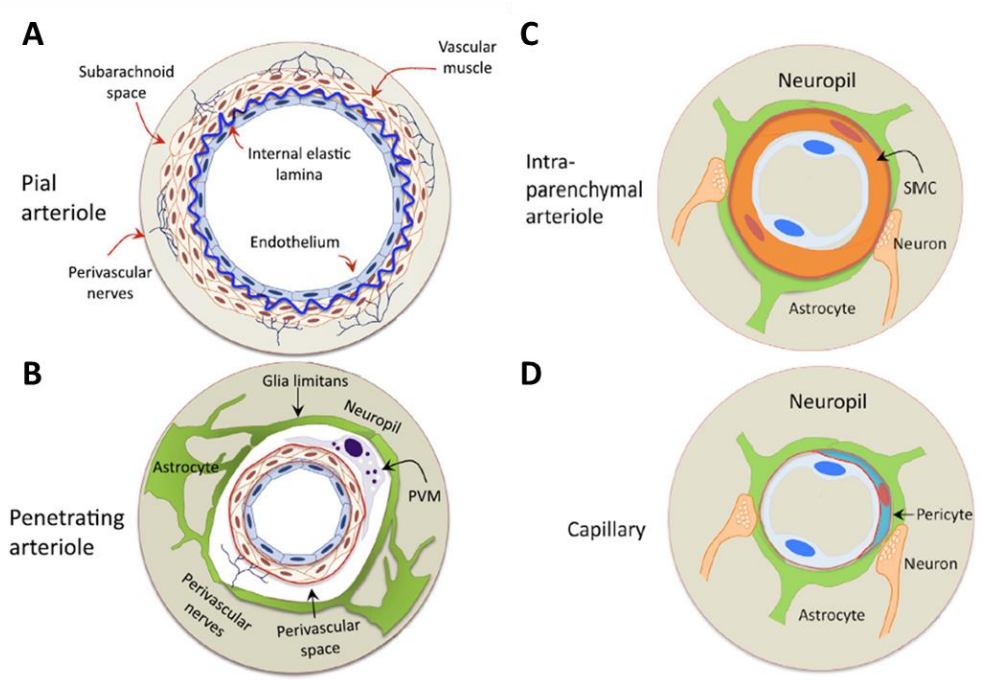

Figure 32 : Les variations de l'architecture de l'unité vasculaire à travers le réseau cérébrovasculaire. Les artères pimériennes (**A**) ont une épaisse couche de cellules musculaires lisses et très innervées par des fibres nerveuses provenant du système nerveux périphérique. Elles sont situées dans l'espace sous-arachnoïdien. Les artères pénétrantes (**B**) plongent vers l'espace périvasculaire (Virchow-Robin) contenant plusieurs types cellulaires, y compris les macrophages périvasculaires (PVM). Les artérioles intra-parenchymateuses (**C**) s'enferment dans les pieds astrocytaires et des neurones provenant du cortex cérébral projettent leur terminaison axonale près du vaisseau. Les capillaires (**D**) sont dépourvus de cellules musculaires lisses mais sont dotés de péricytes qui sont entièrement entourés par la membrane basale de l'endothélium. Des terminaisons axonales sont retrouvées également comme pour les artérioles intra-parenchymateurses (Iadecola, 2017b).

4.3. La régulation du DSC

Le DSC varie en fonction de la consommation énergétique dans les régions cérébrales. En effet, le DSC sera plus élevé dans les régions consommant le plus d'énergie (par exemple, le colliculus inférieur) et plus faible dans les régions consommant le moins (comme la substance blanche ; Sokoloff, 1996). De plus, l'augmentation de l'activité neuronale entraine une augmentation du DSC très

restreinte au niveau des zones activées. Le mécanisme permettant le déclenchement de l'augmentation du DSC se fait principalement via des neurotransmetteurs, en particulier par le glutamate (Bonvento et al., 2002). En effet, la libération de neurotransmetteurs dans la synapse active plusieurs voies de signalisations dans les neurones, les astrocytes et les cellules vasculaires, que nous développerons ci-après.

L'augmentation de l'adénosine triphosphate (ATP) associée à l'activation neuronale conduit à la production d'agents vasodilatateurs tel que l'adénosine, le CO_2, l'hydrogène et le lactate, pouvant potentiellement initier la réponse vasculaire (Freeman & Li, 2016 ; Iliff et al., 2003 ; Ko et al., 1990). Ce mécanisme dépendant du métabolisme neuronal permettant l'augmentation du DSC est également accompagné par un mécanisme indépendant du métabolisme impliquant les neurotransmetteurs, permettant la libération de potassium, de NO ou de prostanoïdes (Attwell et al., 2010 ; Attwell & Iadecola, 2002 ; Drake & Iadecola, 2007).

4.3.1. La signalisation neuronale

Le glutamate libéré dans la fente synaptique va activer les récepteurs NMDA neuronaux, provoquant une entrée de calcium dans le neurone post-synaptique et l'activation de la NO-synthase neuronale (*neuronal Nitric Oxyde Synthase*, nNOS), ainsi que le recrutement de la cyclooxygénase 2 (COX-2). La synthèse et la libération de NO et de prostanoïdes vont participer à la relaxation des cellules musculaires lisses, donc à la dilatation du vaisseau (Busija et al., 2007 ; Lecrux & Hamel, 2016). En effet, l'inhibition des nNOS induit une réduction de l'augmentation du DSC en réponse à l'activité neuronale, suggérant le rôle du NO dans le CNV (Ma et al., 1996). Des interneurones peuvent également à dans la modulation du CNV (Lecrux et al., 2011). En effet, les neurotransmetteurs et les neuromodulateurs libérés par les interneurones ont un effet sur les microvaisseaux aux alentours. Dans le cortex et le cervelet, les interneurones sont capables d'induire une vasoconstriction via la libération du neuropeptide Y, ou une vasodilatation via le NO libéré (Cauli et al., 2004 ; Cauli & Hamel, 2010). De plus, les neurones du locus coeruleus, des noyaux de raphé ou du télencéphale basal sont capables de projeter leurs terminaisons axonales vers le

néocortex pour libérer respectivement de la noradrénaline, de la sérotonine, ou de l'acétylcholine (ACh) afin de moduler le DSC (Cohen et al., 1996 ; Hamel, 2006 ; Toussay et al., 2013 ; Zhang et al., 1995).

4.3.2. La signalisation astrocytaire

Les astrocytes sont situés au niveau des synapses et des microvaisseaux se trouvant à proximité. Ce positionnement très stratégique permet aux astrocytes de faire le relais entre l'activité neuronale et la réponse hémodynamique des vaisseaux. Les astrocytes peuvent augmenter le DSC en réponse à une activation neuronale via la libération de potassium au niveau des pieds astrocytaires en contact avec les artérioles, induisant une hyperpolarisation et une relaxation des cellules musculaires lisses (Knot et al., 1996). En effet, les astrocytes vont jouer le rôle de « siphonage » en recapturant le potassium libéré par l'activité neuronale puis en le libérant vers les pieds astrocytaires (Paulson & Newman, 1987).

Lors de l'activation neuronale, du glutamate va être libéré dans la fente synaptique. Une partie de ce glutamate va activer les mGluR présents à la surface des astrocytes, provoquant une augmentation du flux calcique intracellulaire (**Figure 33** ; Porter & Mccarthy, 1996 ; Zonta et al., 2003). L'élévation de calcium intracellulaire induit la libération de potassium vers les cellules musculaires lisses, mais également l'activation des PLA_2 permettant la libération d'acide arachidonique (AA) le précurseur de la prostaglandine E2 (PGE_2) et des acides époxyeicosatriénoiques (EET), pouvant induire une vasodilatation (Filosa et al., 2006 ; Mishra, 2017).

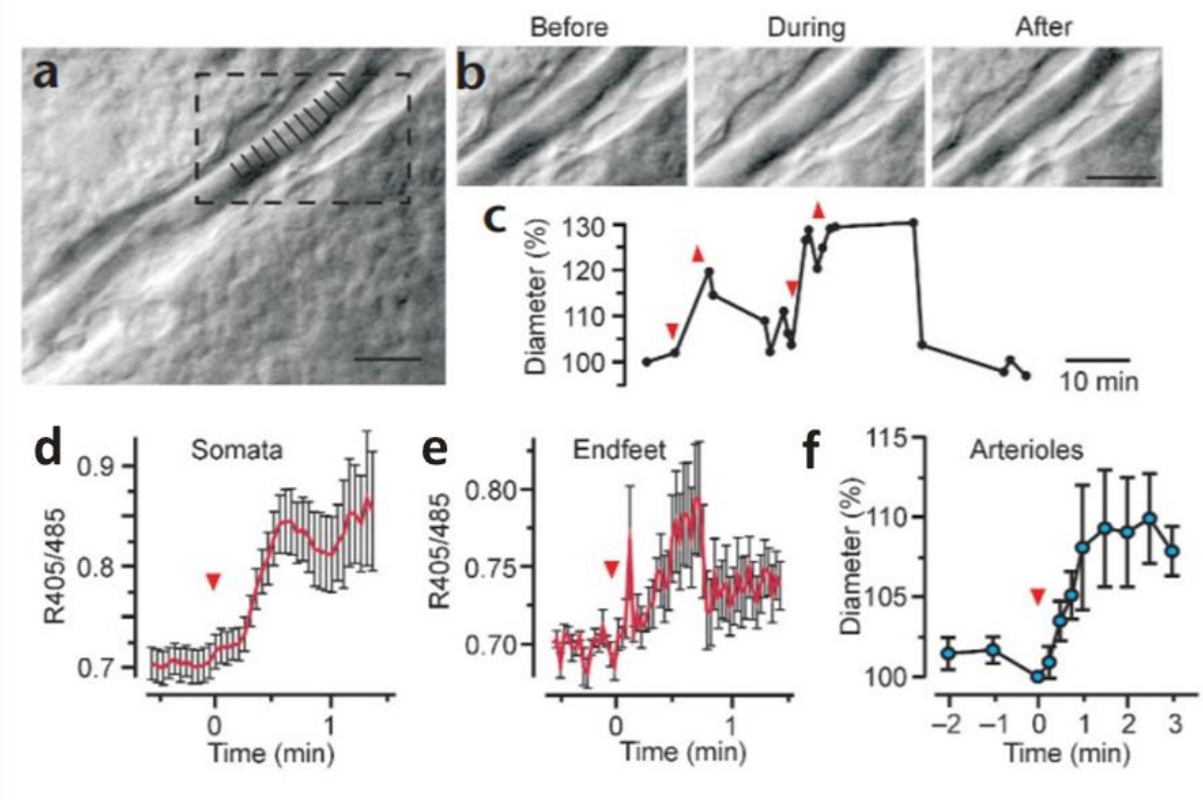

Figure 33 : La stimulation neuronale sous-tend la dilatation des artérioles cérébrales via l'augmentation intracellulaire de calcium dans les astrocytes. Une artériole corticale (**a**) et la réponse vasculaire (**b, c**) lors d'une stimulation de la zone par une électrode intracorticale. Les triangles représentent le début et la fin de la stimulation. Cinétiques de l'augmentation intracellulaire de calcium dans les astrocytes, plus précisément dans le corps cellulaire (**d**) et le pied astrocytaire (**e**). (**f**) Courbe représentant la dilatation de l'artériole obtenue en moyennant la réponse vasculaire entre chaque stimulation (Zonta et al., 2003).

Pour comprendre davantage le rôle des astrocytes dans le CNV, des études avec ablation des astrocytes ont été menées. En effet, l'utilisation de gliotoxines, comme le fluoroacétate pour endommager les astrocytes du cortex a permis d'observer une diminution de 50% de l'augmentation du DSC induite par la stimulation du prosencéphale basal (Paulsen et al., 1987). De la même façon, une réduction du flux sanguin après une stimulation lumineuse a été observé lorsque des yeux de chats ont été traité avec une gliotoxine (Song et al., 2015). Bien que ces études suggèrent que les astrocytes jouent un rôle dans le CNV, elles doivent être interprétées avec prudence car la suppression des astrocytes va également avoir un effet indirect sur les neurones tels que le recyclage de glutamate, du potassium, la régulation du pH

extracellulaire et du métabolisme du glucose (Hassel et al., 1992 ; Lian & Stringer, 2004 ; Stringer & Aribi, 2003).

4.3.3. La signalisation vasculaire

Les cellules endothéliales sont capables de synthétiser de puissants agents vasoactifs tels que le NO ou les prostanoïdes, et sont connues pour réguler le DSC en réponse à des agents pharmacologiques, mais leur rôle dans le CNV n'est pas tout à fait élucidé. Des études suggèrent que les cellules endothéliales peuvent propager de façon rétrograde la signalisation induite par le CNV le long des artérioles. L'administration brève d'agents vasoactifs à l'aide d'une micropipette sur la paroi d'une artériole permet de confiner le stimulus initial dans un rayon égal au diamètre de la micropipette. L'application d'ACh sur l'artériole provoque une propagation de la vasodilatation en amont et en aval de la zone initiale ; cela n'est pas le cas lors de l'application d'histamine, de potassium, d'hydrogène ou d'élédoisine (**Figure 34** ; Duling & Berne, 1970). Également, des études en IRM fonctionnelle (IRMf) ont révélé que pendant l'activation somatosensorielle, les réponses vasculaires sont d'abord observées dans les régions corticales profondes, puis plus superficiellement, suggérant une propagation rétrograde de la réponse vasculaire (Silva & Koretsky, 2002 ; Uhlirova et al., 2016). Le mécanisme de propagation de la vasodilatation dans les vaisseaux périphériques est connu au niveau des muscles squelettiques. En effet, cela implique des canaux potassiques rectifiant entrant (K_{IR}) et des canaux potassiques calcium dépendant (K_{Ca}), déclenchant la libération de NO endothéliale et de prostanoïdes (Segal, 2015 ; Tallini et al., 2007). Dans la circulation cérébrale, ce mécanisme impliquerait plus les K_{IR} du fait que les cellules endothéliales cérébrales expriment en abondance les K_{IR} mais pas les K_{Ca}. En effet, les capillaires cérébraux sont très sensibles au potassium libéré par les pieds astrocytaires pendant l'activité neuronale (Longden et al., 2017).

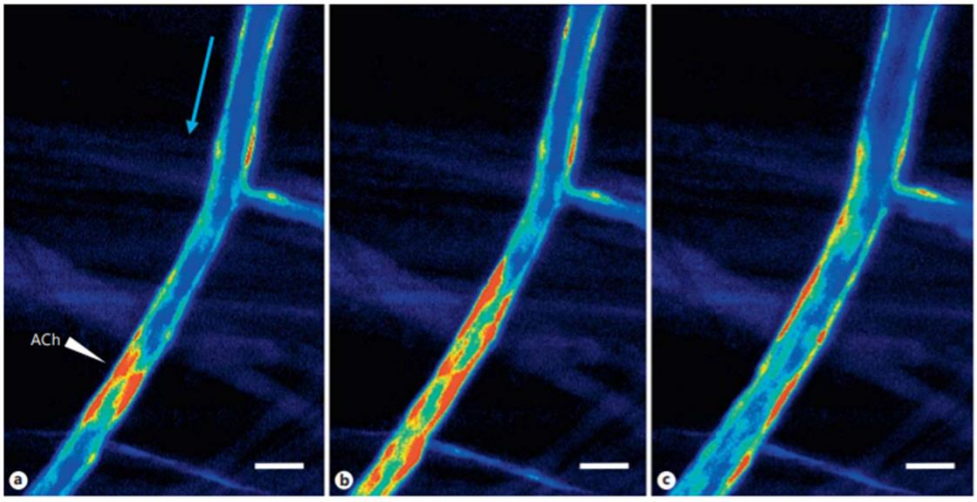

Figure 34 : L'application d'ACh sur l'artériole conduit à une propagation ascendante de la vasodilatation. Images séquentielles d'une artériole d'une souris GCaMP2 dans les cellules endothéliales, la flèche bleue indique le sens du flux sanguin. L'initiation de la stimulation avec l'administration brève d'ACh engendre une augmentation locale de calcium intracellulaire (**a**). La transmission de l'influx calcique se fait de façon bidirectionnelle (**b**), puis la vasodilatation s'observe dans les zones affectées par l'influx calcique (**c**). Les zones présentant un fort influx calcique sont représentées par des couleurs chaudes (Tallini et al., 2007).

Le rôle des péricytes dans la vasodilatation des capillaires est mal connu dû à la taille des vaisseaux et le manque d'identification spécifique des capillaires. Des études suggèrent la présence de péricytes contractiles contenant de l'actine (α-SMA) comme les cellules musculaires lisses, et d'autres non contractiles autour des capillaires (Attwell et al., 2016 ; Hartmann et al., 2015).

4.4. La réponse hémodynamique

Les capillaires sont impliqués dans la détection des signaux envoyés par les neurones et les astrocytes, ce qui conduit à l'hypothèse que le CNV pourrait être initié dans les capillaires. L'hyperpolarisation se propagerait en amont (Cox et al., 1993 ; Iadecola, 1993). La transmission de la signalisation se ferait via les canaux K_{IR} à travers les jonctions communicantes des cellules endothéliales, pour atteindre les cellules contenant de l'α-SMA et les cellules musculaires lisses en amont et permettant

leur relaxation (Longden et al., 2017). La relaxation des cellules musculaires lisses artériolaires se complète en plus avec la propagation de l'hyperpolarisation via les cellules endothéliales, par l'action directe des agents vasoactifs libérés par les neurones et les astrocytes comme le NO, l'adénosine ou les prostanoïdes. Enfin, la relaxation des artérioles pimériennes, éloignées du site d'activation, peut résulter de deux mécanismes : la vasodilatation se propageant à partir des artérioles en aval, et la vasodilatation induite localement. Les artérioles pimériennes n'étant pas directement en contact avec les neurones et les astrocytes, les signaux voyagent de manière rétrograde depuis les capillaires et les artérioles activées plus profondément dans le parenchyme.

4.5. Facteurs influençant le couplage neurovasculaire

4.5.1. Implication du tPA dans le CNV

L'implication du tPA dans le tonus vasculaire via sa fixation sur les récepteurs NMDA des cellules endothéliales est connu. En effet, le tPA peut induire une vasodilatation via l'activation des eNOS (Nassar et al., 2004, 2010).

L'implication du tPA dans le CNV a été rapportée par l'équipe de Iadecola. En effet, il a été observé que l'hyperémie fonctionnelle induite par la stimulation des vibrisses était atténuée chez des souris déficientes en tPA. Ce déficit est restauré via l'application directe de tPA recombinant (rtPA) dans le cortex sensoriel. Le mécanisme d'action du tPA se fait via son interaction avec les récepteurs NMDA synaptiques et post-synaptiques pour promouvoir l'activation des nNOS et la libération de NO (**Figure 35** ; Park et al., 2008).

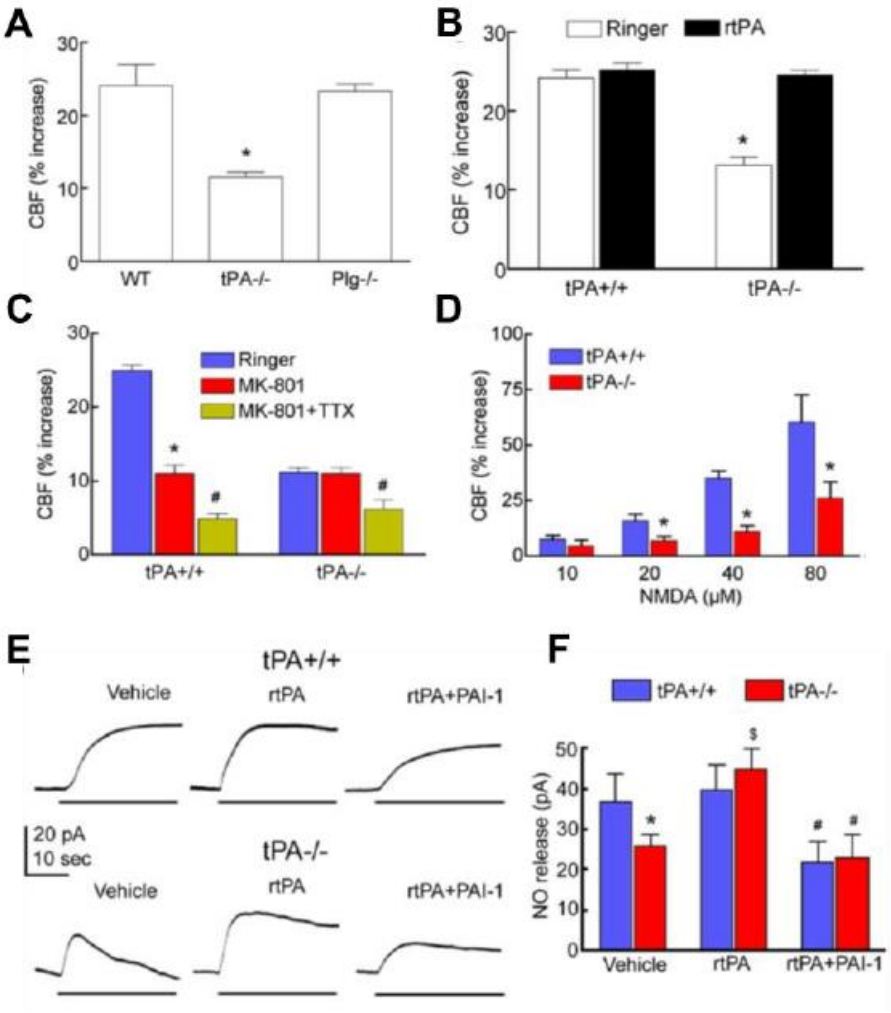

Figure 35 : Le tPA cortical a un effet vasodilatateur sur le CNV. A : L'augmentation du DSC induit par la stimulation des vibrisses est réduite chez les souris déficientes en tPA. **B** : Le déficit de cette réponse hémodynamique peut être restauré chez les souris déficientes en tPA par l'application corticale de rtPA. **C** : L'hyperhémie fonctionnelle peut être réduite en inhibant les récepteurs NMDA mais pas chez les souris déficientes en tPA. La tétrodoxine (TTX), un bloqueur des canaux sodiques, réduit l'hyperémie vasculaire à la fois chez les souris déficientes en tPA et WT. **D** : L'application topique de NMDA induit une augmentation du DSC moins importante chez les souris déficientes en tPA. **E-F** : La production de NO est réduite chez les souris déficientes en tPA et en présence de PAI-1, elle peut être restaurée via l'application corticale de rtPA (Park et al., 2008)

En plus de l'effet vasodilatateur du tPA sur le CNV au niveau cortical, le tPA peut également avoir ce même effet au niveau vasculaire, toujours par son interaction avec les récepteurs NMDA, mais cette fois-ci endothéliaux. En effet, l'injection

intraveineuse de rtPA induit une restauration de l'hyperhémie fonctionnelle chez des souris déficientes en tPA (**Figure 36** ; Anfray et al., 2020).

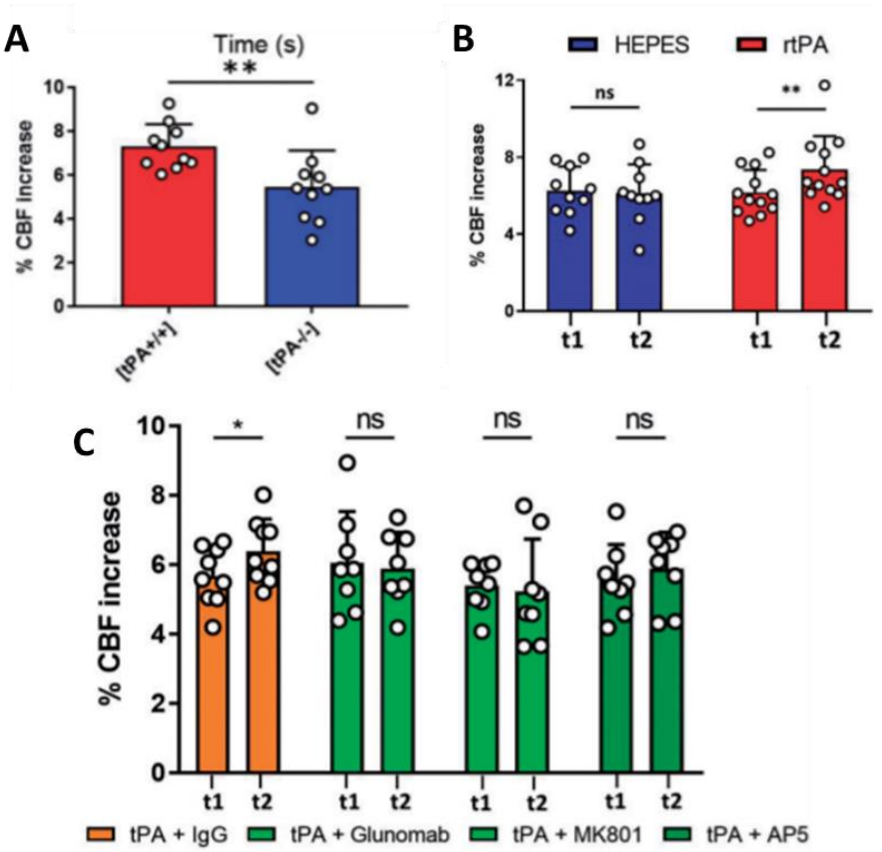

Figure 36 : Le tPA vasculaire a un effet vasodilatateur sur le CNV. A : L'augmentation du DSC induit par la stimulation des vibrisses est réduite chez les souris déficientes en tPA. **B** : Le déficit de cette réponse hémodynamique peut être restauré chez les souris déficientes en tPA par l'injection intraveineuse de rtPA. **C** : L'effet vasodilatateur du rtPA lors du CNV peut être inhibé via l'injection intraveineuse de différents inhibiteurs des récepteurs NMDA chez les souris déficientes en tPA. t1 représente l'augmentation du DSC induit par la stimulation des vibrisses avant l'injection des produits pharmacologiques, t2 représente l'augmentation du DSC après injection des produits pharmacologiques (Anfray et al., 2020)

4.5.2. Effet des agents anesthésiques sur le couplage neurovasculaire

L'anesthésie est largement utilisée dans les études précliniques pour l'étude du CNV chez l'animal in vivo et peut avoir des effets sur les cellules cérébrales comme

sur l'activité neuronale, la réactivité vasculaire ou le métabolisme cérébrale. Ces différents effets peuvent avoir un impact sur le CNV. Ainsi l'anesthésie est un facteur pouvant interférer avec l'hyperhémie fonctionnelle.

L'α-chloralose est l'agent anesthésique le plus couramment utilisé pour l'étude du CNV chez le rongeur car cet agent est connu pour préserver le CNV au niveau hémodynamique et métabolique (Lindauer et al., 1993 ; Ueki et al., 1992). Au niveau de la physiologie de l'animal, l'α-chloralose provoque une dépression respiratoire, une acidose métabolique et une hyperréactivité (Arfors et al., 1971). De plus, l'utilisation de l'α-chloralose requiert l'administration d'un autre agent anesthésique du fait de sa faible capacité analgésique, pouvant alors contribuer à plus de variabilité du CNV (Bonvento et al., 1994).

Les agents anesthésiques par inhalation tels que l'halothane, l'enflurane ou l'isoflurane sont assez pratiques car l'induction et le réveil de l'animal sont très rapides et peuvent être utilisés de manière répétée pour les études longitudinales. Cependant, ces anesthésiques volatiles sont de puissants vasodilatateurs, même au niveau cérébral, et conduisent à une augmentation basale du DSC et une diminution du métabolisme cérébral (van Aken & van Hemelrijck, 1991).

Les anesthésiques barbituriques comme le pentobarbital et le thiopental, réduisent le débit cardiaque et conduisent à une hypotension, de plus, ils induisent une dépression respiratoire. Pour exemple, l'uréthane provoque une hypotension, une réduction du débit cardiaque modéré, et une hyperventilation (Fieldi et al., 1993).

La médétomidine et la xylazine sont des agonistes spécifiques aux récepteurs α2-adrénergiques, qui bloquent la libération de la noradrénaline. En raison des propriétés analgésiques limitées de ces produits, les interventions chirurgicales doivent être effectués en combinaison avec d'autres agents anesthésiques. Elles peuvent affecter la fonction cardiovasculaire et provoquer des dépressions respiratoires. Les animaux peuvent récupérer après l'administration d'un antagoniste

α2-adrénergique, rendant une utilisation répétée possible pour les études longitudinales (Pawela et al., 2009 ; Sinclair, 2003 ; Weber et al., 2006).

Le couplage neurovasculaire est un phénomène qui permet de préserver le bon fonctionnement neuronal. La dilatation des vaisseaux sanguins permet aux neurones de bénéficier d'un apport supplémentaire en énergie lorsqu'ils sont en activité.

La vasodilatation ainsi que l'augmentation du débit sanguin cérébral peuvent être déclenchées par plusieurs voies de signalisation.

Les neurones et les astrocytes sont capable de libérer des neurotransmetteurs comme le glutamate, et permettre la synthèse d'agents vasodilatateurs comme le monoxyde d'azote.

Le tPA peut également moduler l'hyperémie fonctionnelle par son interaction avec les récepteurs NMDA.

Neurovascular coupling is an important phenomenon in order to preserve good neuronal functioning. Dilatation of blood vessels allows neurons to benefit from a supply of energy when they are active.

Vasodilatation and the increase of cerebral blood flow can be triggered by several signalling pathways.

Neurons and astrocytes are able to release neurotransmitters like glutamate, and allow the synthesis of vasodilating agents such as nitric oxide.

tPA may also modulate functional hyperemia through its interaction with NMDA receptors.

Objectifs

Le tPA est une sérine protéase d'abord découvert dans la circulation sanguine et connu pour sa capacité fibrinolytique. Depuis, le tPA a été étudié pour ses nombreuses autres fonctions physiologiques et pathologiques. Les principales sources de production du tPA vasculaire étant les cellules endothéliales et les hépatocytes, une fois libéré, le tPA est rapidement inhibé par le PAI-1, limitant ses interactions dans la circulation sanguine. Il est également capable d'agir comme neuromodulateur dans différents types cellulaires grâce à la présence des récepteurs NMDA.

Les récepteurs NMDA sont exprimés au sein du SNC dans plusieurs types cellulaires, et participent à des fonctions vitales comme la plasticité synaptique, la régulation du tonus vasculaire ou encore l'hyperémie fonctionnelle.

Le couplage neurovasculaire est un mécanisme important pour le bon fonctionnement des neurones, n'ayant pas ou peu de réserves énergétiques propre. Le tPA joue un rôle dans la modulation de l'hyperémie fonctionnelle à la fois par sa présence dans le parenchyme cérébrale mais aussi dans la circulation sanguine. Cependant, la quantité de tPA libre circulant étant très limitée pour pouvoir jouer un rôle hyperémiant dans le CNV, le tPA doit être libéré par les cellules endothéliales et les hépatocytes au moment d'une activation neuronale afin d'exercer son rôle.

Le tPA peut être libéré dans la circulation par les cellules endothéliales via l'activation des récepteurs B2 par la BK, une molécule impliquée dans la vasodilatation et l'hypotension. Inversement, l'AngII peut stimuler la libération de PAI-1 via l'activation des récepteurs AT1. L'AngII est capable d'induire une vasoconstriction ainsi qu'une hypertension.

Mes travaux de thèse visent à mieux comprendre le rôle du tPA circulant dans le CNV induit par la stimulation des vibrisses, son mode de libération dans la circulation, son effet lors de la présence de PAI-1 et son interaction avec les récepteurs NMDA endothéliaux.

Plusieurs modèles animaux et différents agents pharmacologiques ont été utilisés, et ont permis de répondre aux problématiques suivantes :

- Quelle est l'influence de l'axe tPA/PAI-1 sur l'hyperémie fonctionnelle induite par la stimulation des vibrisses ?
- La quantité basale de tPA circulant influence-t-elle le CNV ?
- Les récepteurs NMDA endothéliaux sont-ils responsables de l'hyperémie vasculaire induite par le tPA lors de la stimulation des vibrisses ?
- L'activation du SKK favorise-t-elle la libération de tPA circulant par les cellules endothéliales via l'activation des récepteurs B2 par la BK et influence-t-elle le CNV ?
- L'activation du SRA influence-t-elle l'hyperémie fonctionnelle par la libération de PAI-1 par les cellules endothéliales via l'activation des récepteurs AT1 par l'AngII ?
- Le tPA libéré par les cellules endothéliales hépatiques contribue-t-il à la régulation du CNV ?

Résultats

1. Le tPA circulant sécrété par les cellules endothéliales hépatiques module l'activité des récepteurs NMDA endothéliaux au niveau cérébral et contribue au couplage neurovasculaire.

Vascular tPA of liver origin contributes to neurovascular coupling involving brain endothelial NMDA receptors.

Mervé Yetim,[1] Jonathane Furon,[1] Sara Martinez de Lizarrondo,[1] Esla Pouettre,[1] Eric Maubert,[1] Yannick Hommet,[1] Laurent Lebouvier,[1] Ze Zheng,[2-3] Carine Ali,[1] and Denis Vivien[1-4 *]

[1]Normandie University, UNICAEN, INSERM UMR-S U1237, Physiopathology and Imaging of Neurological Disorders (PhIND), GIP Cyceron, Institut Blood and Brain @ Caen-Normandie (BB@C), 14000 Caen, France; [2]Department of Medicine, Medical College of Wisconsin, Milwaukee, WI, USA; [3]Blood Research Institute, Versiti Blood Center of Wisconsin, Milwaukee, WI, USA; and [4]Department of clinical research, Caen-Normandie University Hospital, CHU, Avenue de la côte de Nacre, Caen, France.

Corresponding author (*): Prof. Denis Vivien, PhD, Normandie Univ, UNICAEN, INSERM UMR-S U1237, Physiopathology and Imaging of Neurological Disorders (PhIND), GIP CYCERON, Institut Blood and Brain @ Caen-Normandie (BB@C), Bvd Becquerel, BP 5229, 14074 Caen Cedex, France; Tel: + 33 2 31470166; Fax: + 33 2 31470222; E-mail: vivien@cyceron.fr

Key Points

Endogenous levels of circulating tPA influence neurovascular coupling induced by whiskers stimulation in mice.

Endothelial NMDA receptors mediate the tPA-dependent modulation of neurovascular coupling induced by whiskers stimulation in mice.

Abstract

Regulation of the cerebral blood flow (CBF) involves complex mechanisms with direct influences on brain functions and dysfunctions. Among these mechanisms it was proposed that the serine protease tissue-type plasminogen activator (tPA) could play a role in the control of neurovascular coupling (NVC) induced by whiskers stimulation in rodents through its action on N-methyl-D-Aspartate receptors (NMDARs). In the present study, using tPA^{Null} mice, conditional deletions of either endothelial tPA ($VECad\text{-}Cre^{\Delta tPA}$) or endothelial NMDARs GluN1 subunit ($VECad\text{-}Cre^{\Delta GluN1}$), parabioses between wild-type and tPA^{Null} mice, hydrodynamic transfections-induced deletion of liver tPA, hepatectomy and pharmacological approaches in mice, we have unveiled this mechanism in detail. We thus demonstrate that physiological concentrations of vascular tPA, produced and released by the liver endothelial cells in a bradykinin type 2 receptors-dependent manner, promotes NVC, by a mechanism dependent of brain endothelial NMDA receptors. These data highlight a new mechanism of the regulation of NVC involving both endothelial tPA and NMDA receptors.

Introduction

Functional hyperemia, also named neurovascular coupling (NVC), allows local energy supply to brain cells, with key roles in the pathophysiology of the brain[1,2]. For instance, brain disorders such as stroke or Alzheimer's Disease are associated with CBF dysregulations[3].

Initially described by its ability to activate plasminogen into plasmin in the blood[4], the tissue-type Plasminogen Activator (tPA) is a serine protease widely expressed in the central nervous system (CNS)[5,6], especially by neurons and endothelial cells[7,8]. Extending its functions above the conversion of plasminogen into plasmin, tPA interferes with a variety of neuronal receptors[9], including *N*-Methyl-D-Aspartate receptors (NMDARs). Through these mechanisms, tPA is considered as a neuromodulator implicated in various brain functions and dysfunctions, including learning and memory processes[10,11], anxiety behavior[12,13] and neurovascular diseases such as stroke, in which it contributes to the homeostasis of the blood brain barrier and the neuronal survival[14,15].

Park et al. proposed tPA as an actor of NVC by its ability to influence NMDAR signaling[16]and proposed that the PAI-1/tPA (type 1 plasminogen activator inhibitor) pathway could counteract the harmful neurovascular and cognitive effects of Aβ[17]. In parallel, Anfray et al. have proposed that the circulating tPA could contribute to NVC[18]. It is thus interesting to note that, in the central nervous system, the tPA initially reported to be expressed and released by endothelial cells is also expressed and released by neurons; both cells also express NMDA receptors[19–22].

Endothelial cells and hepatocytes are thought to be the main sources of vascular tPA[23], with the level of free tPA counterbalanced by its serpin PAI-1[24,25]. The control of this balance between the levels of blood tPA and PAI-1 thus plays a major contribution in a number of neurovascular diseases[17,27,28]. There is a growing body of evidence that activation of endothelial luminal bradykinin receptors promotes the luminal release of tPA by endothelial cells[29], whereas angiotensin-II leads to release of PAI-1[30]. Nevertheless, regulation of plasma levels of PAI-1 cannot be explained solely by the renin-angiotensin system[31].

These observations raise the possibility that modifications of the physiological levels of vascular tPA may contribute to modifications of neurovascular coupling and subsequent brain functions/dysfunctions. Therefore, we further examined the role of tPA, especially the circulating tPA, in functional hyperemia induced by whiskers stimulation in mice, by using a large set of genetic tools, including tPA deficient mice, PAI-1 deficient mice, conditional deletion of either the endothelial tPA or for endothelial NMDA receptors and finally parabiosis between wild type and tPA deficient mice. We thus demonstrated that vascular tPA, from liver endothelial cells origin, contributes to neurovascular coupling through modulation of brain endothelial NMDA receptors signaling. Using parallel pharmacological and genetic approaches we also demonstrated a bradykinin dependent control of the vascular tPA levels with direct impact on functional hyperemia.

Materials and methods

Animals

All experiments were conducted in accordance with the French ethical law (Decree 2013-118) and the European Communities Council guidelines (2010/63/EU). Protocols were approved by our local ethics committee dependent on the French Ministry of Research and Higher Education (agreement numbers Cenomexa #19208, #19978 and Ce5/2012/062). All applicable international, national, and/or institutional guidelines for the care and use of animals were followed.

All experiments were performed on 8-10 weeks old male C57BL/6 (Janvier Labs, Le Genest-Saint-Isle, France), tPA Null mice and their wild type (WT) littermates (see mouse lines section), VeCadCre/tPAlox mice and their WT littermates (see mouse lines section), VeCadCre/Grin1lox mice and their WT littermates (see mouse lines section) were bred in our animal facilities (CURB, Caen, France) and housed in a 12h light/12h dark cycle with free access to water and food.

Mouse lines

tPA Null mice and tPAlox mice were generated by our group[32] in collaboration with the Mouse Clinical Institute (ICS, Illkirch, France, http://www.ics-mci.fr). To induce tPA Null mice, tPAlox mice (C57BL6J background) in which exon 3 of the Plat gene was flanked by loxP sites were crossed with CMV-Cre mice to induce of Cre-mediated excision the third exon of the Plat gene in germline. PAI-$1^{-/-}$ mice were obtained from professor H.R. Lijnen, Centre for Molecular and Vascular Biology, University of Leuven, Belgium. Grin1lox mice (B6.129S4-Grin1tm2Stl/J; # 005246) were obtained from The Jackson Laboratory[33]. VE-Cadherin-Cre mice (B6.FVB-Tg(Cdh5-cre)7Mlia/J; # 006137) were obtained from F. Millat[34], Institute of Radioprotection and Nuclear Safety, Fontenay-aux-Roses, France. tPAlox and Grin1lox mice were crossed with VE-Cadherin-Cre mice to obtain VE-Cadherin-Cre/tPAlox (VECad-$Cre^{\Delta tPA}$) and VE-Cadherin-Cre/Grin1lox mice (VECad-$Cre^{\Delta GluN1}$).

Pharmacological treatments

Different treatments were injected intravenously during experiments. Recombinant tPA (rtPA) (10mg/kg) prepared as previously described[18] was infused for ten minutes (a bolus of 150µl for a total volume of 300µl). A selective bradykinin type 2 receptor agonist (B2Rag) ([Phe8 Ψ(CH-NH)-Arg9]-Bradykinin, Tocris) was used at 7, 15, 30 µg/kg, 0.1ml for each dose or a unique dose for ELISA (60µg/kg, 0.1ml) or for mean arterial pressure (MAP) measure (30µg/kg, 0.1ml). Angiotensin II (Angiotensin II acetate, Sigma, 1µg/kg/min), was infused during 20 minutes to obtain a MAP of 120mmHg for acute hypertension.

Animal preparation prior measurement of the cerebral blood flows induced by whiskers stimulation

Animals were anesthetized using 5% isoflurane (Isoflurane Belamont) in 70% N_2O/30% O_2. Mice were intubated and placed under mechanical ventilation (120 BPM, 10ml/kg) by maintaining anesthesia with 2% isoflurane in 70% N_2O/30% O_2. Caudal vein and femoral artery were catheterized for pharmacological injections (see pharmacological treatments section) and to evaluate physiological parameters: pCO_2, pH and MAP. As previously described[18], mice were placed in a stereotaxic frame. An incision was made along the midline head skin to expose the skull and lidocaine spray (Xylocaine, 5% spray®, AstraZeneca) was applied on the head. Whiskers on the left side were cut to let a length of 1 cm. Anesthesia was switched with subcutaneous infusion of medetomidine (Domitor®, Pfizer, 0.1mg/kg) then isoflurane, N_2O and O_2 were stopped ten minutes later and replaced by air. For isoflurane's effects dissipation and CBF stabilization, twenty minutes have waited before acquisitions.

Laser Doppler Speckle Flowmetry

Laser Doppler Flowmetry (LDF) was used to measure relative cerebral blood flow (CBF) during whiskers stimulations, of the whole surface of the brain with intact skull. Acquisitions were made with a laser speckle contrast imager (MoorFLPI-2, Moor Instrument, Exposure Time: 20s, Filter: 25 frames, Sample Interval: 1000ms, Image Resolution: 752 x 580p). The whole whiskers were mechanically shaken (4Hz) during

30s three times between 60s of resting time. Analysis was made with MoorFLPI-2 Review V5.0 software, stimulation frames and resting frames were averaged and subtracted to obtain an activation map corresponding of the barrel cortex. CBF of this area was calculated to obtain a percentage of CBF change from baseline, then the three stimulations were averaged together.

Parabiosis

For parabiosis[35], mice were anesthetized (see animal preparation section), Buprenorphine (Buprecare®, Axience, 0.1mg/kg) to proceed with the surgery. Animals were placed in the lateral position, back-to-back. A longitudinal skin incision was performed, gently the skin was detached and joints were attached with non-absorbable suture. The skin of the two mice were connected with non-absorbable sutures. Controls were performed to assess the efficacy of parabiosis, using measurements of blood glucose levels and DOTA-Gd MRI analyses (Supplemental figure 2).

Partial hepatectomy

Animals were anesthetized (see animal preparation section), Buprenorphine (Buprecare®, Axience, 0.1mg/kg) to proceed with the surgery. Briefly, a transverse laparotomy was made. Left lateral lobe, left and right median lobes were ligatured using non-resorbable sutures, allowing a resection of around 70% of the total liver. For sham condition, only a transverse laparotomy was made. experiments were performed 24h after partial hepatectomy (see Laser Doppler Speckle section).

ELISA for tPA

Plasma total tPA from mice was analysed using commercial ELISA kits (Innovative Research, Inc.) according to the manufacturer's instructions. Blood samples were collected by intracardiac puncture as previously described[18].

Immunohistochemistry

Deeply anesthetized mice were transcardially perfused with cold heparinized saline (15 ml/min), then with 4% paraformaldehyde in 0.1 M sodium phosphate buffer, pH 7.4 (150 ml, 15 ml/min). Brain and liver sections were incubated overnight at room temperature with primary antibodies rabbit anti-tPA (1:1500, generous gift from R. Lijnen, Leuven) and rat anti-CD31 (1:1000, 553370, BD Biosciences). Primary antibodies were revelated using Fab'2 fragment anti-rabbit IgG linked to CY3 and anti-rat IgG linked to FITC (1:800, 711-096-152 / 112-546-072, Jackson ImmunoReasearch) co-incubated 90 min at room temperature, then coverslipped using mounting medium containing DAPI. Images were digitally captured using an epifluorescence microscope (Leica DM6000). Images were assessed using ImageJ software (NIH).

Statistical analyses

Results are expressed as box plots with medians, 1st and 3rd quartiles, min and max with values for each mouse. Time courses represent the mean ± the standard error of the mean (SEM) in transparency. Statistical analysis was performed using Mann-Whitney test, Kruskal Wallis test or ANOVA with GraphPad software. Data were considered statistically different if probability values (p) were at least <0.05.

Results

The tPA/PAI-1 axis influences functional hyperemia induced by wiskers stimulation.

We decided to perform our experiments by maintaining the skull of animals intact and closed, to prevent any artefacts due to craniectomy. Also, importantly, our animals were maintained sedated using medetomidine instead of ketamine to prevent possible interferences with NMDA receptors signaling. We showed that the CBF increase evoked by whiskers stimulation is significantly impaired in tPA-deficient mice (tPA^{Null}) when compared to WT littermates (**Figure 37A-C**) (+5.65 ± 0.49% for tPA^{Null} mice, n=16, vs. +7.16 ± 0.46% of CBF increase for WT mice, n=18, i.e. -21% of CBF increase for tPA^{Null} mice compared to tPA^{WT} mice, p-value 0.0167). In parallel, similar experiments were performed in 8-10 weeks old wild type and PAI-1 deficient. As expected, CBF increase evoked by whiskers stimulation is significantly increased in PAI-1-deficient mice ($PAI\text{-}1^{KO}$) when compared to WT littermates (**Figure 1A, D-E**) (+10.9 ± 0.67% for $PAI\text{-}1^{KO}$ mice, n=10, vs. +9.17 ± 0.35% of CBF increase for $PAI\text{-}1^{WT}$ mice, n=10, i.e. +19.1% of CBF increase for $PAI\text{-}1^{KO}$ mice compared to $PAI\text{-}1^{WT}$ mice, p-value 0.0433). These data demonstrate that the endogenous ratio tPA/PAI-1 plays a key role in modulating the patency of neurovascular coupling.

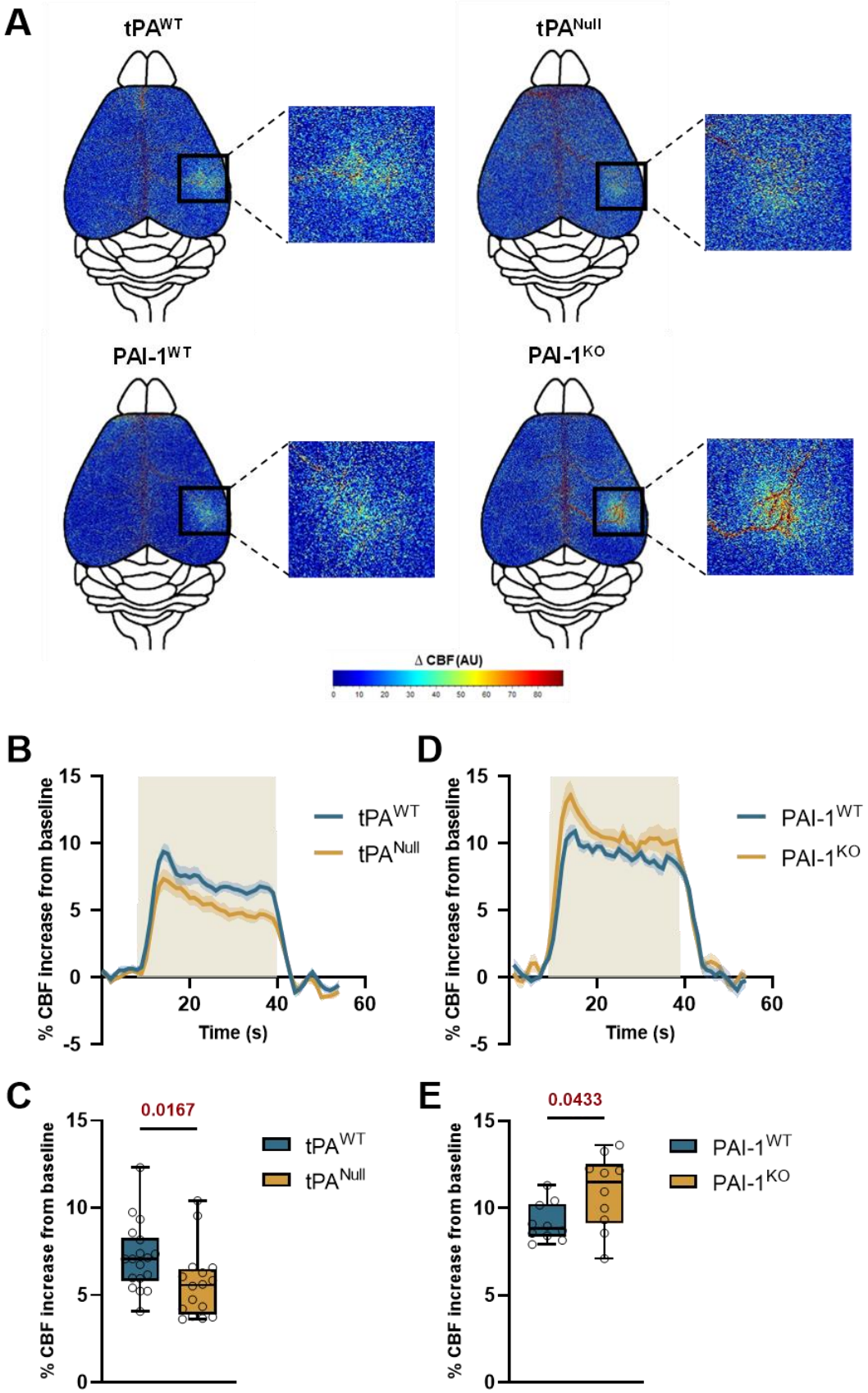

Figure 37 : The tPA/PAI-1 axis controls NVC.

Figure 37 : The tPA/PAI-1 axis controls NVC. A: Colormap corresponds to the activation map related ΔCBF changes during whiskers stimulations of tPA^{Null}, $PAI\text{-}1^{KO}$ mice and their wild type littermates. Maps were obtained by subtraction of stimulation frames and resting frames. Warm colours indicate an elevation of CBF during whiskers stimulations. **B, D**: Time course of % CBF increase (mean ± SEM) during whiskers stimulations ( ) of tPA^{Null} (**B**) and $PAI\text{-}1^{-/-}$ (**D**) mice ( ) and their littermates ( ). **C, E**: Box plots show the variations of % CBF increase from baseline during whiskers stimulations of tPA^{Null} (**C**) and $PAI\text{-}1^{-/-}$ (**E**) mice and their littermates. Box plot with medians, 1st and 3rd quartiles, min and max with values for each mouse. *$p < 0.05$ from tPA^{WT} or $PAI\text{-}1^{WT}$, Mann-Whitney test, n=18/16 tPA^{WT}/tPA^{Null}, n=10 $PAI\text{-}1^{WT}/PAI\text{-}1^{KO}$.

Physiological level of circulating tPA influences NVC

Additional questions are whether these phenotypes are due to the levels of tPA present in the bloodstream. To address this point we decided to use a model of parabiosis between tPA^{WT} and tPA^{Null} mice (**Figure 38A**, and **Supplementary figure 2**). We used three types of parabiosis, tPA^{WT}/tPA^{WT}, tPA^{Null}/tPA^{Null} and tPA^{WT}/tPA^{Null} maintained during a period of 3 weeks, prior to whiskers stimulation-induced NVC assays (the stimulated animal appeared in bold. As reported for individual animals, when testing a tPA^{Null} mice (**tPA^{Null}**) of a parabiosis composed of a pair of tPA^{Null} (**tPA^{Null}**/tPA^{Null}), we revealed an impaired NVC compared to a **tPA^{WT}** animal from a pair of tPA^{WT} animals (**tPA^{WT}**/tPA^{WT}) (**Figure 38B-D**) (+9.2 ± 0.4% for **tPA^{Null}**/tPA^{Null} mice, n=8, vs. +11.3 ± 0.4% of CBF increase for **tPA^{WT}**/tPA^{WT} mice, n=7, i.e. -18.5% of CBF increase for **tPA^{Null}**/tPA^{Null} mice compared to **tPA^{WT}**/tPA^{WT} mice, p-value 0.0122). Interestingly, parallel experiments performed from tPA^{Null} mice of hetero-parabiosis (tPA^{Null}/tPA^{WT}) animals, revealed a rescue of NVC to levels similar to the tPA^{WT} animals (**Figure 38B, D-E**) (+12 ± 0.6% of CBF increase for tPA^{Null} mice from a pair of **tPA^{Null}**/tPA^{WT} mice, n=10, vs. +9.2 ± 0.4% for tPA^{Null} mice from a pair of **tPA^{Null}**/tPA^{Null} mice, n=8, p-value 0.0007). All together, these data demonstrate that endogenous levels of circulating tPA directly influence NVC.

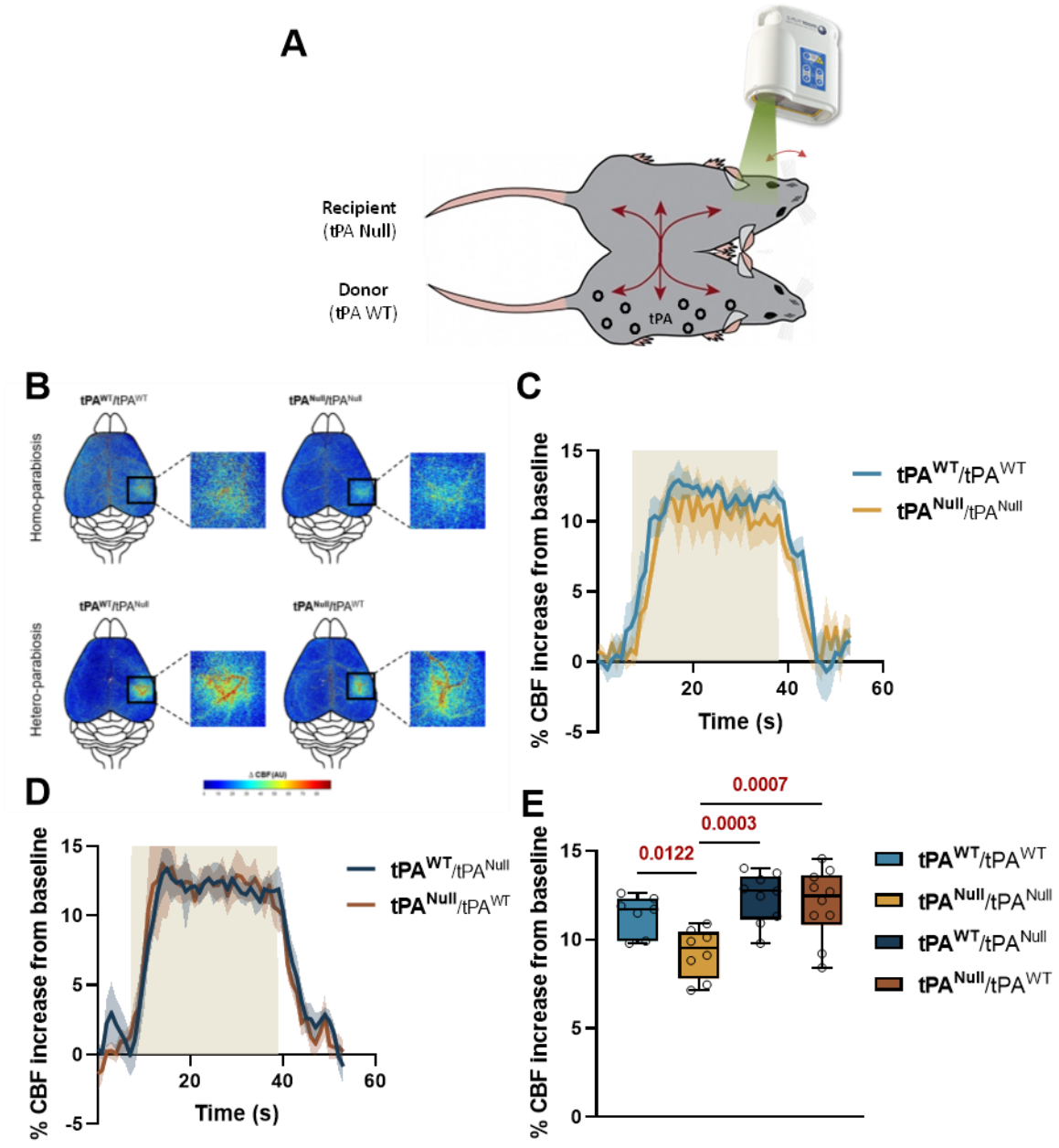

Figure 38 : Endogenous tPA levels influence NVC.

Figure 38 : Endogenous tPA levels influence NVC. A: Schematic representation of the procedure of whiskers stimulations paradigm between two mice (tPA^{Null} and tPA^{WT}) in parabiosis. tPA from the donor (tPA^{WT}) will be share to the recipient (tPA^{Null}). **B**: Colormap corresponds to the activation map related ΔCBF changes during whiskers stimulations in parabiont tPA^{Null} or tPA^{WT} mice. Warm colours indicate an elevation of CBF during whiskers stimulations. **C-D**: Time course of % CBF increase (mean ± SEM) during whiskers stimulations (▭) in homo-parabiosis (**C**) tPA^{WT} (▭) and tPA^{Null}(▭) mice and hetero-parabiosis (**D**) tPA^{WT} (▭) and tPA^{Null}(▭) mice. **E**: Box plots show the variation of % CBF increase from baseline during whiskers stimulations in homo-parabiosis **tPA^{WT}**/tPA^{WT} and **tPA^{Null}**/tPA^{Null}, and hetero-parabiosis **tPA^{WT}**/tPA^{Null} and **tPA^{Null}**/tPA^{WT} (the stimulated mice is mentioned in bold). Box plot with medians, 1st and 3rd quartiles, min and max with values for each mouse. *p < 0.05 and from **tPA^{Null}**/tPA^{Null}, ANOVA and Uncorrected Fisher's LSD tests, n=7 **tPA^{WT}**/tPA^{WT}, n=8 **tPA^{Null}**/tPA^{Null}, n=9 **tPA^{WT}**/tPA^{Null}, n=10 **tPA^{Null}**/tPA^{WT} (n represents the number of stimulated animals).

Endothelial NMDA receptors mediate the vascular tPA-dependent NVC induced by whiskers stimulation.

Our data first revealed an increased neurovascular coupling in VECad-$Cre^{\Delta GluN1}$ mice[20,33] (conditional deletion of endothelial GluN1, **Figure 39A**) compared to VECad-Cre^{WT} control mice (**Figure 39B-F**) (+10 ± 0.7% for VECad-$Cre^{\Delta GluN1}$ mice, n=10, vs. +7.5 ± 0.8% of CBF increase for VECad-Cre^{WT} mice, n=8, i.e. +33.8% of CBF increase for VECad-$Cre^{\Delta GluN1}$ mice compared to VECad-Cre^{WT} mice, p-value 0.0454). The intravenous injection of rtPA (10 mg/kg) was tested in parallel on the two strains. Although intravenous (iv) rtPA led to an increased neurovascular coupling in wild type (VECad-Cre^{WT}) mice, it did not in endothelial deleted GluN1 transgenic mice (VECad-$Cre^{\Delta GluN1}$) (**Figure 39B-F**) (+12.2 ± 1.8% of CBF increase for VECad-Cre^{WT} mice treated by rtPA, n=8, vs. +7.4 ± 0.8% for untreated VECad-Cre^{WT} mice, n=10, i.e. +62.2% of CBF increase VECad-Cre^{WT} mice treated with rtPA compared to untreated VECad-Cre^{WT} mice, p-value 0.0119, +3% of CBF increase for VECad-$Cre^{\Delta GluN1}$ mice treated with rtPA compared to untreated VECad-$Cre^{\Delta GluN1}$ mice, p-value > 0.999). This set of original data demonstrate first that it is the circulating tPA which underlies neurovascular coupling induced by whiskers stimulation in mice; and second, the endothelial NMDA receptors are required to mediate this effect of vascular tPA.

Importantly, these data also demonstrate that the presence of endothelial NMDA receptors is a key mediator of the function of tPA.

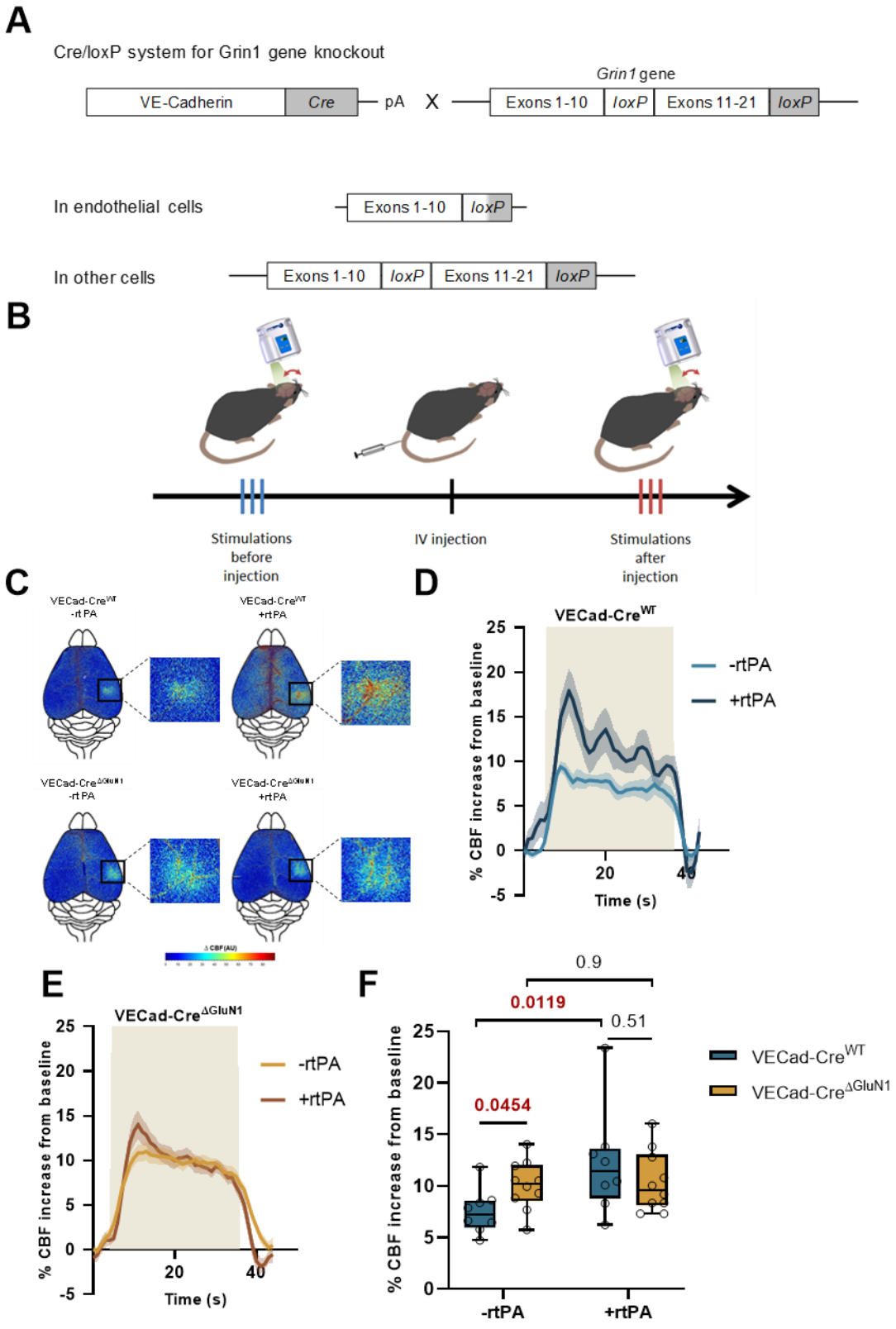

Figure 39 : Endothelial NMDAR controls NVC, an effect mediated by vascular tPA.

Figure 39 : Endothelial NMDAR controls NVC, an effect mediated by vascular tPA. A: Schematic representation of the generation of VE-Cadherin Cre/Grin-1 Lox mice. The cadherin 5 promoter was used to drive expression of CRE in the vascular endothelium. LoxP sites were flanked in the transmembrane and C-term regions of Grin-1 gene (exons 11-21). This configuration carries out the deletion of endothelial Grin-1 gene while conserving Grin-1 in other cells. **B**: Schematic representation of the experimental timeline of whiskers stimulation paradigm. 3 trains of stimulations were made on laser speckle flowmetry before IV infusion of rtPA for 10 minutes and 3 additional trains after. **C**: Colormap corresponds to the activation map related ΔCBF changes during whiskers stimulations in VECad-Cre$^{\Delta GluN1}$ mice and their littermate before and after IV infusion of rtPA. Warm colours indicate an elevation of CBF during whiskers stimulations. **D-E**: Time course of % CBF increase (mean ± SEM) during whiskers stimulations ( ) in VECad-Cre$^{\Delta GluN1}$ mice (**E**) and their littermate (**D**), before (/) and after (/) IV infusion of rtPA. **F**: Box plots show the variations of % CBF increase from baseline during whiskers stimulations in VECad-Cre$^{\Delta GluN1}$ mice and their wild type littermates before and after IV infusions of rtPA. Box plot with medians, 1st and 3rd quartiles, min and max with values for each mouse. *p < 0.05 from VECad-Cre^{WT} or -rtPA, Kruskal-Wallis and Uncorrected Dunn's tests, n=8 VECad-Cre^{WT}, n=10 VECad-Cre$^{\Delta GluN1}$.

Activation of the bradykinin pathway promotes release of tPA in the blood stream and neurovascular coupling.

In order to further investigate how endothelial function/dysfunction may contribute to the ability of vascular tPA to modulate NVC, we decided to test how the couple angiotensin and bradykinin (and related pathways) may be involved, respectively reported to contribute to the regulation of the levels of PAI-1 and tPA in the circulation[36,37]. Thus, animals subjected to whiskers stimulation induced NVC, were previously subjected to intravenous injections of either [Phe8Ψ(CH-NH)-Arg9]-Bradykinin (see methods section) as an agonist for bradykinin type II receptors (B2Rag) (**Figure 40A**) or angiotensin-II (Ang-II, 1 µg/kg/min) (see methods section, **Supplemental figure 5A**). As expected, the B2R agonist (30 µg/kg) led to a decrease of basal mean arterial blood pressure (60 ± 4 mmHg for B2Rag treated animals vs. 91.5 ± 2.9 mmHg for control animals, n=4 per group, p-value 0.0286, **Supplemental figure 3**) and angiotensin-II (1µg/kg/min) led to an increase of basal arterial blood pressure (122.5 ± 4.7 mmHg for Angiotensin-II treated animals vs. 85.75 ± 4 mmHg for control animals, n=4 per group, p-value 0.0286, without affecting physiopathological parameters (**Supplemental figure 4**). Using this procedure, we showed that the CBF

increase evoked by whiskers stimulation was not significantly modified in angiotensin-II treated wild type animals (**Supplemental figure 5B-E**) (+9 ± 0.6% of CBF increase for tPA^{WT} mice treated with Ang-II, n=10, vs. +10.1 ± 0.3% of CBF increase for tPA^{WT} mice, n=10, p-value 0.1067), but that it was significantly increased in B2Rag treated animals compared to the control non treated group (**Figure 40B-E**) (+6 ± 0.4% of CBF increase for tPA^{WT} mice, n=8, vs. +9.7 ± 1.1% of CBF increase for tPA^{WT} treated with B2Rag at 30µg/kg, n=8, p-value 0.0251). We then compared tPA^{WT} and tPA^{Null} mice, treated intravenously with increasing concentrations of the agonist of B2Rag (0, 7, 15, 30 µg/kg). Our data (**Figure 40B-E**), clearly revealed a dose dependent potentiation of the NVC by the agonist of B2R in tPA^{WT} animals and no effect on the tPA^{Null} mice (+18.4% of CBF increase for tPA^{Null} mice at 7 µg/kg of B2Rag, n=6, p-value 0.1951, vs. +28.5% of CBF increase for tPA^{WT} mice, n=8 at 7 µg/kg of B2Rag, p-value 0.0472, when compared to the non-treated tPA^{Null} or tPA^{WT} mice). Parallel experiments were performed to estimate the levels of circulating tPA in the circulation of tPA^{WT} mice subjected to 60 µg/kg of B2Rag as described above (**Figure 40F**). In agreement with our previous data on NVC, B2Rag led to an increase of vascular tPA (+8.7 ng/ml of total tPA after injection of B2Rag, n=4-5, p-value 0.0159, **Figure 40F**). Altogether, these data reveal that activation the bradykinin pathway leads to an increased release of tPA in the blood stream and subsequent potentiation of whiskers stimulation-induced NVC.

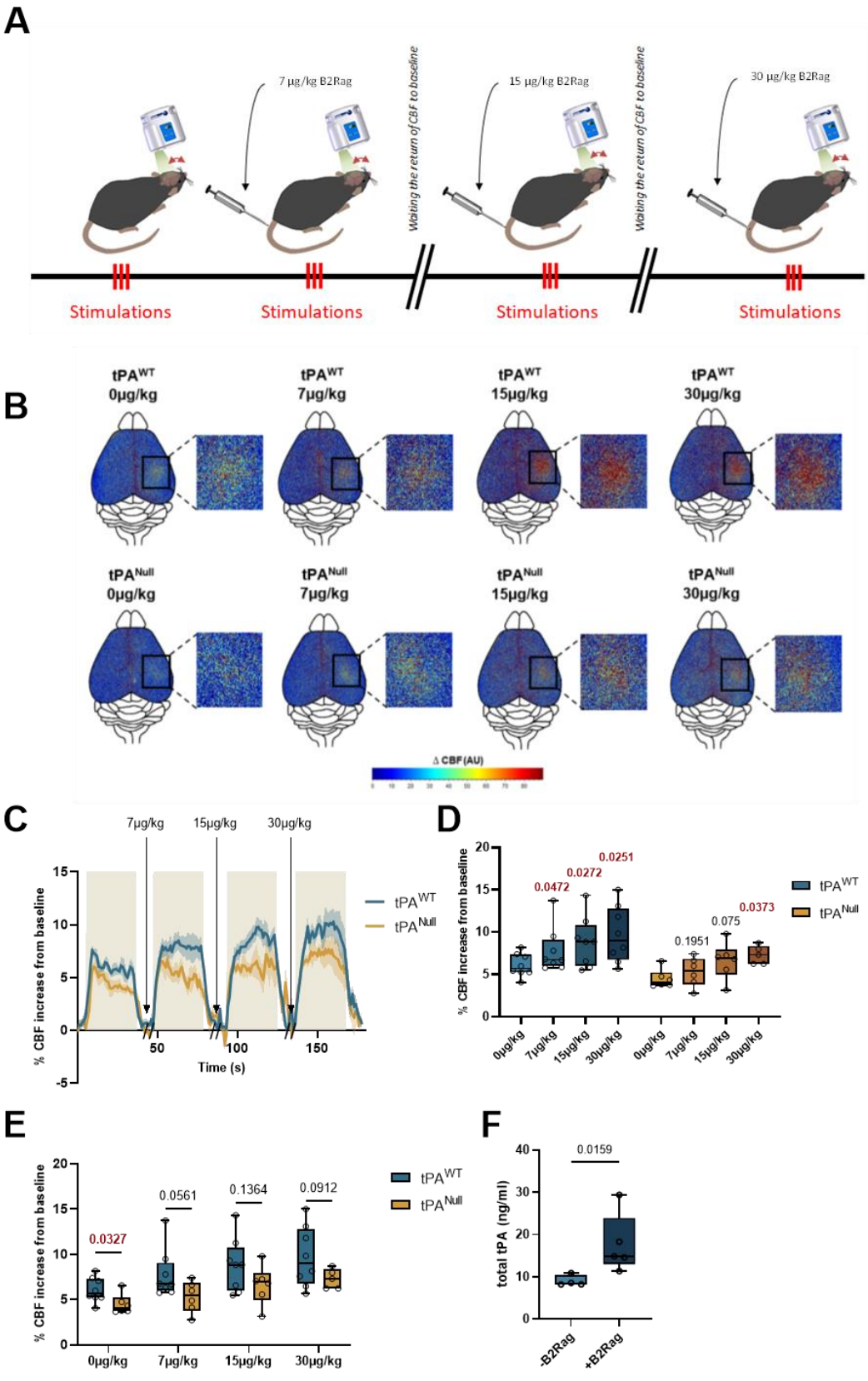

Figure 40 : Intravenous administration of a bradykinin type 2 receptor agonist (B2Rag) influences NVC in a tPA-dependent manner.

Figure 40 : Intravenous administration of a bradykinin type 2 receptor agonist (B2Rag) influences NVC in a tPA-dependent manner. A: Schematic representation of the experimental timeline of whiskers stimulation paradigm. 3 trains of stimulations were made on laser speckle flowmetry 10 minutes after IV injection of B2Rag at different doses (0, 7, 15 and 30 µg/kg). Between each dose, the return of CBF to baseline was waited. **B**: Colormap corresponds to the activation map related ΔCBF changes during whiskers stimulation in tPA^{Null} mice and their wild type littermates for the different doses of B2Rag (0, 7, 15 and 30 µg/kg). Warm colours indicate an elevation of CBF during whiskers stimulations. **C**: Time course of % CBF increase (mean ± SEM) during whiskers stimulations ( ) in tPA^{Null} mice ( ) and their littermate ( ), at different doses of B2Rag (0, 7, 15 and 30 µg/kg). **D-E**: Box plots show the variations of % CBF increase from baseline during whiskers stimulation in tPA^{Null} mice and their wild type littermates for the different doses of B2Rag (0, 7, 15 and 30 µg/kg). Box plot with medians, 1st and 3rd quartiles, min and max with values for each mouse. *p < 0.05 from 0mg/kg or tPA^{WT}, Two-Way-ANOVA and Uncorrected Fisher's LSD tests, n=8 tPA^{WT}, n=6 tPA^{Null}. **F**: Box plots representing ELISA analyses of total tPA in tPA^{WT} mice treated or not with the B2Rag. A saline solution or 60µg/kg of B2Rag were injected intravenously and plasma samples were collected 5 minutes later and subjected to ELISA analysis. Box plots with medians, 1st and 3rd quartiles, min and max with values for each mouse. *p < 0.05 from Vehicle, Mann-Whitney test, n=4 Vehicle, n=5 B2Rag.

tPA released from liver endothelial cells contributes to the regulation of NVC.

We then investigated the cell originate of the circulating tPA involved in the control of NVC. Our data revealed a reduced neurovascular coupling in VECad-$Cre^{\Delta tPA}$ mice[34] (conditional deletion of endothelial tPA, **Figure 41A**) compared to VECad-Cre^{WT} control mice (+10.02 ± 0.3% for VECad-$Cre^{\Delta tPA}$ mice, n=17, vs. +11.4 ± 0.5% of CBF increase for VECad-Cre^{WT} mice, n=14, i.e. -12% of CBF increase for VECad-$Cre^{\Delta tPA}$ mice compared to VECad-Cre^{WT} mice, p-value 0.0358, **Figure 41B-D**). This set of data demonstrate that the tPA produced and released by endothelial cells directly contribute to the modulation of NVC. Since tPA was also expressed from liver, possibly from hepatocytes[38], we decided to investigate whether partial hepatectomy (see methods section) may influence NVC induced by whiskers stimulation (**Figure 42**). These experiments were performed both on tPA^{WT} and tPA^{Null} mice. As reported above (**Figure 37A-C**), tPA^{Null} mice displayed a deficit in NVC induced by whiskers stimulation compared to WT animals (+7.16 ± 0.46% of CBF increase for WT mice, n=18, vs. +5.67

± 0.49% for tPA^{Null} mice, n=16, i.e. -20.5% of CBF increase for tPA^{Null} mice compared to tPA^{WT} mice, p-value 0.0167), an effect also observed in WT animals following partial hepatectomy (+9.58 ± 0.45% for Ligatured tPA^{WT} mice, n=9, vs. +11.63 ± 0.63% of CBF increase for Sham tPA^{WT} mice, n=4, i.e. -17.5% of CBF increase for Ligatured tPA^{WT} mice compared to Sham tPA^{WT} mice, p-value 0.037). No difference was observed between tPA^{WT} and tPA^{Null} mice following partial hepatectomy (+10.38 ± 0.7% for Ligatured tPA^{Null} mice, n=10, vs. +9.58 ± 0.45% of CBF increase for Ligatured tPA^{WT} mice, n=9, i.e. +8.3% of CBF increase for Ligatured tPA^{Null} mice compared to Ligatured tPA^{WT} mice, p-value 0.41). The data suggest that the vascular tPA involved in NVC induced by whiskers stimulation is from liver origin. To determine whether this tPA from liver originate was produced by endothelial cells or hepatocytes, we performed conditional deletion of possible hepatocytic tPA (see methods section) (**Supplemental figure 7**). Using the VECad-$Cre^{\Delta tPA}$ mice, we performed hydrodynamic transfection of hepatocytes using a pLIVE-Cre-GFP promoter. Anti-GFP and anti-CRE immunostainings confirmed the hepatocytic expression of the Cre-GFP in hepatocytes (**Supplemental figure 6**), leading to an additional conditional deletion (in addition of the endothelial deletion of tPA reported above (see **Figure 6**) of a putative hepatocytic tPA. Our data revealed no modification of neurovascular coupling in VECad-$Cre^{\Delta tPA}$ mice transfected with a pLIVE-Cre-GFP (conditional deletion of endothelial and heptacytic tPA) compared to VECad-$Cre^{\Delta tPA}$ mice transfected with an empty-pLIVE (conditional deletion of endothelial tPA only) (**Supplemental figure 7**) (+10.45 ± 0.59% of CBF increase for VECad-$Cre^{\Delta tPA}$ mice transfected with pLIVE-CRE-GFP, n=6, vs. +11.36 ± 0.7% for VECad-$Cre^{\Delta tPA}$ mice transfected with empty-pLive, n=10, i.e. +8.64% of CBF increase for VECad-$Cre^{\Delta tPA}$ mice transfected with pLIVE-CRE-GFP compared to VECad-$Cre^{\Delta tPA}$ mice transfected with an empty-pLIVE, p-value 0.29). Altogether, these data demonstrate that the tPA involved in NVC induced by whiskers stimulation is from liver endothelial origin. These data are in agreement with the immunohistochemistry performed from mouse brain and liver tissues (**Figure 7**), confirming the presence of tPA in both liver and brain endothelial cells.

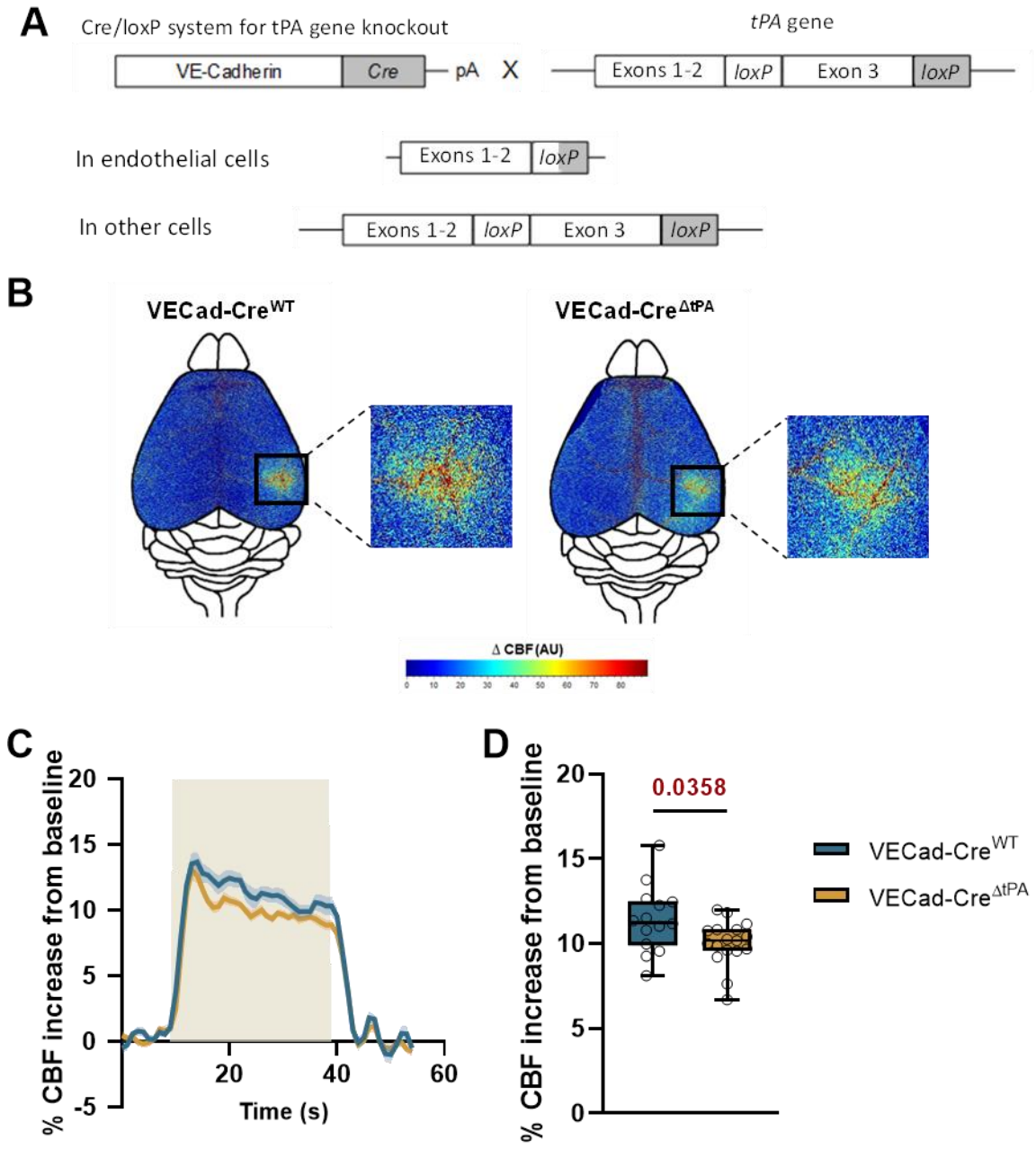

Figure 41 : Endothelial tPA controls NVC.

Figure 41 : Endothelial tPA controls NVC. A: Schematic representation of the generation of VE-Cadherin Cre/tPA Lox mice. The cadherin 5 promoter was used to drive expression of Cre in the vascular endothelium. LoxP sites were flanked in the exon 3 of tPA gene. This configuration carries out the deletion of endothelial tPA gene while conserving tPA in other cells. **B:** Colormap corresponds to the activation map related ΔCBF changes during whiskers stimulations of VECad-Cre$^{\Delta tPA}$ mice and their wild type littermates. Maps were obtained by subtraction of stimulation frames and resting frames. Warm colours indicate an elevation of CBF during whiskers stimulations. **C:** Time course of % CBF increase (mean ± SEM) during whiskers stimulations ( ) of VECad-Cre$^{\Delta tPA}$ ( ) and their littermates ( ). **D:** Box plots show the variations of % CBF increase from baseline during whiskers stimulation of VECad-Cre$^{\Delta tPA}$ mice and their littermates. Box plot with medians, 1st and 3rd quartiles, min and max with values for each mouse. *p < 0.05 from VECad-Cre^{WT}, Mann-Whitney test, n=14/17 VECad-Cre^{WT}/ VECad-Cre$^{\Delta tPA}$.

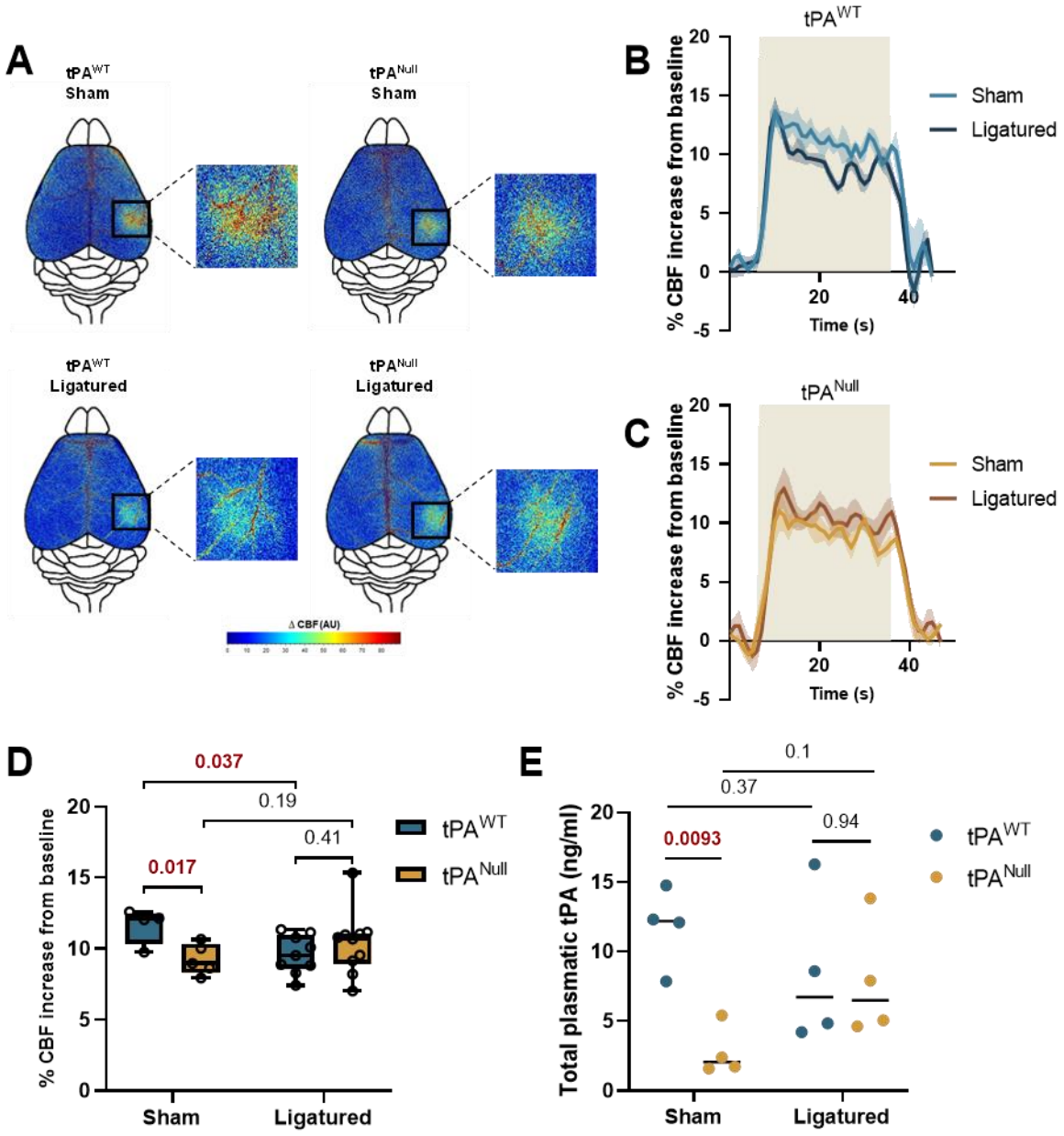

Figure 42 : Partial hepatectomy influences NVC.

Figure 42 : Partial hepatectomy influences NVC. A: Colormap corresponds to the activation map related ΔCBF changes during whiskers stimulations in tPA^{Null} mice and their littermate in sham and ligatured conditions 24h after partial hepatectomy. Warm colours indicate an elevation of CBF during whiskers stimulations. **B-C**: Time course of % CBF increase (mean ± SEM) during whiskers stimulations ( ) in tPA^{Null} mice (**C**) and their littermate (**B**), in sham (—/—) or ligatured (—/—) conditions. **D**: Box plots show the variation of % CBF increase from baseline during whiskers stimulations in tPA^{Null} mice and their littermate in sham and ligatured conditions. Box plot with medians, 1st and 3rd quartiles, min and max with values for each mouse. **E**: Mean ± SEM representing ELISA analyses of total tPA in tPA^{Null} mice and their littermate in sham and ligatured conditions (n=4 for each group). 24h after partial hepatectomy, plasma samples were collected and subjected to ELISA analysis. *p < 0.05 from sham tPA^{WT}, Kruskal-Wallis and Uncorrected Dunn's tests, n=4 sham tPA^{WT}, n=9 ligatured tPA^{WT}, n=5 sham tPA^{Null}, n=10 ligatured tPA^{Null}.

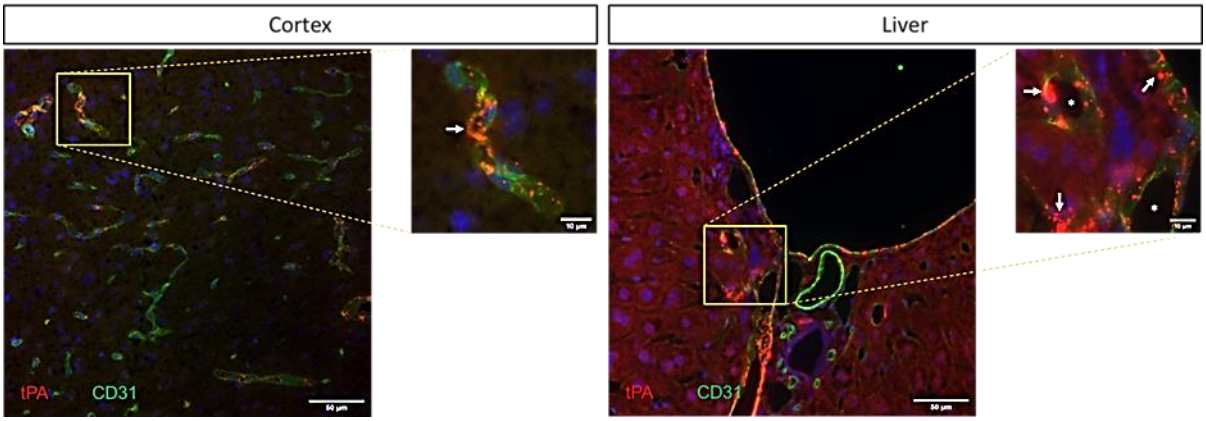

Figure 43 : tPA is present in brain and liver endothelial cells. Epifluorescence images of brain cortex and liver slices from C57BL/6 adult mice (Scale bar = 50 µm, zooms = 10 µm) revealing tPA (red), CD31 (green) and cells nuclei (DAPI, blue). tPA was observed in endothelial cells (arrow) in both brain cortex and liver. Lumen of vessels was represented by stars. Images were digitally captured using a camera (CoolSNAP; Photometrics) and/or with an inverted confocal microscope (SP5, Leica). Images were visualized respectively with Metavue 5.0 software (Molecular Devices, USA) and LAS AF lite software (LEICA).

Discussion

We have demonstrated that physiological levels of vascular tPA, from liver origin, contributes to the modulation of functional hyperemia mediated by brain endothelial NMDAR activation. Indeed, deficiency in tPA reduced functional hyperemia induced by whiskers stimulation in mice, whereas deficiency of PAI-1 increased it. Deletion of tPA is rescued by intravenous injection of tPA or by parabiosis with WT animals. Our data also reveal a key role of endothelial cells in this process, with conditional deletion of endothelial tPA leading to reduced functional hyperemia induced by whiskers stimulation and deletion of endothelial NMDA receptors leading to lack of response to tPA induced NVC. We also show that bradykinin receptors type 2 activation induces both release of tPA in the vasculature and subsequent potentiation of NVC. Our data also demonstrate that physiological levels of vascular tPA directly contribute to the efficiency of neurovascular coupling. Finally, we evidenced that the vascular tPA involved in the NVC induced by whiskers stimulation is from liver endothelial cells origin. Altogether, these data unmask a new pathway contributing to the complex neurovascular coupling regulation.

This new mechanism may explain, some of the physiological and pathological brain functions of tPA reported so far. For instance, tPA was reported to display important functions in learning and memory processes[10,11], cognitive processes directly linked with neuronal activation and subsequent neurovascular coupling[39]. Similarly, tPA and its inhibitor PAI-1 have been reported to interfere with Aβ-induced attenuation of neurovascular coupling[17]. Up to know and in agreement with an extensive literature, mechanisms of NVC associated with these phenotypes, were mainly associated with events occurring from the parenchyma to the vasculature. Our present data lead to integrate that NVC also involved mechanisms occurring from the blood stream to the vasculature[3]. It is thus interesting to note, that blood transfusion from young to old mice, was reported to revitalize old brain and to reverse subsequent decline[40].

Neurovascular coupling has been linked to neuronal activation in general, mediated by a wide variety of vasoactive agents targeting different segments of the cerebrovascular tree[1]. Of these, Nitric Oxyde (NO) derived from NMDAR activity mediates a significant fraction of the response, and tPA is required for the full expression of this component

by enabling NO production during NMDAR activation[16,18]. Here we found that the levels of circulating tPA activity also contribute to neurovascular coupling. NMDA receptors signaling is a key process of neuronal mediated NVC[41]. Here, we demonstrate that the NMDA receptors-dependent control of NVC also involve the NMDA receptors expressed at the luminal side of the endothelial cells. Endothelial NMDA receptors have been already identified as key actors of neuroinflammatory processes[20], also known to influence the efficiency of NVC[42].

Some studies have indicated that tPA modulates Ca^{2+} influx through NMDAR by interacting with the extracellular domain of the GluN1 subunit[43]. Other studies have suggested that tPA does not act on NMDAR directly, but through LRP1 (Low Density Lipoprotein Related Protein-1)[44–46], which, like neuronal Oxyde Nitric Synthase (nNOS), is bridged to the NMDA receptor complex through the adaptor protein Post Synaptic Density Protein-95 (PSD-95)[47–50]. All these studies were reported from neuronal investigations. But NMDA receptors are also exhibited by endothelial cells[22,51] and LRP1 too[52,53]. On endothelial cells, tPA was reported to mediate NMDAR-dependent signaling, involving differential phosphorylation of proteins associated with tight-junctions, such as the myosin light chain (MLC-1)[51]. Our observation that the effects of vascular tPA on functional hyperemia are prevented by the conditional deletion of endothelial GluN1 subunit of NMDA are supported by the above literature. Our data also suggest that endothelial NMDA receptors play a negative vasoconstrictive tonus on the vessels in basal conditions, a process inhibited by tPA.

Increases in PAI-1 expression have also been described in relation with neurovascular and cardiovascular diseases[54–56]. PAI-1 levels are also modulated in neurodegenerative disorders, especially in the context of Alzheimer's disease[57], a disease in which neurovascular coupling is dramatically affected[58–60]. Thus, targeting the tPA dependent and NMDAR dependent modulation of NVC may have important clinical applications. Bradykinin (BK) is a vasoactive polypeptide that has cardioprotective effects[61], causing endothelium-dependent vasodilation by activating its endothelial B2 receptors, present in the lumen side of the vessels[62]. Interestingly, BK has been shown to promote tPA secretion in isolated perfused vascular systems[63]. Here, we evidenced that BK, and not angiotensin, promotes the release of active tPA in the blood stream in vivo via B2R, leading to a tPA-dependent specific increase of NVC. PAI-1 is among the factors released in the circulation by endothelial cells in the

context of endothelial dysfunction[64]. At the opposite release of tPA is more usually associated with normal endothelial function[65,66]. In parallel, it is widely accepted that vascular endothelial cells, through the release of NO, prostacyclin, tPA and PAI-1, play important roles in the regulation of thrombosis and fibrinolysis, mechanisms also highly related with impaired NVC[67–69].

The consensus would be that the main amount of tPA in the blood stream would come from hepatocytes and that the endothelial cells would contribute to the local and/or fast changes in tPA levels[70,71] . Our present data reveal that the vascular tPA involved in the control of the NVC induced by whiskers stimulation is coming from the liver, but from endothelial origin.

In conclusion, we have demonstrated that changes in circulating tPA levels, modulated by activation of endothelial bradykinin receptors, presumably coming from the liver endothelial cells, contributed to the regulation of NVC, through modulation of cerebral endothelial NMDA receptors. The data unveil a previously unappreciated role of the circulating tPA in the control of neurovascular coupling and subsequent cerebral physiopathology axis with potential therapeutic implications.

Acknowledgments

This work was supported by grants from the Ministère de l'Enseignement Supérieur et de la Recherche and INSERM (French National Institute for Health and Medical Research) (HCERES U1237-2017/2022) and the PLATMED European program (EURONANOMED2020-143).

Conflict of Interest

The authors declare that the research was conducted in the absence of any commercial or financial relationships that could be construed as a potential conflict of interest.

Authorship contributions

D.V., C.A., SMDL., Y.H., MY, JF designed the study. D.V., C.A., Z.Z., M.Y. wrote the manuscript; M.Y., J.F., E.P., E.M., Y.H., L.L. performed experiments. All authors analyzed the data and reviewed the manuscript.

References

1. Iadecola C. The Neurovascular Unit Coming of Age: A Journey through Neurovascular Coupling in Health and Disease. Neuron. 2017;96(1):17–42.

2. Sweeney MD, Kisler K, Montagne A, Toga AW, Zlokovic B v. The role of brain vasculature in neurodegenerative disorders. Nature Neuroscience. 2018;21(10):1318–1331.

3. Girouard H, Iadecola C. Neurovascular coupling in the normal brain and in hypertension, stroke, and Alzheimer disease. Journal of Applied Physiology. 2006;100(1):328–335.

4. Collen D, Lijnen HR. Tissue-type plasminogen activator: a historical perspective and personal account. 2004.

5. Teesalu T, Kulla A, Simisker A, et al. Tissue plasminogen activator and neuroserpin are widely expressed in the human central nervous system. Thrombosis and Haemostasis. 2004;92(2):358–368.

6. Louessard M, Lacroix A, Martineau M, et al. Tissue Plasminogen Activator Expression Is Restricted to Subsets of Excitatory Pyramidal Glutamatergic Neurons. Molecular Neurobiology. 2016;53(7):5000–5012.

7. Lochner JE, Honigman LS, Grant WF, et al. Activity-dependent release of tissue plasminogen activator from the dendritic spines of hippocampal neurons revealed by live-cell imaging. Journal of Neurobiology. 2006;66(6):564–577.

8. Angles-Cano E, Balaton A, le Bonniec B, et al. Production of monoclonal antibodies to the high fibrin-affinity, tissue- type plasminogen activator of human plasma. Demonstration of its endothelial origin by immunolocalization. Blood. 1985;66(4):.

9. Thiebaut AM, Gauberti M, Ali C, et al. The role of plasminogen activators in stroke treatment: fibrinolysis and beyond. The Lancet. Neurology. 2018;17(12):.

10. Hébert M, Anfray A, Chevilley A, et al. Distant Space Processing is Controlled by tPA-dependent NMDA Receptor Signaling in the Entorhinal Cortex. Cerebral Cortex. 2017;27(10):4783–4796.

11. Benchenane K, Castel H, Boulouard M, et al. Anti-NR1 N-terminal-domain vaccination unmasks the crucial action of tPA on NMDA-receptor-mediated toxicity and spatial memory. Journal of Cell Science. 2007;120(4):578–585.

12. Pawlak R, Magarinos AM, Melchor J, McEwen B, Strickland S. Tissue plasminogen activator in the amygdala is critical for stress-induced anxiety-like behavior. Nature Neuroscience. 2003;6(2):168–174.

13. Matys T, Pawlak R, Matys E, et al. Tissue plasminogen activator promotes the effects of corticotropin-releasing factor on the amygdala and anxiety-like behavior. Proceedings of the National Academy of Sciences of the United States of America. 2004;101(46):.

14. Wardlaw JM, Doubal FN, Valdes-Hernandez M, et al. Blood-brain barrier permeability and long-term clinical and imaging outcomes in cerebral small vessel disease. Stroke. 2013;44(2):525–527.

15. Marcos-Contreras OA, Martinez de Lizarrondo S, Bardou I, et al. Hyperfibrinolysis increases blood-brain barrier permeability by a plasmin- and bradykinin-dependent mechanism. Blood. 2016;128(20):.

16. Park L, Gallo EF, Anrather J, et al. Key role of tissue plasminogen activator in neurovascular coupling. 2008.

17. Park L, Zhou J, Koizumi K, et al. TPA deficiency underlies neurovascular coupling dysfunction by amyloid-b. Journal of Neuroscience. 2020;40(42):8160–8173.

18. Anfray A, Drieu A, Hingot V, et al. Circulating tPA contributes to neurovascular coupling by a mechanism involving the endothelial NMDA receptors. Journal of Cerebral Blood Flow and Metabolism. 2020;40(10):2038–2054.

19. Nakazawa K, McHugh TJ, Wilson MA, Tonegawa S. NMDA receptors, place cells and hippocampal spatial memory. Nature Reviews Neuroscience. 2004;5(5):361–372.

20. Macrez R, Ortega MC, Bardou I, et al. Neuroendothelial NMDA receptors as therapeutic targets in experimental autoimmune encephalomyelitis. Brain. 2016;139(9):2406–2419.

21. Reijerkerk A, Kooij G, van der Pol SMA, et al. The NR1 subunit of NMDA receptor regulates monocyte transmigration through the brain endothelial cell barrier. Journal of Neurochemistry. 2010;113(2):447–453.

22. Peters EC, Gee MT, Pawlowski LN, et al. Amyloid-β disrupts unitary calcium entry through endothelial NMDA receptors in mouse cerebral arteries. Journal of cerebral blood flow and metabolism : official journal of the International Society of Cerebral Blood Flow and Metabolism. 2021;

23. Zheng Z, Nayak L, Wang W, et al. An ATF6-tPA pathway in hepatocytes contributes to systemic fibrinolysis and is repressed by DACH1. Blood. 2019;133(7):.

24. Samad F, Yamamoto K, Loskutoff DJ. Distribution and regulation of plasminogen activator inhibitor-1 in murine adipose tissue in vivo: Induction by tumor necrosis factor-α and lipopolysaccharide. Journal of Clinical Investigation. 1996;97(1):37–46.

25. Ny T, Sawdey M, Lawrence D, Millan JL, Loskutoff DJ. Cloning and sequence of a cDNA coding for the human beta-migrating endothelial-cell-type plasminogen activator inhibitor. Proceedings of the National Academy of Sciences of the United States of America. 1986;83(18):.

26. Ny T, Sawdey M, Lawrence D, Millant JL, Loskutoff DJ. Cloning and sequence of a cDNA coding for the human a-migrating endothelial-cell-type plasminogen activator inhibitor (vascular fibrinolysis/serine protease inhibitor/placental cDNA expression library/DNA sequence analysis). 1986.

27. Medcalf RL. Fibrinolysis: from blood to the brain. Journal of Thrombosis and Haemostasis. 2017;15(11):2089–2098.

28. Shi K, Zou M, Jia DM, et al. TPA Mobilizes Immune Cells That Exacerbate Hemorrhagic Transformation in Stroke. Circulation Research. 2021;62–75.

29. Brown NJ, Gainer J v, Murphey LJ, Vaughan DE. Bradykinin Stimulates Tissue Plasminogen Activator Release From Human Forearm Vasculature Through B 2

Receptor-Dependent, NO Synthase-Independent, and Cyclooxygenase-Independent Pathway. 2000.

30. Kerins DM, Hao Q, Vaughan DE. Angiotensin induction of PAI-1 expression in endothelial cells is mediated by the hexapeptide angiotensin IV. Journal of Clinical Investigation. 1995;96(5):2515–2520.

31. Nordt TK, Lohrmann J, Bode C. Regulation of PAI-1 expression by genetic polymorphisms. Impact on atherogenesis. Thrombosis research. 2001;103 Suppl 1:

32. Pasquet N, Douceau S, Naveau M, et al. Tissue-Type Plasminogen Activator Controlled Corticogenesis Through a Mechanism Dependent of NMDA Receptors Expressed on Radial Glial Cells. Cerebral Cortex. 2019;29(6):2482–2498.

33. Léger C, Dupré N, Aligny C, et al. Glutamate controls vessel-associated migration of GABA interneurons from the pial migratory route via NMDA receptors and endothelial protease activation. Cellular and Molecular Life Sciences. 2020;77(10):1959–1986.

34. Alva JA, Zovein AC, Monvoisin A, et al. VE-cadherin-cre-recombinase transgenic mouse: A tool for lineage analysis and gene deletion in endothelial cells. Developmental Dynamics. 2006;235(3):759–767.

35. Kamran P, Sereti KI, Zhao P, et al. Parabiosis in mice: a detailed protocol. Journal of visualized experiments : JoVE. 2013;(80):.

36. Vaughan DE, Lazos SA, Tong K. Angiotensin II Regulates the Expression of Plasminogen Activator Inhibitor-1 in Cultured Endothelial Cells: A Potential Link between the Renin-Angiotensin System and Thrombosis. Journal of Clinical Investigation. 1995;95(3):995–1001.

37. Minai K, Matsumoto T, Horie H, et al. Bradykinin stimulates the release of tissue plasminogen activator in human coronary circulation: effects of angiotensin-converting enzyme inhibitors. Journal of the American College of Cardiology. 2001;37(6):.

38. Ping Zhang L, Takahara T, Yata Y, et al. Increased expression of phninogen activator and phsminogen activator inhibitor during liver fibrogenesis of ratx role of stellate cells. Journal of Hepatology. 1999;31:703–711.

39. Lefferts WK, Deblois JP, Barreira T v, Heffernan KS. Neurovascular coupling during cognitive activity in adults with controlled hypertension. J Appl Physiol. 2018;125:1906–1916.

40. Wyss-Coray T. Ageing, neurodegeneration and brain rejuvenation. Nature. 2016;539(7628):180–186.

41. Mapelli L, Gagliano G, Soda T, et al. Granular layer neurons control cerebellar neurovascular coupling through an NMDA receptor/NO-dependent system. Journal of Neuroscience. 2017;37(5):1340–1351.

42. Fulop GA, Ahire C, Csipo T, et al. Cerebral venous congestion promotes blood-brain barrier disruption and neuroinflammation, impairing cognitive function in mice. GeroScience. 2019;41(5):575–589.

43. Nicole O, Docagne F, Ali C, et al. The proteolytic activity of tissue-plasminogen activator enhances NMDA receptor-mediated signaling. Nature medicine. 2001;7(1):.

44. Martin AM, Kuhlmann C, Trossbach S, et al. The functional role of the second NPXY motif of the LRP1 β-chain in tissue-type plasminogen activator-mediated activation of N-methyl-D-aspartate receptors. Journal of Biological Chemistry. 2008;283(18):12004–12013.

45. Samson AL, Nevin ST, Croucher D, et al. Tissue-type plasminogen activator requires a co-receptor to enhance NMDA receptor function. Journal of Neurochemistry. 2008;107(4):1091–1101.

46. Mantuano E, Lam MS, Gonias SL. LRP1 assembles unique co-receptor systems to initiate cell signaling in response to tissue-type plasminogen activator and Myelin-associated glycoprotein. Journal of Biological Chemistry. 2013;288(47):34009–34018.

47. Gotthardt M, Trommsdorff M, Nevitt MF, et al. Interactions of the low density lipoprotein receptor gene family with cytosolic adaptor and scaffold proteins suggest diverse biological functions in cellular communication and signal transduction. Journal of Biological Chemistry. 2000;275(33):25616–25624.

48. May P, Rohlmann A, Bock HH, et al. Neuronal LRP1 Functionally Associates with Postsynaptic Proteins and Is Required for Normal Motor Function in Mice. Molecular and Cellular Biology. 2004;24(20):8872–8883.

49. Nakajima C, Kulik A, Frotscher M, et al. Low density lipoprotein receptor-related protein 1 (LRP1) modulates N-methyl-D-aspartate (NMDA) receptor-dependent intracellular signaling and NMDA-induced regulation of postsynaptic protein complexes. Journal of Biological Chemistry. 2013;288(30):21909–21923.

50. Norris EH, Strickland S. Modulation of NR2B-regulated contextual fear in the hippocampus by the tissue plasminogen activator system. Proceedings of the National Academy of Sciences of the United States of America. 2007;104(33):.

51. Mehra A, Guérit S, Macrez R, et al. Nonionotropic action of endothelial NMDA receptors on blood–brain barrier permeability via Rho/ROCK-mediated phosphorylation of myosin. Journal of Neuroscience. 2020;40(8):1778–1787.

52. Shibata M, Yamada S, Ram Kumar S, et al. Clearance of Alzheimer's amyloid-β1-40 peptide from brain by LDL receptor-related protein-1 at the blood-brain barrier. Journal of Clinical Investigation. 2000;106(12):1489–1499.

53. Storck SE, Pietrzik CU. Endothelial LRP1 – A Potential Target for the Treatment of Alzheimer's Disease: Theme: Drug Discovery, Development and Delivery in Alzheimer's Disease Guest Editor: Davide Brambilla. Pharmaceutical Research. 2017;34(12):2637–2651.

54. Jung RG, Simard T, Labinaz A, et al. Role of plasminogen activator inhibitor-1 in coronary pathophysiology. Thrombosis Research. 2018;164:54–62.

55. Yu BY, Subudeng G, Du CG, et al. Plasminogen activator, tissue type regulates germinal vesicle breakdown and cumulus expansion of bovine cumulus-oocyte complex in vitro. Biology of Reproduction. 2019;100(6):1473–1481.

56. Rosenberg RD, Aird WC. Vascular-bed--specific hemostasis and hypercoagulable states. The New England journal of medicine. 1999;340(20):.

57. Oh J, Lee HJ, Song JH, Park SI, Kim H. Plasminogen activator inhibitor-1 as an early potential diagnostic marker for Alzheimer's disease. Experimental Gerontology. 2014;60:87–91.

58. Tarantini S, Tran CHT, Gordon GR, Ungvari Z, Csiszar A. Impaired neurovascular coupling in aging and Alzheimer's disease: Contribution of astrocyte dysfunction and endothelial impairment to cognitive decline. Experimental Gerontology. 2017;94:52–58.

59. Nicolakakis N, Aboulkassim T, Ongali B, et al. Complete rescue of cerebrovascular function in aged Alzheimer's disease transgenic mice by antioxidants and pioglitazone, a peroxisome proliferator-activated receptor γ agonist. Journal of Neuroscience. 2008;28(37):9287–9296.

60. Kisler K, Nelson AR, Montagne A, Zlokovic B v. Cerebral blood flow regulation and neurovascular dysfunction in Alzheimer disease. Nature Reviews Neuroscience. 2017;18(7):419–434.

61. Starkopf J, Bugge E, Ytrehus K. Preischemic bradykinin and ischaemic preconditioning in functional recovery of the globally ischaemic rat heart. Cardiovascular research. 1997;33(1):.

62. van Guilder GP, Pretorius M, Luther JM, et al. Bradykinin type 2 receptor BE1 genotype influences bradykinin-dependent vasodilation during angiotensin-converting enzyme inhibition. Hypertension. 2008;51(2 PART 2):454–459.

63. Emeis JJ. Perfused rat hindlegs. A model to study plasminogen activator release. Thrombosis research. 1983;30(3):.

64. Jacobs A, Schutte AE, Ricci C, Pieters M. Plasminogen activator inhibitor-1 activity and the 4G/5G polymorphism are prospectively associated with blood pressure and hypertension status. Journal of Hypertension. 2019;37(12):2361–2370.

65. Stein CM, Brown N, Vaughan DE, Lang CC, Wood AJ. Regulation of local tissue-type plasminogen activator release by endothelium-dependent and endothelium-independent agonists in human vasculature. Journal of the American College of Cardiology. 1998;32(1):.

66. Muldowney JA, Vaughan DE. Tissue-type plasminogen activator release: new frontiers in endothelial function. Journal of the American College of Cardiology. 2002;40(5):.

67. Thors B, Halldórsson H, Jónsdóttir G, Thorgeirsson G. Mechanism of thrombin mediated eNOS phosphorylation in endothelial cells is dependent on ATP levels after stimulation. Biochimica et Biophysica Acta - Molecular Cell Research. 2008;1783(10):1893–1902.

68. Koide M, Bonev AD, Nelson MT, Wellman GC. Inversion of neurovascular coupling by subarachnoid blood depends on large-conductance Ca2+-activated K+(BK) channels. Proceedings of the National Academy of Sciences of the United States of America. 2012;109(21):.

69. Braaten J v, Handt S, Jerome WG, et al. Regulation of fibrinolysis by platelet-released plasminogen activator inhibitor 1: light scattering and ultrastructural examination of lysis of a model platelet-fibrin thrombus. Blood. 1993;81(5):.

70. Zheng Z, Nakamura K, Gershbaum S, et al. Interacting hepatic PAI-1/tPA gene regulatory pathways influence impaired fibrinolysis severity in obesity. Journal of Clinical Investigation. 2020;140(8):4348–4359.

71. Emeis J. The Control of tPA and PAI-1 Secretion from the Vessel Wall. Vascular Medicine Review. 1995;vmr-6(2):.

Supplemental materials and methods

Magnetic Resonance Imaging (MRI)

The MRI studies were realized 3 weeks after parabiosis surgery. Parabionts were placed in a rat cradle (to image both animals at the same time). Animals were anesthetized using 5% isoflurane (Isoflurane Belamont) in 50% N_2O/50% O_2, then maintained under 2% isoflurane in 100% N_2O/100% O_2. They were monitored by a breathing module in order to adapt the anesthesia according to the respiratory rate and they were thermoregulated by a heating blanket beeween 36.5°C and 37.5°C. The chimerism validation was assessed by injecting DOTA-Gd (Dotarem®), 0.01mMol/ml through a tail vein catheter in MRI. Then MRI sequences (7T MRI, Bruker, Germany) of T2-weighted and T1-weighted are respectively realized on whole animals' body. MRI analyses were performed until 75 minutes after the injection. Images analysis were made with an extension of ImageJ (Fiji). We obtained final images by making substraction between "After Injection Time" and "Before Injection Time", to correct the signal difference for T1-weighted sequence.

Hydrodynamic transfection

Hydrodynamic transfections were performed as previously described[34]. Awake mice were injected with either 100µg engineered pLIVE encoding Cre-green fluorescent protein (pLIVE-Cre-GFP) or pLIVE plasmid alone (empty-pLIVE). A large volume (10% of body weight) of plasmid-containing saline buffer (0.9% NaCl) was injected into the caudal vein in less than 5 seconds for hepatic transfection. After 48 hours, Laser Doppler Speckle was realized (see Laser Doppler Speckle section) to measure modifications of the CBF induced by whiskers stimulations. Liver tissues were collected after transcardiac perfusions with cold heparinized saline (15 ml/min) followed by a solution of 4% paraformaldehyde (see Supplemental materials and methods section).

Immunohistochemistry

Deeply anesthetized mice were transcardially perfused with cold heparinized saline (15 ml/min), then with 4% paraformaldehyde in 0.1 M sodium phosphate buffer, pH 7.4

(150 ml, 15 ml/min). Liver segments were removed and washed in veronal buffer containing 20% sucrose for 24h, and frozen in Tissue-Tek (Miles Scientific). Transversal sections of liver (10 µm) were cut on a cryostat, then collected on poly-D-lysine slides and stored at -80°C. Liver sections were incubated overnight at room temperature with primary antibodies rabbit anti GFP (1:1000, ab6556, Abcam), mouse anti Cre-recombinase (1:1000, MAB3120, Millipore) and phalloidin (1:1000, ab176759, Abcam). Primary antibodies were revelated using Fab'2 fragment anti-rabbit IgG linked to FITC and anti-mouse linked to CY3 (1:800, 711-546-155 / 715-165-150, Jackson ImmunoReasearch) co-incubated 90 min at room temperature. Sections were then coverslipped using mounting medium containing DAPI. Images were digitally captured using an epifluorescence microscope (Leica DM6000). Images were assessed using ImageJ software (NIH).

Supplemental figures

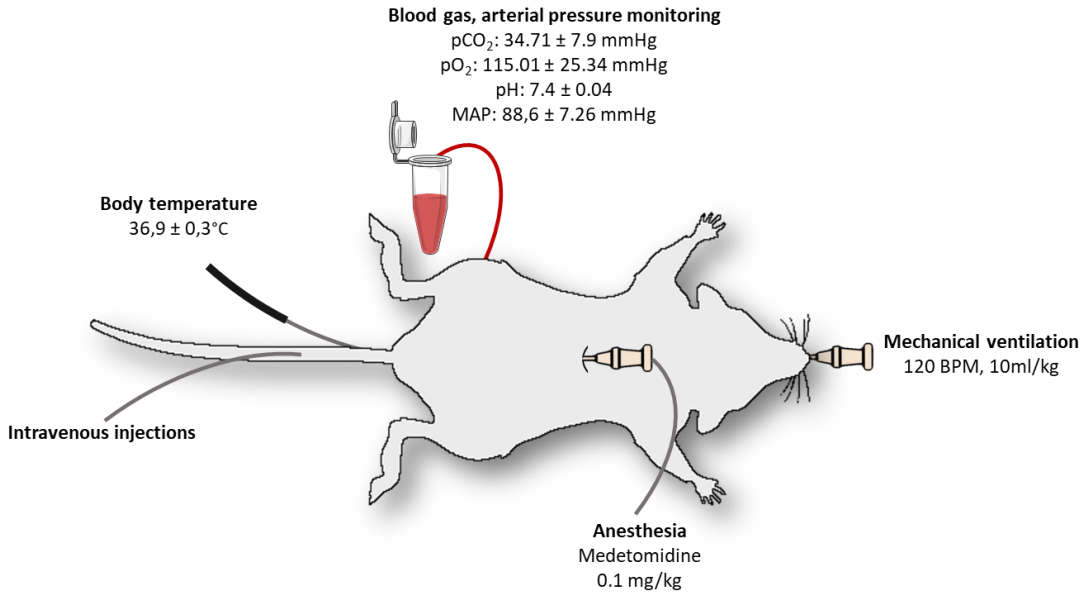

Supplemental figure 1 : Mice physiological parameters measured during whiskers stimulations. Mice physiological parameters during experimental procedure of whiskers stimulations. Mice were mechanically ventilated (120 BPM, 10 ml/kg). Blood samples were collected by a femoral catheter and mean arterial pressure (MAP) was measured. Pharmacological treatments were injected via a tail vein catheter. Data are mean with SD, n=8.

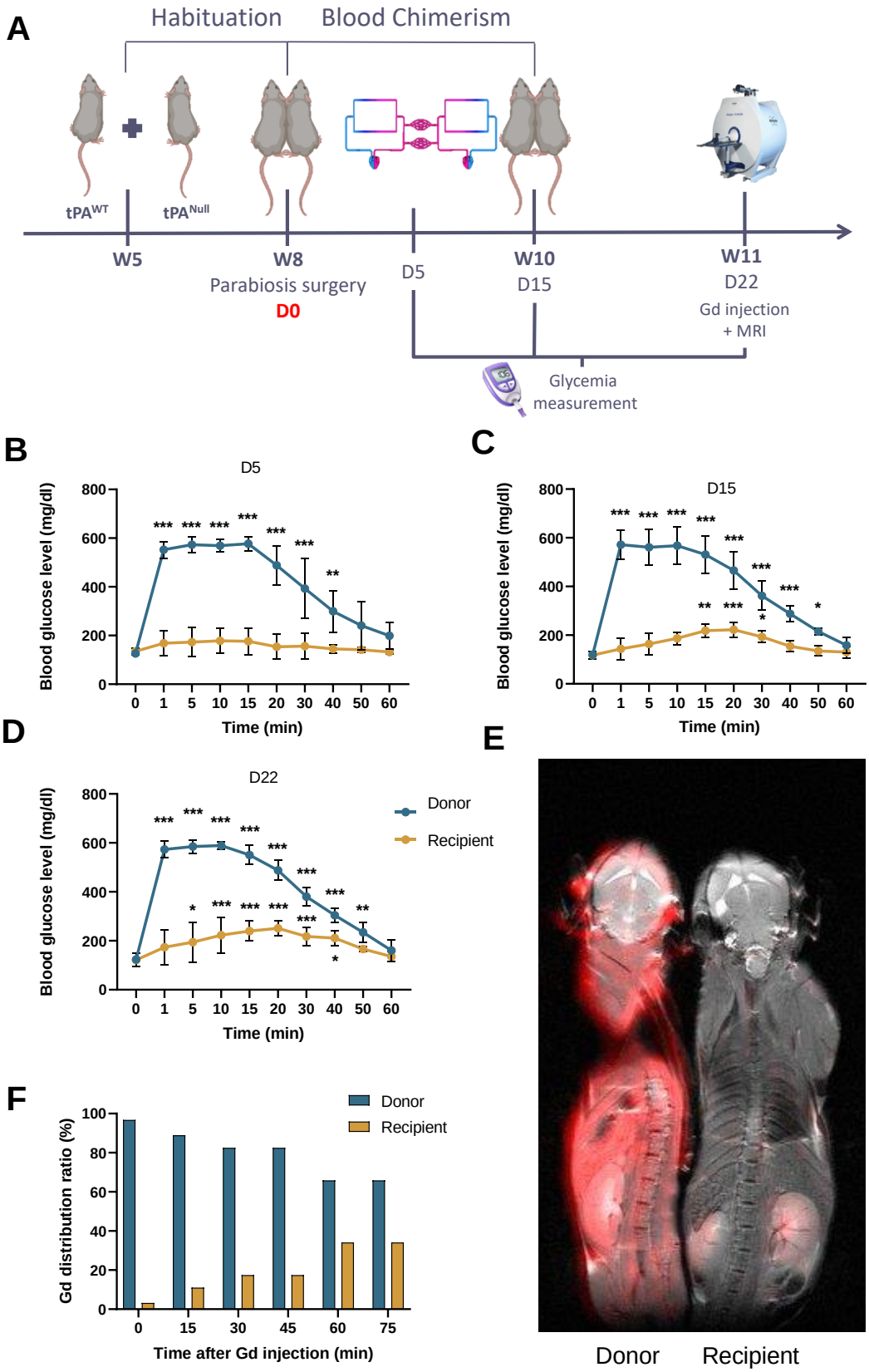

Supplemental figure 2 : Parabiosis model and chimerism validation methods.

Supplemental figure 2 : Parabiosis model and chimerism validation methods. **A**: Schematic representation of experimental study design for parabiosis surgery and chimerism validation. **B-D**: Parabiosis chimerism validation by IV injection of glucose (100µl, 1.2 g/kg) at T0 in tail vein of donor mice, glycemia (mg/dl) of both donor and recipient mice was measured during 1 hour, at different time points following parabiosis surgery (D5, n=5, figure **B**; D15, n=7, figure **C**; D22, n=7, figure **D**). **E**: Representative MRI acquisition of parabionts after IV DOTA-gd injection (200 µl, 0.01 mMol/ml) in donor mice to validate parabiosis model. T1-weighted image (red) represents DOTA-Gd signal and was superposed on anatomical T2-weighted image. **F**: Quantification of DOTA-Gd distribution between parabionts at different time points. Data are mean with SD for each group. *p < 0.05, **p < 0.005 and ***p < 0.001 from T0, 2-way ANOVA test.

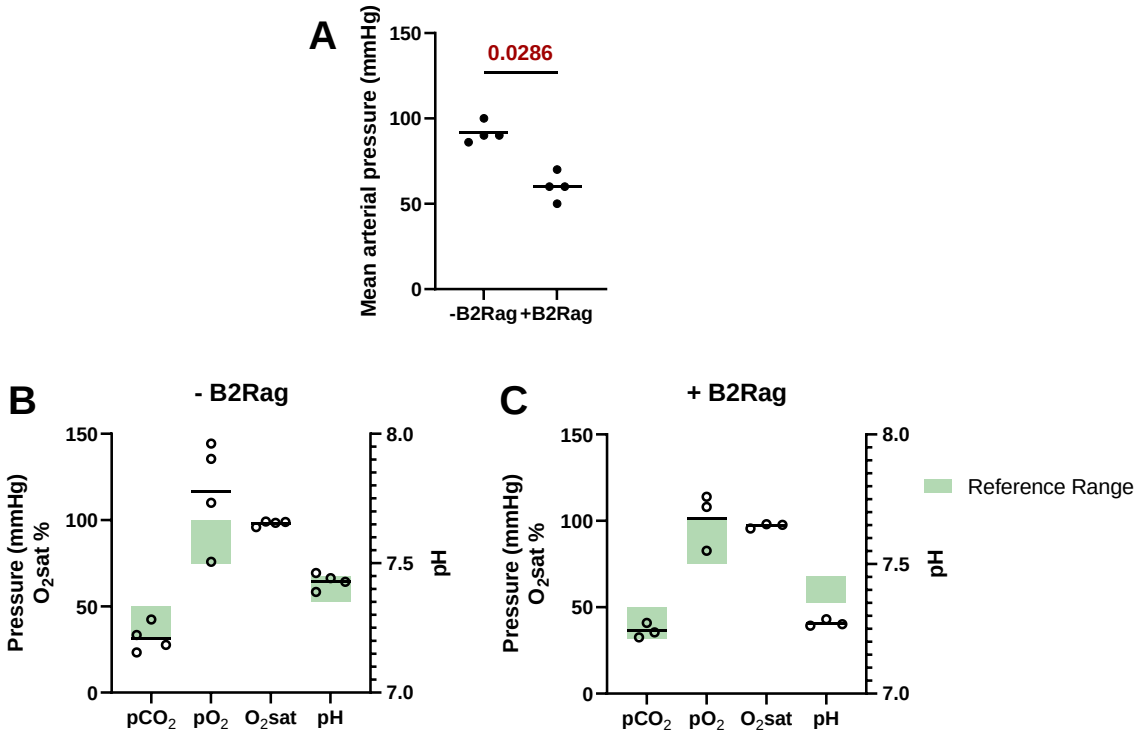

Supplemental figure 3 : Mean arterial blood pressure and blood gases before and after injection of B2Rag in mice. **A**: Mean arterial pressure (MAP, mmHg) before (-B2Rag) and 25 minutes after IV injection of 30 µg/kg of B2Rag (+B2Rag). Data are Mean with values for each mouse. **B-C**: Measurement of arterial blood gas before (-B2Rag, **C**) and 25 minutes after IV infusion of 30 µg/kg of B2Rag (+B2Rag, **D**). pCO_2, pO_2, O_2sat and pH were measured with 100µl of blood on RAPIDLab® 348EX Blood Gas System. Data are mean with values for each mouse and reference range for these measurements. *p < 0.05 from - B2Rag, Mann-Whitney test, n=4 per group.

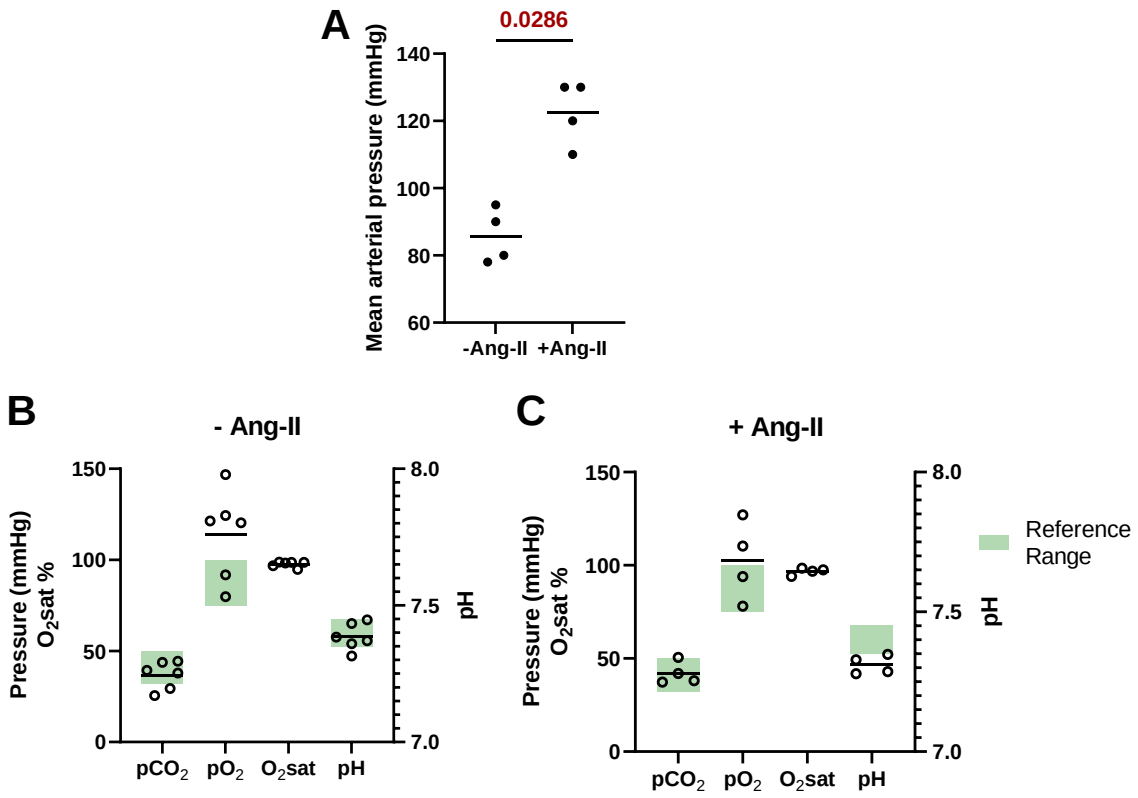

Supplemental figure 4 : Mean arterial blood pressure and blood gases before and after injection of Ang-II in mice. A: Mean arterial pressure (MAP, mmHg) before (-Ang-II) and 25 minutes after IV infusion of 1 µg/kg/min of Ang-II (+Ang-II). Data are Mean with values for each mouse. **B-C**: Measurement of arterial blood gas before (-Ang-II, **B**) and 25 minutes after IV infusion of 1 µg/kg/min of Ang-II (+Ang-II, **C**). pCO_2, pO_2, O_2sat and pH were measured with 100µl of blood on RAPIDLab® 348EX Blood Gas System. Data are mean with values for each mouse and reference range for these measurements. *p < 0.05 from -Ang-II, Mann-Whitney test, n=4 per group.

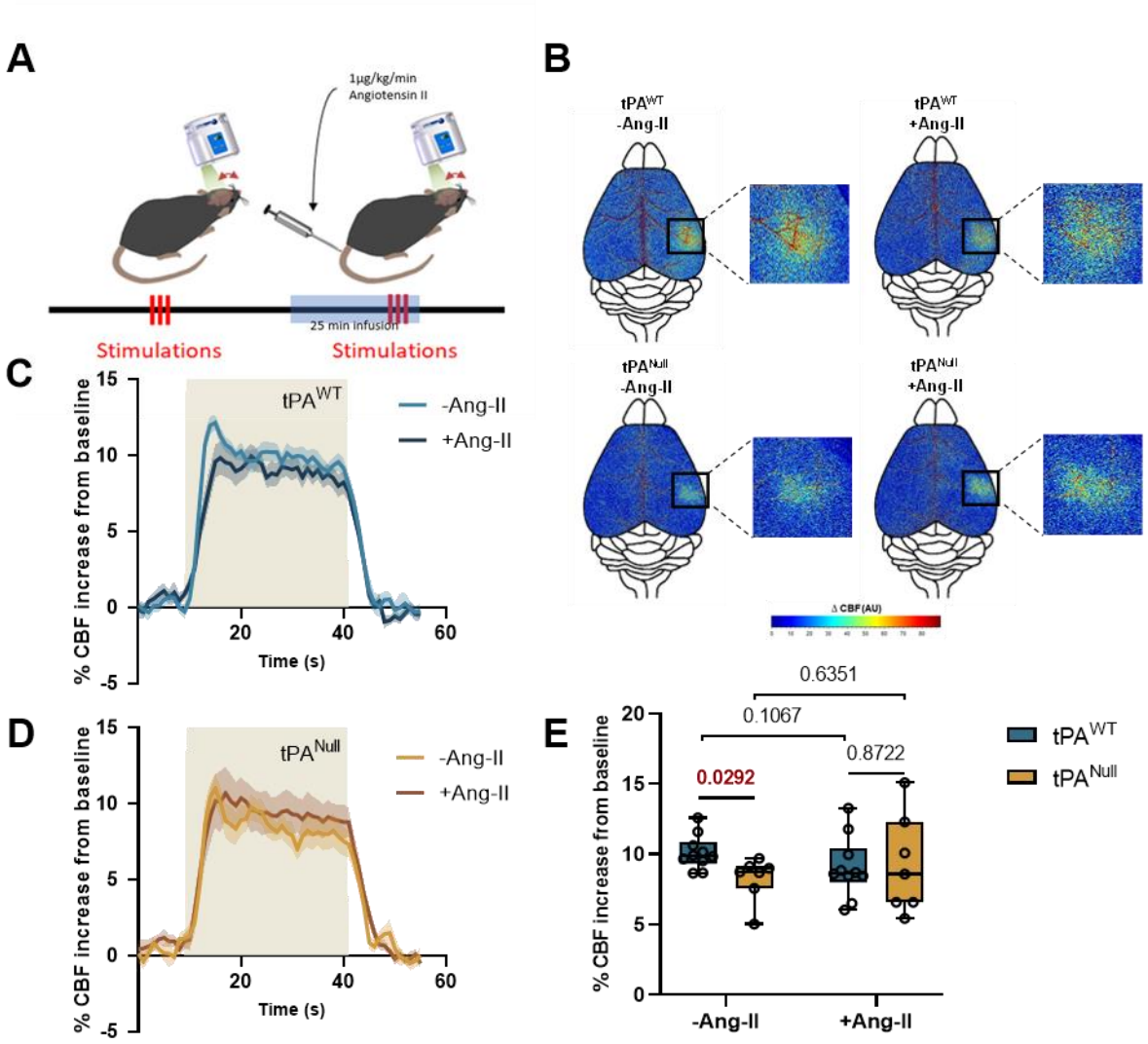

Supplemental figure 5 : Intravenous administration of angiotensin-II (Ang-II) does not influence NVC in a tPA dependent manner.

Supplemental figure 5 : Intravenous administration of angiotensin-II (Ang-II) does not influence NVC in a tPA dependent manner. A: Schematic representation of the experimental timeline of whiskers stimulations paradigm. 3 trains of stimulations were made on laser speckle flowmetry before IV infusion of angiotensin-II (1 µg/kg/min) during 25 minutes, then 3 trains of stimulations were made again. **B**: Colormap corresponds to the activation map related ΔCBF change during whiskers stimulations in tPA^{Null} mice and their littermate before and after IV infusion of Ang-II. Warm colours indicate an elevation of CBF during whiskers stimulations. **C-D**: Time course of % CBF increase (mean ± SEM) during whiskers stimulations ( ) in tPA^{Null} mice (**D**) and their littermate (**C**), before (/) and after (/) IV infusion of Ang-II. **E**: Box plots show the variation of % CBF increase from baseline during whiskers stimulations in tPA^{Null} mice and their littermate before and after IV infusion of Ang-II. Box plot with medians, 1st and 3rd quartiles, min and max with values for each mouse. *p < 0.05 from tPA^{WT}, Kruskal-Wallis and Uncorrected Dunn's tests, n=10 tPA^{WT}, n=7 tPA^{Null}.

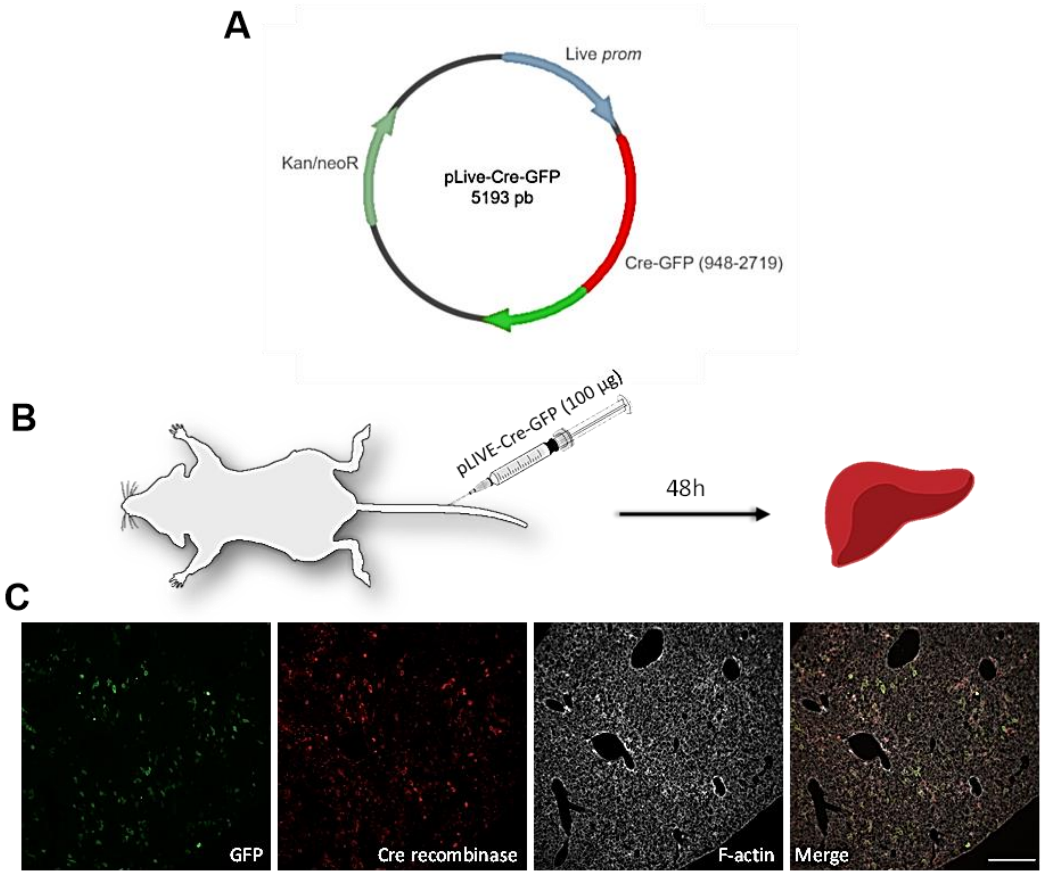

Supplemental figure 6 : Hydrodynamic transfection of pLIVE-Cre-GFP in VECad-$Cre^{\Delta tPA}$ mice.

Supplemental figure 6 : Hydrodynamic transfection of pLIVE-Cre-GFP in VECad-Cre$^{\Delta tPA}$ mice. A: Construction scheme of plasmid pLIVE-Cre-GFP. The cDNA of Cre-GFP was PCR amplified from a pCAG-Cre-GFP plasmid and fused into multiple cloning sites of the pLIVE plasmid between BamHI and NotI. **B**: Experimental schematic representation of hydrodynamic transfection of pLIVE-Cre-GFP. 48 h after transfection of the plasmid, livers from transfected VECad-Cre$^{\Delta tPA}$ mice were collected. **C**: Epifluorescence images of liver slice from transfected VECad-Cre$^{\Delta tPA}$ mice with pLIVE-Cre-GFP (scale bar = 500µm). Immunostaining reveals GFP (green), Cre-recombinase (red) and actin filaments with phalloidin (grey), confirming the transfection of the plasmid in hepatocytes. Images were digitally captured using a camera (CoolSNAP; Photometrics) and/or with an inverted confocal microscope (SP5, Leica). Images were visualized respectively with Metavue 5.0 software (Molecular Devices, USA) and LAS AF lite software (LEICA).

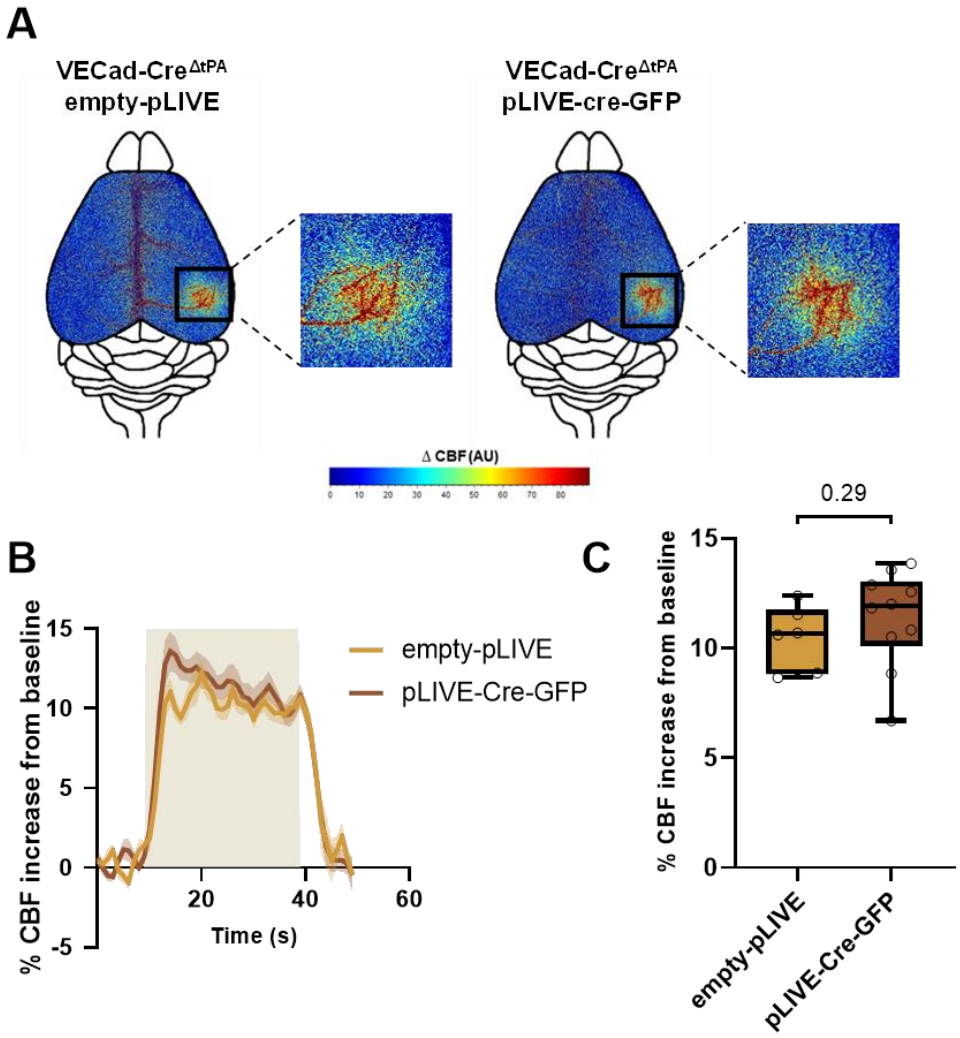

Supplemental figure 7 : Deletion of tPA in hepatocytes does not influence NVC in VECad-Cre$^{\Delta tPA}$ mice.

Supplemental figure 7 : Deletion of tPA in hepatocytes does not influence NVC in VECad-Cre$^{\Delta tPA}$ mice. A: Colormap corresponds to the activation map related ΔCBF changes during whiskers stimulations in VECad-Cre$^{\Delta tPA}$ mice transfected with promotors empty-pLIVE or pLIVE-Cre-GFP. Warm colours indicate an elevation of CBF during whiskers stimulations. **B:** Time course of % CBF increase (mean ± SEM) during whiskers stimulations ( ) of VECad-Cre$^{\Delta tPA}$ transfected with empty-pLIVE ( ) or pLIVE-Cre-GFP ( ). **C:** Box plots show the variations of % CBF increase from baseline during whiskers stimulations of VECad-Cre$^{\Delta tPA}$ mice transfected with promotors empty-pLIVE or pLIVE-Cre-GFP. Box plot with medians, 1st and 3rd quartiles, min and max with values for each mouse. *p < 0.05 from empty-pLIVE, Mann-Whitney test, n=6 empty-pLIVE, n=10 pLIVE-Cre-GFP.

Discussion

1. Le tPA vasculaire est impliqué dans le couplage neurovasculaire

Pour étudier le CNV chez la souris, nous avons choisi d'utiliser le paradigme de stimulation des vibrisses. En effet, les vibrisses des souris sont des organes extrêmement sensibles pour obtenir des informations tactiles spatiales. Le cortex somatosensoriel des vibrisses est hautement organisé en une carte somatotopique qui occupe une grande partie du cortex cérébral (**Figure 44** ; Petersen, 2007). Du fait de sa bonne accessibilité sur la partie dorsale du cerveau, il est très facile d'imager cette zone. Nous avons également choisi d'étudier le CNV par imagerie laser à contraste de Speckle. Cet outil permet de mesurer le DSC directement à travers le crâne, préservant ainsi l'intégrité du cerveau et la pression intracrânienne.

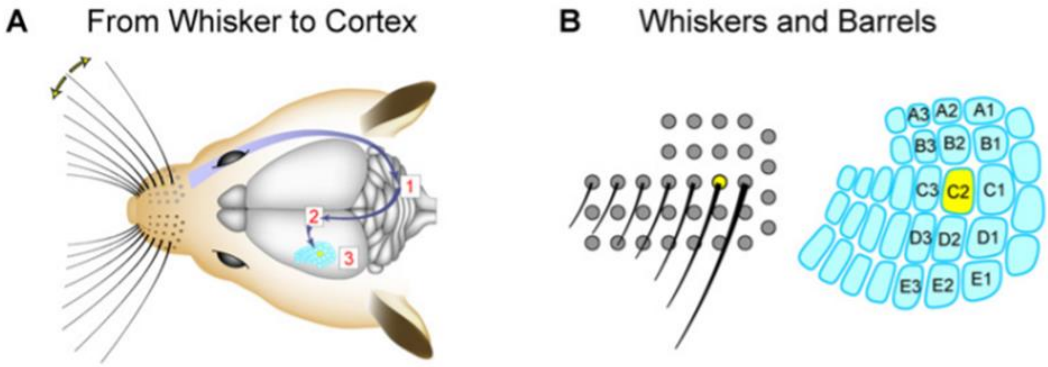

Figure 44 : Organisation du cortex somatosensoriel des vibrisses et représentation de la voie de transmission de l'information des vibrisses vers le cortex. A : La stimulation d'une vibrisse induit des potentiels d'actions dans les neurones sensoriels du nerf trijumeau, libérant du glutamate au niveau d'une première synapse dans le tronc cérébral (1). Les neurones du tronc cérébral transmettent à leur tours l'information au niveau du thalamus (2) par l'intermédiaire du glutamate. Les neurones thalamocorticaux se projettent vers le cortex somatosensoriel des vibrisses (3), également appelé barrel cortex. **B** : Carte somatotopique représentant la disposition des follicules des vibrisses sous la forme de tonneaux dans le cortex somatosensoriel des vibrisses. (Petersen, 2007).

Nous avons choisi comme agent anesthésique pour cette étude, la médétomidine, un agoniste des récepteurs α2-adrénergiques, qui exerce peu d'effets vasculaires (Sinclair, 2003). Afin de maintenir les paramètres physiologiques en conditions normales, nous avons placé les souris sous ventilation mécanique, afin d'avoir un contrôle sur la respiration des animaux (**Supplemental figure 1**).

1.1. Le tPA vasculaire contribue à l'augmentation de l'hyperémie fonctionnelle

1.1.1. L'absence de tPA conduit à une diminution de la réponse vasculaire induite par la stimulation des vibrisses

La première étape de notre étude a été d'évaluer la différence d'augmentation du DSC lors de la stimulation des vibrisses sur une nouvelle souche de souris déficiente en tPA, les tPA^{Null}. Les résultats ont permis d'observer un déficit de 20% sur la réponse vasculaire induite par la stimulation des vibrisses chez les tPA^{Null} par rapport aux souris tPA^{WT} (**Figure 37**). Nos résultats sont en adéquations avec les résultats obtenus par l'équipe de Iadecola et avec une précédente étude réalisée au sein de notre laboratoire sur des souris tPA KO (Anfray et al., 2020 ; Park et al., 2008). Ces résultats permettent de valider le modèle via l'utilisation d'une nouvelle souche de souris déficiente en tPA.

La parabiose est une union chirurgicale de deux organismes permettant le partage de la circulation sanguine. L'attachement de la peau de deux animaux va favoriser la formation de microvaisseaux au niveau du site de l'inflammation (Kamran et al., 2013). Ce modèle est utilisé principalement pour étudier le phénomène de réjuvénation (Zhang et al., 2020).

L'utilisation d'un modèle de parabiose entre une souris tPA^{Null} et tPA^{WT} a permis d'observer que le tPA circulant de la souris tPA^{WT} donneuse pouvait être retrouvé chez la souris tPA^{Null} receveuse, grâce au partage de la circulation sanguine entre les deux souris. Le partage de tPA circulant entre ces deux phénotypes permet à la souris

tPA^{Null} d'influencer l'hyperémie fonctionnelle induite par la stimulation des vibrisses de façon positive. En effet, la parabiose entre deux souris tPA^{Null} (**tPA^{Null}**/tPA^{Null}) montre bien un déficit de 18.5% sur la réponse vasculaire induite par la stimulation des vibrisses par rapport à une parabiose entre deux souris tPA^{WT} (**tPA^{WT}**/tPA^{WT}). La parabiose entre une souris tPA^{WT} et une souris tPA^{Null} a permis d'observer chez la souris tPA^{Null} (**tPA^{Null}**/tPA^{WT}) une augmentation de 23% de l'augmentation du DSC induite par la stimulation des vibrisses en comparaison à une parabiose entre deux souris tPA^{Null} (**tPA^{Null}**/tPA^{Null} ; **Figure 38**). Les résultats permettent de conclure que le tPA endogène circulant de la souris donneuse suffit à restaurer le déficit d'hyperhémie fonctionnelle qu'avait la souris receveuse. Cependant, le niveau de tPA circulant produit par une souris a suffi pour garder une hyperémie fonctionnelle adéquate pour deux souris. En effet, nous observons une variation de l'augmentation du DSC de 0.3% entre les souris tPA^{WT} et tPA^{Null} au sein d'une parabiose **tPA^{Null}**/tPA^{WT}, et la variation de l'augmentation du DSC entre deux souris tPA^{WT} issues des parabioses **tPA^{WT}**/tPA^{WT} et **tPA^{WT}**/tPA^{Null} est seulement de 1% (**Figure 38**). Or, au vu du partage de la circulation entre les deux souris **tPA^{WT}**/tPA^{Null}, par des principes physico-chimiques, la concentration de tPA circulant doit être plus faible lors de la parabiose. De plus, le PAI-1 contenu dans la circulation sanguine chez la souris tPA^{Null} receveuse se retrouve également chez la souris tPA^{WT} donneuse, donc il devrait avoir davantage de tPA circulant complexé à PAI-1, c'est-à-dire moins de tPA circulant actif et donc, une diminution de l'hyperémie fonctionnelle chez les parabioses **tPA^{WT}**/tPA^{Null} par rapport à des parabioses **tPA^{WT}**/tPA^{WT}, or ce n'est pas le cas. La cause plausible qui pourrait expliquer ces résultats serait que la souris tPA^{WT} donneuse produit davantage de tPA circulant pour conserver une quantité de tPA circulant normale.

Une analyse sanguine afin de quantifier la quantité de tPA circulant et de PAI-1 chez la souris tPA^{WT} donneuse au sein d'une parabiose **tPA^{WT}**/tPA^{Null} et de la comparer à une souris tPA^{WT} au sein d'une parabiose **tPA^{WT}**/tPA^{WT} pourrait confirmer en partie cette hypothèse.

1.1.2. L'absence de tPA provenant des cellules endothéliales vasculaires conduit à une diminution de la réponse vasculaire lors de l'hyperémie fonctionnelle

Pour s'affranchir de toute provenance du tPA circulant autre que celle des cellules endothéliales, nous avons généré une nouvelle souche de souris transgénique avec une délétion conditionnelle du tPA dans les cellules endothéliales par croisement d'une souris VE-Cadherin-Cre avec une souris tPA-loxP. Les résultats permettent d'observer une diminution de 12% sur la réponse vasculaire induite par la stimulation des vibrisses chez la souris déficiente en tPA issu des cellules endothéliales par rapport aux souris WT (**Figure 41**). Ces résultats démontrent que le tPA produit par les cellules endothéliales contribue directement à la modulation du CNV.

Comme expliqué dans l'introduction (voir la partie « **1.3.1. Expression et distribution du tPA circulant** »), le tPA peut être également exprimé à partir des hépatocytes (Zheng et al., 2019). Pour connaitre l'implication du foie dans la libération de tPA vasculaire et son implication dans la modulation du CNV, nous avons procédé à une hépatectomie partielle sur des souris tPA^{Null} et tPA^{WT}. L'hépatectomie partielle consiste en une résection d'environ 70% du foie total en ligaturant la base du lobe latéral gauche, et les lobes médians droit et gauche (Hori et al., 2012).

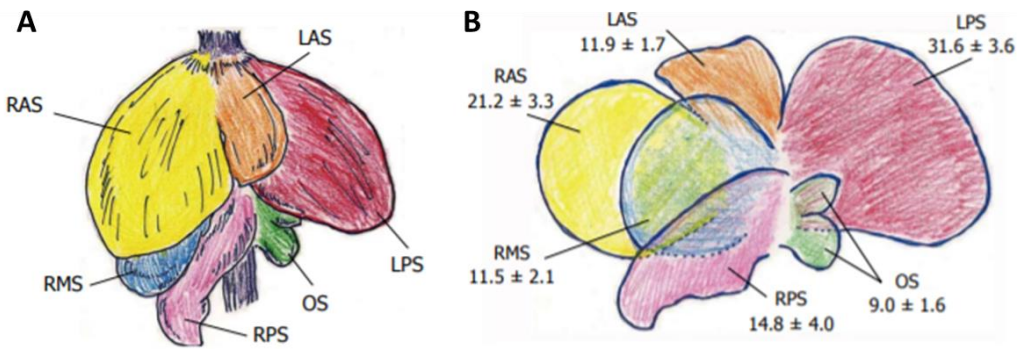

Figure 45 : Représentation des différents lobes d'un foie d'une souris. A : Le foie d'une souris est divisé en six lobes, le lobe médian droit (RAS), le lobe médian gauche (LAS), le lobe latéral gauche (LPS), deux lobes droits (RMS et RPS) et le lobe caudé (OS). **B** : Représentation en pourcentage du volume total de chaque lobe. (Hori et al., 2012).

Après hépatectomie partielle, les souris tPA^{WT} présentent une diminution de 17.5% sur la réponse vasculaire induite par la stimulation des vibrisses par rapport aux souris tPA^{WT} en condition sham. Il n'y a pas de différence observée concernant l'hyperémie fonctionnelle entre les souris tPA^{Null} et tPA^{WT} ayant reçu une hépatectomie partielle, ni entre les tPA^{Null} ayant reçu une hépatectomie partielle et leur homologue sham (**Figure 42**). Les résultats suggèrent que le tPA vasculaire impliqué dans la modulation du CNV induit par la stimulation des vibrisses serait d'origine hépatique.

Pour déterminer si l'implication du tPA dans la modulation du CNV provient des hépatocytes ou des cellules endothéliales du foie, nous avons procédé à la délétion de tPA au niveau des hépatocytes sur des souris délétées en tPA dans les cellules endothéliales, via l'utilisation d'un plasmide pLIVE-Cre-GFP qui sera transfecté dans les hépatocytes par la technique de transfection hydrodynamique (Marcos-Contreras et al., 2016 ; **Supplemental figure 6**). La délétion du tPA dans les hépatocytes via la transfection de pLIVE-Cre-GFP chez les souris déficientes en tPA dans les cellules endothéliales n'influence pas l'hyperémie fonctionnelle par rapport aux souris délétées en tPA dans les cellules endothéliales, transfectées avec un plasmide contrôle (**Supplemental figure 7**). De plus, l'immunohistologie réalisée sur des coupes de foie confirment la présence de tPA dans les cellules endothéliales hépatiques mais

indétectable dans les hépatocytes (**Figure 43**). Ces résultats permettent de conclure que le tPA d'origine hépatique, impliqué dans la modulation du CNV induite par la stimulation des vibrisses, serait plutôt sécrété au sein des cellules endothéliales hépatiques plutôt que les hépatocytes.

Selon les résultats obtenus par Zheng et collaborateurs, le tPA contribuant à l'activité basale du tPA circulant serait d'origine hépatocytaire. En effet, l'utilisation d'un adénovirus-associé AAV8-TBG-Cre, spécifique aux hépatocytes, délétant ainsi DACH1 dans les hépatocytes a permis d'observer une augmentation de l'expression de tPA dans le foie, une augmentation de la quantité et de l'activité du tPA plasmatique, et une plus forte activité fibrinolytique. La délétion d'ATF6 dans les hépatocytes par le même principe, induit une réduction de l'expression de tPA dans le foie, une diminution de la quantité et de l'activité du tPA plasmatique et une baisse de l'activité fibrinolytique (**Figure 46** ; Zheng et al., 2019). Dans notre modèle de transfection hydrodynamique, seulement une partie des hépatocytes est transfectée pour le plasmide pLIVE-Cre-GFP (**Supplemental figure 6**), donc il est possible que la quantité d'hépatocytes transfectés ne soit pas suffisante pour que le tPA délété dans ces cellules aient un impact sur la modulation du CNV. L'expression du gène Plat par ATF6 doit se faire de manière constitutive, vu que l'expression du tPA par les hépatocytes participe au maintien de la quantité basale du tPA circulant.

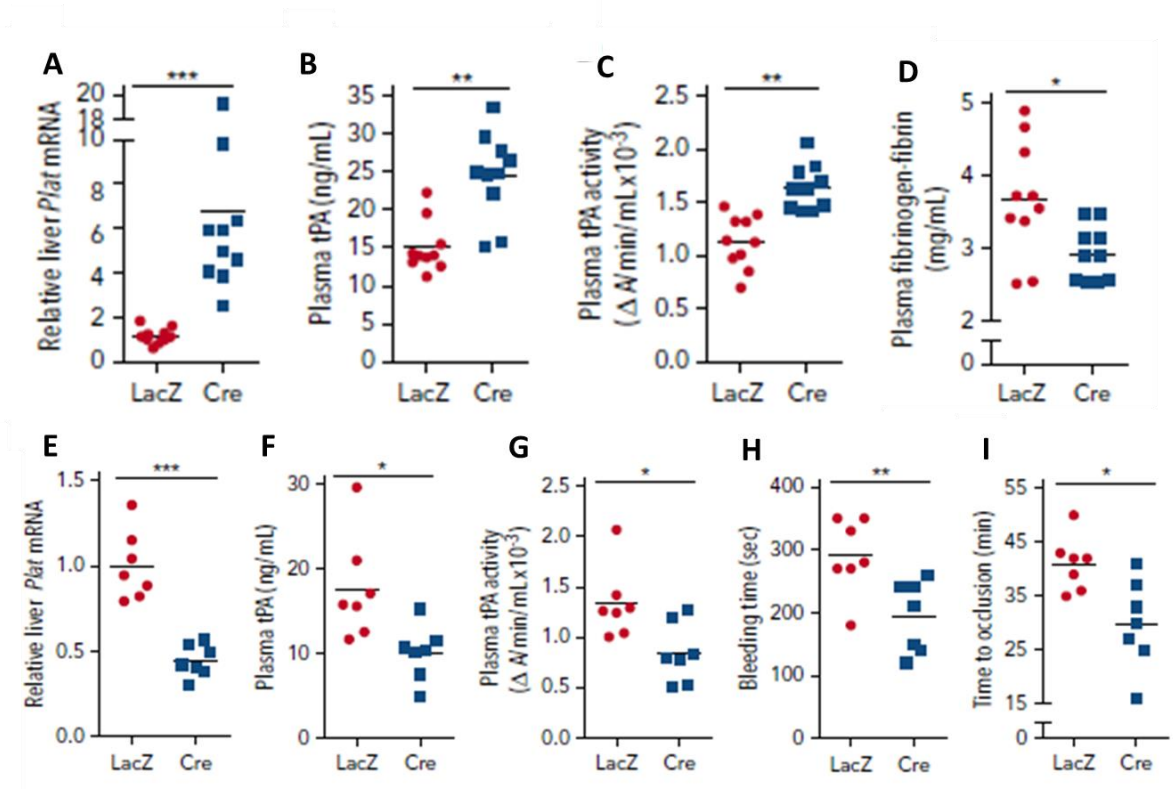

Figure 46 : La délétion de DACH1 et de ATF6 dans les hépatocytes induisent des modifications sur l'expression et l'activité du tPA plasmatique. Quantité relative d'ARNm du gène Plat codant pour le tPA dans le foie chez les souris délétées en DACH1 dans les hépatocytes (**A**) et chez les souris déficientes en ATF6 dans les hépatocytes (**E**) et leur condition contrôle (LacZ). Concentration plasmatique de tPA chez les souris délétées en DACH1 (**B**) et chez les souris déficientes en ATF6 (**F**) dans les hépatocytes. Activité du tPA plasmatique chez les souris délétées en DACH1 (**C**) et chez les souris déficientes en ATF6 (**G**) dans les hépatocytes. **D** : Concentration de fribrinogène-fibrine plasmatique chez les souris délétées en DACH1 dans les hépatocytes. Temps de saignement de la queue (**H**) et d'occlusion de l'artère carotidienne induite par une lésion photochimique (**I**) chez les souris déficientes en ATF6 dans les hépatocytes (Adaptée de (Zheng et al., 2019)

L'hyperémie fonctionnelle est un processus où la réponse vasculaire doit être très rapide lors de l'activité neuronale, si ATF6 n'exprime pas davantage le tPA lors d'une activité neuronale, il est difficile de concevoir que le tPA provenant des hépatocytes puisse participer à la modulation du CNV. De plus, PAI-1 étant entre autres exprimé par les hépatocytes, une régulation fine entre la libération de tPA ou de PAI-1 doit être mise en place. En effet, dans certaines pathologies comme l'obésité,

les hépatocytes expriment en plus grande quantité le PAI-1 par rapport au tPA (Zheng et al., 2020).

1.1.3. L'absence de PAI-1 induit une plus forte augmentation du DSC lors du CNV

PAI-1 est l'inhibiteur du tPA le plus répandu dans la circulation et inhibe en grande partie le tPA circulant. Nous nous sommes intéressés à l'intensité de modulation du tPA dans le CNV si PAI-1 était absent dans la circulation. En effet, pour répondre à cette problématique, nous avons utilisé des souris déficientes en PAI-1. L'absence de PAI-1 chez les souris PAI-1^{KO} induit une augmentation de 19% sur la réponse vasculaire induite par la stimulation des vibrisses par rapport aux souris PAI-1^{WT} (**Figure 37**). Ces résultats permettent de mieux comprendre le fort potentiel modulateur du tPA sur l'hyperémie fonctionnelle et le fait que PAI-1 régule le tPA dans la modulation du CNV.

Par la même occasion, nous avons également utilisé l'infusion intraveineuse d'AngII sur des souris tPA^{Null} et tPA^{WT}, afin de libérer du PAI-1 dans la circulation via l'activation des récepteurs AT1 endothéliaux. L'infusion intraveineuse d'AngII induit bien une augmentation de la pression artérielle moyenne, passant de 85 mmHg à 122 mmHg, sans altérer les gaz du sang (**Supplemental figure 4**). La stimulation des vibrisses chez les souris tPA^{WT} recevant l'infusion d'AngII, n'induit pas de différence sur la réponse vasculaire par rapport aux conditions contrôles. Le même effet est constaté pour les tPA^{Null} ayant reçu une infusion d'AngII (**Supplemental figure 5**). Ces résultats suggèrent que l'infusion intraveineuse d'AngII n'induit pas d'altération du CNV chez les souris tPA^{Null} et tPA^{WT}. De plus, la libération de PAI-1 par l'activation des récepteurs AT1 par l'AngII, n'a pas d'influence sur l'hyperémie fonctionnelle chez les tPA^{WT}. Cependant, une étude a réussi à obtenir une altération du CNV, à la suite d'une infusion intraveineuse aigue d'AngII chez les souris mâles mais pas les femelles (**Figure 47** ; Girouard et al., 2008).

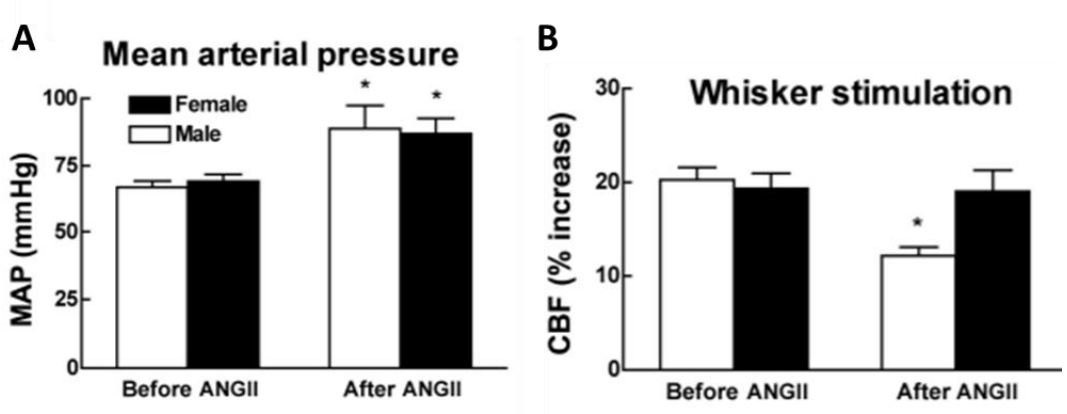

Figure 47 : Les effets cérébrovasculaire d'une administration intraveineuse aigue d'AngII chez des souris mâles et femelles. A : Effet de l'AngII sur la pression artérielle moyenne. **B** : Effet de l'AngII sur l'augmentation du DSC produite par la stimulation des vibrisses (Adaptée de (Girouard et al., 2008)).

Notre infusion lente d'AngII fonctionne correctement car après 25 min, nous observons une augmentation de la pression artérielle moyenne stable d'environ 40 mmHg. Ceci prouve bien la sollicitation des récepteurs AT1 par l'AngII, mais aucune altération du CNV n'est observée contrairement aux études de Girouard et collaborateurs. La possible libération de PAI-1 par l'activation des récepteurs AT1 n'était pas suffisante pour inhiber le tPA libre circulant, ou bien la quantité basale de tPA circulant étant déjà faible, l'inhibition de ces derniers ne provoque pas une altération significative du CNV. Cependant, au vu de cette dernière suggestion, si la quantité de tPA libre circulant était insuffisante pour moduler de façon positive le CNV, nous n'aurions pas pu observer une baisse de la réponse vasculaire lors de la stimulation des vibrisses lorsque le tPA endothéliale est délété. Une autre explication tout à fait plausible serait que malgré la libération de PAI-1 dans la circulation sanguine via l'AngII, la libération locale de tPA par les cellules endothéliales vasculaires au niveau la zone où a lieu l'activité neuronale, n'empêche pas le tPA d'exercer son rôle de modulation dans la réponse vasculaire.

1.2. Le mécanisme d'action du tPA lors de l'hyperémie fonctionnelle

1.2.1. L'absence de sous-unité GluN1 des récepteurs NMDA conduit à une augmentation de la réponse vasculaire lors de l'hyperémie fonctionnelle

Pour étudier le rôle des récepteurs NMDA dans la modulation du CNV par le tPA, nous avons généré une nouvelle souche de souris transgénique avec une délétion conditionnelle de la sous-unité GluN1 dans les cellules endothéliales par croisement d'une souris VE-Cadherin-Cre avec une souris Grin-1-loxP. La délétion de la sous-unité GluN1 des récepteurs NMDA dans les cellules endothéliales induit une augmentation de 35% sur la réponse vasculaire induite par la stimulation des vibrisses par rapport aux souris WT (**Figure 39**). Ces résultats, bien que surprenants, laissent suggérer que le récepteur NMDA en conditions basales, contribue à un tonus vasoconstricteur.

1.2.2. Le tPA agit sur la sous-unité GluN1 des récepteurs NMDA endothéliaux

L'administration intraveineuse de rtPA chez les souris déficientes en sous-unité GluN1 dans les cellules endothéliales n'influence pas l'hyperémie fonctionnelle. Cependant, nous pouvons observer une augmentation de 23% sur la réponse vasculaire induite par la stimulation des vibrisses lorsque du rtPA est injecté par voie intraveineuse chez les souris WT (**Figure 39**). Ces résultats suggèrent que le tPA peut moduler l'hyperémie vasculaire via son interaction avec la sous-unité GluN1 des récepteurs NMDA. En effet, il est connu que le domaine kringle 2 du tPA est capable d'interagir avec la sous-unité GluN1 du récepteur NMDA (Lopez-Atalaya et al., 2008). De plus, il a été montré que le domaine kringle 2 serait impliqué dans la modulation du CNV via son interaction avec les récepteurs NMDA, grâce à l'utilisation d'une forme mutée du tPA sur son domaine kringle 2 (tPA K2*), empêchant le tPA d'interagir avec le récepteur NMDA (**Figure 48** ; Anfray et al., 2020). Le tPA pourrait également interagir avec la LRP-1, qui est liée avec PSD-95 (*Protein Postsynaptic Density 95*) et pourrait moduler la signalisation du récepteur NMDA par l'activation de la PKA (Herz & Strickland, 2001).

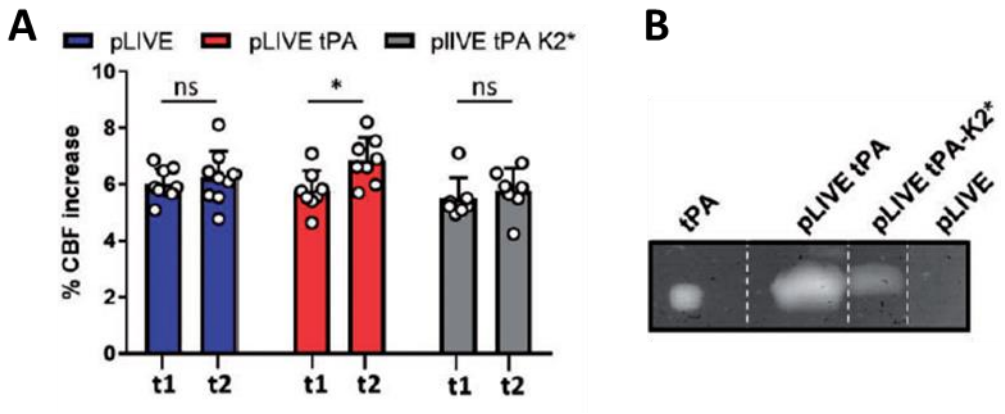

Figure 48 : L'expression chronique de tPA restreint dans la circulation sanguine favorise l'hyperémie fonctionnelle. A : Mesure de l'augmentation du DSC pendant la stimulation des vibrisses avant (t1) et après (t2) transfection hydrodynamique de plasmides pLIVE, pLIVE-tPA ou pLIVE-tPA-K2* sur des souris déficientes en tPA. **B** : Représentation d'une zymographie de fibrine-agar réalisée à partir de plasma de souris déficientes en tPA transfectées soit avec un pLIVE, un pLIVE-tPA ou un pLIVE-tPA-K2*. Les bandes représentent la présence de tPA libre plasmatique (Adaptée de (Anfray et al., 2020)).

Comme vu dans la partie précédente, le récepteur NMDA induirait un effet vasoconstricteur dans des conditions basales. L'injection de rtPA par voie intraveineuse induit une augmentation de la réponse vasculaire lors du CNV par rapport aux conditions salines. Le tPA aurait donc un effet qui viendrait « inhiber » cet effet vasoconstricteur en favorisant la vasodilatation des vaisseaux, via la production de NO (Park et al., 2008).

1.3. La provenance du tPA vasculaire

1.3.1. Le tPA vasculaire impliqué dans la modulation du CNV est libéré par les cellules endothéliales vasculaires

En conditions basales, le tPA est sécrété de manière constitutive dans la circulation sanguine et est rapidement inhibé par le PAI-1 circulant. Pour que le tPA puisse moduler l'hyperémie fonctionnelle dans la zone activée, il est nécessaire qu'il

soit libéré dans la circulation au moment de l'activation. Jusque-là, les hypothèses tendaient à ce que le tPA vasculaire impliqué dans la modulation du CNV, était libéré par les cellules endothéliales à proximité de la région activée. Seulement, dans notre étude, nous avons pu constater que les cellules endothéliales hépatiques pouvaient également libérer du tPA dans la circulation et moduler le CNV. Or, la distance que le tPA a à parcourir entre le foie et le cerveau est suffisante pour qu'il soit inhibé par PAI-1 en chemin. L'hypothèse la plus probable pour que le tPA circulant en provenance du foie module le CNV est qu'il soit libéré en grande quantité. Seulement, une question demeure floue, pourquoi solliciter une libération du tPA circulant systémique pour le CNV ? Une libération locale de tPA dans la zone activée par les cellules endothéliales vasculaire environnantes n'est-elle pas suffisante ?

1.3.2. La libération du tPA peut se faire via l'activation des récepteurs B2 endothéliaux

Comme mentionné dans l'introduction (voir la partie « **3.1.5. tPA et bradykinine** »), la BK est capable de stimuler la libération de tPA par les cellules endothéliales vasculaires via son interaction avec les récepteurs B2 (Brown et al., 1999 ; Rahman et al., 2014). Pour étudier ce phénomène, et comprendre si le tPA libéré par les cellules endothéliales via la BK influence l'hyperémie fonctionnelle, nous avons décidé d'utiliser un puissant agoniste des récepteurs B2, la [Phe^{8}Ψ(CH-NH)-Arg^{9}]-Bradykinin (Drapeau et al., 1988). La BK induisant une vasodilatation et une hypotension, nous avons pris le temps de mesurer la pression artérielle moyenne des souris ainsi que de vérifier les gaz du sang, afin d'être certain d'être dans des conditions physiologiques. La pression artérielle de nos souris passe de 91 mmHg à 60 mmHg lors de l'injection de l'agoniste des récepteurs B2, les gaz du sang restent également dans les normes (**Supplemental figure 3**). Pour étudier l'implication du tPA libéré par la BK dans le CNV, nous avons utilisé notre nouvelle souche de souris déficiente en tPA, les souris tPA^{Null} et des souris contrôles tPA^{WT}. Nous observons une augmentation de la réponse vasculaire induite par la stimulation des vibrisses dose dépendante à l'agoniste des récepteurs B2 injecté par voie intraveineuse, à la fois pour les souris tPA^{Null} et tPA^{WT}. En effet, la BK est un agent vasodilatateur, l'activation des récepteurs B2 va activer la eNOS pour produire du NO induisant ainsi une relaxation

des cellules musculaires lisses (Mathis et al., 1996). Chez les tPA^{Null}, l'augmentation de la réponse vasculaire lors de la stimulation des vibrisses devient significativement plus importante à une dose d'agoniste des récepteurs B2 injectée de 30 µg/kg, soit la plus forte dose administrée. Chez les tPA^{WT}, l'augmentation de la réponse vasculaire devient significativement importante à une dose de 7 µg/kg, soit la plus faible dose administrée (**Figure 40**).

Le paramètre qui varie entre ces deux groupes est la capacité d'expression du tPA. En effet, les tPA^{Null} ne possédant pas de tPA, pour induire une augmentation significative de l'hyperémie lors du CNV après injection d'agoniste des récepteurs B2, seulement le NO produit par l'activation des récepteurs B2 par l'agoniste peut augmenter cette hyperémie. Donc il faut de plus grandes doses d'agoniste afin de produire suffisamment de NO pour augmenter significativement la réponse vasculaire induite par le CNV. Quant aux tPA^{WT} qui expriment normalement du tPA, l'agoniste peut à la fois induire une production de NO et une libération de tPA circulant via l'activation des récepteurs B2. Une plus faible dose d'agoniste est donc suffidante par rapport aux souris tPA^{Null} pour induire une augmentation significative de la réponse vasculaire lors du CNV. Ainsi, nous pouvons observer à une dose d'agoniste de 7 µg/kg une augmentation de 18% de la réponse vasculaire lors de la stimulation des vibrisses chez les tPA^{Null} contre 28% chez les tPA^{WT} (**Figure 40**). De plus, la quantification du tPA total plasmatique a permis de montrer qu'après injection d'une dose de 60 µg/kg d'agoniste, la quantité de tPA total plasmatique a bien augmenté par rapport à une injection de sérum physiologique (**Figure 40**).

Dans l'ensemble, ces résultats révèlent que l'activation du SKK entraine une libération de tPA dans la circulation sanguine par les cellules endothéliales vasculaire, pouvant participer à la modulation du CNV.

1.3.3. La libération du tPA vasculaire via d'autres facteurs

La libération supplémentaire de tPA nécessite une stimulation des cellules endothéliales. Cette libération se fait via des médiateurs vasoactifs agissant sur les cellules endothéliales (**Tableau 1** ; Oliver et al., 2005). D'autres composés vasoactifs comme la trombine ou l'histamine, augmentent la synthèse du tPA (Levin et al., 1984 ; van Hinsbergh et al., 1987).

	Libération de tPA	Mécanisme	Dose	Commentaires
Bradykinine	++++	Dépendant des récepteurs B2 Indépendant du NO et des prostaglandines	0.02 à 3 nmol/min	Implication de la libération du tPA par la bradykinine pour la voie de la coagulation et l'action des ACE
Substance P	+++	Récepteurs NK1	2 à 40 pmol/min	
TNF-α	+++	Incertain	80 à 240 ng/min	L'initiation de la libération du tPA est lente au début puis se maintien > 3 heures après l'arrêt de la perfusion
Desmopressine	++	Récepteurs V_2	21 à 70 ng/min	
Isoprénaline	++	Récepteurs adrénergiques	400 ng/min	
ATP	++	Récepteurs P2X ou P2Y	10 à 200 nmol/min	
UTP				
Méthacholine	+	Récepteurs muscariniques	0.8 à 12.8 µg/min	

Norépinéphrine	+	Récepteurs adrénergiques	1.2 µg/min	

Tableau 1 : Les substances qui peuvent stimuler la libération de tPA par les cellules endothéliales chez l'Homme. Les différents médiateurs et leur capacité de libération du tPA, leur site d'action ainsi que la dose injectée chez l'Homme sont renseignés (Adaptée de (Oliver et al., 2005)).

1.4. L'implication de la voie du tPA dans la modulation de l'hyperhémie fonctionnelle

1.4.1. tPA et maladie d'Alzheimer

La maladie d'Alzheimer est caractérisée par une augmentation de dépôts de peptides β-amyloïde dans le parenchyme cérébral sous forme de plaques et dans les vaisseaux sanguins, ainsi qu'une accumulation de protéine Tau dans les neurones. Cette maladie est associée avec des altérations du DSC et du CNV qui surviennent tôt dans la maladie (Iadecola, 2017 ; Iturria-Medina et al., 2016). La quantité de tPA est réduite dans le SNC des souris modèles de cette maladie, qui surexpriment la protéine précurseur de l'amyloïde, en raison de l'augmentation de l'activité de PAI-1 (Cacquevel et al., 2007 ; Cortes-Canteli & Iadecola, 2020 ; Jacobsen et al., 2008). Ce déficit de tPA atténue l'hyperémie fonctionnelle, via la suppression de la production de NO suite à l'activation des récepteurs NMDA pendant l'activité neuronale. L'inhibition de PAI-1 permet au tPA de moduler le CNV de façon positive lors d'une activité neuronale (Park et al., 2020).

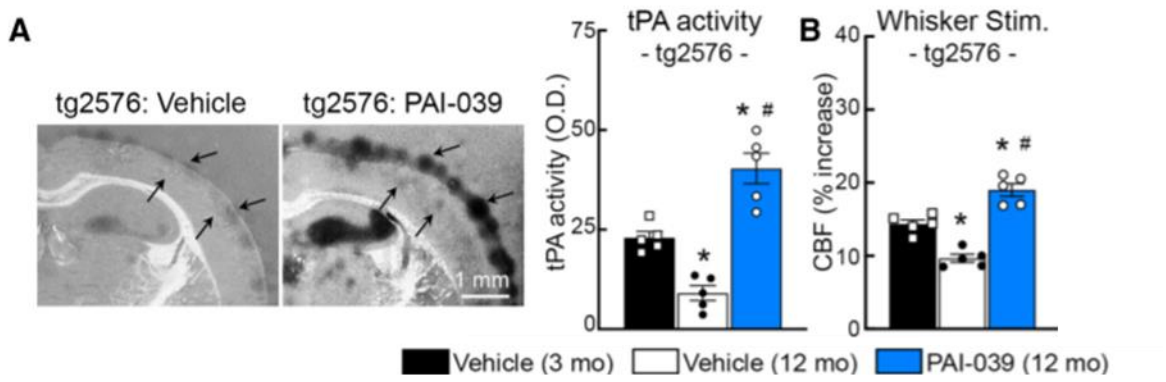

Figure 49 : L'inhibition de PAI-1 inverse le dysfonctionnement neurovasculaire. A : L'administration intracérébroventriculaire d'un inhibiteur de PAI-1 pendant 4 semaines sur des souris surexprimant la protéine précurseur de l'amyloïde (tg2576), restaure l'activité du tPA en zymographie *in situ*. **B** : L'inhibiteur PAI-1-039 améliore également la réponse vasculaire induit par la stimulation des vibrisses (Adaptée de (Park et al., 2020)).

1.4.2. tPA et AVC ischémique

L'ischémie cérébrale focale ou globale induit des effets non négligeables sur la régulation du DSC. En effet, après un AVC ischémique, la réactivité vasculaire face aux stimuli et l'autorégulation sont altérées (Girouard & Iadecola, 2006). Après une ischémie cérébrale, le cerveau produirait moins de tPA, et l'activité de PAI-1 serait exacerbée (Hosomi et al., 2001). Les résultats suggèrent qu'en l'absence de tPA, le CNV est altéré, que ce soit le tPA neuronal ou vasculaire (Anfray et al., 2020 ; Park et al., 2008). Donc lors d'une ischémie, une réduction de tPA pourrait entrainer une dérégulation du CNV post-ischémique.

Conclusion générale

L'ensemble des résultats de ma thèse a permis de mieux comprendre l'implication du tPA vasculaire dans un processus physiologique qui est le couplage neurovasculaire.

Nous avons démontré que le tPA vasculaire contribue à la modulation de l'hyperémie fonctionnelle, médiée par l'activation des récepteurs NMDA endothéliaux. En effet, une déficience en tPA altère l'hyperémie fonctionnelle induite par la stimulation des vibrisses, alors qu'une déficience en PAI-1 l'augmente. La diminution de la réponse vasculaire lors du CNV chez les souris déficientes en tPA peut être rétablie via l'injection intraveineuse de tPA ou par le chimérisme du système sanguin entre une souris déficiente en tPA et une WT.

Nos données révèlent également un rôle clé des cellules endothéliales dans le CNV. Une délétion conditionnelle du tPA endothélial conduit à une réduction de l'hyperémie fonctionnelle induite par la stimulation des vibrisses. Une délétion des sous-unités GluN1 des récepteurs NMDA endothéliaux conduit à une absence de modulation du CNV par le tPA.

Nous avons également observé que l'activation des récepteurs B2 favorise la libération de tPA circulant, pouvant moduler de façon positive l'hyperémie fonctionnelle induite par la stimulation des vibrisses. Ainsi, les niveaux physiologiques de tPA circulant contribuent directement à l'efficacité du CNV.

Enfin, nous avons mis en évidence que le tPA circulant impliqué dans la modulation de l'hyperémie fonctionnelle pourrait provenir des cellules endothéliales vasculaire du foie. Ces résultats dévoilent une nouvelle voie contribuant à la régulation complexe du CNV, impliquant des récepteurs NMDA endothéliaux, dépendant du tPA endothélial et un axe de communication cerveau-foie.

Autres travaux

Original Article

JCBFM

Journal of Cerebral Blood Flow & Metabolism
2020, Vol. 40(10) 2038–2054

DOI: 10.1177/0271678X19883599
journals.sagepub.com/home/jcbfm
SAGE

Circulating tPA contributes to neurovascular coupling by a mechanism involving the endothelial NMDA receptors

Antoine Anfray[1], Antoine Drieu[1], Vincent Hingot[2], Yannick Hommet[1], Mervé Yetim[1], Marina Rubio[1], Thomas Deffieux[2], Mickael Tanter[2], Cyrille Orset[1,*] and Denis Vivien[1,3,*]

Abstract

The increase of cerebral blood flow evoked by neuronal activity is essential to ensure enough energy supply to the brain. In the neurovascular unit, endothelial cells are ideally placed to regulate key neurovascular functions of the brain. Nevertheless, some outstanding questions remain about their exact role neurovascular coupling (NVC). Here, we postulated that the tissue-type plasminogen activator (tPA) present in the circulation might contribute to NVC by a mechanism dependent of its interaction with endothelial N-Methyl-D-Aspartate Receptor (NMDAR). To address this question, we used pharmacological and genetic approaches to interfere with vascular tPA-dependent NMDAR signaling, combined with laser speckle flowmetry, intravital microscopy and ultrafast functional ultrasound in vivo imaging. We found that the tPA present in the blood circulation is capable of potentiating the cerebral blood flow increase induced by the activation of the mouse somatosensorial cortex, and that this effect is mediated by a tPA-dependent activation of NMDAR expressed at the luminal part of endothelial cells of arteries. Although blood molecules, such as acetylcholine, bradykinin or ATP are known to regulate vascular tone and induce vessel dilation, our present data provide the first evidence that circulating tPA is capable of influencing neurovascular coupling (NVC).

Keywords

Endothelial cells, NDMA receptors, neurovascular coupling, tissue-type plasminogen activator, vascular biology

Received: 30 May 2019; Revised: 16 September 2019; Accepted: 25 September 2019

Introduction

Regulation of the cerebral blood flow (CBF) plays a critical role in brain functions with its alteration as a cause or a consequence of several brain disorders, including stroke and Alzheimer's Disease.[1] Therefore, understanding the cellular and molecular mechanisms underlying physiological and/or pathophysiological hemodynamic signals elicited by neuronal activation should lead to a better understanding of brain health and diseases. The control of the functional hyperemia, also known as neurovascular coupling (NVC),[1] has been reported to involve almost all cells of the neurovascular unit (neurons, astrocytes, vascular smooth muscle cells, pericytes and endothelial cells),[1,2] with mechanisms that may differ between arteries/arterioles and capillaries.[3,4]

[1]Normandie University, UNICAEN, INSERM, UMR-S U1237, Physiopathology and Imaging of Neurological Disorders (PhIND), GIP Cyceron, Caen, France
[2]Institut Langevin, CNRS, INSERM, ESPCI Paris, PSL Research University, Paris, France
[3]CHU Caen, Department of Clinical Research, Caen Normandie University Hospital, Avenue de la Côte de Nacre, Caen, France

*These authors equally participated in the elaboration of the article.

Corresponding author:
Denis Vivien, INSERM UMR-S U1237 "Physiopathology and Imaging of Neurological Disorders", University Caen Normandie, GIP Cyceron, Bd Becquerel, BP5229, Caen 14074, France.
Email: vivien@cyceron.fr

Tissue-type plasminogen activator (tPA) is a serine protease initially characterized for its role in fibrinolysis by its ability to convert plasminogen into plasmin,[5] and is therefore used in the treatment of stroke.[6] tPA was also described as a neuromodulator[7,8] and a gliotransmitter[9] implicated in various brain functions.[10–12] A number of its cerebral parenchymal effects are related to its ability to influence N-methyl-D-Aspartate receptor (NMDAR) signaling.[8,13,14] Therefore, tPA was previously described as an actor of NVC via a mechanism involving neuronal NMDAR signaling.[15] However, the complete mechanism of action of tPA on NVC remains to be clarified since tPA may originate either from neurons[16] or endothelial cells[17] and NMDAR also being expressed on neurons and on endothelial cells.[18–20] When expressed on brain endothelial cells, NMDAR is involved in the maintenance of the integrity of the blood–brain barrier (BBB),[18,19] and their tPA-dependent modulation results in the passage of immune cells across the BBB in neuroinflammatory conditions.[21]

Whereas important studies have described signaling pathways in astrocytes, vascular smooth muscle cells, pericytes and endothelial cells involved in the control of hemodynamic signal induced by neuronal activity, some outstanding questions remain. Endothelial cells are key component in the regulation of vascular tone in the brain, and many circulating molecules are capable to have an influence on it, such as acetylcholine, bradykinin or ATP.[22,23] As endothelial cells are localized at the interface between the circulation and the brain parenchyma, the question whether blood components are capable of specifically influencing NVC is still debated. Here, we hypothesized that circulating tPA may participate in hemodynamic responses induced by neuronal activation. To address this question, we took advantages of laser speckle contrast imaging, functional UltraSound (fUS) imaging[24] and intravital imaging along with pharmacological and genetic approaches. We found that plasmatic tPA can potentiate the CBF increase evoked by activation of the mouse barrel cortex. Moreover, our study shows that this effect is mediated by a tPA-dependent activation of NMDAR expressed on endothelial cells of arteries and arterioles. Thus, while mechanisms reported so far to control NVC mainly arise from the parenchyma towards the vessels, we provide here the evidences of a secondary mechanism coming from the blood stream towards endothelial cells in the control of NVC.

Materials and methods

Animals

All experiments were performed on male tPA wt, tPA$^{-/-}$ (Centre Universitaire de Ressources Biologiques, Caen, France) or C57BL/6 (Janvier labs, Le Genest-Saint-Isle, France) aged from 8 to 12 weeks. Mice were housed in plastic cages on a 12-h light cycle with ad libitum access to water and food. During experiments, body temperature was maintained with electric heating pads with thermal feedback, and hearth rate and blood O2 saturation were monitored using the MouseOx+ device (Starr Life Sciences Corporation). All experiments and analysis were randomized and performed blind. Experiments were performed in accordance with the European directive (2010/63/UE) and French ethical laws (act no. R214; 87–137 du code rural). The project was approved by the ethical committee CENOMEXA (under the identification number #11104) and the experiments were performed following the ARRIVE guidelines (Animal Research: Reporting of in Vivo Experiments; http://www.nc3rs.org.uk).

Animals preparation

Anesthesia was initially induced using 5% isoflurane (Forene®, AbbVie) in 70% N_2O/30% O_2 and then maintained using 2% isoflurane in 70% N_2O/30% O_2. Mice were intubated, placed under mechanical ventilation, and fixed in a stereotaxic frame. The skull was exposed, and lidocaine (Xylocaine 5% spray®, AstraZeneca) was applied. Whiskers on the left side of the mouse were cut to let only about 1 cm. A catheter was placed in the tail vein, to allow further IV injection. Anesthesia was then switch to medetomidine (Domitor®, Pfizer, 0.1 mg/kg). Isoflurane, N_2O and O_2 were stopped 10 min after the bolus injection. A waiting time of a least 20 min was then respected to discard N_2O and isoflurane from the mouse body and to allow the stabilization of the CBF. Preliminary experiments were performed in order to evaluate physiological parameters, especially blood pCO2 and pH, in mice placed in experimental conditions. Blood pressure was measured using the tail-cuff method. These experiments revealed normal values for these parameters in our conditions. These controls were repeated regularly.

Pharmacology

During experiments, different treatments were injected through the tail vein of the mice. The total volume injected was 300 µL as follows: a bolus of 150 µL, 10 min before the beginning of the CBF response measurement, followed by an infusion (10 µL/min). Dosages were as follows: rtPA = 10 mg/kg; AP5 (2-amino-5-phosphonopentanoic acid, noncompetitive antagonist of NMDARs) = 0.3 mg/kg; MK-801 (competitive antagonist of NMDARs) = 0.3 mg/kg; Glunomab® and control IgG = 5 mg/kg. As a control, HEPES (0.3 M) and saline (0.9%) were injected.

rtPA preparation

rtPA was prepared from Actilyse® (Boehringer Ingelheim). In order to eliminate the arginine buffer contained in the commercial solution, rtPA was dialyzed in HEPES buffer (4-(2-hydroxyethyl)-1-piperazineethanesulfonic acid, 0.3 M, pH 7.4, Sigma-Aldrich) using dialysis cassettes (Slide-A-Lyzer® 10 K; ThermoScientific).

Laser speckle flowmetry

CBF responses to whiskers stimulations in medetomidine-anesthetized mice were determined using laser speckle flowmetry directly through the skull. Images were acquired using a Laser Speckle Contrast Imager (moorFLPI-2, Moor Instruments; Sample interval: 1 Hz, exposure time: 20 ms, FOV = 6 mm × 11.3 mm, images resolution 752 × 580). Stimulation were performed by mechanically shaking (4–5 Hz) mice whiskers on the left side over a period of 30 s, followed by a 90-s rest periods, three times (total time = 390 s). Images were analyzed using the moorFLPIReviewV40 software (moorFLPI-2, Moor Instruments). The average of the images obtained during rest was subtracted to the average of the images obtained during stimulation, revealing the area where the CBF had changed during the stimulation. The average CBF signal of this area was then extracted, and the percent of increase of the CBF was calculated based on the baseline signal during rest. Values of the 3 stimulations were then averaged (See Suppl. Figure 1).

Intravital microscopy

The day before the experiment, animals were anesthetized with isoflurane and placed in a stereotaxic device. The skull was exposed, and the area above the S1bf cortex was thinned with a drill. On the day of the experiment, anesthetized mice were placed in a stereotaxic device and aqueous medium was deposed between the thin-skull window and the ×25 immersive objective. Just before the imaging, an IV injection of FITC Dextran (100 µL; 70,000 kDa; Sigma Aldrich) was performed to visualize the lumen of blood vessels. Acquisitions were performed using a Leica TCS SP5 MP microscope on confocal mode (1392 × 1040 pixels; 0702 µm/pixel, 145 ms/frame).

Mechanical whiskers stimulation was performed during a single 10-s period. Images were analyzed using ImageJ software (NIH) as follows: images obtained during rest and during stimulation were averaged separately and a line ROI was drawn perpendicularly to the vessel. An intensity curve of fluorescence along the line was obtained from this ROI, and vessel diameter was measured by measuring the distance between the two borders of the curve at 50% of the peak of intensity. Vessels were then separated in three groups depending on their resting diameter size (>25 µm; 25 µm>×>15 µm; <15 µm).

Hydrodynamic transfection

Hydrodynamic transfection was conducted as previously described.[25] Mice were injected with 100 µg of pLIVE plasmid alone, as a control, pLIVE plasmid encoding wild-type rat tPA (pLIVE-tPA) or tPA mutants (pLIVE-tPA-K2*). Briefly, a large volume (10% of body weight) of plasmid-containing saline buffer (0.9% NaCl) was injected in the tail vein of the mice in less than 5 s. This approach with the pLIVE vector allows the constitutive hepatic expression of the insert during few days. Laser speckle flowmetry was realized before the transfection (see Laser speckle flowmetry section). At the end of this first measurement, mice received an intraperitoneal injection of atipamezole (0.5 mg/kg, Antisedan®, Pfizer) to facilitate their wake up; 48 h after the transfection, a second CBF measurement was realized (see Laser speckle flowmetry section). Right after, blood sampling was performed by retro-orbital puncture. Blood was anticoagulated using citrate. Blood samples were then subject to a 1500*g* centrifugation for 15 min, to separate cells from plasma. Supernatant was separated and subjected to a 10,000*g* centrifugation, to separate plasma from remaining platelets.

Zymography

The presence of free plasmatic tPA after hydrodynamic transfection was detected by direct fibrin autography following sodium dodecylsulphate polyacrylamide gel electrophoresis (SDS-PAGE) performed as previously described.[26] Plasma samples and reference tPA (0.25 nM, 10 µL) were subjected to SDS electrophoresis (8% polyacrylamide gels, under non-reducing conditions). SDS was then exchanged with 2.5% Triton X-100. After washing off excess Triton X-100 with distilled water, the gel was carefully overlaid on a 1% agarose gel containing 1 mg/mL bovine fibrinogen, 100 nM plasminogen and 0.2 NIH U/mL of bovine thrombin. Zymograms were allowed to develop at 37°C for 12 h and photographed at regular intervals using dark-ground illumination. Active proteins in plasma samples were identified by reference to the migration of known tPA.

Functional ultrasound imaging

Introduced in Macé et al.,[24] functional ultrasound (fUS) enables a fast tracking of hemodynamic changes

in depth in animal brains summited to an external stimulation. fUS sequences and parameters in the present study reproduce the methology described in Tiran et al.,[27] where fUS was applied to different models of rodents, especially in mice's and describes the response to whiskers stimulation.

The day before the experiment, animals were anesthetized with isoflurane and placed in a stereotaxic frame. The skin was cut to expose the skull and the area above the S1bf cortex was thinned with a drill.

The animal preparation was then the same as for the Laser speckle flowmetry experiments (see Laser speckle flowmetry section), except that ultrasound gel was applied between the ultrasound probe and the mouse skull to ensure good acoustic coupling. The probe was positioned over the coronal plane corresponding to the somatosensory barrel field cortex (S1bf; bregma −1.5 mm). Stimulations were performed the same way as for the Laser speckle flowmetry experiments (see Laser speckle flowmetry section).

Ultrafast acquisition was performed using an ultrasonic sequence based on compounded plane wave transmission (11 angles from −10° to 10° by steps of 2°) and a 15 MHz ultrasonic probe (Vermon, France, 100 µm × 100 µm in plane pixels, 300 µm slice thickness, elevation focus 8 mm) with a frame rate of 500 Hz; 200 images were acquired every second for 390 s. For each block of 200 images, blood signal was extracted from tissue signal using singular value decomposition filters[28] and excluding the 60 most energetic singular values.

For each pixel, the correlation coefficient was calculated between the normalized Power Doppler (PD) intensity along time and a step function following the stimulation pattern. An activation map was reconstructed by keeping only pixels with a correlation coefficient higher than 0.2 and superimposing the corresponding pixels on the mean Doppler image. An artefact caused by the mechanical respirator was masked on the bottom left of the image, without significant impact on the activation in the cortex.

The activated area was determined as the pixels with a correlation coefficient higher than 0.2 corresponding to two times the spatial standard deviation of CBV baseline estimated in a non-activated area. The quantification of the relative PD increase is performed of the mean PD signal in the activated area.

Immunohistochemistry on isolated brain vessels

Brain vessels of C57BL/6 mice were isolated as previously described.[29] Deeply anesthetized mice were transcardially perfused with cold heparinized saline (15 mL/min). Brain were then dissociated in a solution of HEPES and HBSS and then centrifuged at 2000*g* at 4°C during 10 min. The pellet was then resuspended in a solution of HEPES/HBSS and Dextran (Dextran from *Leuconostoc spp*. Mr ~70,000, Sigma-Aldrich) and centrifuged at 4400*g* at 4°C during 15 min. Vessels were then suspended in a solution of HEPES/HBSS and BSA 1% and filtrated on a 20-µm mesh filter. Vessels were then detached from the filter in a PBS solution. Vessels were then put on a poly-lysine coated slides, cryoprotected overnight in a 20% sucrose PBS solution and fixated during 15 min with PBS 0.1 M. pH 7.4 containing 2% paraformaldehyde and 0.2% picric acid. Slide was stored at −80°C before processing. Vessels were then co-incubated overnight with rabbit anti-PDGF-Rβ (1:1000, ab32570, Abcam) primary antibodies and FITC-conjugated mouse anti-αSMA (1:500, ab8211, Abcam) primary antibodies, or with goat anti-GluN1 (1:200, sc-1467, Santa-Cruz) primary antibodies, FITC-conjugated mouse anti-αSMA (1:500, ab8211, Abcam) primary antibodies and rabbit anti-laminin (1:2000, ab11575, Abcam) primary antibodies. Primary antibodies were revealed using Fab'2 fragment anti rabbit and goat IgG linked to CY3 and Alexa Fluor 647 (1:600, Jackson ImmunoResearch) co-incubated 90 min at room temperature. Vessels were then coverslipped using mounting medium containing DAPI. Images were digitally captured using an epifluorescence microscope (Leica DM6000). Fluorescent intensity of the GluN1 staining in vessels was assessed using ImageJ software (NIH).

Statistical analysis

Results are expressed as the mean ± the standard deviation (SD). For curves displayed, curves in transparency represent the SEM in order to preserve the scale. Statistical analysis was performed using Mann–Whitney test, Wilcoxon test or t-test with the Statistica software (Statsoft). For the GluN1 fluorescence intensity and the pool meta-analysis, normality was assessed using D'Agostino and Pearson normality test. Values were considered statistically different if probability value, $p < 0.05$.

Results

Circulating tPA contributes to the increase of CBF during NVC

We examined the CBF increase produced by the activation of the whisker barrel cortex in wild type (WT) versus tPA-deficient mice ($tPA^{-/-}$) by using time-lapse laser speckle flowmetry (Suppl. Figure 1). Using this procedure, we showed that the CBF increase evoked by whiskers stimulation is significantly impaired in tPA-deficient mice ($tPA^{-/-}$) when compared to WT

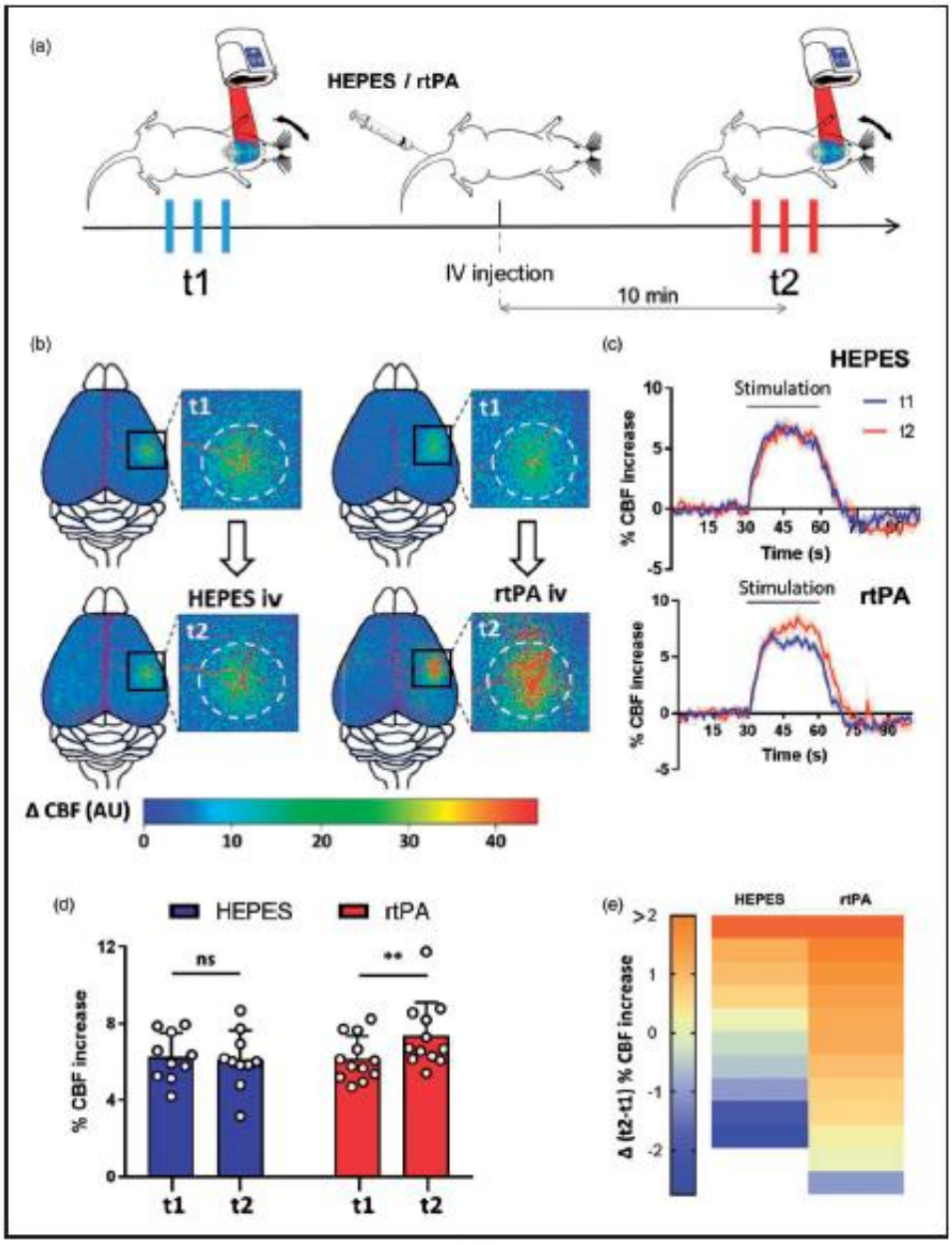

Figure 2. Vascular rtPA increases the functional hyperemia in $tPA^{-/-}$ mice. (a) Schematic representation of the experimental timeline, including a first train of stimulations as a control followed by an IV injection and a second train of stimulations 10 min after the injection. (b) Pseudo colored representative subtraction maps of the CBF highlighting CBF change during whiskers stimulation of $tPA^{-/-}$ mice before and after the injection of HEPES (200 µL, 0.3 M) or rtPA (200 µL, 10 mg/kg). Color intensity goes from blue (no change during stimulations) to red (strong CBF increase during stimulation). (c) Mean CBF signal trace from the S1bf during whiskers stimulation of $tPA^{-/-}$ mice before and after the injection of HEPES (200 µL, 0.3 M; —) or rtPA (200 µL, 10 mg/kg; —) extracted from Laser Doppler speckle images (curves in transparency define the SEM, $n = 10$ for the HEPES group, $n = 12$ for the rtPA group). (d) Quantification of the CBF increase during whiskers stimulation in $tPA^{-/-}$ mice before (t1) and after (t2) IV injection of HEPES (200 µL, 0.3 M) or rtPA (200 µL, 10 mg/kg). Circles represent values for each mouse (Mean ± SD, Wilcoxon test, $n = 10$ for the HEPES group, $n = 12$ for the rtPA group). (e) Diagram showing the evolution (delta) of the hemodynamic response of each mouse between the control condition and after the IV injection of HEPES (200 µL, 0.3 M) or rtPA (200 µL, 10 mg/kg).

for t2/t1, p-value = 0.0068; n = 10/12). These data demonstrate that the rtPA present in the bloodstream contributes to the increase of CBF during NVC.

A similar set of experiments was performed using wild-type animals instead of $tPA^{-/-}$ mice, in order to determine whether increasing the levels of circulating tPA may promote NVC. Our data demonstrate that even in the presence of endogenous tPA, increasing rtPA levels in the bloodstream leads to an increase of the hyperemia induced by whiskers stimulation (Suppl. Figure 6(a) to (d); HEPES injected tPA WT mice, 6.31% at t1 vs. 6.17% at t2, i.e. −2.21% for t2/t1, p-value = 0.8438; rtPA injected tPA WT mice, 6.17% at t1 vs. 7.12% at t2, i.e. +15.39% for t2/t1, p-value = 0.0117; n = 8–9 per group). A pooled analysis comparing all $tPA^{-/-}$ mice (n = 38), treated or not with rtPA during our experiments confirms that plasmatic tPA promotes CBF increase induced by whiskers stimulation (Suppl. Figure 7(a) to (c); HEPES injected $tPA^{-/-}$ mice, 6.27% at t1 vs. 6.31% at t2, i.e. +0.64% for t2/t1, p-value = 0.8982; rtPA injected $tPA^{-/-}$ mice, 6.05% at t1 vs. 6.98% at t2, i.e. +15.18% for t2/t1, p-value = 0.001; n = 38 in each group).

We then used in vivo functional ultrasound (fUS) imaging to confirm the function of tPA on NVC (Figure 3(a) to (e)). As reported above, when injected intravenously, rtPA led to an increase of the hyperemia induced by whiskers stimulation in the corresponding barrel cortex (+7.31% at t1 vs. +11.91% at t2 for rtPA-treated $tPA^{-/-}$ mice (n = 7), i.e. +62.93% for t2/t1, p-value = 0.0042, n = 7). Altogether, these multimodal data demonstrate that intravenous rtPA is implicated in the modulation of the CBF increase during NVC.

Circulating tPA enhances Whiskers stimulation-induced vasodilation, a phenomenon restricted to larger vessels

We used intravital microscopy in $tPA^{-/-}$ mice with or without intravenous infusions of rtPA to examine responses of individual vessels. We observed that rtPA treatment leads to a more pronounced dilation of the vessels in the barrel cortex during whiskers stimulation (Figure 4(a) and (b)). We then separated vessels according to their diameter (d) as follows: d > 25 µm, 15 < d < 25 and d < 15 µm (Figure 4(c)). All types of vessels showed a dilation in response to whiskers stimulation: +6.3% for vessels of d > 25 µm; +11.8% for 15 < d < 25 µm; +16.5% for d < 15 µm). However, a differential effect of rtPA was observed according to the diameter of vessels. Indeed, although rtPA treatment led to an increase of the dilation of the larger vessels, rtPA did not affect the dilation of small vessels (Figure 4(b) and (c); d > 25 µm, +3.8%, p = 0.0391; 15 < d < 25 µm, +3.8%, p = 0.0391; d < 15 µm, −0.7%, p = 0.6406; n = 8 vessels in each group).

NMDAR expressed on endothelial cells mediates the tPA-dependent modulation of NVC

We then postulated that the tPA present in the bloodstream could influence NVC by its ability to modulate NMDAR signaling on endothelial cells. In order to address this question, we used a molecular tool, tPA-K2*, a tPA mutated on the amino-acid in position 254 of the Lysine Binding Site (LBS) containing kringle 2 domain which is not capable to bind and activate NMDAR.[30] Then, we proposed that a chronic overexpression of tPA by the liver cells and its subsequent release in the circulation may promote the increased CBF induced by whiskers stimulation in $tPA^{-/-}$ mice. We thus used a set of expression vectors driven by a liver-specific promoter (pLIVE plasmids) that promotes sustained tPA secretion in the circulation, as we previously characterized[25] encoding for either a WT tPA (tPAWT) or a tPA-K2* (pLIVE-tPAWT, pLIVE-tPA-K2*; Figure 5). The liver was transfected in vivo by a hydrodynamic transfection of pLIVE constructs. Each animal was tested before (d1) and after (d3) hydrodynamic transfection and was thus its own control (Figure 5(a)). Our data showed that although tPAWT expression promoted the CBF increase induced by whiskers stimulation, the expression of tPA-K2* did not (Figure 5(b) to (e); pLIVE transfected $tPA^{-/-}$ mice, 6.01% at d1 vs. 6.24% at d3, i.e. +3.82% for d3/d1, p-value = 0.4961; pLIVE-tPAWT transfected $tPA^{-/-}$ mice, 5.77% at d3 vs. 6.86% at d1, i.e. +18.89% for d3/d1, p-value = 0.0391; pLIVE-tPA-K2* transfected $tPA^{-/-}$ mice, 5.50% at d1 vs. 5.77% at d3, i.e. +4.90% for d3/d1, p-value = 0.6875; n = 7–9). To control the efficiency of the transfection, we performed zymography assays from blood samples collected at d3 to measure tPA plasmatic concentration and activity.[25] As expected, we detected tPA proteolytic activity in the plasma of $tPA^{-/-}$ mice transfected with pLIVE-tPAWT or pLIVE-tPA-K2*, but not with the pLIVE empty plasmid (Figure 5(f)). These data demonstrate that tPA can promote the CBF increase induced by whiskers stimulation through a mechanism involving its K2 domain, suggesting a mechanism dependent on NMDAR.

Since the mutation of the LBS within the kringle 2 domain of tPA may also interfere with NMDAR-independent functions of tPA, we performed complementary experiments using Glunomab®. Glunomab® is a monoclonal antibody targeting the binding site of tPA on the GluN1 subunit of NMDAR, used as a competitive antagonist of tPA on NMDAR.[21,31] The aim of this experiment was not to target tPA itself, but

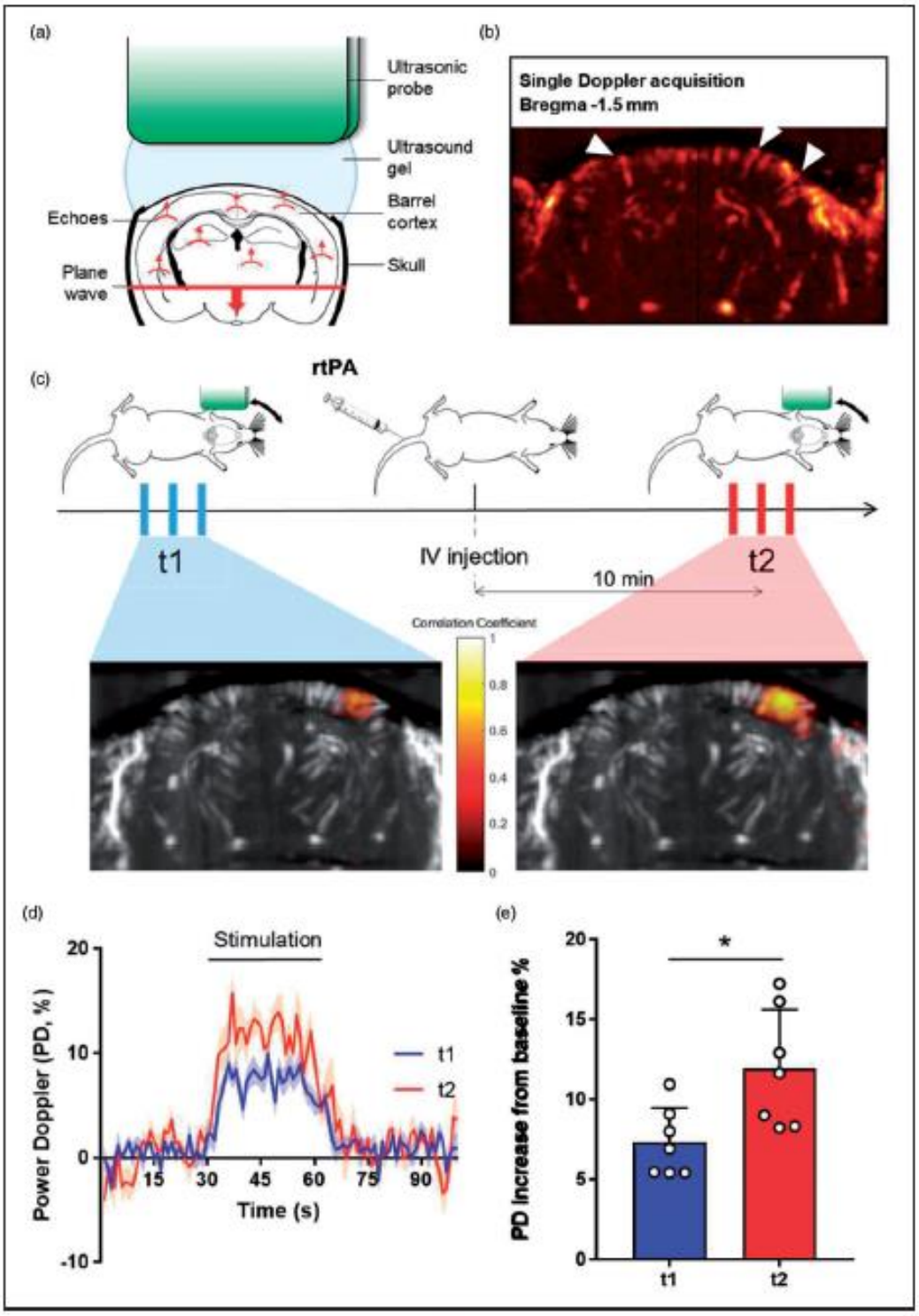

Figure 3. The promotion of the functional hyperemia by rtPA is not restricted to the surface of the brain but involved the whole barrel cortex. (a) Schematic representation of functional ultrasound acquisition. (b) Ultrasensitive Doppler image of the brain of a C57BL/6 mouse through a thinned skull window, revealing blood vessels, and particularly penetrating arterioles (white arrows).

(continued)

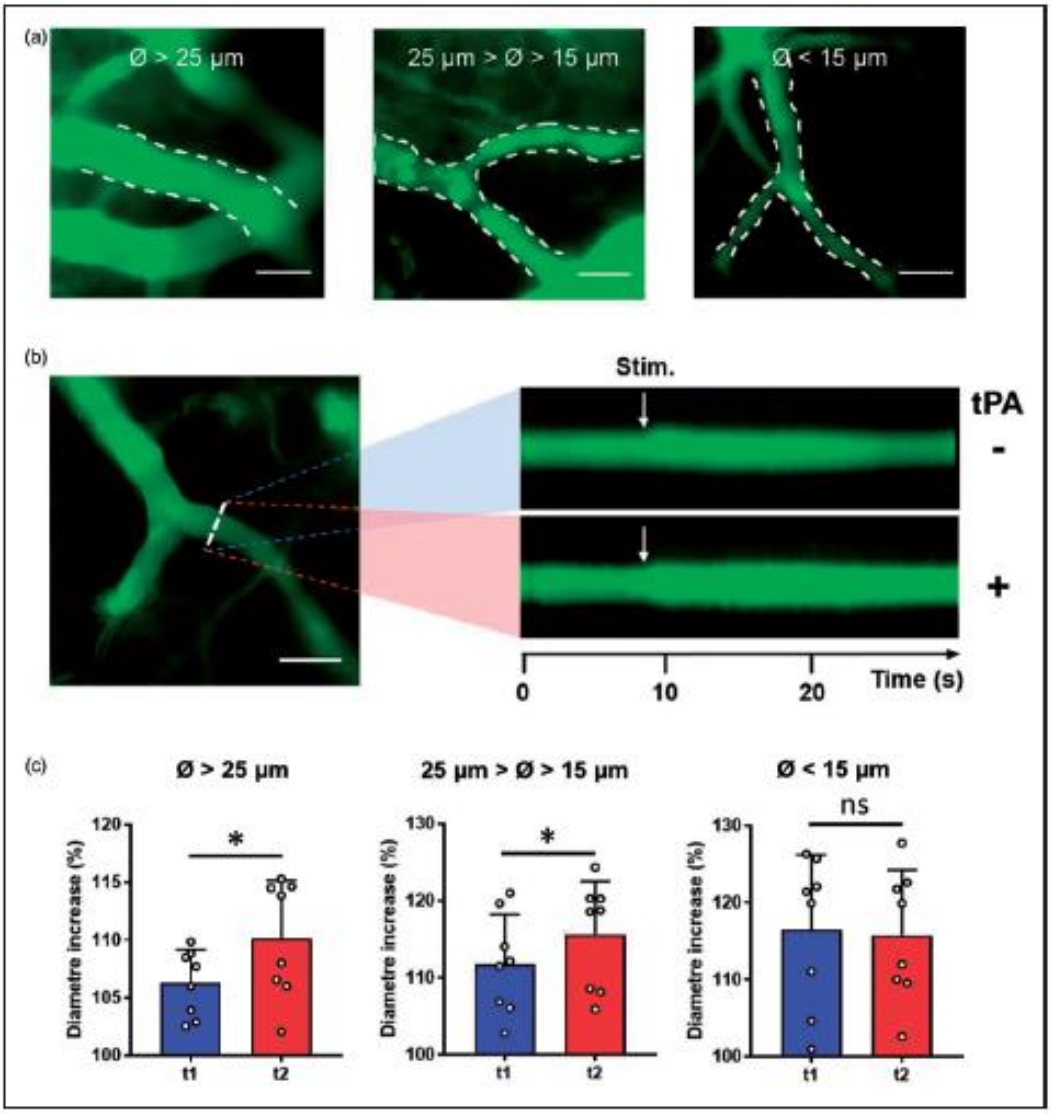

Figure 4. Vascular rtPA promotes whiskers stimulation induced dilation of large vessels. (a) Intravital microscopy images of vessels of different diameters revealed by in IV injection of FITC dextran. Images obtained from the S1bf cortex of $tPA^{-/-}$ mice (scale bar = 50 µm). (b) Left: Intravital microscopy images of a vessel from the S1bf cortex of a $tPA^{-/-}$ mouse (scale bar = 50 µm). Vessels were labelled using an IV injection of FITC dextran. Right: line-scans of the same vessel during whiskers stimulation before (top) and after (bottom) rtPA (10 mg/kg) injection. (c) Quantification from intravital microscopy images of the vessels dilation during whiskers stimulation according to their diameters before (●) and after (●) rtPA (10 mg/kg) injection. Circles represent values for each vessel (Mean ± SD, Wilcoxon test, $n = 8$–9 per group).

Figure 3. Continued
(c) Schematic representation of the experimental timeline, including a first train of stimulations as control followed by an IV injection of rtPA and a second train of stimulations 10 min after the injection. Bottom images represent an example of the activation maps when stimulating the left whiskers before and after the injection of rtPA. Colormap corresponds to the correlation coefficient between the normalized PD intensity along time and a step function representing the stimulation pattern. (d) Relative augmentation of the Power Doppler in the activated area (seen in c) during whiskers stimulation of $tPA^{-/-}$ mice before (—) or after (—) intravenous injection of rtPA (curves in transparency define the SEM, $n = 7$). (e) Quantification of the relative PD intensity increase in the activated area (seen in c) during whiskers stimulation in $tPA^{-/-}$ mice. Circles represent values for each mouse (Mean ± SD, Wilcoxon test, $n = 7$).

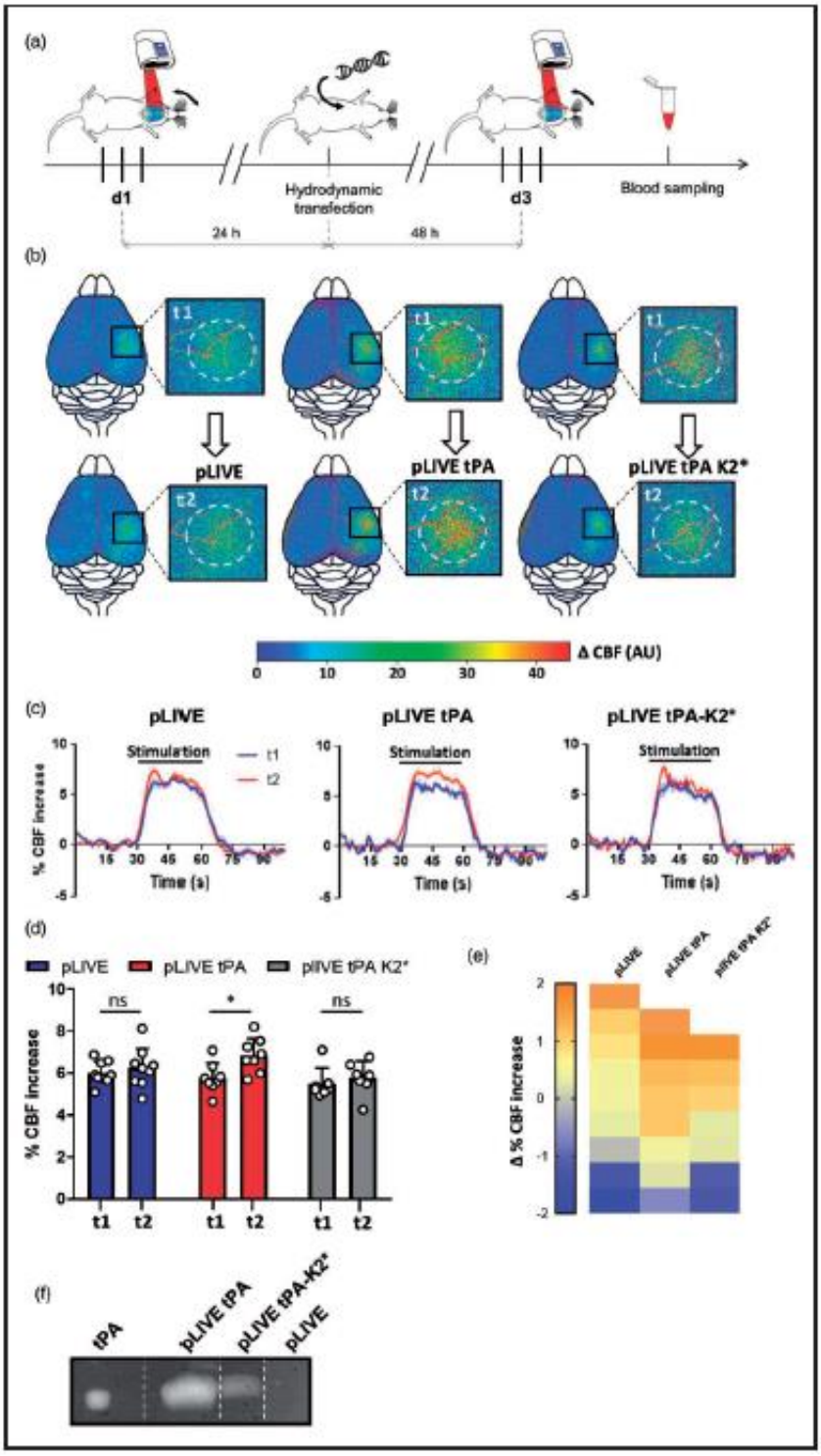

Figure 5. Chronic expression of tPA restrained to the blood circulation promotes functional hyperemia in tPA$^{-/-}$ mice.
(a) Schematic representation of the experimental timeline, including a first train of stimulations as control followed 24 h later by the

(continued)

directly the binding site of tPA on NMDAR and thus to block subsequent NMDAR signaling.[21,31] In agreement with the above data and our hypothesis that circulating tPA may contribute to NVC by acting on NMDAR expressed on endothelial cells, Glunomab® blocked the rtPA-induced increase of hyperemia during whiskers stimulation (Figure 6(a) to (d); rtPA + control IgG injected $tPA^{-/-}$ mice, 5.66% at t1 vs. 6.39% at t2, i.e. +12.89% for t2/t1, p-value = 0.0391; rtPA + Glunomab® injected $tPA^{-/-}$ mice, 6.05% at t1 vs. 5.89% at t2, i.e. −2.64% for t2/t1, p-value > 0.9999; $n = 8$–9).

Furthermore, these data were confirmed by using common NMDAR antagonists: MK-801 (Dizocilpine), a non-competitive NMDAR antagonist, and D-2-amino-5-phosphonopentanoate (AP5), a competitive antagonist of NMDAR (Figure 6(a) to (d)). Both MK-801 and AP5 blocked the rtPA effect on the CBF increase induced by whiskers stimulation (rtPA + MK801 injected $tPA^{-/-}$ mice, 5.39% at t1 vs. 5.23%, at t2 i.e. −2.96% for t2/t1, p-value = 0.7422; rtPA + AP5 injected $tPA^{-/-}$ mice, 5.54% at t1 vs. 5.89% at t2, i.e. +6.31% for t2/t1, p-value = 0.6406; $n = 9$ per groups). Control experiments with injection of MK801 or AP5 alone showed no effect of these molecules on NVC (Suppl. Figure 8(a) to (d)). Altogether, these data demonstrate that the plasmatic tPA triggers NVC through a mechanism dependent of its ability to activate the NMDAR present at the surface of endothelial cells.

To understand why the dilation of only larger vessels is affected by rtPA, we sought to investigate the distribution of NMDAR in brain vessels. To do so, we performed immunostaining for GluN1-containing NMDAR from isolated brain vessels. Vessels were discriminated by positive or negative immunostaining for alpha-SMA (smooth muscle actin; Figure 7(a)). As expected, αSMA staining was positive for vessels of more than 8–9 µm in diameter (Figure 7(b)). In agreement with the above data, immunostainings revealed the presence of NMDAR preferentially on alpha-SMA positive vessels, i.e. arteries and arterioles (Figure 7(c) to (f); $n = 34$ for alpha-SMA positive vessels, $n = 29$ for alpha-SMA negative vessels, p-value = 0.011).

Overall, we demonstrate here for the first time that circulating tPA is necessary for the full increase of CBF during NVC by promoting the signaling of NMDAR expressed at the luminal side of endothelial cells, a phenomenon restricted to larger vessels (arteries and arterioles).

Discussion

CBF rapidly increases in response to neural activation, a phenomenon termed functional hyperemia or neurovascular coupling (NVC), providing a local supply of substrates and energy to neurons.[1] NVC is a complex mechanism involving several different cell types and signaling pathways among the neurovascular unit, especially in neurons and astrocytes. Many different molecules are involved, and their mechanisms of action are not yet completely understood. At the synaptic level, NMDAR activation contributes to this process.[1] Indeed, an important part of the vascular response is mediated by the activation of postsynaptic NMDAR. NMDAR are associated to the neuronal NO synthase (nNOS),[32] whose activation leads to the production and release of the vasodilator nitric oxide (NO).[33] Accordingly, NMDAR can regulate nNOS activity by increasing intra-cellular Ca^{2+} concentration and regulating the phosphorylation of the nNOS.[34]

The serine protease tPA (69 kDa), in addition to its role in fibrinolysis,[6] has more recently emerged as a pleiotropic neuromodulator implicated in various aspects of brain functions, including learning and memory processes and anxiety behavior.[7,14] In 2008, using a mouse model of whiskers stimulation,[15] Park et al., proposed tPA as an actor of NVC[15] for its ability to influence NMDAR signaling.[8] When compared with wild-type mice, CBF increase in the barrel cortex of tPA deficient mice showed a sustained attenuation

Figure 5. Continued
hydrodynamic transfection, and by a second train of stimulations 48 h after the transfection; Three different plasmids were transfected: pLIVE (empty), pLIVE-tPA and pLIVE- tPA-K2*. (b) Pseudo colored representative subtraction maps of the CBF highlighting CBF change during whiskers stimulation of $tPA^{-/-}$ mice before and after the transfection. Color intensity goes from blue (no change during stimulations) to red (strong CBF increase during stimulation). (c) Mean CBF signal trace from the S1bf during whiskers stimulation of $tPA^{-/-}$ mice before (—) and after (—) the transfection extracted from Laser Doppler speckle images (curves in transparency define the SEM, $n = 7$–9 per group). (d) Quantification of the CBF increase during whiskers stimulation in $tPA^{-/-}$ mice before (t1) and after (t2) the transfection. Circles represent values for each mouse (Mean ± SD, Wilcoxon test, $n = 7$–9 per group). (e) Diagram showing the evolution (delta) of the hemodynamic response of each mouse between the control condition and after the hydrodynamic transfection. (f) Representative fibrin-agar zymography assays performed from plasma of pLIVE, pLive-tPA and pLIVE-tPA-K2* transfected mice, which demonstrate the presence of free plasmatic tPA and tPA-K2* after the transfection. rtPA was used as standard in the zymography assays.

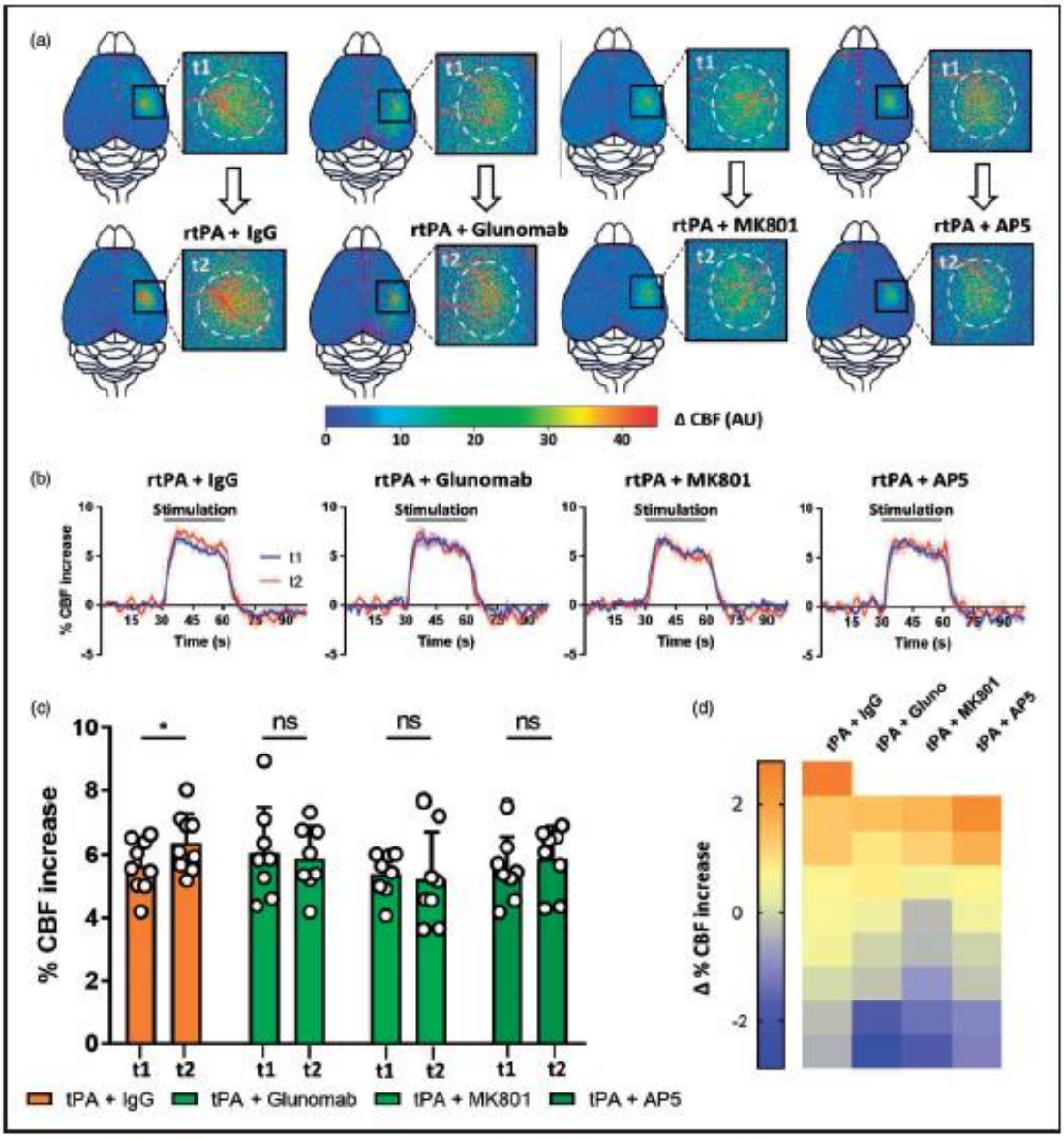

Figure 6. Inhibition of the interaction between vascular rtPA and NMDARs prevents the rtPA-induced potentiation of functional hyperemia. (a) Pseudo colored representative subtraction maps of the CBF highlighting CBF change during whiskers stimulation of $tPA^{-/-}$ mice before and after the injection of rtPA (10 mg/kg) and a control IgG (5 mg/kg), rtPA (10 mg/kg) and Glunomab® (5 mg/kg), rtPA (10 mg/kg) and MK-801 (0.4 mg/kg), or rtPA (10 mg/kg) and AP5 (0.4 mg/kg). Color intensity goes from blue (no change during stimulations) to red (strong CBF increase during stimulation). (b) Mean CBF signal trace from the S1bf during whiskers stimulation of $tPA^{-/-}$ mice before (—) and after (—) the injection of rtPA (10 mg/kg) and a control IgG (5 mg/kg), rtPA (10 mg/kg) and Glunomab® (5 mg/kg), rtPA (10 mg/kg) and MK-801 (0.4 mg/kg), or rtPA (10 mg/kg) and AP5 (0.4 mg/kg) extracted from Laser Doppler speckle images (curves in transparency define the SEM, $n = 8$–10 per group). (c) Quantification of the CBF increase during whiskers stimulation in $tPA^{-/-}$ mice before (t1) and after (t2) IV injection of rtPA (10 mg/kg) and a control IgG (5 mg/kg), rtPA (10 mg/kg) and Glunomab® (5 mg/kg), rtPA (10 mg/kg) and MK-801 (0.4 mg/kg), or rtPA (10 mg/kg) and AP5 (0.4 mg/kg). Circles represent values for each mouse (Mean ± SD, Wilcoxon test, $n = 8$–10 per group). (d) Diagram showing the evolution (delta) of the hemodynamic response of each mouse between the control condition and after the IV injection of rtPA (10 mg/kg) and a control IgG (5 mg/kg), rtPA (10 mg/kg) and Glunomab® (5 mg/kg), rtPA (10 mg/kg) and MK-801 (0.4 mg/kg), or rtPA (10 mg/kg) and AP5 (0.4 mg/kg).

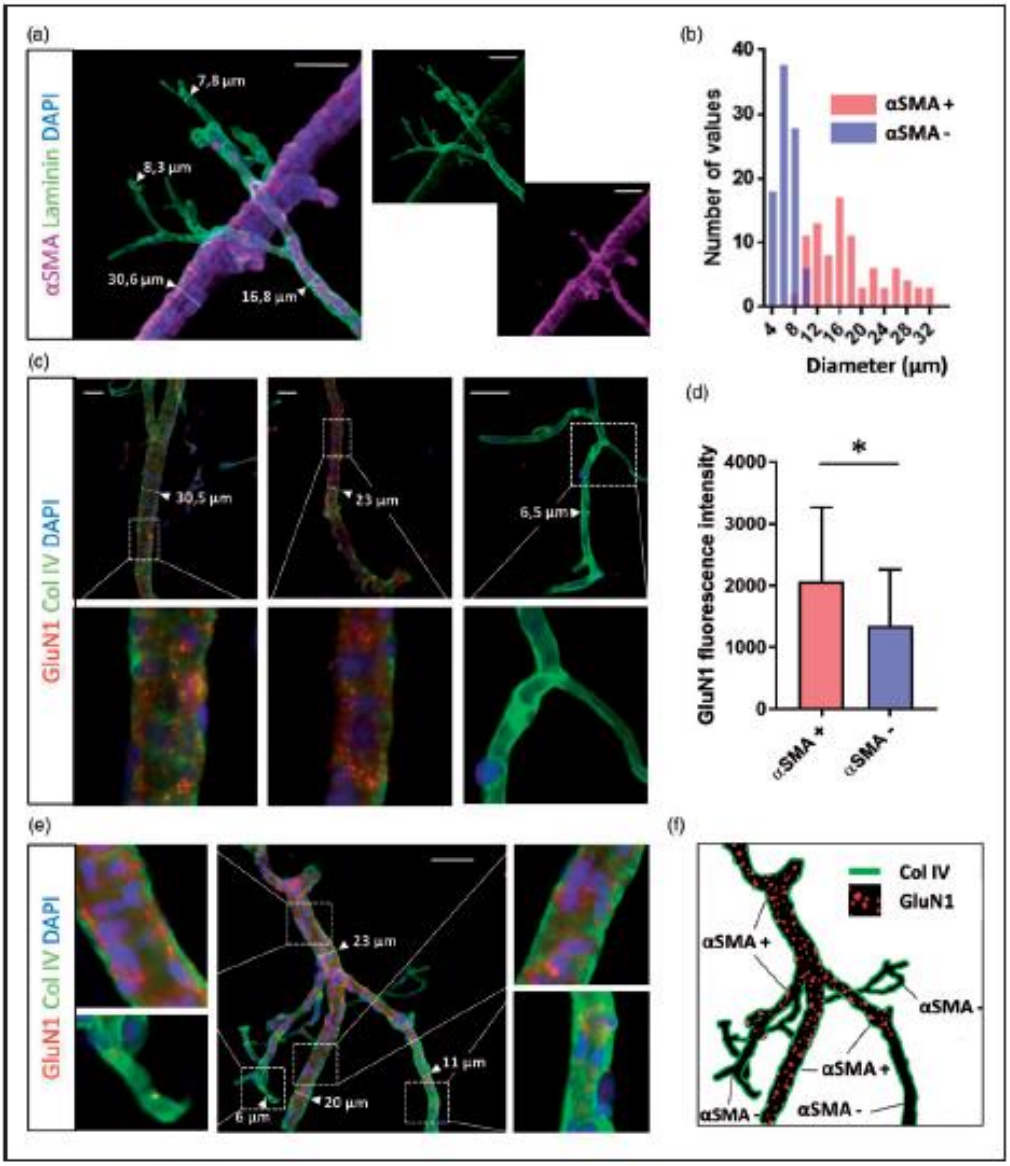

Figure 7. Expression of NMDARs is restricted to arteries and arterioles. (a) Epifluorescence images of isolated vessels from C57BL/6 mice brain revealing (scale bar = 50 µm): α-SMA (purple), laminin (green) and cells nuclei (blue). (b) Quantification of the number of vessels positive (red) or negative (blue) for α-SMA staining depending on their diameter. Only vessels over 8–9 µm in diameter express α-SMA. (c) Epifluorescence images of isolated vessels from C57BL/6 mice brain revealing GluN1 subunit of the NMDAR (red), collagen IV (green) and cells nuclei (blue), depending on vessel diameter. (d) Quantification of the GluN1 staining fluorescence intensity in α-SMA positive vessels and in α-SMA negative vessels (ANOVA test, $n = 34$ for the α-SMA + group and $n = 29$ for the α-SMA – group, from four different mice). (e–f) Epifluorescence images of isolated cerebrovascular tree from C57BL/6 mice brain revealing GluN1 staining (red), Col IV (green) and cells nuclei (blue), and (f) corresponding schematic representation.

during whiskers stimulation. In this pioneer publication, superfusion of rtPA on the surface of the brain parenchyma of tPA-deficient mice restored NVC, with NMDAR and activation of NOS implicated as mediators of this response.[15] Our present data confirm the role of tPA in NVC, providing the demonstration that in addition to its role at the synapse level, circulating tPA plays also a significant role. Indeed,

although tPA deficient mice showed an impaired CBF increase induced by whiskers stimulation, this lack of response can be rescued after intravenous injection of rtPA. Besides similarities in our model and the one used by Park et al., we can note a difference in the increase produced by whiskers stimulation of mice. In their study, whiskers stimulation induced a 20% increase of the CBF, whereas our model provides an 8% increase of CBF. This can be explained by our use of a laser speckle imaging system instead of a Doppler laser fiber, allowing us to measure the blood flow of the entire brain surface through the intact skull, and giving us the advantage to measure the mean CBF increase of the whole S1bf. We also choose to anesthetize our mice with medetomidine. Medetomidine is an alpha-2-adrenergic receptor antagonist having little effect on brain vessels, and widely used for rodent functional magnetic resonance imaging (fMRI) studies. Medetomidine can be used for longitudinal studies such as hydrodynamical transfection model (Figure 5). On the other hand, medetomidine causes a bradycardia that can diminish the CBF increase. Overall, when looking at the difference in the CBF increase between tPA WT and tPA KO mice (Figure 1(b)), the effect size is comparable between studies.

Emerging evidence suggest an important role of endothelial cells in NVC, but the nature of how it contributes to the dialogue between neurons, smooth muscle cells and astrocytes in NVC remains unknown. Endothelial cells would indeed be the support of the propagation of a retrograde activity-induced signal that would triggers the dilation of larger vessels upstream of the activated area.[1,2] Furthermore, the presence of NMDAR on endothelial cells was reported by several groups[18–20] with roles in the control of the homeostasis of the BBB on healthy and injured brains.[35] NMDAR was also reported to act on the cerebral blood vessel tone.[36,37] Particularly, several studies have showed that NMDAR expressed on endothelial cells is involved in the dilation mechanism of middle cerebral arteries isolated from mice.[38] The activation of endothelial NMDAR elicited by astrocytes thus leads to the production of NO by the eNOS and to the dilation of brain vessels.[39,40] A recent study demonstrated that loss of function of endothelial NMDAR leads to a 50% reduction of CBF increased during whiskers stimulation.[41] This study used grin1 fl/fl· $Cre^{+/-}$ mice in which the Cre recombinase is driven by Tie2 promoter elements, leading to a complete loss of function of all endothelial NMDAR, while we have performed intravenous injections of NMDA receptors inhibitors in $tPA^{-/-}$ mice with an effect only on the luminal NMDA receptors. Additional investigations are needed to investigate whether the specific contribution of endothelial NMDAR to NVC is dependent on their localization side and signalization input (luminal or parenchymal). Interestingly, and consistent with our data, this loss of function has no effect on resting CBF.[41]

Accordingly, plasmatic tPA was also reported to have vasodilation properties on peripherical vessels and to reduce brain vessels reactivity,[42–44] cerebral vascular resistance and systemic blood pressure,[45] suggesting that tPA may modulate cerebrovascular tone during functional hyperemia. It is also interesting to note that an inactive tPA variant (tPA-S481A) was capable of preventing the impairment of autoregulation when administered 30 min after fluid percussion injury through the inhibition of the NMDAR over-activation.[46] Similarly, a tPA variant tPA-(A296-299), characterized to prevent the binding of endogenous tPA to NMDAR, was reported to prevent impairment of cerebral autoregulation and necrosis of hippocampal neurons after stroke.[47] Here we demonstrate that the circulating tPA can act on endothelial NMDAR to promote brain vessels dilation during functional hyperemia. Thus, deletion and rescue experiments were performed using a mutated form of tPA, tPA-K2* previously reported to not bind with NMDAR and thus to not promote their signaling,[30] and a monoclonal antibody (Glunomab®) characterized as an antagonist of tPA on NMDAR signaling.[21] Our data were also confirmed by using different modalities of in vivo imaging including the largely used laser speckle imaging and intravital microscopy imaging, in addition to the more recent promising methodology of fUS.[24,27,48] Our data show that the intravenous injection of rtPA has no effect on the resting CBF (Suppl. Figure 1), which can be surprising given the previous discussed studies reporting an effect of both tPA and NMDAR on vascular tone.[38,42] However, those studies were not performed in vivo, but mostly on isolated arteries, thus may be lacking other regulatory mechanisms compensating this phenomenon in vivo, such as autoregulation. tPA is also mostly inhibited in the blood circulation in physiological conditions, and a large part of the rtPA injected in our model is dedicated to the saturation of the inhibitors present in the blood stream. This could explain the lack of direct effect of rtPA on vessel tone just after its injection.

In addition, it is interesting to note that tPA was previously reported to influence NO and reactive oxygen species (ROS) production on endothelial cells by a mechanism dependent of NMDAR.[19] This is to be compared with the study of LeMaistre et al., which has showed that the dilation of the middle cerebral artery mediated by the activation of NMDAR required an intact endothelium and the presence of eNOS, supporting the hypothesis of an action of tPA directly on the vessels.

Traditionally, regulation of CBF is thought to occur at the level of arterioles.[3] However, capillaries in the brain are also wrapped by contractile cells called pericytes,[49] for which the exact role in NVC is debated. However, we found that rtPA only promotes vasodilation of large vessels of at least 15 µm of diameter, corresponding to arterioles and arteries (Figure 4). Consistent with this, we show that the expression of NMDAR is restricted to the vessels of these diameters. These data are correlated with the fact that during NVC, NMDAR and the subsequent signaling pathways are associated with arteriolar dilation rather than capillaries, suggesting different signalization pathways between arteries and capillaries.[50] This leads us to think that similar organization could occur in endothelial cells, and that endothelial NMDAR activation is specific of arterial dilation. In agreement with that, previous findings have shown that tPA is primarily associated with precapillary arterioles in the CNS.[51]

It is known for a long time that blood molecules, such as acetylcholine, bradykinin or ATP can regulate vascular tone and induce vessel dilation. Other events such as shear stress can also induce vessel dilation in the brain. However, the effects of these molecules are independent of the NVC by itself. Our study reports for the first time that a molecule present in the circulation (here tPA) contributes to the CBF increase observed during NVC. We found that circulating tPA, potentially released in the blood circulation by endothelial cell during neuronal activity, can interact with endothelial NMDAR and promote the dilation of large vessels surrounded by smooth muscle cells. Circulating tPA is thus necessary for the full increase of CBF during NVC.

Although NVC is the basis of blood oxygen level dependent (BOLD) fMRI, our understanding of the underlying signaling mechanisms is still incomplete. Our study provides important information to understand the complexity of fMRI, with the demonstration that a vascular molecule such as tPA may contribute to NVC by interacting with NMDAR expressed on the luminal side of endothelial cells. The finding that tPA modulates functional hyperemia raises the possibility that levels of plasmatic tPA may contribute to the alterations in NVC that occur in aging[1,52] or brain pathologies such as Alzheimer's disease or ischemic stroke.[1] Indeed, the levels of the principal inhibitor of tPA in the blood stream, PAI-1, that are increased during Alzheimer Disease,[53] raise the possibility that this increased tPA inhibition in the circulation could participate in the impairment of NVC. Moreover, stroke leads to a profound alteration in NVC in the acute phase after the ischemic event, worsening cerebral perfusion and promoting brain damages,[1] an effect which could be explained by alterations of the vascular levels of active tPA.

Altogether, our present study demonstrates that the vascular tPA plays a role in neurovascular coupling by influencing endothelial NMDA receptors. Further investigations are needed to understand how this new mechanism of action of tPA contributes to brain functions and dysfunctions.

Funding

The author(s) disclosed receipt of the following financial support for the research, authorship, and/or publication of this article: This work was funded by the Institut National de la Santé et de la Recherche Médicale (INSERM), Caen Normandie University, the Regional Council of Lower Normandy. This project is also part of the following European research programs: 1/European Marie Curie International Training Network "NeuroInflammation, FP7; 2/ NeuroAtlantic, An Atlantic innovation platform on diagnosis and treatment of neurological diseases and aging, EAPA_791/ 2018-NEUROATLANTIC; 3/H2020, International Marie Curie Training Network, ENTRAIN, Neuroinflammation, H2020-MSCA-ITN-2018 number 813294.

Declaration of conflicting interests

The author(s) declared no potential conflicts of interest with respect to the research, authorship, and/or publication of this article.

Authors' contributions

Study design: DV, AA and CO Conducting experiments and acquiring data: AA, AD, VH, CO, TD, MR, YH and MY Analyzing data: AA, VH and YH. Writing the article: DV, AA, and MT.

Supplemental material

Supplemental material for this article is available online.

References

1. Iadecola C. The neurovascular unit coming of age: a journey through neurovascular coupling in health and disease. *Neuron* 2017; 96: 17–42.
2. Chen BR, Kozberg MG, Bouchard MB, et al. A critical role for the vascular endothelium in functional neurovascular coupling in the brain. *J Am Heart Assoc* 2014; 3: e000787.
3. Hill RA, Tong L, Yuan P, et al. Regional blood flow in the normal and ischemic brain is controlled by arteriolar smooth muscle cell contractility and not by capillary pericytes. *Neuron* 2015; 87: 95–110.
4. Hall CN, Reynell C, Gesslein B, et al. Capillary pericytes regulate cerebral blood flow in health and disease. *Nature* 2014; 508: 55–60.
5. Collen D and Lijnen HR. Basic and clinical aspects of fibrinolysis and thrombolysis. *Blood* 1991; 78: 3114–3124.

6. Vivien D, Gauberti M, Montagne A, et al. Impact of tissue plasminogen activator on the neurovascular unit: from clinical data to experimental evidence. *J Cereb Blood Flow Metab* 2011; 31: 2119–2134.
7. Samson AL, Medcalf RL. Tissue-type plasminogen activator: a multifaceted modulator of neurotransmission and synaptic plasticity. *Neuron* 2006; 50: 673–678.
8. Nicole O, Docagne F, Ali C, et al. The proteolytic activity of tissue-plasminogen activator enhances NMDA receptor-mediated signaling. *Nat Med* 2001; 7: 59–64.
9. Cassé F, Bardou I, Danglot L, et al. Glutamate controls tPA recycling by astrocytes, which in turn influences glutamatergic signals. *J Neurosci* 2012; 32: 5186–5199.
10. Pawlak R, Nagai N, Urano T, et al. Rapid, specific and active site-catalyzed effect of tissue-plasminogen activator on hippocampus-dependent learning in mice. *Neuroscience* 2002; 113: 995–1001.
11. Pawlak R, Magarinos AM, Melchor J, McEwen B, Strickland S. Tissue plasminogen activator in the amygdala is critical for stress-induced anxiety-like behavior. *Nat Neurosci* 2003; 6: 168–174.
12. Chevilley A, Lesept F, Lenoir S, Ali C, Parcq J, Vivien D. Impacts of tissue-type plasminogen activator (tPA) on neuronal survival. *Front Cell Neurosci* 2015; 9: 415.
13. Parcq J, Bertrand T, Montagne A, et al. Unveiling an exceptional zymogen: the single-chain form of tPA is a selective activator of NMDA receptor-dependent signaling and neurotoxicity. *Cell Death Differ* 2012; 19: 1983–1991.
14. Hébert M, Anfray A, Chevilley A, et al. Distant space processing is controlled by tPA-dependent NMDA receptor signaling in the entorhinal cortex. *Cereb Cortex* 2017; 27: 4783–4796.
15. Park L, Gallo EF, Anrather J, et al. Key role of tissue plasminogen activator in neurovascular coupling. *Proc Natl Acad Sci U S A* 2008; 105: 1073–1078.
16. Lochner JE, Honigman LS, Grant WF, et al. Activity-dependent release of tissue plasminogen activator from the dendritic spines of hippocampal neurons revealed by live-cell imaging. *J Neurobiol* 2006; 66: 564–577.
17. Angles-Cano E, Balaton A, Bonniec BL, et al. Production of monoclonal antibodies to the high fibrin-affinity, tissue- type plasminogen activator of human plasma. Demonstration of its endothelial origin by immunolocalization. *Blood* 1985; 66: 913–920.
18. András IE, Deli MA, Veszelka S, et al. The NMDA and AMPA/KA receptors are involved in glutamate-induced alterations of occludin expression and phosphorylation in brain endothelial cells. *J Cereb Blood Flow Metab* 2007; 27: 1431–1443.
19. Reijerkerk A, Kooij G, Van Der Pol SMA, et al. The NR1 subunit of NMDA receptor regulates monocyte transmigration through the brain endothelial cell barrier. *J Neurochem* 2010; 113: 447–453.
20. Scott GS, Bowman SR, Smith T, et al. Glutamate-stimulated peroxynitrite production in a brain-derived endothelial cell line is dependent on N-methyl-D-aspartate (NMDA) receptor activation. *Biochem Pharmacol* 2007; 73: 228–236.
21. Macrez R, Ortega MC, Bardou I, et al. Neuroendothelial NMDA receptors as therapeutic targets in experimental autoimmune encephalomyelitis. *Brain* 2016; 139: 2406–2419.
22. Kisler K, Nelson AR, Montagne A, et al. Cerebral blood flow regulation and neurovascular dysfunction in Alzheimer disease. *Nat Rev Neurosci* 2017; 18: 419–434.
23. Hillman EMC. Coupling mechanism and significance of the BOLD signal: a status report. *Annu Rev Neurosci* 2014; 37: 161–181.
24. Macé E, Montaldo G, Cohen I, et al. Functional ultrasound imaging of the brain. *Nat Methods* 2011; 8: 662–664.
25. Marcos-Contreras OA, Martinez de Lizarrondo S, Bardou I, et al. Hyperfibrinolysis increases blood-brain barrier permeability by a plasmin- and bradykinin-dependent mechanism. *Blood* 2016; 128: 2423–2434.
26. Gaussem P, Grailhe P and Anglès-Cano E. Sodium dodecyl sulfate-induced dissociation of complexes between human tissue plasminogen activator and its specific inhibitor. *J Biol Chem* 1993; 268: 12150–12155.
27. Tiran E, Ferrier J, Deffieux T, et al. Transcranial functional ultrasound imaging in freely moving awake mice and anesthetized young rats without contrast agent. *Ultrasound Med Biol* 2017; 43: 1679–1689.
28. Demené C, Deffieux T, Pernot M, et al. Spatiotemporal clutter filtering of ultrafast ultrasound data highly increases Doppler and fUltrasound sensitivity. *IEEE Trans Med Imaging* 2015; 34: 2271–2285.
29. Boulay A-C, Saubaméa B, Declèves X, et al. Purification of mouse brain vessels. *J Vis Exp JoVE* 2015; 10: e53208.
30. Parcq J, Bertrand T, Baron AF, et al. Molecular requirements for safer generation of thrombolytics by bioengineering the tissue-type plasminogen activator A chain. *J Thromb Haemost* 2013; 11: 539–546.
31. Macrez R, Obiang P, Gauberti M, et al. Antibodies preventing the interaction of tissue-type plasminogen activator with N-Methyl-d-Aspartate receptors reduce stroke damages and extend the therapeutic window of thrombolysis. *Stroke* 2011; 42: 2315–2322.
32. Christopherson KS, Hillier BJ, Lim WA, et al. PSD-95 Assembles a ternary complex with the N-Methyl-d-aspartic acid receptor and a bivalent neuronal NO synthase PDZ domain. *J Biol Chem* 1999; 274: 27467–27473.
33. Busija DW, Bari F, Domoki F, Louis T. Mechanisms involved in the cerebrovascular dilator effects of N-methyl-D-aspartate in cerebral cortex. *Brain Res Rev* 2007; 56: 89–100.
34. Rameau GA, Chiu L-Y and Ziff EB. NMDA receptor regulation of nNOS phosphorylation and induction of neuron death. *Neurobiol Aging* 2003; 24: 1123–1133.
35. Mehra A, Ali C, Parcq J, et al. The plasminogen activation system in neuroinflammation. *Biochim Biophys Acta* 2016; 1862: 395–402.
36. Fiumana E, Parfenova H, Jaggar JH, et al. Carbon monoxide mediates vasodilator effects of glutamate in isolated pressurized cerebral arterioles of newborn pigs. *Am J Physiol* 2003; 284: H1073–H1079.
37. Parfenova H, Fedinec A and Leffler CW. Ionotropic glutamate receptors in cerebral microvascular endothelium

are functionally linked to heme oxygenase. *J Cereb Blood Flow Metab* 2003; 23: 190–197.
38. LeMaistre JL, Sanders SA, Stobart MJ, et al. Coactivation of NMDA receptors by glutamate and d-serine induces dilation of isolated middle cerebral arteries. *J Cereb Blood Flow Metab* 2012; 32: 537–547.
39. Lu L, Hogan-Cann AD, Globa AK, et al. Astrocytes drive cortical vasodilatory signaling by activating endothelial NMDA receptors. *J Cereb Blood Flow Metab* 2019; 39: 481–496.
40. Stobart JLL, Lu L, Anderson HDI, et al. Astrocyte-induced cortical vasodilation is mediated by D-serine and endothelial nitric oxide synthase. *Proc Natl Acad Sci U S A* 2013; 110: 3149–3154.
41. Hogan-Cann AD, Lu P and Anderson CM. Endothelial NMDA receptors mediate activity-dependent brain hemodynamic responses in mice. *Proc Natl Acad Sci USA* 2019; 116: 10229–10231.
42. Nassar T, Akkawi S, Shina A, et al. In vitro and in vivo effects of tPA and PAI-1 on blood vessel tone. *Blood* 2004; 103: 897–902.
43. Nassar T, Yarovoi S, Fanne RA, et al. Regulation of airway contractility by plasminogen activators through N-Methyl-D-aspartate receptor–1. *Am J Respir Cell Mol Biol* 2010; 43: 703–711.
44. Heyman SN, Hanna Z, Nassar T, et al. The fibrinolytic system attenuates vascular tone: effects of tissue plasminogen activator (tPA) and aminocaproic acid on renal microcirculation. *Br J Pharmacol* 2004; 141: 971–978.
45. Cipolla MJ, Lessov N and Clark WM. Postischemic attenuation of cerebral artery reactivity is increased in the presence of tissue plasminogen activator. *Stroke* 2000; 31: 940–945.
46. Armstead WM, Bohman L-E, Riley J, et al. tPA-S481A prevents impairment of cerebrovascular autoregulation by endogenous tPA after traumatic brain injury by upregulating p38 MAPK and inhibiting ET-1. *J Neurotrauma* 2013; 30: 1898–1907.
47. Armstead WM, Hekierski H, Yarovoi S, et al. tPA variant tPA-A296-299Prevents impairment of cerebral autoregulation and necrosis of hippocampal neurons after stroke by inhibiting upregulation of ET-1. *J Neurosci Res* 2018; 96: 128–137.
48. Errico C, Pierre J, Pezet S, et al. Ultrafast ultrasound localization microscopy for deep super-resolution vascular imaging. *Nature* 2015; 527: 499–502.
49. Kisler K, Nelson AR, Rege SV, et al. Pericyte degeneration leads to neurovascular uncoupling and limits oxygen supply to brain. *Nat Neurosci* 2017; 20: 406–416.
50. Mishra A, Reynolds JP, Chen Y, et al. Astrocytes mediate neurovascular signaling to capillary pericytes but not to arterioles., Astrocytes mediate neurovascular signaling to capillary pericytes but not to arterioles. *Nat Neurosci Nat Neurosci* 2016; 19: 1619–1627.
51. Levin EG and del Zoppo GJ. Localization of tissue plasminogen activator in the endothelium of a limited number of vessels. *Am J Pathol* 1994; 144: 855–861.
52. Toth P, Tarantini S, Tucsek Z, et al. Resveratrol treatment rescues neurovascular coupling in aged mice: role of improved cerebromicrovascular endothelial function and downregulation of NADPH oxidase. *Am J Physiol* 2014; 306: H299–H308.
53. Wilkerson WR and Sane DC. Aging and thrombosis. *Semin Thromb Hemost* 2002; 28: 555–568.

Theranostics 2020, Vol. 10, Issue 17 7480

IVYSPRING INTERNATIONAL PUBLISHER

Theranostics

2020; 10(17): 7480-7491. doi: 10.7150/thno.44233

Research Paper

Early Ultrafast Ultrasound Imaging of Cerebral Perfusion correlates with Ischemic Stroke outcomes and responses to treatment in Mice

Vincent Hingot[1†], Camille Brodin[2†], Florent Lebrun[2,5], Baptiste Heiles[1], Audrey Chagnot[2], Mervé Yetim[2], Maxime Gauberti[3], Cyrille Orset[2], Mickael Tanter[1], Olivier Couture[1], Thomas Deffieux[1‡], Denis Vivien[2,4‡]

1. Institute Physics for Medicine Paris, Inserm U1273, ESPCI Paris, CNRS FRE 2031, PSL University.
2. Normandie Univ, UNICAEN, INSERM, GIP Cyceron, Institut Blood and Brain @Caen-Normandie (BB@C), UMR-S U1237, Physiopathology and Imaging of Neurological Disorders (PhIND), Caen, France.
3. CHU Caen, Department of radiology, Caen University Hospital, Avenue de la Côte de Nacre, Caen, France.
4. CHU Caen, Department of Clinical Research, Caen University Hospital, Avenue de la Côte de Nacre, Caen, France.
5. STROKOLLIANCE, ETAP-Lab, 2 rue des Rochambelles, Caen, France

†These co-first authors equally contributed to this work.

‡These co-last authors equally contributed to this work.

✉ Corresponding author: Denis VIVIEN, PhD, INSERM UMR-S U1237 "Physiopathology and Imaging of Neurological Disorders", University Caen Normandie, GIP Cyceron, Institut Blood and Brain @ Caen-Normandie (BB@C), Bd Becquerel, BP5229, 14074 Caen, France. Phone: +33 2 31 47 01 66; Fax: +33 2 31 47 02 22; E-mail: vivien@cyceron.fr.

Received: 2020.01.23; Accepted: 2020.04.28; Published: 2020.06.12

Abstract

In the field of ischemic cerebral injury, precise characterization of neurovascular hemodynamic is required to select candidates for reperfusion treatments. It is thus admitted that advanced imaging-based approaches would be able to better diagnose and prognose those patients and would contribute to better clinical care. Current imaging modalities like MRI allow a precise diagnostic of cerebral injury but suffer from limited availability and transportability. The recently developed ultrafast ultrasound could be a powerful tool to perform emergency imaging and long term follow-up of cerebral perfusion, which could, in combination with MRI, improve imaging solutions for neuroradiologists.

Methods: In this study, in a model of *in situ* thromboembolic stroke in mice, we compared a control group of non-treated mice (N=10) with a group receiving the gold standard pharmacological stroke therapy (N=9). We combined the established tool of magnetic resonance imaging (7T MRI) with two innovative ultrafast ultrasound methods, ultrafast Doppler and Ultrasound Localization Microscopy, to image the cerebral blood volumes at early and late times after stroke onset and compare with the formation of ischemic lesions.

Results: Our study shows that ultrafast ultrasound can be used through the mouse skull to monitor cerebral perfusion during ischemic stroke. In our data, the monitoring of the reperfusion following thrombolytic within the first 2 h post stroke onset matches ischemic lesions measured 24 h. Moreover, similar results can be made with Ultrasound Localization Microscopy which could make it applicable to human patients in the future.

Conclusion: We thus provide the proof of concept that in a mouse model of thromboembolic stroke with an intact skull, early ultrafast ultrasound can be indicative of responses to treatment and cerebral tissue fates following stroke. It brings new tools to study ischemic stroke in preclinical models and is the first step prior translation to the clinical settings.

Key words: Ischemic stroke; Thrombolysis; Ultrasound Imaging; Ultrasound Localization Microscopy; Outcome

Introduction

Cerebral arterial recanalization and tissue reperfusion are the major prognostic factors of good functional outcomes following ischemic stroke. The only FDA approved pharmacological treatment of

stroke remains thrombolytic therapy, using recombinant tissue plasminogen activator (rtPA), with a therapeutic window of 4.5 h after stroke onset [1]. The Extend clinical trial suggests the safe use of rtPA alone, even 9 h after stroke onset [2]. The overall acute recanalization rate after rtPA treatment is below 35 %, with its efficacy affected by the time to treatment, poor collaterals, clot localization and the size of thrombi [3, 4]. This efficacy is dramatically improved when combined with endovascular thrombectomy (EVT) when treated within 6-24 h of the onset of symptoms [5, 6].

The main imaging techniques dedicated to brain hemodynamics are positron emission tomography (PET), single photon emission computed tomography (SPECT), Xenon-enhanced computed tomography (XeCT), dynamic perfusion computed tomography (PCT), MRI dynamic susceptibility contrast (DSC), arterial spin labeling (ASL) and transcranial Doppler ultrasonography (TCD). Finer estimation of cerebral perfusion can be obtained in Perfusion Weighted Imaging (PWI) but requires the injection of MR contrast agents and only provide one reading [7]. Currently, there are no tools that could be performed at bedside (as TCD), repeatable (as ASL), provides quantitative measurement (as PET and XeCT) and measures multiple perfusion parameters (as PCT) [8,9]. The recent development of ultrafast ultrasound and progresses in probe technologies combined all these criteria in a unique system [10]. Unlike optical methods that are used for cerebral perfusion imaging, ultrasound allows the imaging in depth in living tissues. Specifically, ultrafast Doppler allows the monitoring of subtle Cerebral Blood Volume (CBV) changes without contrast agents and led to the development of the ultrasound analog of functional MRI (fMRI): functional Ultrasound (fUS) [11-16]. Ultrafast ultrasound also allows the detection of injected intravascular microbubbles, a clinical ultrasound contrast agent, and led to the development of Ultrasound Localization Microscopy (ULM) [17-20] which, unlike ultrafast Doppler, may allow transcranial imaging in adults patients [21,22]. In this study, we demonstrate that both modalities are adapted to the study of stroke in a mouse model, with ultrafast Doppler producing longitudinal monitoring and ULM proving an increased sensitivity and definition, two criteria which are mandatory for clinical applicability.

In preclinical studies where the skull was removed, ultrafast Doppler have been showed to detect vessels with flow as slow as 1 $mm.s^{-1}$ with a 100 µm precision whereas ULM detected vessels under 1 $mm.s^{-1}$ with a 10 µm resolution. In this study, the skull was kept intact and image quality was degraded but still enabled quality imaging of cerebral perfusion. Our present work demonstrates in an intact skull setup with a clinically relevant model of Middle Cerebral Artery (MCA) occlusion [23-25] that ultrafast Doppler and ULM can provide characterization of cerebral perfusion during an ischemic episode and follow-up in mice. The potential of ULM for transcranial imaging in human patients might allow the imaging of cerebral perfusion very early after stroke onset and possible improvement in medical care.

Materials and Methods

Animals

Experiments were performed on swiss male mice (35-40 g; Janvier Labs, France, 8-10 weeks old) in accordance with French ethical laws (Decree 2013-118) and European Communities Council guidelines (2010/63/EU).

Middle Cerebral Artery occlusion in the thromboembolic model

Micropipettes were filled with 1 µL of purified murine alpha thrombin (1 UI = 0.05 mg; Stago BNL). The pipettes were introduced in the lumen of the MCA and murine thrombin was slowly injected to form a fibrin clot. Micropipettes were left in place for 10 min to stabilize the clot.

Tissue-Type Plasminogen Activator induced thrombolysis

To induce thrombolysis, 10 mice received intravenous injection of 200 µL of rtPA (10 mg/kg, Actilyse), 10% as a bolus and 90% as an infusion for 40 min at a steady rate of 4.5 µL/min. A control group of 10 mice was injected with saline under similar conditions. One animal was excluded from the rtPA group due to poor sterotactic fixing.

Ultrafast ultrasound

Acquisitions were performed on an ultrafast scanner (Verasonics, 128 channels, 62.5 MHz sampling rate) with Neuroscan live acquisition software (ART Inserm U1273 & Iconeus; Paris, France) with a custom ultrasound probe (15 MHz, 0.11 mm pitch, 128 elements, 14 mm width, Vermon, France) which enables a 110 µm × 100 µm in plane resolution at a depth of 10 mm. The probe was mounted on 4 motors (3 translation + 1 rotation, Pi, Germany). A schematic of the setup can be found in Figure 1A. As both stereotactic frame and motorization system were fixed to the table, a common coordinate system was set so each animal could be imaged later in similar configuration. In this study, the coordinate system is (z, x, y) with z the axial axis, x the lateral axis and y the

elevation axis as shown in Figure 1A. The coordinate system was adapted to match stereotactic coordinates by taking a reference on the antero-posterior axis at the vertical plane under the Bregma suture β=0.

Ultrafast Doppler

200 compounded frames (11 angles between -10°: 10°) were acquired at 500 Hz. Singular Value Decomposition filters were used (removal of the 60 first singular values) to separate blood signal from tissues and summed to produce a power Doppler image [26-30]. Between two images, a 1.2 s pause was added to let the motor move to the next slice. 24 coronal planes were imaged every 0.3 mm to reconstruct a 10 mm × 14 mm × 8 mm volume between β+2 mm and β-6 mm with an in plane resolution of 110 µm × 100 µm and a step of 300 µm every 40 s (Figure 1B).

Temporal profiles

Two regions of interest were defined on the body of the MCA and on the hypoperfused part of the cortex. The mean Doppler intensity in the ROI was calculated at each time to produce temporal profiles proportional to cerebral blood volumes in the ROI. The profiles were normalized on the basis of pre-occlusion levels.

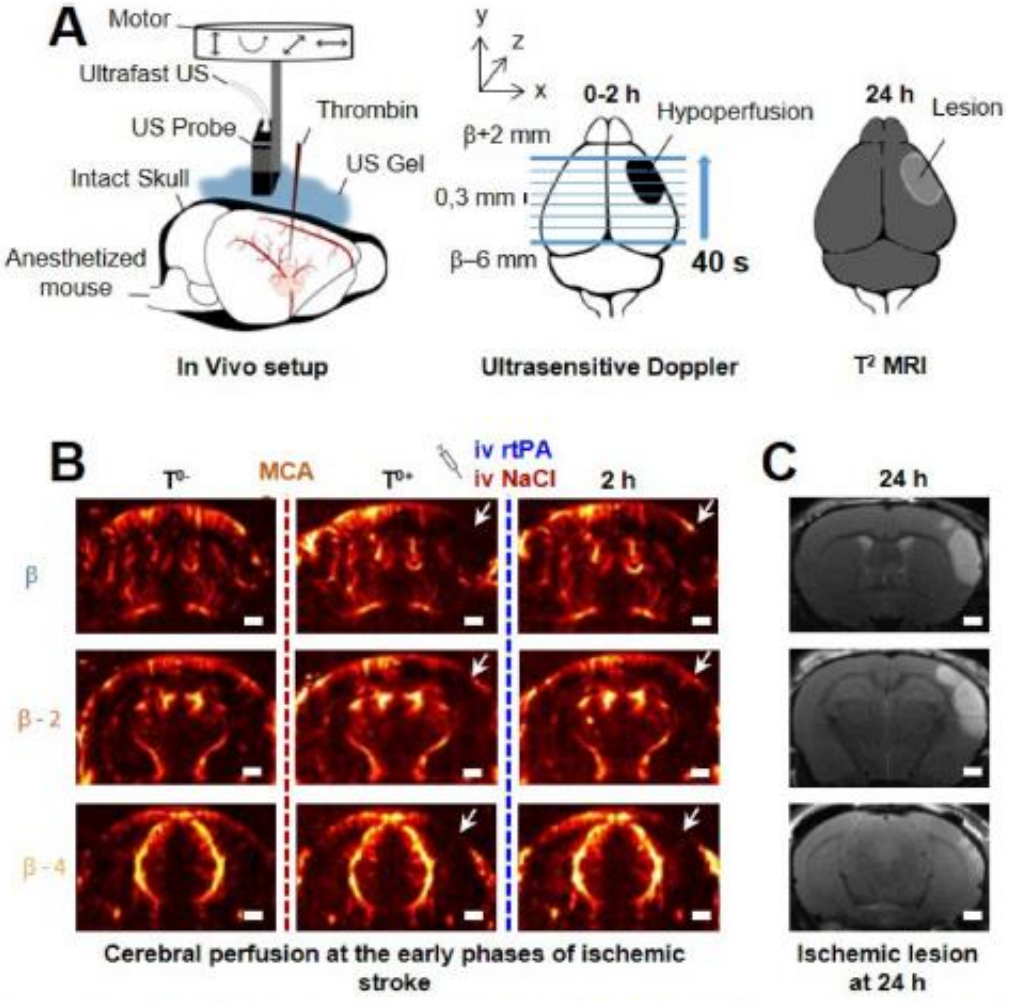

Figure 1. Transcranial ultrafast ultrasound imaging to monitor cerebral perfusion before, during and after stroke A. Experimental setup with an ultrasound probe connected to an ultrafast ultrasound acquisition system (Inserm Accelerator of Technological Research) and mounted on a 4 axis-motor for 3D scanning over the whole mice brain by steps of 0.3 mm. A volume over the whole brain is reconstructed every 40 s. Ultrafast Ultrasound monitors cerebral perfusion during the early phase of the ischemic episode, before, during and after onset, including treatment with the gold standard recombinant-tPA (rtPA). At 24 h MRI reveals the final ischemic lesion. B. Ultrafast Doppler reveals hypoperfusion in the ipsilateral cortices subjected to thrombin injection (clot formation) in the middle cerebral artery (MCA) and reperfusion of the corresponding territory after injection of the thrombolytic, rtPA. C. Registration and comparison with MRI reveal tight relationships between cerebral perfusions at the early phase of stroke and the final lesion volumes. Scale bar 1 mm.

Ultrasound Localization Microscopy

To perform ULM, acquisition and post processing steps were adapted from the reference methods [17-20]. For each image, 100 µL of Sonovue microbubbles were injected in the tail vein. Blocks of 800 compounded frames (-5° 0° 5°) at 1 kHz were acquired for 800 ms and saved for 200 ms and this scheme repeated for 180 s. A combination of Butterworth high pass filter (second order, 20 Hz) and SVD filters (removal of the 10 first singular values) were used to separate microbubbles echoes from tissues. Microbubbles centroid positions were localized using a weighted average algorithm. Microbubbles were tracked through consecutive frames using *simpletracker* (Mathworks). Tracks were interpolated and smoothed using a sliding window of 5 points and cleaned from redundant positions. A density image was reconstructed on an 11 µm × 10 µm grid.

Magnetic Resonance Imaging

Acquisitions were performed on a 7T Brucker system. T2-weighted images were acquired using a multislice multiecho sequence: TE/TR 33 ms/2500 ms and reconstructed with a 0.7 mm × 0.7 mm × 0.5 mm resolution. Lesions were manually segmented on T2 acquisitions. MRI and ultrafast Doppler volumes were registered on anatomical similarities using *imregister* (Mathworks), an intensity-based function for multimodal registration. As the coordinate system was the same for ultrafast Doppler and ULM, the volumetric registration used for ultrafast Doppler was applied to ULM to ensure registration with MRI. Segmentation of ischemic lesion was performed manually and blind to ultrasound images.

Quantifications and statistical analyses

To account for tissue swelling due to the edema, a first correction factor had to be calculated for every mouse. On T_2 MRI images, the distance between the skull and the corpus callosum was measured on both hemisphere of the mouse brain. Because skull thickness increases at the front of the head, ultrasound imaging in the most anterior parts of the head suffered from stronger wave attenuation. Consequentially, the contrast and sensitivity to the vasculature was strongly impaired and meaningful analysis could not be performed reliably after β+1.5 mm. As lesions spread up to β+3 mm, the parts between β+1.5 mm and β+3 mm were not included in lesion quantifications in the analysis in Figure 5 under the mention adjusted volume of lesion.

Quantifications are expressed as mean ± std (Figure 5A and 5B). Statistical analysis was performed using GraphPad®. We first assessed normal distribution of all samples by Shapiro-Wilk tests. In the panels A, B and E unpaired two-tailed t tests were performed. Pearson correlation tests were used for panels C and D. Sidak's multiple comparisons tests were used to assess multiple comparisons in panel F. Differences were considered statistically significant for a probability value $p < 0.05$.

Ultrafast ultrasound TICI score

In human, the TICI score is used to describe the perfusion following stroke [34,35]. We adapted a TICI-like score for ultrafast Doppler. The scoring was estimated by an operator from a combination of markers: recanalisation and reperfusion profiles reaching 50% or pre-occlusion levels, and the presence of significant remaining hypoperfused volumes at 2 h. Grade 0: No Recanalisation. Grade 1: Recanalisation but no Reperfusion Grade 2: Recanalisation and partial reperfusion. Grade 3: Complete recanalisation and reperfusion.

Results

Transcranial ultrafast ultrasound monitors hypoperfusion following thromboembolic stroke

On ultrafast Doppler, the body of the MCA can be observed on a coronal slice over 1 mm. Directly after thromboembolic occlusion of the MCA (Figure 1A), blood flow in the artery is completely blocked and the appearance of a large hypoperfused area can be observed in the ipsilateral cortex to the occluded MCA and spreading between β -3 mm and β -4 mm (Figure 1B). In the lateral part of the cortex, fed by the MCA, the blood supply is completely stopped. The most central part of the cortex, fed by the Anterior Cerebral Artery (ACA) is sometimes subjected to small and rapid changes in cerebral blood volumes (CBVs). During the 2 h following MCAo and rtPA treatment, restoration of perfusion can be assessed. At 24 h post-stroke onset and treatment, T_2 weighted MRI reveals areas with high water content corresponding to the ischemic lesion (Figure 1C). The edema as seen on T_2 MRI is known to correlate with tissue damage seen by histopathological staining [23,24]. Moreover, the edema only appears several hours after the stroke onset which makes it ineffective to image tissue damage during the early phase of stroke (Figure S1).

Without rtPA treatment, the ischemic lesion is the hypoperfused volume measured early in ultrafast ultrasound

In the control group, 10 mice were injected with saline 20 min after MCAo, corresponding to the sham of the rtPA-treated group (Figure 2B). Variations in

ultrafast Doppler before and after occlusion exhibit hypoperfusion in the corresponding ipsilateral cortices (Figure 2B). Additionally, differences in ultrafast Doppler between post-occlusion time and 2 h after the stroke onset is displayed in Figure 2C and reveal the absence of any reperfusion. After identification of the MCA on ultrafast Doppler image, recanalization profiles were plotted and exhibited the absence of recanalization for saline treated mice (Figure 2D). Deep in the tissues fed by the MCA, no reperfusion was observed in any of the mice (Figure 2E). Profiles directly after MCAo can be reconstructed and reveal a peak around β-1 mm and spreading between β-4 mm and further than β+3 mm (Figure 2F). Total measured volumes at risk were 16 mm^3 ± 3 mm^3. Similar measurements were performed 2 h post MCAo and show little evolutions and hypoperfused volumes stayed similar within the margin of error (Figure 2G). Infarct areas on T_2 weighted MRI reveal lesion spreading between β-5 mm and β+3 mm with a peak also around β-1 mm and co-localization with the hypoperfused areas (Figure 2H). To account for late edema and ultrasound blindness between β+1 mm and β+3 mm, two corrections were made to the volume of lesions with adjusted volumes of 17 mm^3 ± 3 mm^3 (24 mm^3 ± 5 mm^3 without correction). This represents a 6% difference between ultrasound and MRI. In these conditions, the lesions measured by MRI at 24 h appear to be the totality of the hypoperfused volumes measured by ultrafast Doppler at 2 h post stroke onset. This hypothesis was validated in a supplementary group of 5 mice in which the MCA has been permanently occluded through electrocoagulation thus allowing neither recanalization nor reperfusion of the tissue (Figure S2). As expected, no reperfusion was observed, and similar hypoperfused volumes were observed in ultrafast Doppler imaging together with similar ischemic lesions on T_2 weighted MRI. The volumes at risk were 19 mm^3 ± 3 mm^3 while the volumes of lesion were 18 mm^3 ± 5 mm^3 (24 mm^3 ± 7 mm^3 before adjustments). This represents a 5 % difference between ultrasound and MRI.

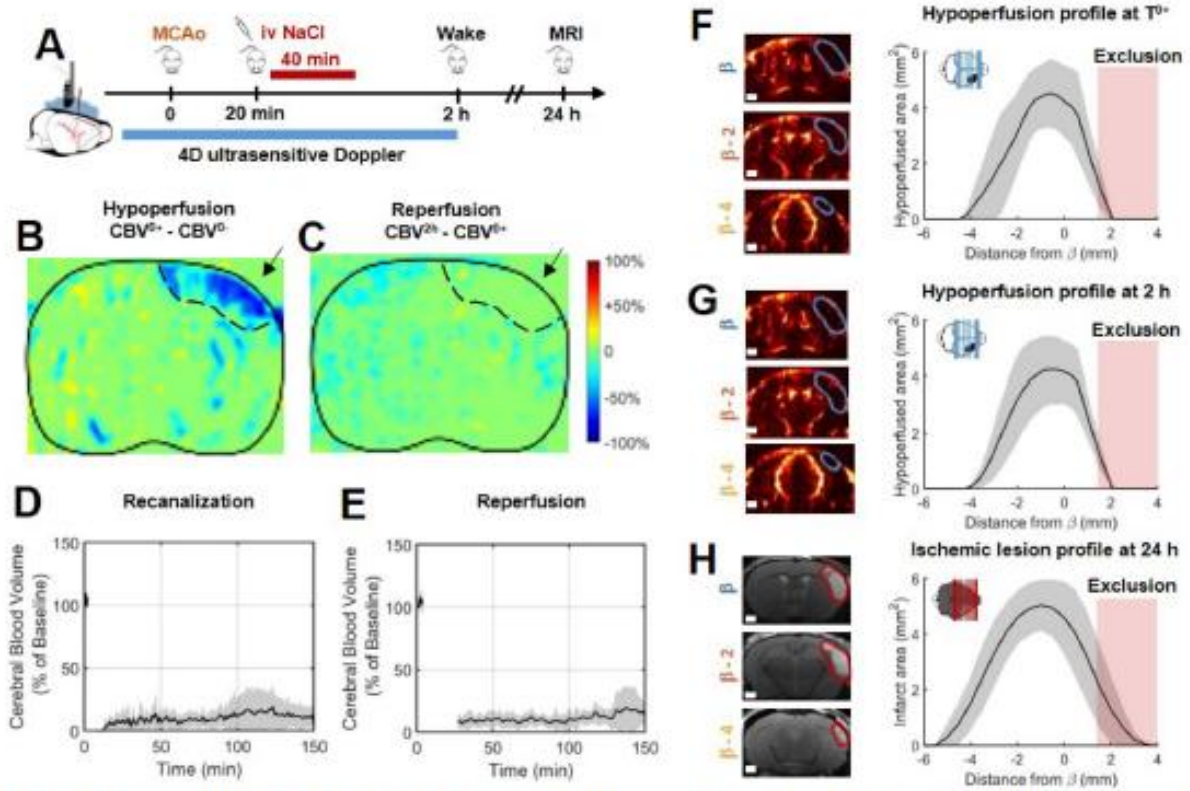

Figure 2. In the absence of treatment, the final volume of lesion corresponds to the early hypoperfused area. A. Experimental timeline for ultrasound monitoring of cerebral blood volumes after MCAo and comparison with MRI. **B.** Differences between ultrafast Doppler imaging performed before and after occlusion of the middle cerebral artery (MCAo) reveal hypoperfusion in the corresponding ipsilateral cortices. **C.** Differences between ultrafast Doppler imaging just after MCAo and 2 h later show no sign of reperfusion in the corresponding ipsilateral cortices. **D.** Monitoring of blood flows in the MCA on ultrafast Ultrasound over β+1 mm shows permanent occlusion with no clear recanalization occurring during the first 2 h. **E.** Monitoring of cerebral perfusion in the hypoperfused volume shows no sign of reperfusion. **F.** Patterns of hypoperfusions directly after MCAo reveal large hypoperfused volumes in the cortex. **G.** Patterns of hypoperfusions 2 h after MCAo reveal similar hypoperfused volumes. **H.** Patterns of the final ischemic lesions measured at 24 h after MCAo revealed by T_2 MRI.

Theranostics 2020, Vol. 10, Issue 17 7485

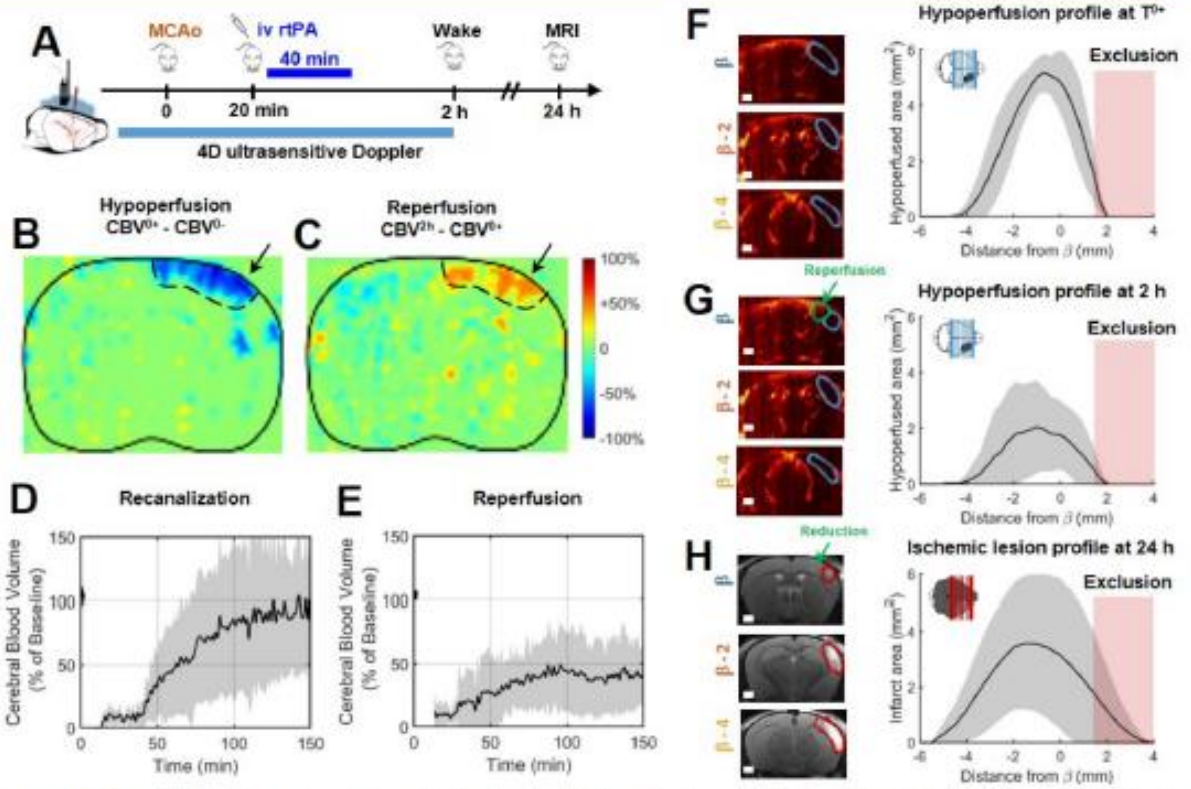

Figure 3. Early injection of rtPA causes arterial recanalization, tissue reperfusion and reduces the volume of lesion. A. Differences between ultrafast Doppler before and after MCAo reveal hypoperfusion in the corresponding ipsilateral cortices. **B.** Differences between ultrafast Doppler just after MCAo and 2 h later show reperfusion in the hypoperfused part of the corresponding cortices. **C.** Corresponding MRIs reveal the formation of smaller lesions. **D.** Monitoring of flows in the MCA on ultrafast ultrasound images over β+1 mm shows rapid and effective recanalization. **E.** Monitoring of cerebral perfusion in the hypoperfused volumes show some tissue reperfusions. **F.** Patterns of hypoperfusions directly after MCAo revealed by ultrafast ultrasound imaging. **G.** Patterns of hypoperfusions 2 h after MCAo revealed by ultrafast ultrasound imaging. **H.** Patterns of the ischemic lesions 24 h after MCAo revealed by MRI in rtPA treated animals.

rtPA induces recanalization and reperfusion can be monitored transcranially with ultrafast ultrasound

In a group of 9 mice, the gold standard fibrinolytic treatment, rtPA was injected intravenously 20 min after occlusion of the MCA, 10 % in bolus and 90 % in infusion as in clinic (Figure 3A). The differences of ultrafast Doppler images from before and after MCAo exhibit the hypoperfusion in the ipsilateral cortices (Figure 3B) whereas the differences between just after occlusion and 2 h after this time display the reperfused areas (Figure 3C). The monitoring of the recanalization of the body of the MCA reveals an overall improvement in arterial recanalization (Figure 3D). Although tissue reperfusion can be observed, it does not appear as effective as arterial recanalization (Figure 3E). The areas at risk in ultrafast Doppler were measured as previously (sham control group, Figure 2) directly after MCAo (before rtPA treatment) and reveal the same behaviors, a peak around β-1 mm and spreading between β-4 mm and further than β+1 mm with total hypoperfused volumes of 17 mm^3 ± 3 mm^3 (Figure 3F). 2 h post MCAo however, the action of rtPA treatment can be quantified as the hypoperfused volumes are reduced to 7 mm^3 ± 7 mm^3 (Figure 3G). In agreement with recanalization-reperfusion of the ischemic brain tissue, revealed by a rescue of the CBV, the final infarct areas on T_2 weighted MRI at 24 h are 11 mm^3 ± 3 mm^3 (14 mm^3 ± 11 mm^3 before adjustment), (Figure 3H) i.e. reduced by 30 % of the lesion volumes compared to the initially identified areas at risk measured before rtPA treatment. There remains a 30 % difference between ultrasound and MRI which highlights the fact that although they are reperfused, some tissues can still be infarcted. The variability in the response to rtPA treatment comes from the thromboembolic model and is rather representative of what happens in human patients. This variability of behaviors can be more finely observed with ultrafast ultrasound.

Theranostics 2020, Vol. 10, Issue 17 7486

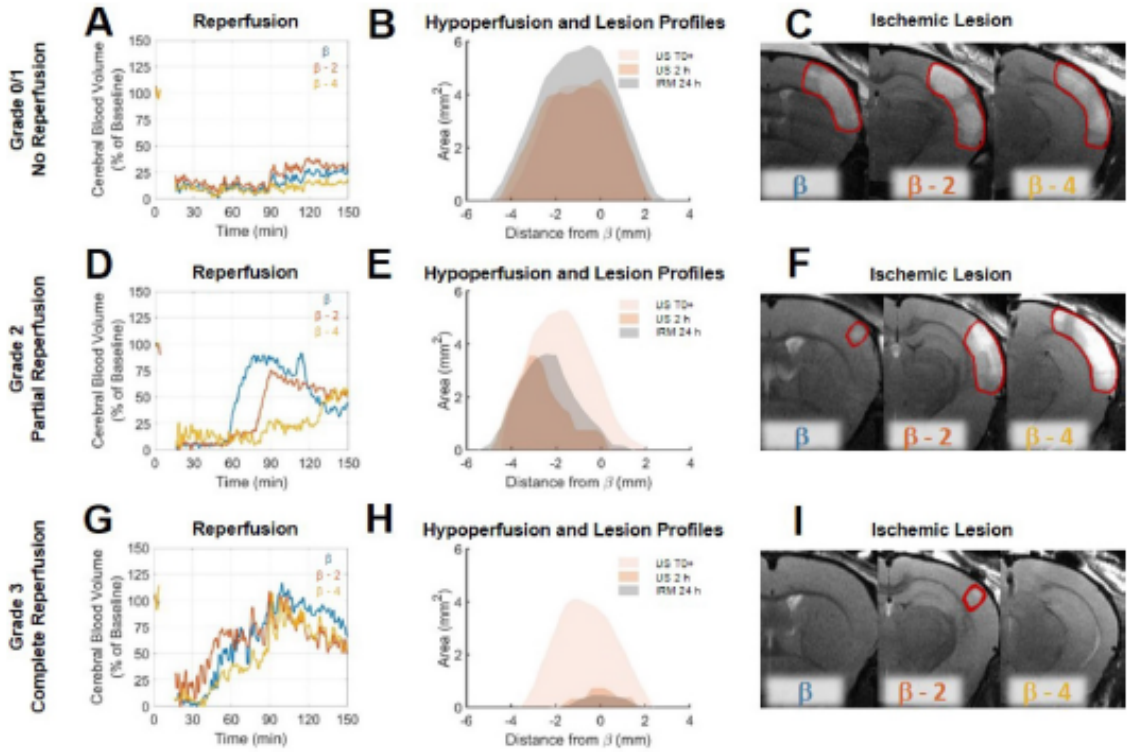

Figure 4. Differences in reperfusion patterns revealed by ultrafast ultrasound imaging correspond to the formation of ischemic lesions. A. For a typical Grade 0/1 mouse, the reperfusion curves in three different parts of the hypoperfused areas show no reperfusion. B. Hypoperfused profiles immediately post MCAo and after 2 h show no significant evolution of the formation of the ischemic lesions co-localized with hypoperfusions. C. Ischemic lesions on the corresponding areas. D. For a typical Grade 2 mouse, the reperfusion curves in three different parts of the hypoperfused areas show inhomogeneous reperfusions. E. Hypoperfused profiles immediately post MCAo and after 2 h show significant evolutions of the formation of the ischemic lesions co-localized with the remaining hypoperfusions at 2h. F. Ischemic lesions on the corresponding areas. G. For a typical Grade 3 mouse, the reperfusion curves in three different parts of the hypoperfused areas show early and effective reperfusions. H. Hypoperfused profiles immediately post MCAo and after 2 h show significant reductions of hypoperfusions associated with the formation of reduced ischemic lesions. I. Ischemic lesions on the corresponding areas.

Transcranial ultrafast ultrasound allows a fine spatiotemporal follow-up of the cerebral blood volumes following stroke and treatment

Analysis of individual animals of the rtPA treated group, unmasks fine correspondence between reperfusion patterns and volumes of lesion. In two animals, some degree of arterial recanalization was observed without any tissue reperfusion. In two other animals, complete tissue reperfusions were achieved. In the other animals, recanalization was followed by some form of incomplete reperfusions. To highlight these differences and how ultrafast ultrasound can be used to understand lesion formation, reperfusion profiles were reconstructed in three different coronal planes to explore spatial temporal differences in reperfusion. To standardize the analysis of reperfusion, a grading system similar to the clinical TICI grading system [31,32] (Thrombolysis In Cerebral Ischemia) from 0 to 3 was used to describe the reperfusion, 0 being no recanalization, 1 being recanalization but no reperfusion, 2 being a partial reperfusion and 3 being a complete reperfusion. This scoring was performed based on the ultrafast Doppler images. On Figure 4 are given three examples of mice with different reperfusion patterns. The first mouse showed little arterial recanalization and no tissue reperfusion corresponding to a TICI grade of 1. The whole hypoperfused volume directly after MCAo remains hypoperfused for the duration of the experiment as shown by reperfusion curves at β (in blue), β-2 (in red) and β-4 (in yellow) (Figure 4A). The hypoperfusion profiles show no significant evolution 2 h after MCAo and the lesion is the entire hypoperfused volume (Figure 4B). MRI reveals a large lesion over the hypoperfused areas (Figure 4C). The second mouse showed good arterial recanalization but inhomogeneous tissue reperfusion corresponding to a TICI grade of 2. Some parts of the hypoperfused volume directly after MCAo are reperfused within the first 2 h as shown by reperfusion curves at β, β-2 mm and β-4 mm (Figure 4D). The hypoperfusion profiles show significant reduction 2 h after MCAo and the lesion matches the remaining hypoperfused volume (Figure 4E). MRI reveals the inhomogeneity of the lesion (Figure 4F). The third mouse showed good

arterial recanalization and good tissue reperfusion corresponding to a TICI grade of 3. All the hypoperfused volume directly after MCAo is reperfused within the first 2 h as shown by reperfusion curves at β, β-2 mm and β-4 mm (Figure 4G). The hypoperfusion profiles show a complete reduction 2 h after MCAo and the absence of lesion (Figure 4H). MRI reveals the absence of lesion (Figure 4I). Eventually, the prediction ability of ultrafast ultrasound can be tested on all the animals.

Transcranial ultrafast ultrasound at 2 h predicts responses to thrombolytic treatment and final outcomes

The effect of rtPA in this model reduces the lesion by more than 30 % (P=0.032) (Figure 5A). The saving of tissue caused by early reperfusion can be observed in rtPA animals (P=0.0206) (Figure 5B). To represent the link between hypoperfusion and the formation of a lesion, the adjusted volumes of lesion can be plotted as a function of the volumes at risk defined as the hypoperfusion directly after the occlusion of the MCA (Figure 5C). For the control group, the outcome of the stroke can be predicted since, after adjustments, all points align along the diagonal (R^2=0.8273, p=0.0003). This means that when no early reperfusion is observed, the final volumes of lesion are the whole volumes at risk measured by using CBV only, just after stroke onset. For animals receiving rtPA, the volumes of lesion are reduced compared to the volumes at risk, meaning that tissue areas were effectively saved (R^2=0.4001, p=0.0675). The size of the lesion depends on two factors: the initial size of the hypoperfused zone and the efficiency of the reperfusion. When plotting the adjusted volumes of lesion as a function of the hypoperfusion at 2 h after stroke onset (control and treated groups) (Figure 5D), all points align around the diagonal (NaCl: R^2=0.8186, p=0.0003) (rtPA: R^2=0.4438, p=0.05) with a strong correlation, even in the rtPA group with a large variability of outcome. This means that in both cases, the volumes of lesion are the hypoperfused volumes measured at 2 h using CBV only.

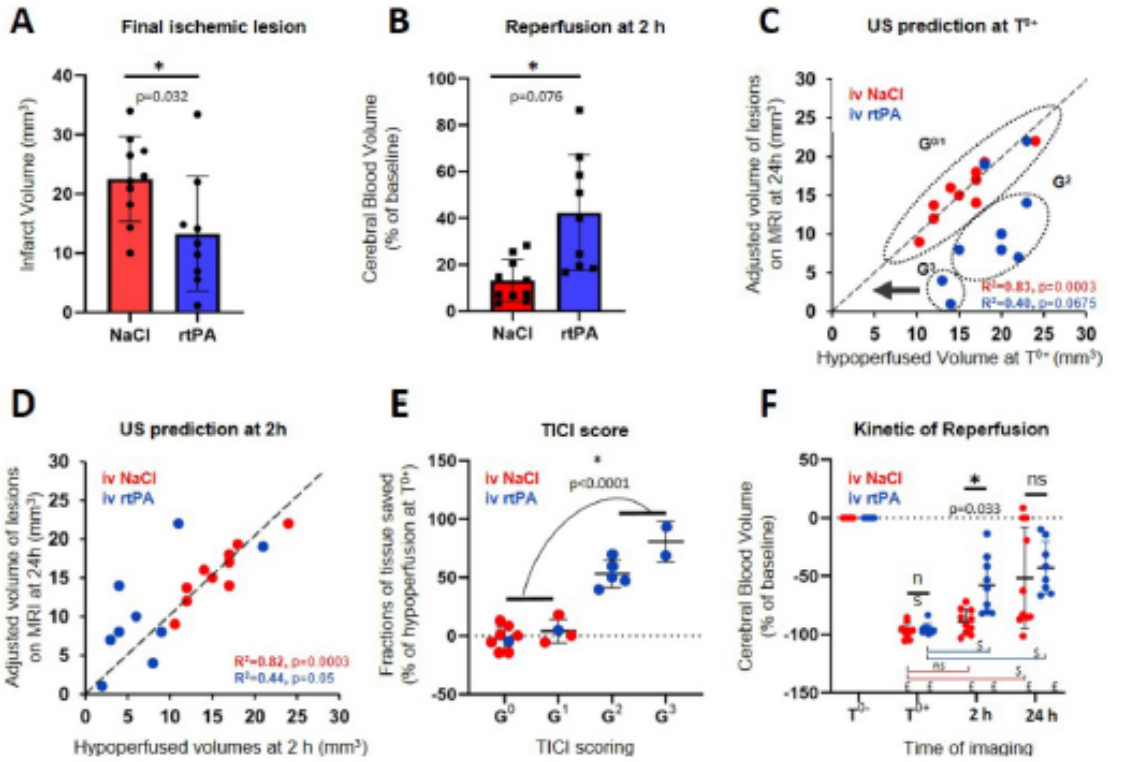

Figure 5. Prediction of lesions and responses to treatment based on early Transcranial ultrafast Doppler imaging. A, B, E = Unpaired t test Two-tailed (n=10; 9); C, D = Pearson correlation (n=10; 9); F = Sidak's multiple comparisons test (n=10; 9), *Intergroup differences; $ Intragroup differences; £ significant compared to T0. A. Final ischemic lesions determined at 24 h indicate reduction of lesions in animals treated with rtPA. B. State of reperfusion 2 h after MCAo shows improved reperfusions in the rtPA treated group. C. Directly after MCAo, the hypoperfused volume in ultrafast Doppler imaging is a marker of final ischemic lesion volumes for the NaCl treated animals (red) with the lesions that correspond to the complete hypoperfused volumes, aligned around the diagonal. For the rtPA treated group (blue), the lesions are smaller than the volumes at risk defined directly after occlusion because of effective tissue reperfusions. D. After rtPA treatment, the remaining hypoperfused volumes are predictive of the final lesion volumes in both groups. E. Effectiveness of the prediction of lesions based on reperfusion using the ultrafast ultrasound based TICI score. F. Evolutions of perfusions in the volumes at risk at the early time after stroke onset (0 and 2 h) and at 24 h show that after a therapeutic window of 2 h, perfusion is no longer predictive of the lesion.

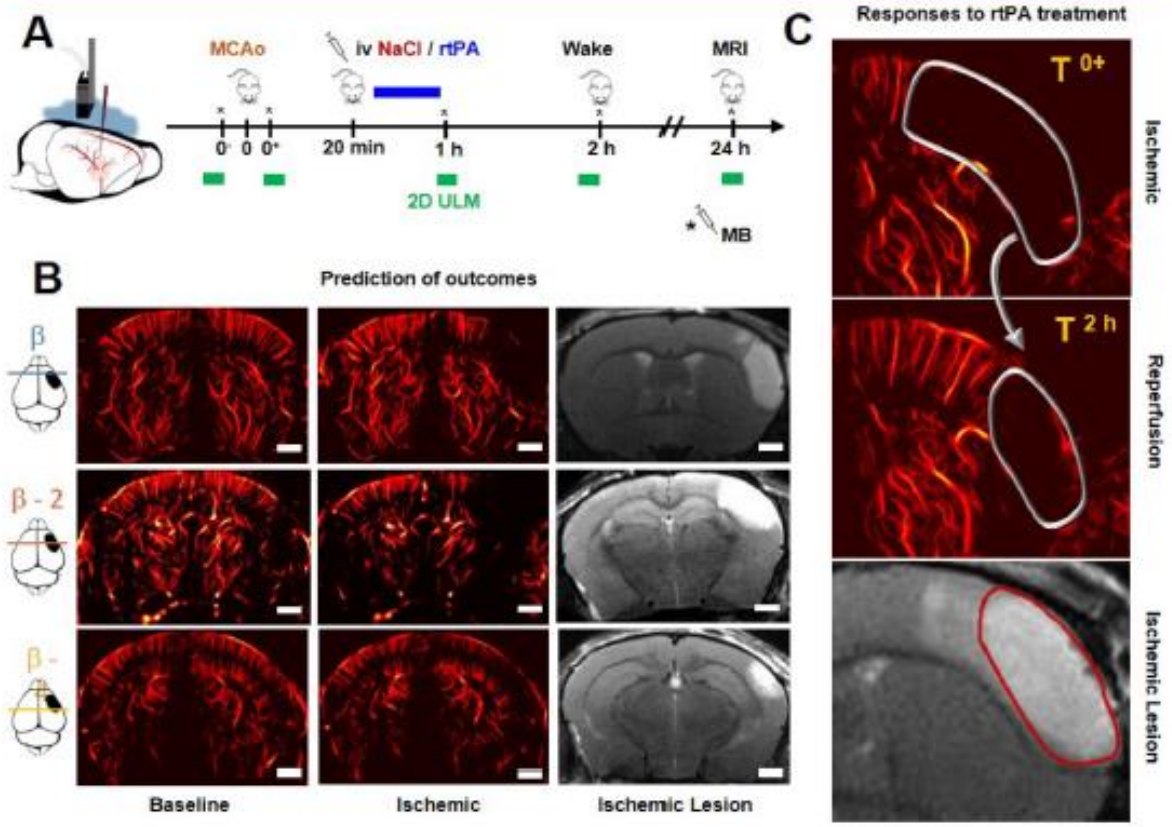

Figure 6. Predicting the outcomes and evaluating responses to treatment with transcranial ULM. A. Timeline for ULM acquisitions. **B.** For mice treated with NaCl, a large lesion can be seen in ULM just after ischemia and very little reperfusion can be observed 2 h after the onset. In ultrafast Doppler, the hypoperfused area is the infarcted lesion seen in MRI. **C.** On rtPA treated mice, the reperfusion can be evaluated with ULM and predicts the formation of the lesion. Scale bar 1 mm.

However, this representation does not consider the quality of the reperfusion in saving tissues. All mice in the control group are attributed a TICI score of 0 or 1, meaning that no reperfusion was ever observed. Four mice in the rtPA treated group were attributed TICI scores of 0 or 1 meaning that thrombolysis was not effective enough to reperfuse the tissues. In these conditions, the prognostic of lesions is similar to the control saline group. Six mice in the rtPA group were attributed TICI scores of 2 or 3, meaning that reperfusions were achieved. In these conditions, the lesions were reduced compared to the volumes at risk and compared to the control group, implying that the better the reperfusion is, the more tissues are saved. Using the ultrafast Doppler based TICI grading system, we can represent how much tissue was effectively saved by an early and effective reperfusion compared to the initial areas at risk measured by CBV (Figure 5E). It is no surprise that for grades 0 and 1, no tissue is saved. On the contrary, major improvements can be observed for mice with grade 2 and 3 with preservation of more than half of the tissue ($P<0.0001$). All animals were imaged again at 24 h. Some reperfusion 24 h after the onset of the stroke is observed in both the saline and rtPA groups, with an improved reperfusion for the rtPA treated animals when measured at 2 h ($p=0.033$) (Figure 5F).

Transcranial Ultrasound Localization Microscopy to image hypoperfusion

In four mice in each group, ULM was performed in a single coronal plane at particular times, just before and after occlusion of the MCA, 1 and 2 h later and again after 24 h (Figure 6A). On the given examples in Figure 6B, although there is still shadowing by the skull, ULM can be performed and reveals the vasculature with enhanced spatial resolution and sensitivity. ULM reveals the localization and extent of the hypoperfusion. 24 h after the onset of the stroke, we can compare the lesions seen in T_2 weighted MRI with the hypoperfused areas. The given examples in Figure 6B, shows the formation of a large lesion. The hypoperfused area is large to begin with, and the injection of NaCl does not induce efficient reperfusion. 2 h after the onset of the ischemia, only a

small area is reperfused, which we can easily identify as saved on the corresponding T_2 image. The given example in Figure 6C shows the formation of a reduced lesion after rtPA treatment and reperfusion. These examples give an idea of how ULM could be used to image the hypoperfused areas and monitor the response to treatment.

Discussion

An important goal to improve stroke therapy is to identify how the lesion will extend with time, whether the patient will respond to treatment and ultimately to predict the functional outcome. To address these important questions, neurologists and neuroradiologists use a combination of prediction tools with the severity of stroke, its location, age, previous risk factors and comorbid disease (such as high blood pressure, diabetes, etc.) as key factors. Despite all these criteria, their answer remains most often very evasive and is usually postponed until the evolution of permanent neurological deficits. An early biomarker to accurately identify salvageable tissues and to predict functional outcome after stroke is, therefore, mandatory [33] and could be met with the assistance of neuroimaging techniques [34].

In our study, we demonstrate that ultrafast Doppler and Ultrasound Localization Microscopy can be relevant neuroimaging modalities for stroke. We show here that early assessment of the cerebral perfusion using *in vivo* ultrafast Doppler brain imaging, when performed early after stroke onset (here 2 h in rodents) is indicative of final lesion volumes measured by MRI at 24 h. We also demonstrate, that when performed just after thrombolytic treatment (rtPA-induced fibrinolysis), the methodology can be used to monitor the treatment efficacy.

Ultrafast Doppler for functional imaging was demonstrated in different animal models [11–14] and in clinical settings: in newborns [15] or intraoperatively [16]. In the context of stroke, it was first investigated in 2012 [35] and recent works confirmed its relevance [36,37], but not in a model of thromboembolic stroke as it occurs in clinic and without considering prognostic and/or responses to the gold standard treatment. However, the translation of results to human should always be done carefully, especially in the context of stroke. Indeed, all strategies identified so far to save the brain excepted rtPA treatment have failed in the clinic, mainly because of poor animal modeling. The model of stroke we have used here [23,24] is relevant with the actual clinical setting [25,38]. Moreover, ultrasound imaging of the early phases following stroke was also performed with optical contrast using photoacoustic imaging but in a simpler mouse model of photo thrombose and filament induced MCA occlusion [39]. Unlike ultrafast Doppler and ULM, photoacoustic imaging is sensitive to oxygen saturation in tissue and not blood volumes but can nonetheless provide similar results in terms of temporal dynamics and formation of lesion [40]. Although its translation to human patients might be severely limited by the strong absorption of light through the skull, photoacoustic can be complementary with ultrafast Doppler and ULM for preclinical studies to provide both cerebral blood volume and tissue oxygenation in tissues with different sets of sensitivity and resolutions.

Similarly, the translation of ultrasound imaging methods to human has always been a challenge because of a strong attenuation by the skull bone. As demonstrated previously, ultrafast Doppler can be performed through the fontanel [15] and could thus contribute to the diagnosis of stroke in babies. However, there are clear limitations about the possibility to use ultrafast ultrasound in adult due to strong aberrations and absorptions by the skull bone. The more recent improvements of both contrast and resolution of ULM may allow transcranial imaging [21,22], all the more so than microbubbles are commonly used in human as contrast agent for ultrasound imaging (Sonovue, Bracco), and in particular in MCA infarction to improve the signal to noise ratio [41]. This is a major point considering the recent report made by the Food and Drug Administration (FDA) about a Safety Announcement related to gadolinium-based contrast agents (GBCAs) administered for MRIs [42]. Nonetheless, the quality of the imaging through the skull will be critical to determine the quality of the readings, as there is a priori no way to distinguish ischemic from shadowed areas.

A proper clinical trial has yet to demonstrate the ability of ULM to provide quality reading through the human skull. The clinical use of ULM in this context could be performed through the temporal window, and would benefit from the extension of the field of view from 2D to 3D to access large areas of the brain which may reduce the dependency of the imaging procedure to the operator and allow the detection of scattered lesion. It may also enable the estimation of quantitative biomarkers of vascular suffering over large areas of the brain. Such extension is envisioned to become possible in the next years with the advent of piezocomposite 2D Matrix Arrays or Capacitive Micromachined Ultrasonic Transducers (CMUT) technologies and development of 3D ultrafast ultrasound modalities [43-45].

The possibility to have access to an easy to use,

cheap, operator independent and transportable machine to image cerebral perfusion would undoubtedly increase the number of patients eligible for treatment, with the possibility to use this imaging method in the ambulance. Although recanalization is associated with rapid clinical improvement in some patients, for others despite recanalization, they show delayed or impaired reperfusion. Ideal patient selection for thrombolysis alone or combined to thrombectomy should therefore not be based on therapeutic windows but rather on perfusion imaging to determine "a signature" of response to treatments. In addition, such type of monitoring could be very useful for long term recording of recovery and to prevent and treat recurrent stroke.

In conclusion, we provide here, in a relevant model of thromboembolic stroke model in mice with rtPA treatment, the demonstration that ultrafast ultrasound *in vivo* imaging can be used in the context of stroke to diagnose ischemic injury, to prognose outcomes and responses to treatment, in an early time frame after stroke onset.

Supplementary Material

Supplementary figures and tables.
http://www.thno.org/v10p7480s1.pdf

Acknowledgments

This work was supported by Agence Nationale de la Recherche (ANR), within the project ANR Predic, the European Research Council under the European Union Horizon H2020 programme/ERC Consolidator grant agreement No 772786-ResolveStroke, the RHU project Marvelous (16-RHUS-0009), the LABEX WIFI (Laboratory of Excellence ANR -10 -LABX -24) within the French Program "Investments for the Future" under reference ANR -10 - IDEX -0001 -02 PSL* and performed with the technical and scientific support of the INSERM Accelerator of Technological Research in Biomedical Ultrasound and the institute Blood and Brain @ Caen-Normandie (BB@C).

Author contributions

All authors designed the research, V.H., C.B. and C.O. did the experiments, V.H., C.B., T.D., M.T. and D.V. analyzed the data, T.D. developed parts of the sequence, acquisition and processing software, VH, B.H. and O.C. developed the algorithms for ULM, all the authors discussed the results and wrote the paper.

Disclosure

O.C. and M.T. are depositor of the patent /FR2011/052810. T.D. and M.T. are cofounder of Iconeus.

Competing Interests

The authors have declared that no competing interest exists.

References

1. Zivin J, Fisher M, DeGirolami U, Hemenway C, Stashak J. Tissue plasminogen activator reduces neurological damage after cerebral embolism. Science. 1985; 230: 1289–92.
2. Campbell BCV, Ma H, Ringleb PA, Parsons MW, Churilov L, Bendszus M, et al. Extending thrombolysis to 4·5–9 h and wake-up stroke using perfusion imaging: a systematic review and meta-analysis of individual patient data. Lancet. 2019; 394: 139-147.
3. Berkhemer OA, Fransen PSS, Beumer D, van der Berg LA, Lingsma HF, Yoo AJ, et al. A Randomized Trial of Intraarterial Treatment for Acute Ischemic Stroke. N Engl J Med. 2015; 372: 11–20.
4. Coutinho JM, Liebeskind DS, Slater LA, Nogueira RG, Clark W, Davalos A, et al. Combined Intravenous Thrombolysis and Thrombectomy vs Thrombectomy Alone for Acute Ischemic Stroke: A Pooled Analysis of the SWIFT and STAR Studies. JAMA Neurol. 2017; 74: 268-274.
5. Nogueira RG, Jadhav AP, Haussen DC, Bonafe A, Budzik RF, Bhuva P, et al. Thrombectomy 6 to 24 h after Stroke with a Mismatch between Deficit and Infarct. N Engl J Med. 2018; 378: 11–21.
6. Thiebaut AM, Gauberti M, Martinez De Lizarrondo S, Vivien D, Yepes M, Roussel BD. The role of plasminogen activators in stroke treatment: fibrinolysis and beyond. Lancet Neurol. 2018; 17: 1121–1132.
7. Shen Q, Duong T. Magnetic resonance imaging of cerebral blood flow in animal stroke models. Brain Circ. 2016; 2:20-27.
8. Wintermark M, Sesay M, Barbier M, Borbely K, Dillon WP, Eastwood JD, et al. Comparative Overview of Brain Perfusion Imaging Techniques. Stroke. 2005; 36:e83-99
9. Essig M, Shiroishi MS, Nguyen TB, Saake M, Provenzale JM, Enterline D, et al. Perfusion MRI: The Five Most Frequently Asked Technical Questions. AJR Am J Roentgenol. 2013; 200:24–34.
10. Tanter M, Fink M. Ultrafast imaging in biomedical ultrasound. IEEE Trans Ultrason Ferroelectr Freq Control. 2014; 61: 102–119.
11. Deffieux T, Demene C, Pernot M, Tanter M. Functional ultrasound neuroimaging: a review of the preclinical and clinical state of the art. Curr Opin Neurobiol. 2018; 50:128–135.
12. Mace E, Montaldo G, Cohen I, Baulac M, Fink M, Tanter M. Functional ultrasound imaging of the brain. Nat Methods. 2011; 8: 662–4.
13. Demene C, Tiran E, Sieu LA, Bergel A, Gennisson JL, Pernot M, et al. 4D microvascular imaging based on ultrafast Doppler tomography. NeuroImage. 2016; 127: 472–483.
14. Tiran E, Ferrier J, Deffieux T, Gennisson JL, Pezet S, Lenkei Z, et al. Transcranial Functional Ultrasound Imaging in Freely Moving Awake Mice and Anesthetized Young Rats without Contrast Agent. Ultrasound Med Biol. 2017; 43: 1679–1689.
15. Demene C, Baranger J, Bernal M, Delanoe C, Auvin S, Biran V, et al. Functional ultrasound imaging of brain activity in human newborns. Sci Transl Med. 2017; 9(411).
16. Imbault M, Chauvet D, Gennisson JL, Capelle L, Tanter M. Intraoperative Functional Ultrasound Imaging of Human Brain Activity. Sci Rep. 2017; 7: 7304.
17. Errico C, Pierre J, Pezet S, Dessailly Y, Lekei Z, Couture O, et al. Ultrafast ultrasound localization microscopy for deep super-resolution vascular imaging. Nature. 2015; 527(7579): 499–502.
18. Couture O, Hingot V, Heiles B, Muleki-Seya P, Tanter M. Ultrasound Localization Microscopy and Super-Resolution: A State of the Art. IEEE Trans Ultrason Ferroelectr Freq Control. 2018; 65: 1304–1320.
19. Hingot V, Errico C, Heiles B, Rahal L, Tanter M, Couture O. Microvascular flow dictates the compromise between spatial resolution and acquisition time in Ultrasound Localization Microscopy. Sci Rep. 2019; 9: 2456.
20. Heiles B, Correia M, Hingot V, Pernot M, Provost J Tanter M, et al. Ultrafast 3D Ultrasound Localization Microscopy using a 32×32 Matrix Array. IEEE Trans Med Imaging. 2019; 38: 2005-2015.
21. O'Reilly MA, Hynynen K. A super-resolution ultrasound method for brain vascular mapping. Med Phys. 2013; 40: 110701.
22. Soulioti De, Espindola D, Dayton PA, Pinton GF. Super-Resolution Imaging Through the Human Skull. IEEE Trans Ultrason Ferroelectr Freq Control. 2020; 67: 25-36.
23. Orset C, Haelewyn B, Allan SM, Ansar S, Sampos F, Cho TH, et al. Efficacy of Alteplase in a Mouse Model of Acute Ischemic Stroke: A Retrospective Pooled Analysis. Stroke. 2016; 47: 1312–1318.
24. Orset C, Macrez R, Young AR, Panthou D, Angles-Cano E, Maubert E, et al. Mouse Model of In Situ Thromboembolic Stroke and Reperfusion. Stroke. 2007; 38: 2771–2778.
25. Llovera G, Hofmann K, Roth S, Salas-Perdomo A, Ferrer-Ferrer M, Perego C, et al. Results of a preclinical randomized controlled multicenter trial (pRCT): Anti-CD49d treatment for acute brain ischemia. Sci Transl Med. 2015; 7(299): 299ra121.

26. Demene C, Deffieux T, Pernot M, Osmanski BF, Gennisson JL, Sieu LA, et al. Spatiotemporal Clutter Filtering of Ultrafast Ultrasound Data Highly Increases Doppler and fUltrasound Sensitivity. IEEE Trans Med Imaging. 2015; 34: 2271-85.
27. Baranger J, Arnal B, Perren F, Baud O, Tanter M, Demene C. Adaptive Spatiotemporal SVD Clutter Filtering for Ultrafast Doppler Imaging Using Similarity of Spatial Singular Vectors. IEEE Trans Med Imaging. 2018; 37: 1574-1586.
28. Shung KK, Sigelmann R, Reid JM. Scattering of ultrasound by blood. IEEE Trans Biomed Eng. 1976; 23: 460-467.
29. Cloutier G, Qin Z. Ultrasound backscattering from non-aggregating and aggregating erythrocytes--a review. Biorheology. 1997; 34: 443-470.
30. Bercoff J, Montaldo G, Loupas T, Savery D, Meziere F, Find M, et al. Ultrafast compound Doppler imaging: providing full blood flow characterization. IEEE Trans Ultrason Ferroelectr Freq Control. 2011; 58: 134-147.
31. Zaidat OO, Lazzaro MA, Liebeskind DS, Janjua N, Wechsler L, Nogueira RG, et al. Revascularization grading in endovascular acute ischemic stroke therapy. Neurology. 2012; 79: S110-S116.
32. Zerna C, Thomalla G, Campbell BCV, Rha JH, Hill MD. Current practice and future directions in the diagnosis and acute treatment of ischaemic stroke. Lancet. 2018; 392: 1247-1256.
33. Stinear CM. Prediction of motor recovery after stroke: advances in biomarkers. Lancet Neurol. 2017; 16: 826-836.
34. Thomalla G, Gerloff C. Acute imaging for evidence-based treatment of ischemic stroke. Curr Opin Neurol. 2019; 32: 521-529.
35. Martin A, Mace E, Boisgard R, Montaldo G, Theze B, Tanter M, et al. Imaging of perfusion, angiogenesis, and tissue elasticity after stroke. J Cereb Blood Flow Metab. 2012; 32: 1496-1507.
36. Brunner C, Isabel C, Martin A, Dussaux C, Savoye A, Emmrich J, et al. Mapping the dynamics of brain perfusion using functional ultrasound in a rat model of transient middle cerebral artery occlusion. J Cereb Blood Flow Metab. 2017; 37: 263-276.
37. Brunner C, Korostelev M, Raja S, Montaldo G, Urban A, Baron JC. Evidence from functional ultrasound imaging of enhanced contralesional microvascular response to somatosensory stimulation in acute middle cerebral artery occlusion/reperfusion in rats: A marker of ultra-early network reorganization? J Cereb Blood Flow Metab. 2018; 38: 1690-1700.
38. Martinez de Lizarrondo S, Gakuba C, Herbig BA, Repesse Y, Ali C, Denis CV, et al. Potent Thrombolytic Effect of N -Acetylcysteine on Arterial Thrombi. Circulation. 2017; 136: 646-660.
39. Lv J, Shi L, Jingde Z, Fei D, Zhiyou W, Ronghe C, et al. In vivo photoacoustic imaging dynamically monitors the structural and functional changes of ischemic stroke at a very early stage. Theranostics. 2020; 10:816-828.
40. Cao R, Li J, Kharel Y, Zhang C, Morris E, Santos WL, et al. Photoacoustic microscopy reveals the hemodynamic basis of sphingosine 1-phosphate-induced neuroprotection against ischemic stroke. Theranostics. 2018; 8:6111-6120.
41. Seidel G, Meyer-Wiethe K, Berdien G, Hollstein D, Toth D, Aach T. Ultrasound Perfusion Imaging in Acute Middle Cerebral Artery Infarction Predicts Outcome. Stroke. 2004; 35:1107-1111.
42. Levine D, McDonald RJ, Kressel HY. Gadolinium Retention After Contrast-Enhanced MRI. JAMA. 2018; 320:1853.
43. Provost J, Papadacci C, Arango JE, Imbault M, Fink M, Gennisson JL, et al. 3D ultrafast ultrasound imaging in vivo. Phys Med Biol. 2014; 59: L1-L13.
44. Provost J, Papadacci C, Demene C, Gennisson JL, Tanter M, Pernot M. 3-D ultrafast Doppler imaging applied to the noninvasive mapping of blood vessels in vivo. IEEE Trans Ultrason Ferroelectr Freq Control. 2015; 62: 1467-1472.
45. Rabut C, Correia M, Finel V, Pezet S, Pernot M, Deffieux T, et al. 4D functional ultrasound imaging of whole brain activity in rodents. Nat Methods. 2019; 16: 994-997.

Megalencephalic leukoencephalopathy with subcortical cysts is a developmental disorder of the gliovascular unit

Alice Gilbert[1,2], Xabier Elorza-Vidal[1], Armelle Rancillac[3*], Audrey Chagnot[4*], Mervé Yetim[4*], Vincent Hingot[5], Thomas Deffieux[5], Anne-Cécile Boulay[1], Rodrigo Alvear-Perez[1], Salvatore Cisternino[6], Sabrina Martin[7], Sonia Taib[7], Antoinette Gelot[8], Virginie Mignon[9], Maryline Favier[10], Isabelle Brunet[7], Xavier Declèves[6, 11], Mickael Tanter[5], Raul Estevez[12, 13], Denis Vivien[4], Bruno Saubaméa[6, 9] and Martine Cohen-Salmon[1]

[1] Physiology and Physiopathology of the Gliovascular Unit Research Group, Center for Interdisciplinary Research in Biology (CIRB), College de France, CNRS Unité Mixte de Recherche 724, INSERM U1050, Labex Memolife, Université PSL, 75005 Paris, France.

[2] École doctorale Cerveau Cognition Comportement "ED3C" N°158, Pierre and Marie Curie University, 75005 Paris, France.

[3] Neuroglial Interactions in Cerebral Physiopathology Research Group, Center for Interdisciplinary Research in Biology (CIRB), College de France, CNRS Unité Mixte de Recherche 724, INSERM Unité 1050, Labex Memolife, Université PSL, 75005 Paris, France.

[4] Normandie University, UNICAEN, INSERM, GIP Cyceron, Institut Blood and Brain @Caen-Normandie (BB@C), UMR-S U1237, Physiopathology and Imaging of Neurological Disorders (PhIND), 14014 Caen, France.

[5] Physics for Medicine Paris, Inserm U1273, CNRS UMR 8063, ESPCI Paris, PSL University, 75005 Paris, France.

[6] Université de Paris, Faculté de Santé, INSERM UMR-S 1144, 75015, Paris.

[7] Molecular control of the neurovascular development Research Group, Center for Interdisciplinary Research in Biology (CIRB), College de France, CNRS Unité Mixte de Recherche 724, INSERM U1050, Labex Memolife, Université PSL, 75005 Paris, France.

[8] Service d'anatomie et cytologie pathologie de l'hôpital Armand Trousseau, 75012 Paris, France.

[9] Cellular and Molecular Imaging facility, US25 INSERM, UMS3612 CNRS, Faculty of Pharmacy, University of Paris, 75014 Paris, France.

[10] Plateforme HistIM Institut Cochin, 75014 Paris, France.

[11] Biologie du médicament et toxicologie, Assistance Publique – hôpitaux de Paris, APHP, Hôpital Cochin, 75014, Paris.

[12] Unitat de Fisiología, Departament de Ciències Fisiològiques, IDIBELL-Institute of Neurosciences, Universitat de Barcelona, L'Hospitalet de Llobregat, 08907 Barcelona, Spain.

[13] Centro de Investigación en Red de Enfermedades Raras (CIBERER), ISCIII, 08907 Barcelona, Spain.

* coauthors

Corresponding author: Martine Cohen-Salmon, Collège de France, Center for Interdisciplinary Research in Biology (CIRB), CNRS, UMR 7241, INSERM, U1050, 11 place Marcelin Berthelot, 75005 Paris, France. Tel: Tel: +33-144-271-242; E-mail: martine.cohen-salmon@college-de-france.fr

Abstract

Absence of the astrocyte-specific membrane protein MLC1 is responsible for megalencephalic leukoencephalopathy with subcortical cysts (MLC), a rare type of leukodystrophy characterized by early-onset macrocephaly and progressive white matter vacuolation that lead to ataxia, spasticity, and cognitive decline. During postnatal development (from P5 to P15 in the mouse), MLC1 forms a membrane complex with GlialCAM (another astrocytic transmembrane protein) at the junctions between perivascular astrocytic processes. Perivascular astrocytic processes along with blood vessels form the gliovascular unit. It was not previously known how MLC1 influences the physiology of the gliovascular unit. Here, using the *Mlc1* knock-out (KO) mouse model of MLC, we demonstrated that MLC1 controls the postnatal development and organization of perivascular astrocytic processes, vascular smooth muscle cell contractility, neurovascular coupling and intraparenchymal interstitial fluid clearance. Our data suggest that MLC is a developmental disorder of the gliovascular unit, and perivascular astrocytic processes and vascular smooth muscle cell maturation defects are primary events in the pathogenesis of MLC and therapeutic targets for this disease.

Keywords: Megalencephalic leukoencephalopathy with subcortical cysts; MLC1; Astrocytes; Gliovascular unit; Development

Introduction

Megalencephalic leukoencephalopathy with subcortical cysts (MLC) is a rare type of leukodystrophy (OMIM 604004) mainly caused by mutations in the *MLC1* gene (MIM #605908) (Leegwater et al., 2001; Topcu et al., 2000). Patients with MLC display early-onset macrocephaly and progressive white matter vacuolation, leading to slowly progressive ataxia, spasticity, and cognitive decline. Most mutations in *MLC1* result in the degradation of the encoded protein MLC1 (Duarri et al., 2008; Lanciotti et al., 2016; Leegwater et al., 2001), a membrane protein that is specifically expressed by the astrocytic lineage in the brain and present at high levels at the junctions between perivascular astrocytic processes (Hoegg-Beiler et al., 2014; Wang et al., 2020). At present, there is no cure for MLC, only symptomatic treatments and supportive care are available. Although the physiopathological mechanisms leading to MLC have not been characterized, the strong expression of MLC1 in perivascular astrocytic processes and other recent observations suggest that the protein has a role in gliovascular functions, in particular the regulation of ion/water homeostasis (Capdevila-Nortes et al., 2013; Hoegg-Beiler et al., 2014; Ridder et al., 2011). Indeed, MLC patients present widespread brain edema and swollen perivascular astrocytic processes (Bugiani et al., 2017; Dubey et al., 2015). GlialCAM, another transmembrane protein forming a complex with MLC1 and responsible for its endoplasmic reticulum exit, is an auxiliary subunit of ClC-2, an inward rectifier chloride channel expressed in a subtype of astrocytes (Benesova et al., 2012; Bugiani et al., 2017; Estevez et al., 2018; Hoegg-Beiler et al., 2014; Jeworutzki et al., 2012). Recessive and dominant mutations in GlialCAM cause MLC subtypes MLC2A and MLC2B, respectively (van der Knaap et al., 1993). *In vitro*, the MLC1/GlialCAM complex indirectly regulates other ion channels, such as TRPV4 and LRRC8 (Elorza-Vidal et al., 2018).

Despite the above observations, it is still not known whether and how MLC1 influences the physiology of the gliovascular unit, the functional interface comprising perivascular astrocytic processes and the brain vessels. We recently reported that MLC1 expression in mouse perivascular astrocytic processes starts around postnatal day (P)5 and that the MLC1/GlialCAM complex forms progressively from P5 to P15, with the protein deposits creating a meshwork between the astrocytes' perivascular membranes (Gilbert et al., 2019). We also demonstrated that this postnatal period is a developmental

97 window for the molecular maturation of brain endothelial cells, particularly with regard to their efflux
98 properties and for the contractility of vascular smooth muscle cells (Gilbert et al., 2019; Slaoui et al.,
99 2021). Given that astrocytes are key regulators of cerebrovascular development and function (e.g. blood
100 brain barrier integrity, immune quiescence and perivascular homeostasis, neurovascular coupling)
101 (Abbott et al., 2006; Alvarez et al., 2013; Castro Dias et al., 2019; Cohen-Salmon et al., 2021), we
102 hypothesized that the MLC1/GlialCAM complex might influence the postnatal differentiation of the
103 vascular system.
104 Here, we characterized key aspects of the molecular and functional organization of the
105 gliovascular unit in *Mlc1* KO mice, a preclinical model of MLC that recapitulates several important
106 features of the disease and that can be used to examine the pathological cascade (Hoegg-Beiler et al.,
107 2014). Our results revealed that MLC1 is a critical factor in the postnatal maturation and function of the
108 gliovascular unit.
109
110

Results

The absence of MLC1 results in accumulation of fluid in the brain but does not alter blood-brain barrier integrity or the organization of the endothelial network

Astrocytes influence several properties of endothelial cells, such as blood brain barrier integrity (Abbott et al., 2006; Alvarez et al., 2013; Castro Dias et al., 2019; Cohen-Salmon et al., 2021). We recently demonstrated that the postnatal maturation of the MLC1/GlialCAM complex in perivascular astrocytic processes from P5 to P15 coincides with the progressive increase in endothelium-specific proteins that contribute to blood brain barrier integrity, such as the tight junction protein claudin5 and the endothelial luminal ATP-binding cassette (ABC) efflux transporter P-glycoprotein (P-gP), suggesting that perivascular astrocytic processes and the blood brain barrier mature in parallel (Gilbert et al., 2019; Slaoui et al., 2021). We therefore investigated whether the absence of MLC1 in the *Mlc1* KO mouse influenced postnatal endothelial maturation. To that end, we used qPCRs to characterize the expression of *Abcb1* (encoding P-gP) and *Cldn5* (encoding claudin5) on P5, P15, and P60 in whole brain microvessels isolated from WT and *Mlc1* KO animals (Boulay et al., 2015) (**Fig. 1A; Fig. 1-source data 1**). In the WT, expression of both analyzed mRNAs on P5 and P15 confirmed the progressive postnatal molecular maturation of endothelial cells (**Fig. 1A**). There were no significant differences between *Mlc1* KO mice and WT mice in this respect (**Fig. 1A**). Consistently, the protein levels of P-gP and claudin5 in purified brain microvessels determined by Western blots were also similar in *Mlc1* KO and WT mice at all stages (**Fig. 1B; Fig. 1-source data 1**). We next assessed the blood brain barrier integrity in *Mlc1* KO and WT mice on P60. We first observed that the apparent diffusion coefficient (measured using magnetic resonance imaging) was higher in *Mlc1* KO mice (**Fig. 1C; Fig. 1-figure supplement1; Fig. 1-source data 1; Fig. 1-figure supplement1-source data1**). Furthermore, the volume of the ventricles and the brain estimated from the anatomical T2-weighted magnetic resonance imaging acquisition was larger in *Mlc1* KO mice than in WT mice (**Fig. 1-figure supplement1**), although the relative ventricular volumes did not differ (**Fig. 1-figure supplement1**). These results reflected the previously described presence of fluid in the parenchyma in *Mlc1* KO mice (Dubey et al., 2015). However, this fluid accumulation was not related to leakage of the blood brain barrier. Indeed,

the vascular volume measured by *in situ* brain perfusion of [^{14}C] sucrose (a marker of vascular space and integrity (Dagenais et al., 2000)) was the same in *Mlc1* KO and WT mice and so suggested that the blood brain barrier was not leaky, even in the shear stress conditions (increased hydrostatic pressure: 180 mmHg) produced by the addition of human serum albumin to the perfusate (Ezan et al., 2012) (**Fig. 1D; Fig. 1-source data 1**). Lastly, we assessed the endothelium architecture by analyzing vessel length, branching and tortuosity in the whole cleared somatosensory cortex of WT and *Mlc1* KO on P60 immunolabeled for the endothelium-specific protein Pecam-1 (**Fig. 1E, F; Fig. 1-source data 1**). There were no differences between WT and *Mlc1* KO mice with regard to these architectural parameters, in either the parenchymal or pial vasculature at the cortical surface (**Fig. 1E, F**).

Hence, the absence of MLC1 leads to fluid accumulation in the brain but has no obvious impact on the postnatal molecular maturation of ECs, blood brain barrier integrity, or endothelium architecture.

MLC1 is crucial for contractile maturation of vascular smooth muscle cells, arterial perfusion, and neurovascular coupling.

We recently showed that vascular smooth muscle cells mature postnatally in mice and humans, with the progressive acquisition of contractility (from P5 onwards in mice and from birth in humans) and the extension of the vascular smooth muscle cell network (Slaoui et al., 2021). Here, we investigated the vascular smooth muscle cells' status in *Mlc1* KO mice during postnatal development. We first used qPCRs to compare the mRNA expression of *Acta2* (encoding smooth muscle actin, SMA) in microvessels purified from WT and *Mlc1* KO whole brain on P5, P15, and P60 (Boulay et al., 2015) (**Fig. 2A; Fig. 2-source data 1**). We also measured the mRNA expression of *Atp1b1* (a vascular-smooth-muscle-cell-specific gene stably expressed during postnatal development) as a marker of vascular smooth muscle cell density in purified brain microvessels (He et al., 2016; Vanlandewijck et al., 2018). In WT mice, the level of *Acta2* mRNA rose progressively from P5 to P15 while the level of *Atp1b1* mRNA remained stable (**Fig. 2A**). In *Mlc1* KO mice, however, *Acta2* was significantly downregulated on P5 and P15, while *Atp1b1* levels were unchanged (**Fig. 2A**). We next analyzed the protein levels of SMA in microvessels purified from WT and *Mlc1* KO whole brain on P5, P15, and P60 by Western blot (**Fig. 2B; Fig. 2-source data 1**). A small decrease in SMA expression was found in

167 *Mlc1* KO microvessels from P15 onwards although it became significant only at P60. Moreover,
168 additional bands of lower molecular weights resembling a degradation pattern were detected at this stage
169 (**Fig. 2B**). To determine whether the decrease in SMA expression and the putative increase in its
170 degradation were related to vascular smooth muscle cell degeneration, we used an immunofluorescence
171 assay to detect SMA on 2-month old WT and *Mlc1* KO whole cleared somatosensory cortices (**Fig. 2C,**
172 **D**). No discontinuities in the labeling were detected in the parenchymal (**Fig. 2C**) or pial vasculature (at
173 the cortical surface) (**Fig. 2D**). Moreover, the SMA-positive vessels' length, branching, tortuosity and
174 number of anastomoses (analyzed only in pial vessels) were the same in *Mlc1* KO and WT mice (**Fig.**
175 **2C, D**). These findings indicate that the absence of MLC1 perturbs the developmental expression of
176 SMA but does not affect the development of the vascular smooth muscle cell network.
177 To further assess the functional consequences of this molecular change, we compared the *ex*
178 *vivo* contractility of vascular smooth muscle cells in brain slices obtained from *Mlc1* KO and WT mice
179 on P5, P15, and P60 (**Fig. 3A-C; Fig. 3-source data 1**). We recorded the vasomotor changes in cortical
180 arterioles upon exposure for 2 min to the thromboxane A_2 receptor agonist U46619 (9,11-dideoxy-
181 11a,9a-epoxymethanoprostaglandin F2α, 5 nM), which acts directly on vascular smooth muscle cells to
182 induce a reversible vasoconstriction. On P5, application of U46619 had a small effect on vessel diameter
183 in both WT and *Mlc1* KO mice (**Fig. 3B, C**). In contrast, a clear vasoconstriction was observed on P15
184 (**Fig. 3B, C**). Strikingly, the amplitude and speed of vasoconstriction were significantly lower in *Mlc1*
185 KO mice from P15 onwards (**Fig. 3B, C; Fig. 3-source data 1**). These results indicate that the postnatal
186 acquisition of contractility is impaired in the absence of MLC1.
187 Given this phenotype, we next hypothesized that arterial tonicity might be impaired in *Mlc1* KO
188 mice. We addressed this question by performing ultrasound localization microscopy *in vivo* imaging to
189 reveal the brain vasculature at a microscopic resolution after intravenous microbubble injection (**Fig.**
190 **3D**). *Mlc1* KO mice displayed significantly lower blood perfusion, suggesting narrower penetrating
191 arteries (**Fig. 3D; Fig. 3-source data 1**). Vasomotricity and cerebral blood flow are tightly coupled to
192 neuronal energy demand, in a process referred to as neurovascular coupling or functional hyperemia
193 (Iadecola, 2017). We then used functional ultrasound imaging to measure the neurovascular coupling,
194 i.e. variations in cerebral blood flow in the barrel cortex in response to whisker stimulation in 2-month-

old WT and *Mlc1* KO mice (Bertolo et al., 2021; Hingot et al., 2020; Osmanski et al., 2014) (**Fig. 3E; Fig. 3-source data 1**). The increase in cerebral blood flow evoked by whisker stimulation was significantly smaller in *Mlc1* KO mice than in WT mice, indicating that neurovascular coupling was impaired in the KO mice (**Fig. 3E; Fig. 3-source data 1**).

In conclusion, the absence of MLC1 impairs the postnatal acquisition of contractile properties by vascular smooth muscle cells and impedes blood perfusion, vessel diameter and neurovascular coupling.

The absence of MLC1 alters the perivascular astrocytic processes' molecular maturation and organization

We next characterized the perivascular astrocytic processes in *Mlc1* KO mice by focusing on membrane proteins known to be strongly expressed in these structures (Cohen-Salmon et al., 2021): the water channel aquaporin 4 (Aqp4), the gap junction protein connexin 43 (Cx43), the adhesion protein GlialCAM and the inward rectifier potassium channel Kir4.1. We first used immunofluorescence to analyze the proteins' location in perivascular astrocytic processes on brain sections on P5, P15, and P60; Kir4.1 was analyzed from P15 onwards, since it is barely detectable before this stage (**Fig. 4A**). The vessels were counterstained with isolectin B4. GlialCAM (whose location at the astrocyte endfoot membrane and immunolabeling depends on MLC1) was not detected around vessel in *Mlc1* KO mice at any stage, as described previously (Hoegg-Beiler et al., 2014). Interestingly, perivascular Aqp4 and Cx43 were almost undetectable on P5 in *Mlc1* KO mice but were detected on perivascular astrocytic membranes from P15 onwards (**Fig. 4A**). Kir4.1 was present on perivascular astrocytic membranes in *Mlc1* KO mice, although the immunofluorescence was less intense. To further quantify these results, we first used Western blots to assess the levels of Aqp4, Cx43, GlialCAM and Kir4.1 in whole brain protein extracts (**Fig. 4B; Fig. 4-source data 1**). In *Mlc1* KO mice, we observed lower levels of Aqp4, Cx43 and GlialCAM on P5 only and lower levels of Kir4.1 on P15 and P60 (**Fig. 4B**). Using stimulated emission depletion (STED) and confocal microscopy, we next quantified the perivascular location of Aqp4, Cx43, GlialCAM and Kir4.1 in WT and *Mlc1* KO mice on P60 (**Fig. 4C**). The vessel's surface was stained by isolectin B4. The Aqp4 signal was similar in the WT and *Mlc1* KO samples. In the *Mlc1*

KO mice, however, the perivascular Cx43 puncta were larger and denser (**Fig. 4C; Fig. 4-source data 1**). GlialCAM labelling was almost undetectable in *Mlc1* KO mice. Kir4.1 perivascular puncta were the same size in both in the WT and *Mlc1* KO samples but were less dense in *Mlc1* KO mice.

These results show that the absence of MLC1 is associated with lower expression of Kir4.1, the delayed expression of Aqp4 and Cx43, the disruption (from P5 onwards) of the GlialCAM's membrane anchoring, and impairment of Cx43's perivascular organization. The data suggest that MLC1 is required for the development and maintenance of the perivascular astrocytic processes' molecular organization.

The absence of MLC1 alters the perivascular astrocytic processes' mechanical cohesiveness

We had demonstrated previously that perivascular astrocytic processes and the associated neuronal fibers remained attached to vessels during their mechanical purification (Boulay et al., 2015) (**Fig. 5E**). The level of Aqp4 in the whole brain extract on P60 was similar in WT and *Mlc1* KO mice (**Fig. 4B**). However, the level of Aqp4 in the extract of mechanically purified brain microvessels was significantly lower in *Mlc1* KO mice than in WT mice (**Fig. 5A; Fig. 5-source data 1**). The same was true for neurofilament protein M (NF-M), a neuronal-specific intermediate filament protein present in neuronal fibers abutting perivascular astrocytic processes. NF-M was similarly present in whole brain extracts from WT and *Mlc1* KO mice but was significantly less present in P60 *Mlc1* KO microvessels (**Fig. 5B; Fig. 5-source data 1**). These data suggested that the perivascular astrocytic processes and the associated neuronal fibers had detached from *Mlc1* KO brain vessels when the latter were mechanically purified. To further validate these results, we assessed the levels of Aqp4 and NF-M immunofluorescence in mechanically purified microvessels from P60 *Mlc1* KO and WT mice (**Fig. 5C, D; Fig. 5-source data 1**). The vessels were counterstained with isolectin B4. In the *Mlc1* KO sample, Aqp4 and NF-M immunolabeling present at the surface of the purified vessels was discontinuous and less intense than in the WT sample (**Fig. 5C, D; Fig. 5-source data 1**).

Taken as a whole, these results suggest that MLC1 influences the mechanical cohesiveness of perivascular astrocytic processes at the vessel surface (**Fig. 5E**).

The absence of MLC1 alters the development and maintenance of astrocyte morphology and polarity

Since tissue cohesivity, cell morphology, and polarity are interdependent, we hypothesized that the absence of MLC1 could perturb the astrocytes' morphology and polarity. We addressed this question by performing a Sholl analysis of glial fibrillary acid protein (GFAP)-immunolabeled astrocytic ramifications in the CA1 region of the hippocampus on P60 (**Fig. 6A**). *Mlc1* KO astrocytes displayed a greater number of processes located between 15 to 25 µm from the soma (**Fig. 6A; Fig. 6-source data 1**). In the hippocampal stratum radiatum, GFAP-positive astrocytic processes are normally polarized perpendicular to the pyramidal cell layer (Nixdorf-Bergweiler et al., 1994). We evaluated this preferential orientation and measured the polarity index, which corresponds to the ratio between parallel (axial) and perpendicular (lateral) crossing points between GFAP-positive processes and a grid oriented with the pyramidal cell layer (**Fig. 6C**). We found that both *Mlc1* KO and WT astrocytes were equally well oriented, with a polarity index > 1 (**Fig. 6C; Fig. 6-source data 1**). However, when taking hippocampal vessels as the reference, *Mlc1* KO astrocytes were abnormally oriented towards vessels in the axial plane (**Fig. 6B; Fig. 6-source data 1).**

MLC1 expression is progressive; in the mouse, it starts at P5 and finishes at P15 (Gilbert et al., 2019). Astrocyte ramification in the stratum radiatum increases greatly between P8 and P16 (Nixdorf-Bergweiler et al., 1994). We therefore wondered whether the abnormal morphology and polarity observed in adult *Mlc1* KO astrocytes might be caused by a developmental defect. Hence, we analyzed the morphology and orientation of GFAP-immunolabeled astrocytic processes on P10 and P15. As previously observed on P60, *Mlc1* KO astrocytes had a larger number of processes located 10 to 25 µm from the soma (**Fig. 6D, F; Fig. 6-source data 1; Fig. 6-figure supplement 1**). On P10 and P15, the *Mlc1* KO processes were also abnormally oriented towards the hippocampal vessels, relative to WT astrocytes (**Fig. 6E, G; Fig. 6-source data 1; Fig. 6-figure supplement 1**).

Taken as a whole, these results indicate that MLC1 is required for the development and maintenance of astrocyte morphology and polarity.

The absence of MLC1 impacts the gliovascular unit's organization and development

We next used transmission electron microscopy to analyze the ultrastructural morphology of perivascular astrocytic processes in the cortex and hippocampus of 2-month old WT and *Mlc1* KO mice, with a focus on vessels up to 10 µm in diameter (**Fig. 7**). In WT mice, endothelial cells were joined by tight junctions and were totally covered by perivascular astrocytic processes, which themselves were joined by gap junctions. Astrocytes and endothelial cells were separated by a thin, homogeneous, regular basal lamina (**Fig. 7A**). In *Mlc1* KO mice, the endothelium appeared to be unaltered: normal tight junctions and basal lamina, and no accumulation of intracellular vesicles (**Fig. 7B-E**). However, the astrocytes' perivascular organization was drastically modified (**Fig. 7B-E**). We observed perivascular astrocytic processes surrounded by basal lamina (**Fig. 7C; Fig. 7-figure supplement 1**) or stacked on top of each other and joined by gigantic gap junction plaques (**Fig. 7D**). Some perivascular astrocytic processes interpenetrated each other (**Fig. 7-figure supplement 1**). No swelling was observed in *Mlc1* KO perivascular astrocytic processes (**Fig. 7B-E, G; Fig. 7-source data 1**) (edematous perivascular astrocytic processes were observed in one-year-old *Mlc1* KO mice (**Fig. 7-figure supplement 2; Fig. 2- figure supplement 2-source data 1**). Strikingly, astrocyte coverage in *Mlc1* KO mice was often discontinuous. In the free spaces, axons (recognizable by their microtubules) (**Fig. 7B, E**) and synapses (recognizable by the large number of vesicles in the presynaptic part and their electron dense postsynaptic density (**Fig. 7-figure supplement 1**) were found to be in direct contact with the endothelial basal lamina. Accordingly, the percentage of microvessels in which the endothelial basal lamina was in direct contact with at least one neuronal process was higher in *Mlc1* KO mice than in WT mice (**Fig. 7F**).

The time course of perivascular astrocyte coverage has not previously been described. Here, we used transmission electron microscopy to quantify the percentage of the perivascular diameter covered by perivascular astrocytic processes in *Mlc1* KO and WT cortex and hippocampus on P5, P10, P15, and P60 (**Fig. 7H; Fig. 7-supplement 1; Fig. 7-source data 1**). On P5, the perivascular astrocytic processes covered about half of the vessel's circumference, and the WT and *Mlc1* KO samples did not differ significantly in this respect (**Fig. 7H**). The perivascular astrocyte coverage increased dramatically between P5 and P15 and was almost complete on P15 in WT mice (**Fig. 7H**). In contrast, *Mlc1* KO mice displayed a lower percentage of perivascular astrocytic process coverage from P10 onwards, and a large

306 number of neuronal processes were inserted into the noncovered areas of the vessels (**Fig. 7H; Fig. 7-**
307 **figure supplement 1; Fig. 7-source data 1**).

308 Our results demonstrate for the first time that the perivascular astrocyte coverage increases
309 rapidly between P5 and P15. This process is impaired in *Mlc1* KO mice and results in incomplete
310 perivascular astrocytic process coverage and direct contact between infiltrating neuronal processes and
311 the endothelial basal lamina (the processes normally remain behind the perivascular astrocyte layer).
312 Taken as a whole, these results indicate that (i) the absence of MLC1 in the gliovascular unit greatly
313 alters the perivascular astrocytic processes' morphology and coverage and (ii) MLC1 is critical for the
314 normal postnatal development of perivascular astrocyte coverage.

315

316 **The absence of MLC1 modifies the parenchymal circulation of cerebrospinal fluid**

317 Several groups have reported a causal link between perivascular astrocytic process
318 disorganization and impaired parenchymal cerebrospinal fluid transport (Haj-Yasein et al., 2012; Kress
319 et al., 2014). We tested this hypothesis by measuring the parenchymal distribution of DOTA-
320 Gadolinium (DOTA-Gd) injected in cerebrospinal fluid through the cisterna magna in 2-month-old mice
321 using T1-weighted magnetic resonance imaging (**Fig. 8A**). Contrast-enhanced T1 mapping was used to
322 quantify changes of the concentration of DOTA-Gd within the brain tissue over time. In line with the
323 conventional models of cerebrospinal solute circulation, tracers injected into the cisterna magna
324 dispersed into the subarachnoid space and then entered the parenchyma through the perivascular spaces
325 (**Fig. 7B**) (Iliff et al., 2012; Iliff et al., 2013). As expected, a high concentration of DOTA-Gd was
326 detected at the border of the brain as early as 10 minutes after injection in both WT and *Mlc1* KO mice;
327 this reflected the initial dispersion of contrast within the subarachnoid space. Forty-five minutes after
328 injection, the DOTA-Gd concentration in brain tissue rose as it penetrated into the parenchyma through
329 the perivascular spaces (**Fig. 8C**). The dispersion kinetics for each route depends on anatomic
330 differences between regions of the brain, such as the presence or absence of a perivascular space and
331 the topology of the vascular network (Iliff et al., 2012; Iliff et al., 2013). For both the WT and *Mlc1* KO
332 genotypes, the distribution of DOTA-Gd appeared to be in line with the literature data (**Fig. 8C**).
333 However, examination of the quantitative maps suggested that DOTA-Gd transport into the

cerebrospinal fluid was less intense in *Mlc1* KO mice than in WT mice. We also analyzed the time courses of DOTA-Gd dispersion in the cerebellum, midbrain, septal area, and cortex (**Fig. 8D-G; Fig. 8-source data 1**). Relative to WT mice, the mean DOTA-Gd concentration in *Mlc1* KO mice was lower in the midbrain (**Fig. 8E; Fig. 8-source data 1**) and the slope was lower in the cerebellum, midbrain, and cortex (**Fig. 8D, E, G; Fig. 8-source data 1**). We therefore conclude that the absence of MLC1 impairs the intraparenchymal circulation and clearance of cerebrospinal fluid.

Developmental perivascular expression of MLC1 in the human cortex

In an attempt to move closer to the context of MLC in humans, we used immunohistochemical techniques to analyze the development of perivascular expression of MLC1 in human cortical sections from 15 weeks of gestation to 17 years of age (**Fig. 9; Fig. 9-source data 1**). Interestingly, perivascular MLC1 was detected as early as 15 weeks of gestation (**Fig. 9A; Fig. 9-source data 1**) and remained stable thereafter (**Fig. 9B-F; Fig. 9-source data 1**). These results suggested that in humans, the MLC1/GlialCAM complex and the astrocyte's perivascular coverage are initiated prenatally.

Discussion

MLC1 (the main gene involved in MLC) encodes an astrocyte-specific protein located in perivascular astrocytic processes, where it forms a junctional complex with GlialCAM. Our previous research showed that, in the mouse, the MLC1/GlialCAM complex forms progressively after birth (between P5 and P15) (Gilbert et al., 2019). Our present work demonstrated for the first time that the P5-P15 time window is also important for the formation of perivascular astrocyte coverage. On P5, perivascular astrocytic processes covered only 50% of the vascular surface, and this coverage increased rapidly until completion on P15. We show that the absence of MLC1 impairs this developmental process together with the astrocytic perivascular processes' molecular maturation, with a lower Kir4.1 expression and a transient decrease in Aqp4 and Cx43 protein levels on P5. GlialCAM (whose anchorage in astrocytic membranes depends on MLC1) is distributed diffusely, as described previously (Hoegg-Beiler et al., 2014). From P10 onwards, perivascular astrocytic processes incompletely cover the vessels and direct contact between neuronal components and the vessel wall are observed. Interestingly, the postnatal period is also an intense synaptogenic phase in the mouse brain (Chung et al., 2015); astrocytes and neurons might compete for the perivascular space during this time. In the absence of MLC1, neurons might either stabilize or insert into the space left free by perivascular astrocytic processes.

Remodeling of the gliovascular interface is accompanied by a loss of astrocyte polarity in *Mlc1* KO. Firstly, the perivascular distribution of Cx43 gap junction at the perivascular surface is modified with more and larger puncta, and the perivascular astrocytic processes are delineated by large gap junction plaques. Interestingly, disorganization of Cx43 was recently reported in *GlialCAM* KO mice (Baldwin et al., 2021); this supports the hypothesis whereby the MLC1/GlialCAM complex organizes gap junction coupling in perivascular astrocytic processes. Secondly, *Mlc1* KO astrocytes have an abnormally high number of ramifications, which tend to project towards the blood vessels. Thirdly, there are changes in the perivascular astrocytic processes' polarity and organization (stacking, interpenetration, and the presence of basal lamina on the parenchymal side). Lastly, astrocytic perivascular processes are less mechanically cohesive. It was recently demonstrated that the astrocyte arborization becomes more complex between P7 and P21 - the period during which the perivascular

377 MLC1/GlialCAM astrocytic complex forms (Clavreul et al., 2019; Gilbert et al., 2019). The formation
378 of perivascular astrocytic process coverage (mediated by the MLC1/GliaCAM complex) might
379 influence this process and thus polarize astrocytes. Taken as a whole, our data demonstrate that MLC1
380 is crucial for the development of astrocyte morphology, perivascular polarity, and perivascular coverage.
381 What impact, then, does the lack of MLC1 have on the gliovascular physiology? Although
382 astrocytes are key regulators of the blood-brain barrier's integrity (Abbott et al., 2006; Alvarez et al.,
383 2013; Castro Dias et al., 2019; Cohen-Salmon et al., 2021), the incomplete perivascular astrocyte
384 coverage, the abnormal astrocytic polarity, and the loss of the perivascular astrocytic processes'
385 mechanical cohesiveness did not alter BBB integrity in *Mlc1* KO. Nevertheless, these changes probably
386 alter the "barrier" formed by perivascular astrocytic processes around the vessels. In turn, this might
387 greatly affect perivascular homeostasis and astrocyte signaling towards the vascular compartment
388 (Abbott et al., 2006; Yao et al., 2020). The astrocytes' perivascular organization is thought to be crucial
389 for regulating the fluxes of cerebrospinal fluid and interstitial fluid into the parenchyma (Abbott et al.,
390 2018). Perivascular astrocytic process alterations in *Mlc1* KO mice might therefore be directly linked to
391 the loss of DOTA-Gd intraparenchymal drainage observed. By reducing the volume of subarachnoid
392 spaces, megalencephaly in *Mlc1* KO mice may also alter the brain's drainage capacity, as suggested by
393 the lower level of DOTA-Gd transport into the cerebrospinal fluid observed in *Mlc1* KO mice. In the
394 presence of an intact blood brain barrier, impaired parenchymal circulation of the cerebrospinal
395 fluid/interstitial fluid might (i) contribute to the fluid accumulation and megalencephaly (Dubey et al.,
396 2015; van der Knaap et al., 2012), (ii) lead to the progressive accumulation of harmful molecules in the
397 brain, and (iii) thus increase susceptibility to neural disorders (Rasmussen et al., 2018).
398 Epilepsy is a significant component of MLC (Yalcinkaya et al., 2003). *Mlc1* KO mice display
399 spontaneous epileptiform activity, an abnormally low threshold for seizure induction, and an elevated
400 extracellular potassium concentration in the hippocampus upon prolonged high-frequency stimulation
401 (Dubey et al., 2018). The absence of Kir4.1 leads to hyperexcitability and epilepsy (Sibille et al., 2014).
402 The low level of perivascular Kir4.1 observed in *Mlc1* KO mice might link MLC to epilepsy.
403 Unlike skeletal or cardiac muscle, SMCs are not terminally differentiated and are extremely
404 plastic. They constantly integrate signals from their local environment and undergo profound phenotypic

changes in response to variations in their local environment (Owens, 1995; Owens et al., 2004). By perturbing perivascular homeostasis, the abnormal development of perivascular astrocytic processes in the absence of MLC1 might affect the postnatal acquisition of vascular smooth muscle cells' contractile properties and thus result in hypoperfusion and defective neurovascular coupling. This hypothesis is supported by the fact that perivascular astrocyte coverage, MLC1 expression (Gilbert et al., 2019) and vascular smooth muscle cell contractile differentiation (Slaoui et al., 2021) develop concomitantly. Interestingly, deletion of astrocytic laminin γ1 was shown to lead to the loss of vascular smooth muscle cell contractile proteins (Chen et al., 2013), which indicated a functional link between astrocytes and vascular smooth muscle cells. Our data now suggest that astrocytes have a critical role in the postnatal differentiation of contractile vascular smooth muscle cells.

Alteration of vascular smooth muscle cell contractility might influence brain perfusion and neurovascular coupling, which are critical for oxygen and nutrient delivery to neurons (Iadecola, 2017); this impairment might compromise neuronal and cerebral functions. Furthermore, the maintenance of axonal myelination makes extraordinary metabolic demands on oligodendrocytes (Harris and Attwell, 2012) (Rosko et al., 2019). The lack of vascular smooth muscle cell contractility and the changes in blood perfusion and cerebral blood flow regulation resulting from the absence of MLC1 might contribute to progressive intramyelinic edema. This hypothesis is also supported by the fact that myelin vacuolation in *Mlc1* KO mice does not start until the age of 3 months (Dubey et al., 2015; Hoegg-Beiler et al., 2014). Finally, alteration of vascular smooth muscle cell contractility could affect circulation of the cerebrospinal fluid and perivascular fluid, although the heart beat is the main driver (Iliff et al., 2013).

Together, the development of perivascular astrocytic process, vascular smooth muscle cell maturation, cerebrospinal fluid flux, and cerebral blood flow defects precede myelin vacuolation in *Mlc1* KO mice and so are probably primary events in the pathogenesis of MLC. Our observation of swollen perivascular astrocytic processes on 1-year but not on P60 *Mlc1* KO mice indicates that edema develops progressively in the absence of MLC1 and suggests that the pathogenic process is irresistible.

In contrast to the mouse, expression of MLC1 and the astrocyte's perivascular coverage are initiated prenatally in humans, as already suggested by earlier observations of perivascular GFAP and

433 AQP4 expression (El-Khoury et al., 2006). These results suggest that in humans, impaired perivascular
434 astrocytic process formation linked to the absence of MLC1 might occur prenatally, deregulating
435 perivascular homeostasis and then the perinatal differentiation of vascular smooth muscle cell
436 contractility (Gilbert et al., 2019; Slaoui et al., 2021) leading to a progressive white matter vacuolation.
437 In conclusion, we showed that the astrocyte-specific protein MLC1, the absence of which causes
438 MLC, is critical for the postnatal development of perivascular astrocyte coverage, the acquisition of
439 vascular smooth muscle cell contractility, and parenchymal CFS/ISF efflux. Our results shed light on
440 the role of astrocytes in the postnatal the acquisition of vascular smooth muscle cell contractility, a
441 crucial component of neurovascular coupling in the brain. Our data indicate that MLC could be
442 considered primarily as an early developmental disorder of the gliovascular unit. Moreover, our study
443 illustrates how looking at physiopathological processes in a rare disease can enlighten important aspects
444 of the brain's physiology.
445

446 **Acknowledgements**

447

448 We are grateful to the donors who support the charities and charitable foundations cited below. This
449 work was funded by grants from the *Association Européenne contre les Leucodystrophies* (ELA, grant
450 reference ELA2012-014C2B), the *Fondation pour la Recherche Médicale* (FRM, grant reference
451 AJE20171039094) and the *Fondation Maladies Rares* (grant reference 20170603). A. Gilbert's PhD
452 was funded by the FRM (grant reference: PLP20170939025p60) and ELA (grant reference: ELA2012-
453 014C2B). The creation of the Center for Interdisciplinary Research in Biology (CIRB) was funded by
454 the "Fondation Bettencourt Schueller". We thank Fawzi Boumezbeur, Aloïse Mabondzo, Corinne
455 Blugeon, Laurent Jourdren and Stéphane Le Crom for helpful discussions. We thank Isabelle Bardou
456 for her help writing ethical documents. We thank Louise Charpentier and Ines Masurel for their help
457 analyzing astrocyte morphology and polarity. Lastly, we thank Virginie Mignon for help with
458 transmission electron microscopy, Julien Dumont for help with STED imaging, and Augustin Walter
459 for help with confocal image analysis. Copy-editing assistance was provided by Biotech
460 Communication SARL (Ploudalmézeau, France) and Life Science Editors. Despite our efforts, our work
461 has not received any funding from the French National Agency for Research (ANR).

462

463

464

Figure Legends

Fig. 1. The absence of MLC1 has no effect on blood brain barrier integrity or the organization of the endothelial network.

A. qPCR determination of mRNA expression of *Abcb1* (encoding P-gP) and *Cldn5* (encoding claudin5) in microvessels purified from WT and *Mlc1* KO whole brains on P5, P15, and P60. Signals were normalized against *Gapdh*. Groups were compared using a two-tailed Mann-Whitney test. The data are presented as a Tukey box plot (n = 3 or 4 samples per genotype; number of brains pooled per sample: 5 for P5; 3 for P15; 2 for P60). **B.** Western blot detection and analysis of P-gP and claudin5 in protein extracts from microvessels purified from WT and *Mlc1* KO whole brains on P5, P15, and P60. Signals were normalized against histone H3. Two-tailed Mann-Whitney test. The data are represented in a Tukey box plot (n = 4 or 5 sample per genotype; number of brains pooled per sample: 5 for P5; 3 for P15; 2 for P60). **C.** Apparent diffusion coefficient values in the cortex of 2-month old WT and *Mlc1* KO mice. Two-tailed Student's T test. The data are represented in a Tukey box plot (n = 7 mice per genotype). **D.** Blood brain barrier integrity, assessed by measuring the brain vascular volume (Vv, in µL/g), after *in situ* brain perfusion with [^{14}C]-sucrose and a normal hydrostatic vascular pressure (without albumin (Albumin-); 120 mmHg) or an elevated hydrostatic vascular pressure (with albumin (Albumin+); 180 mmHg) in 2-month-old WT (in black) and *Mlc1* KO mice (in red). Two-tailed Mann-Whitney test. The data are represented in a Tukey box plot (n = 8 WT and 9 *Mlc1* KO mice for Albumin -; n = 11 WT and 12 *Mlc1* KO mice for Albumin +). Representative 3D images of the endothelial architecture in cleared somatosensory cortex. Parenchymal (Z stack 320 µm; scale bar: 100 µm) **(top)** and pial **(bottom)** vessels (Z stack 50 µm; scale bar: 500 µm) samples from 2-month-old WT and *Mlc1* KO mice, after immunolabeling for Pecam1. **F.** A comparative analysis of vessel length, branching and tortuosity in WT mice (in black) and *Mlc1* KO mice (in red) in the parenchymal cortex **(top)**, normalized on sample volume, and cortical surface **(bottom)**, normalized on sample surface. One-tailed Mann-Whitney test. The data are represented in a Tukey box plot (n = 3 mice per genotype). The data are given in **Fig. 1-source data 1**. *, $p \leq 0.05$, **, $p \leq 0.01$, ***, $p \leq 0.001$, and ns: not significant.

493 **Fig. 2. MLC1 is crucial for the molecular maturation of vascular smooth muscle cell contractility**
494 **A** qPCR results for *Acta2* (encoding SMA) and *Atp1b1* in microvessels purified from WT and *Mlc1* KO
495 whole brains on P5, P15, and p60. Signals are normalized against *Gapdh*. Two-tailed Mann-Whitney
496 test. The data are represented in a Tukey box plot (n = 3 to 5 samples per genotype; number of brains
497 pooled per sample: 5 for P5; 3 for P15; 2 for P60). **B.** Western blot detection and analysis of SMA in
498 protein extracts from microvessels purified from WT and *Mlc1* KO whole brains on P5, P15, and P60.
499 Arrows indicate abnormally low molecular weight SMA-positive bands. Signals were normalized
500 against histone H3. Two-tailed Mann-Whitney test. The data are represented in a Tukey box plot (n = 4
501 or 5 samples per genotype; number of brains pooled per sample: 5 for P5; 3 for P15; 2 for P60). **C. E.**
502 Representative 3D images of the vascular smooth muscle cell arterial network in cleared somatosensory
503 cortex. Parenchymal (Z stack 600 µm; scale bar: 100 µm) (**C**) and pial vessels (Z stack 50 µm; scale
504 bar: 500 µm) (**E**) samples in 2-month-old WT and *Mlc1* KO mice after immunolabeling for SMA. **D. F.**
505 Comparative analysis of arterial length, branching, tortuosity, and anastomosis in WT mice (black
506 boxes) and *Mlc1* KO mice (red boxes) in the cortical parenchyma (**D**), normalized on sample volume,
507 and at the cortical surface (**F**), normalized on sample surface. One-tailed Mann-Whitney test. The data
508 are represented in a Tukey box plot (n = 3 mice per genotype). The data are given in **Fig. 2-source data**
509 **1**. *, $p \leq 0.05$, **, $p \leq 0.01$, ***, $p \leq 0.001$, and ns: not significant.
510
511 **Fig. 3. MLC1 is crucial for the postnatal acquisition of vascular smooth muscle cell contractility,**
512 **arterial diameter, and neurovascular coupling**
513 **A-C.** *Ex vivo* analysis of mean vascular constriction and dilation upon application of U46619 (50 nM)
514 to somatosensory cortical slices from P5, P15, and P60 WT mice (black traces) and *Mlc1* KO mice (red
515 traces). **A.** Representative infrared images of a cortical penetrating arteriole constriction in response to
516 bath application of U46619 and dilation upon washing at P60. The vessel lumen is indicated by dotted
517 lines. Scale bar: 10 µm. **B.** Contraction and dilation slopes on P5, P15 and P60. 0 min corresponds to
518 the addition of U46619 to the recording chamber medium. The data are presented as the mean ± SEM.
519 **C.** Analysis of the amplitude and slope of the contraction. Two-tailed Mann-Whitney test. The data are
520 represented in a Tukey box plot (n = 13 vessels from WT and 13 *Mlc1* KO mice on P5; n = 9 vessels

from WT and 12 *Mlc1* KO mice at P15; n = 8 vessels from WT and 11 *Mlc1* KO mice at P60; 3 mice per group). **D.** *In vivo* ultrasound localization microscopy measurement of cortical arterial vessel diameter after intravenous microbubble injection in 2-month-old WT and *Mlc1* KO mice. **Left:** Schematic representation of the experiment; **Middle:** Cerebrovascular maps of WT and *Mlc1* KO mice, showing the arterial (in red) and venous (in blue) velocities in mm/s (scale bar: 0.15 cm); **Right:** Measurement of the penetrating arteries' diameter using ultrasound localization microscopy imaging of an injected microbubbles. The data are represented in a Tukey box plot. Two-tailed Mann–Whitney test (n=6 WT mice and *Mlc1* KO mice each). **E.** *In vivo* functional ultrasound analysis of cerebral blood flow in the somatosensory cortex after whisker stimulation. **Left:** Schematic representation of the experiment (S1bf: bregma -1.5 mm, somatosensory barrel field cortex); **Middle:** Functional ultrasound power doppler signal traces during whisker stimulation of 2-month-old WT mice (in black) and *Mlc1* KO mice (in red) mice. Baselines before stimulation are aligned; **Right:** Quantification of the normalized percentage of cerebral blood flow variation following whisker stimulation. Two-tailed Mann–Whitney test. The grey areas around the curves correspond to the SEM (n=11 WT mice and 12 *Mlc1* KO mice). The data are given in **Fig. 3-source data 1**. *, $p \leq 0.05$, **, $p \leq 0.01$, ***, $p \leq 0.001$, and ns: not significant. Data presented in A-C are also included in (Slaoui et al., 2021). These panels are not available under the terms of a Creative Commons Attribution License, and further reproduction of these images requires permission from the copyright holder.

Fig. 4. The absence of MLC1 alters the molecular maturation of the perivascular astrocytic processes

A. Representative confocal projection images of the immunofluorescent detection of Aqp4, Cx43, GlialCAM and Kir4.1 (in red) on brain cortex sections from WT and *Mlc1* KO mice on P5 (except for Kir4.1), P15, and P60. Vessels were stained with isolectin B4 (IB4) (in green), and nuclei were stained with Hoechst dye (in blue). Scale bar: 20 µm. **B.** Western blot detection and analysis of Aqp4, Cx43, GlialCAM and Kir4.1 in whole-brain protein extracts from WT and *Mlc1* KO mice on P5 (except for Kir4.1), P15, and P60. Two-tailed Mann-Whitney test. The data are represented in a Tukey box plot (for whole brain: n = 5 samples per genotype (one mouse per sample)). **C.** Representative STED images and

quantification of the immunofluorescent detection of Aqp4, Cx43, GlialCAM and Kir4.1 (in red) on brain cortex sections from WT and *Mlc1* KO mice on P60. Vessels were stained with IB4 (in green). Intravascular diffusion of the IB4 fluorescence is an artifact of STED. Scale bar: 5 µm. Two-tailed Mann-Whitney test. The data are represented in a Tukey box plot (aquaporin 4: n = 18 *Mlc1* KO vessels; n=18 WT vessels; n=3 mice per genotype; Connexin 43: n = 15 *Mlc1* KO vessels; n=15 WT vessels; n=3 mice per genotype; GlialCAM: n = 14 *Mlc1* KO vessels; n=14 WT vessels; n=3 mice per genotype; Kir4.1: n = 18 *Mlc1* KO vessels; n=17 WT vessels; n=3 mice per genotype). The data are given in **Fig. 4-source data 1.** *, $p \leq 0.05$, **, $p \leq 0.01$, ***, $p \leq 0.001$, and ns: not significant.

Fig 5. The absence of MLC1 alters the perivascular cohesiveness of astrocytic processes

A. B. Western blot detection and analysis of Aqp4 (**A**) and NF-M (**B**) in protein extracts from microvessels purified from WT and *Mlc1* KO whole brains on P60 (see **Fig. 4C** for Aqp4 detection in whole brain on P60). The signals were normalized against stain-free membranes. Two-tailed Mann-Whitney test. The data are represented in a Tukey box plot (n = 5 samples per genotype (2 mice per microvessels sample)). **C. D.** Representative confocal projection images of the immunofluorescent detection and quantification of Aqp4 (**C**) and NF-M (**D**) (in red) on microvessels purified from WT and *Mlc1* KO whole brain on P60. Vessels were stained with isolectin B4 (IB4) (in green). Scale bar: 20 µm. Two-tailed Mann-Whitney test. The data are represented in a Tukey box plot (aquaporin 4: n = 17 *Mlc1* KO images; n=22 WT images; n=3 mice per genotype; NF-M: n = 15 *Mlc1* KO images; n=16 WT images; n=3 mice per genotype; each image shows between 1 and 4 vessels). The data are given in **Fig. 5-source data 1**. *, $p \leq 0.05$, **, $p \leq 0.01$, ***, $p \leq 0.001$, and ns: not significant. **E.** Schematic interpretation of the data. In *Mlc1* KO mice, the perivascular astrocytic processes (in green) and neuronal associated fibers (in red) are lost during the microvessel purification process (basal lamina in yellow, mural cells in brown, EC in blue). MLC1 is represented by pink dots in the WT.

Fig. 6. The absence of MLC1 alters the postnatal development and maintenance of astrocyte morphology and polarity

A. A Sholl analysis of the ramification of hippocampal CA1 astrocytes immunolabeled for GFAP (in black) in WT and *Mlc1* KO P60 mice. The concentric circles start from the astrocyte's soma. Scale bar: 20 µm. A two-way analysis of variance, followed by a Bonferroni *post hoc* test. The data are presented as the median ± quartiles. (n=48 *Mlc1* KO cells; n=44 WT cells; n=3 mice per genotype). **B.** Grid-baseline analysis of the orientation of the GFAP-immunolabeled astrocytic processes (in white) toward vessels labeled with isolectin B4 (in green) in WT and *Mlc1* KO P60 mice. The nuclei were labeled with Hoechst dye (in blue). Scale bar: 20 µm. The polarity index is the ratio between axial GFAP contacts and lateral GFAP contacts. A polarity index of 1 means that there is no polarity. Two-tailed Mann-Whitney test. The data are represented in a Tukey box plot (n=41 *Mlc1* KO cells; n= 41 WT cells; 3 mice per genotype). **C.** Grid-baseline analysis of the orientation of the GFAP-immunolabeled astrocytic processes (in white) toward the hippocampal pyramidal cell layer in WT and *Mlc1* KO P60 mice. The nuclei were labeled with Hoechst dye (in blue). Scale bar: 20 µm. The polarity index is the ratio between axial GFAP contacts and lateral GFAP contacts. A polarity index of 1 means that there is no polarity. Two-tailed Mann-Whitney test. The data are represented in a Tukey box plot (n=52 *Mlc1* KO cells; n= 47 WT cells; 3 mice per genotype). **D. F.** Quantitative analyses of astrocyte ramification on P10 (**D**) and P15 (**F**). A two-way analysis of variance, followed by a Bonferroni *post hoc* test (P10: n=53 *Mlc1* KO cells; n=49 WT cells; n=3 mice per genotype; P15: n=51 *Mlc1* KO cells; n=50 WT cells; n=3 mice per genotype). See **Fig. 6-figure supplement 1** for representative images. **E. G.** Quantitative analysis of astrocyte process orientation toward vessels on P10 (**E**) and P15 (**G**). See **Fig. 6-figure supplement 1** for representative images. The polarity index is the ratio between axial GFAP contacts and lateral GFAP contacts. A polarity index of 1 means that there is no polarity. Two-tailed Mann-Whitney test. The data are represented in a Tukey box plot (P10: n=35 *Mlc1* KO cells; n=26 WT cells; n=3 mice per genotype; P15: n=48 *Mlc1* KO cells; n=46 WT cells; n=3 mice per genotype). The data are given in **Fig. 6-source data 1**. *, $p \leq 0.05$, **, $p \leq 0.01$, ***, $p \leq 0.001$, and ns: not significant.

Fig. 7. The absence of MLC1 impacts the organization and development of the gliovascular unit

A-E. Representative transmission electron microscopy images of the gliovascular unit in the hippocampus of P60 WT and *Mlc1* KO mice (n=3 mice per genotype). Images are presented in pairs,

605 with artificial colors in the lower panel: perivascular astrocytic processes in yellow, gap junctions in
606 green, axons or synapses in red, mural cells in light blue, endothelial cells in dark blue, the basal lamina
607 in brown, and tight junctions in purple. **A.** In WT mice, perivascular astrocytic processes fully cover
608 endothelial cells linked by a tight junction and surrounded by a continuous basal lamina. **B-E.** Data from
609 *Mlc1* KO mice. **B.** Perivascular astrocytic processes are separated by an axon, which contacts the
610 endothelial basal lamina (red arrowhead). **C.** A perivascular astrocytic process is surrounded by the
611 basal lamina (red arrowhead). **D.** Several perivascular astrocytic processes are stacked on top of each
612 other and are linked by extended gap junctions (red arrowhead). **E.** Perivascular astrocytic processes are
613 separated by four axons (red arrowhead), which are in direct contact with the vascular basal lamina. **F.**
614 Quantification of capillaries and venules contacted by neural processes (axons or synapses) in P60 mice.
615 Two-tailed Student's T test. The data are represented in a Tukey box plot (n=399 *Mlc1* KO cortical
616 vessels; n=301 *Mlc1* KO hippocampal vessels; n=286 WT cortical vessels; n=287 WT hippocampal
617 vessels; n=3 mice per genotype). **G.** Percentage of vessels contacted by a normal perivascular astrocytic
618 process (swelling = 0), a moderately swollen perivascular astrocytic process (swelling = 1), or an
619 edematous perivascular astrocytic process (swelling = 2) in the hippocampus and cortex of P60 mice.
620 Two-tailed Mann-Whitney test. The data are represented in a Tukey box plot (n=399 *Mlc1* KO cortical
621 vessels; n=301 *Mlc1* KO hippocampal vessels; n=286 WT cortical vessels; n=287 WT hippocampal
622 vessels; n=3 mice per genotype). **H.** Percentage of the vessel diameter covered by perivascular astrocytic
623 processes in the cortex of WT and *Mlc*1 KO mice on P5, P10, P15, and P60. Two-tailed Mann-Whitney
624 test. The data are represented in a Tukey box plot (n = 46 vessels from WT mice and 68 *Mlc1* KO mice
625 on P5, n=3 mice per genotype ; n=121 vessels from WT mice and 81 *Mlc1* KO mice on P10, n=3 mice
626 per genotype; n=207 vessels from WT mice and 144 *Mlc1* KO mice at P15, n=4 mice per genotype;
627 n=143 vessels from WT mice and 134 *Mlc1* KO mice at P60, n=3 mice per genotype). Representative
628 transmission electron microscopy images of the gliovascular interface in the cortex of WT and *Mlc1* KO
629 mice on P10 and P15 are presented in **Fig. 7-figure supplement 1**. The data are given in **Fig. 7-source**
630 **data 1.** *, $p \leq 0.05$, **, $p \leq 0.01$, ***, $p \leq 0.001$, and ns: not significant.
631

Fig. 8 Contrast-enhanced magnetic resonance imaging reveals a low level of tracer dispersion from the CSF into the parenchyma in *Mlc1* KO mice.

A. B. Schematic representation of injecting 1 µL DOTA-Gd into the mouse's CSF through the cisterna magna (**A**) and the disperse of the tracer through the brain into the subarachnoid space before entering the deep parenchyma through the perivascular spaces (**B**). **C.** Quantitative contrast maps in WT and *Mlc1* KO mice, 10 and 45 minutes after contrast injection (scale bar: 1cm). **D-G.** Based on the dynamic acquisitions, the changes over time in contrast agent concentration were extracted, and the mean contrast concentration and the contrast slope were calculated for the cerebellum (**D**), midbrain (**E**), septal area (**F**), and cortex (G). Two-tailed Mann-Whitney test. The data are represented in a Tukey box plot (n = 9 per genotype except 8 in the cortex of WT). The data are given in **Fig. 8-source data 1**. *, $p \leq 0.05$, **, $p \leq 0.01$, ***, $p \leq 0.001$, and ns: not significant.

Fig. 9: Developmental perivascular expression of MLC1 in the human cortex

A-E. Representative images of MLC1-immunostained human cortical slices (left) and a higher magnification image of the parenchyma in the boxed areas (right) at the prenatal stage (weeks of gestation: 15; 21; 28; 30; 39) (**A**); 0 to 1 year of age (ages: 3 weeks; 1 month; 2 months; 3 months; 8 months; 1 year) (**B**); 3 to 4 years of age (3 years; 4 years (n=2)) (**C**); 10 to 13 years of age (10 years; 11 years; 12 years; 13 years (n=2) (**D**); and 16 to 17 years of age (16 years; 17 years) (**E**). Scale bar: 100 µm. MLC1 immunostaining (arrowheads) was revealed with DAB. **F.** 3, 3'-diaminobenzidine (DAB) intensity was quantified and presented as a Tukey box plot. We applied the Kruskal-Wallis test (overall, in bold) and a Two-tailed Mann-Whitney test (for comparing stages). The number of samples per developmental age was 5 for the prenatal samples, 5 for 0-1 years of age, 4 for 3-4 years of age, 4 for 10-13 years of age, and 2 for 16-17 years of age. The data are given in **Fig. 9-source data 1.**

659 **Methods**

660 **Key resources**
661

Reagent type (species) or resource	Designation	Source or reference	Identifier	Additional information
sequence-based reagent	Acta2_F	This study	PCR primers	GTCCCAGACATCAG GGAGTAA
sequence-based reagent	Acta2_R	This study	PCR primers	TCGGATACTTCAGCG TCAGGA
sequence-based reagent	Atp1b1_F	This study	PCR primers	GCTGCTAACCATCAG TGAACT
sequence-based reagent	Atp1b1_R	This study	PCR primers	GGGGTCATTAGGAC GGAAGGA
sequence-based reagent	Mdr1a (Abcb1)_F	This study	PCR primers	GATAGGCTGGTTTGA TGTGC
sequence-based reagent	Mdr1a (Abcb1)_R	This study	PCR primers	TCACAAGGGTTAGCT TCCAG
sequence-based reagent	Cldn5_F	This study	PCR primers	TAAGGCACGGGTAG CACTCA
sequence-based reagent	Cldn5_R	This study	PCR primers	GGACAACGATGTTG GCGAAC
sequence-based reagent	Gapdh_F	This study	PCR primers	AGGTCGGTGTGAAC GGATTTG
sequence-based reagent	Gapdh_R	This study	PCR primers	TGTAGACCATGTAGT TGAGGTCA
antibody	Claudin 5 (Rabbit polyclonal)	THERMO FISHER	34-1600	Western blot (1:500)
antibody	H3 (Mouse monoclonal)	OZYME	14269S	Western blot (1:2000)
antibody	P-gP (Mouse monoclonal)	ENZO	ALX-801-002-C100	Western-blot (1:200)
antibody	SMA_cy3 (Mouse monoclonal)	SIGMA	C6198	Immunofluorescence (1:250) Western blot (1:1000)
antibody	Pecam-1 (Goat polyclonal)	R&D SYSTEMS	AF3628	Immunofluorescence (1:300)
antibody	Connexin 43 (Mouse monoclonal)	BD transduction	610062	Immunofluorescence (1:200) Western blot (1:500)
antibody	GlialCAM (Rabbit polyclonal)	Provided by Raul Estevez, Universitat de Barcelona, Spain.	/	Immunofluorescence (1:500) Western-blot (1:500)
antibody	Aquaporin 4 (Rabbit polyclonal)	SIGMA	A5971	Immunofluorescence (1:500) Western blot (1:500)
antibody	Neurofilament motor N (Mouse monoclonal)	Provided by Beat M. Riederer, University of	/	Immunofluorescence (1:40) Western blot (1:40)

		Lausanne, Switzerland.		
antibody	GFAP (Rabbit polyclonal)	SIGMA	G9269	Immunofluorescence (1:500)
antibody	MLC1human (Rabbit polyclonal)	Provided by Raul Estevez, Universitat de Barcelona, Spain.	/	Immunofluorescence (1:200)
antibody	MLC1pan (Rabbit polyclonal)	Provided by Raul Estevez, Universitat de Barcelona, Spain.	/	Western blot (1:500)
antibody	Kir 4.1 (Rabbit polyclonal)	Alomone labs	APC-035	Western blot (1:5000)
antibody	Kir 4.1 extracellular (Rabbit polyclonal)	Alomone labs	APC-165	Immunofluorescence (1:200)
antibody	anti-rabbit_alexa 555 (Goat polyclonal)	Thermofisher	A21429	Immunofluorescence (1:2000)
antibody	anti-rabbit_alexa 488 (Goat polyclonal)	Thermofisher	A11034	Immunofluorescence (1:2000)
antibody	anti-mouse_alexa 555 (Goat polyclonal)	Thermofisher	A21424	Immunofluorescence (1:2000)
antibody	anti-oat_alexa 647 (Donkey polyclonal)	Thermofisher	A-21447	Immunofluorescence (1:2000)
antibody	anti-rabbit_HRP (Goat polyclonal)	Biovalley	CSA2115	Western blot (1:2500)
antibody	anti-mouse_HRP (goat polyclonal)	Biovalley	CSA2108	Western blot (1:2500)
antibody	anti-rabbit STAR RED (Goat polyclonal)	Abberior	STRED-1002	Immunofluorescence (1:200)
antibody	anti-mouse STAR RED (Goat polyclonal)	Abberior	STRED-1001	Immunofluorescence (1:200)
other	Alexa-conjugated Isolectin (griffonia simplicifolia) 647	Thermofisher	I32450	Immunofluorescence (1:100)
other	Alexa-conjugated Isolectin (griffonia simplicifolia) 594	Thermofisher	I21413	Immunofluorescence (1:100)

662
663

664 **Animals**

665 All animal experiments were carried out in compliance with the European Directive 2010/63/EU on the

666 protection of animals used for scientific purposes and the guidelines issued by the French National

667 Animal Care and Use Committee (reference: 2019021814073504 and 2019022113258393). *Mlc1* KO
668 mice were maintained on a C57BL6 genetic background (Hoegg-Beiler et al., 2014).
669
670 **Brain microvessel purification**
671 Microvessels were isolated from whole brain using selective filtration, as described previously (Boulay
672 et al., 2015). We purified vessels that passed through 100 µm pores but not 20 µm pores (Boulay et al.,
673 2015). Brain vessels from 2 animals were pooled for the 2-month samples, 3 for P15 samples and 5 for
674 P5 samples.
675
676 **Immunohistochemical analysis**
677 Brain slices: Mice were anesthetized with pentobarbital (600 mg/kg, i.p.) and killed by transcardiac
678 perfusion with PBS/PFA 4%. The brain was removed and cut into 40-µm-thick sections using a Leitz
679 (1400) cryomicrotome.
680 Purified microvessels: microvessels were plated on a glass slide coated with Cell Tak (Corning, NY,
681 USA) and fixed in PBS/PFA 4% for 15 min at room temperature.
682 Brain slices or microvessels on glass slides were immersed in the blocking solution (PBS/normal goat
683 serum (NGS) 5%/Triton X-100 0.5%) for 1 h at room temperature (RT) and then incubated with primary
684 antibodies (see the key resource table below) diluted in the blocking solution 12 h at 4 °C. After 3 washes
685 in PBS, slices were incubated for 2 h at RT (or overnight for STED experiments) with secondary
686 antibodies and Hoechst dye, rinsed in PBS, and mounted in Fluormount G (Southern Biotech,
687 Birmingham, AL) for confocal analysis or Abberior Mount solid antifade medium for STED imaging.
688 Tissues were imaged using a 40X objective on a Zeiss Axio-observer Z1 with a motorized XYZ stage
689 (Zeiss, Oberkochen, Germany). For STED imaging, we used a STEDyCON microscope (Abberior
690 Instruments, Göttingen, Germany) with a 100x/1.46 Plan-ApoChromat DIC Oil (Zeiss, Oberkochen,
691 Germany). Alexa 594 and Star-red fluorescence was depleted with a laser at 775 nm. The pixel size was
692 set to 25 nm, with a 1.13 pinhole.
693

Quantification of immunofluorescence

Images were analyzed using ImageJ/Fiji software (Schindelin et al., 2012; Schneider et al., 2012). Microvessels: the isolectin B4 channel was first processed with a *subtract background* filter (rolling ball radius = 50 pixels), a *Gaussian Blur* filter (sigma = 10 pixels) and using the *Tubness* ImageJ plugin (sigma=1). The resulting image was converted to a mask using the *Huang dark* threshold, which was dilated 3 times. A distance map image of this mask was created using *local Thickness* (threshold=1), and the surface area of isolectin-B4-positive vessels was measured. Aqp4 or NF-M channels were processed by *Bleach correction* using the *simple ratio* method. A *subtract background* filter (rolling ball radius = 50 pixels) and a *Median* filter (radius= 2 pixels) were then applied. The resulting picture was converted to a mask using the *Default dark* threshold. A third mask for the Aqp4 or NF-M signal contained in the isolectin B4 channel was created by using the *imageCalculator AND* method to combine the two previously created masks. We calculated the surface ratio of this third mask/isolectin B4.
STED: vessels with a diameter below 15 µm were analyzed. For Aqp4, 6 individual 2 x 0.1 μm^2 surfaces perpendicular to the vessel wall were drawn half inside the vessel and half outside, starting from the contact zone between the Aqp4 staining and the isolectin B4 staining. We then calculated the Aqp4/IB4 ratio. For Cx43, GlialCAM and Kir4.1, the particles' size and number were quantified in a 1 µm perivascular area (the vessel's boundary was based on the isolectin B4 staining). We applied a *Gaussian filter* (sigma=1), with an *Intermodes dark* threshold for Cx43 and GlialCAM and a *Moments dark* threshold for Kir 4.1.

Western blots

Proteins were extracted from one brain hemisphere or from purified microvessels in 2% SDS (500 µl or 50µl per sample, respectively) with EDTA-free Complete Protease Inhibitor (Roche), sonicated three times at 20 Hz (Vibra cell VCX130) and centrifuged for 20 min at 10,000 g at 4 °C. Supernatants were heated in Laemmli loading buffer for 5 min at 56 °C. Proteins were extracted from one brain hemisphere per sample in 500 µL SDS 2%, under the same conditions. The protein content was measured using the Pierce 660 nm protein assay (Thermo Scientific, Waltham, MA, USA). Equal amounts of proteins were

722 separated by denaturing electrophoresis on Mini-Protean TGX stain-free gels (Biorad) and then
723 electrotransferred to nitrocellulose membranes using the Trans-blot Turbo Transfer System (Biorad).
724 Membranes were hybridized, as described previously (Ezan et al., 2012). The antibodies used in this
725 study are listed in the key resource table below. Horseradish peroxidase activity was visualized using
726 enhanced chemiluminescence in a Western Lightning Plus system (Perkin Elmer, Waltham, MA, USA).
727 Chemiluminescent imaging was performed on a FUSION FX system (Vilber, South Korea). At least
728 four independent samples were analyzed in each experiment. The level of chemiluminescence for each
729 antibody was normalized against that of histone H3 or a stain-free membrane (enabling bands to be
730 normalized against the total protein on a blot).
731
732 **Quantitative RT-PCR**
733 RNA was extracted using the Rneasy Lipid Tissue Mini Kit (Qiagen, Hilden, Germany). cDNA was
734 then generated using the Superscript™ III Reverse Transcriptase Kit (Thermo Fisher). Differential
735 levels of cDNA expression were measured using droplet digital PCR. Briefly, cDNA and primers (see
736 the key resource table below) were distributed into approximately 10,000 to 20,000 droplets. cDNAs
737 were then PCR-amplified in a thermal cycler and read (as the number of positive and negative droplets)
738 with a QX200 Droplet Digital PCR System (Biorad). The ratio for each tested gene was normalized
739 against the total number of positive droplets for *Gapdh*.
740
741 ***In situ* brain perfusion**
742 Mice were anesthetized with ketamine-xylazine (140 and 8 mg/kg, respectively, i.p.), and a polyethylene
743 catheter was inserted into the carotid veins. The heart was incised, and the perfusion was started
744 immediately (flow rate: 2.5 mL/min) so as to completely replace the blood with Krebs carbonate-
745 buffered physiological saline (128 mM NaCl, 24 mM $NaHCO_3$, 4.2 mM KCl, 2.4 mM NaH_2PO_4, 1.5
746 mM $CaCl_2$, 0.9 mM $MgCl_2$), 9 mM D-glucose) supplemented with [^{14}C] sucrose (0.3 µCi/mL) (Perkin
747 Elmer Life Sciences, Courtaboeuf, France) as a marker of vascular integrity. The saline was bubbled
748 with 95% O_2/5% CO_2 for pH control (7.4) and warmed to 37 °C. Perfusion was terminated after 120 sec

749 by decapitating the mouse. The whole brain was removed from the skull and dissected out on a freezer
750 pack. Brain hemisphere and two aliquots of perfusion fluid were placed in tared vials and weighed,
751 digested with Solvable® (Perkin Elmer) and mixed with Ultima gold XR® (Perkin Elmer) for ^{14}C dpm
752 counting (Tri-Carb®, Perkin Elmer). In some experiments, human serum albumin (40 g/L) (Vialebex®,
753 Paris, France) was added to the perfusion fluid in order to increase the hydrostatic pressure (~180
754 mmHg) and create shear stress (Ezan et al., 2012). The brain [^{14}C]-sucrose vascular volume (Vv, in
755 µL/g) was calculated from the distribution of the [^{14}C]-sucrose: $Vv = X_v/C_v$ where X_v (dpm/g) is the
756 [^{14}C] sucrose concentration in the hemispheres and C_v (dpm/µL) is the [^{14}C] sucrose concentration in
757 the perfusion fluid (Dagenais et al., 2000). It should be noted that in mammals, the very hydrophilic,
758 low-molecular-weight (342 Da) disaccharide sucrose does not bind to plasma proteins and does not have
759 a dedicated transporter. Accordingly, sucrose does not diffuse passively and thus serves as a marker of
760 blood brain barrier integrity (Takasato et al., 1984). In this context, variations in sucrose's distribution
761 volume in the brain solely reflect changes in the blood brain barrier's physical integrity.
762
763 **Vascular smooth muscle cell responsiveness**
764 Mice were rapidly decapitated, and the brains were quickly removed and placed in cold (~4 °C) artificial
765 cerebrospinal fluid (aCSF) solution containing 119 mM NaCl, 2.5 mM KCl, 2.5 mM CaCl2, 26.2 mM
766 NaHCO3, 1 mM NaH2PO4, 1.3 mM MgSO4, 11 mM D-glucose (pH = 7.35). Brains were constantly
767 oxygenated with 95% O_2 –5% CO_2. Brain cortex slices (400 µm thick) were cut with a vibratome
768 (VT2000S, Leica) and transferred to a constantly oxygenated (95% O_2–5% CO_2) holding chamber
769 containing aCSF. Subsequently, individual slices were placed in a submerged recording chamber
770 maintained at RT under an upright microscope (Zeiss) equipped with a CCD camera (Qimaging) and
771 perfused at 2 ml/min with oxygenated aCSF. Only one vessel per slice was selected for measurements
772 of vascular responsiveness, at the junction between layers I and II of the somatosensory cortex and with
773 a well-defined luminal diameter (10–15 µm). An image was acquired every 30 s. Each recording started
774 with the establishment of a control baseline for 5 min. Vessels with an unstable baseline (i.e. a change
775 in diameter of more than 5%) were discarded from analysis. Vasoconstriction was induced by the
776 application of the thromboxane A_2 receptor agonist U46619 (9,11-dideoxy-11a,9a-

epoxymethanoprostaglandin F2α, 50 nM, Sigma) for 2 min. The signal was recorded until it had returned to the baseline.

Functional ultrasound

Two-month-old mice were anesthetized, and cerebral blood flow responses to whisker stimulation were determined using functional ultrasound imaging. The protocol is described in detail in (Anfray et al., 2019). Briefly, mice were intubated and mechanically ventilated (frequency: 120/min; Tidal volume:10 ml/kg) by maintaining anesthesia with 2% isoflurane in 70% N_2O/30% O_2. Mice were placed in a stereotaxic frame, and the head was shaved and cleaned with povidone-iodine. An incision was made along the midline head skin (to expose the skull), and lidocaine spray was applied to the head. Whiskers on the left side were cut to a length of one centimeter. Anesthesia was switched to a subcutaneous infusion of medetomidine (Domitor®, Pfizer, 0.1 mg/kg) and isoflurane, N_2O and O_2 were withdrawn 10 min later. So that the isoflurane could dissipate and the cerebral blood flow could stabilization, the functional ultrasound measurements were initiated 20 min later. Ultrasound gel was applied between the ultrasound probe and the mouse's skull, to ensure good acoustic coupling. The probe was positioned in the coronal plane, corresponding to the somatosensory barrel field cortex (S1bf; bregma -1.5 mm). Ultrafast acquisition was performed with an ultrasound sequence based on compounded plane wave transmission (11 angles from 10° to 10°, in increments of 2°), using a 15 MHz probe (Vermon, France; 100 µm x 100 µm in-plane pixels; slice thickness: 300 µm; elevation focus: 8 µm; frame rate: 500 Hz). The whiskers were mechanically stimulated three times for 30 s, interspaced with a 60 s rest period (total duration of the experiment: 300s). Using MATLAB (the MathWorks Inc., Natick, Massachussets, United States), we calculated the coefficient for the correlation between the normalized power Doppler (PD) intensity over time and a step function following the stimulation pattern. An activation map was reconstructed by selecting only pixels with a correlation coefficient above 0.2. The relative PD increase was quantified as the mean PD signal in the activated area.

Ultrasound localization microscopy

The acquisition and post processing steps for ultrasound localization microscopy were adapted from (Hingot et al., 2020). For each image, 100 µL of Sonovue microbubbles were injected into the tail vein. Blocks of 800 compounded frames (-5° 0° 5°) at 1 kHz were acquired for 800 ms and saved for 200 ms; this scheme was repeated for 180 s. A combination of a Butterworth high-pass filter (second order, 20 Hz) and a singular value decomposition filter (10 values) was used to separate microbubble echoes from tissue echoes. The microbubbles' centroid positions were localized using a weighted average algorithm. Microbubbles were tracked through consecutive frames using MathWorks (the MathWorks Inc., Natick, Massachussets, United States). The tracks were interpolated and smoothed using a 5-point sliding window, and redundant positions were removed. A density image was reconstructed on an 11 µm × 10 µm grid.

Magnetic resonance imaging

Magnetic resonance imaging was performed on a 7T Pharmascan magnetic resonance imaging system (Bruker, Rheinstetten, Germany) equipped with volume transmit and surface receive coils and operated via Paravision® 6.0 software (Bruker, Rheinstetten, Germany). An anatomical T2-weighted acquisition was performed prior to contrast injection, with the following parameters: echo time (TE) = 40 ms; repetition time (TR) = 3500 ms; flip angle (FA) = 90°; averages = 2; number of echoes = 8; on a 256x256 sagittal matrix with 20 contiguous 0.5 mm thick slices (in-plan resolution = 0.07 x 0.07 mm) for a total duration of 2 min 41 s. The apparent diffusion coefficient was calculated from a multi-b diffusion-weighted echo planar imaging sequence, with following parameters: TE = 35 ms; TR = 2000 ms; FA = 90°; number of segments = 4; 16 b-values = 20 $s.mm^{-2}$, 30 $s.mm^{-2}$, 40 $s.mm^{-2}$, 50 $s.mm^{-2}$, 75 $s.mm^{-2}$, 100 $s.mm^{-2}$, 150 $s.mm^{-2}$, 200 $s.mm^{-2}$, 300 $s.mm^{-2}$, 400 $s.mm^{-2}$, 500 $s.mm^{-2}$, 750 $s.mm^{-2}$, 1000 $s.mm^{-2}$, 1250 $s.mm^{-2}$, 1500 $s.mm^{-2}$, 2000 $s.mm^{-2}$; 12 directions; on a 128x40 sagittal matrix with 9 contiguous 1 mm thick slices (in-plan resolution: 0.15 x 0.15 mm), with use of a saturation band to remove the out-of-matrix signal, over a total duration of 25 min 45 s. The apparent diffusion coefficient acquisition was performed prior to contrast injection. To estimate the concentration of contrast agent, T1 maps before and after contrast injection were computed from a FAIR RARE (flow alternating inversion recovery,

rapid acquisition with refocused echoes) acquisition derived from the Look-Locker T1 mapping sequence (Karlsson and Nordell, 1999), with the following parameters: TE = 5.3 ms; TR = 5000 ms; FA = 90°; RARE factor = 4; 10 inversion times (TI) = 10 ms, 21 ms, 44 ms, 195 ms, 410 ms, 862 ms, 1811 ms, 3807 ms, 8000 ms; on a 64x64 single mediosagittal slice (in-plan resolution: 0.3 x 0.3 mm; thickness: 0.8 mm) for a total duration of 4 min 25 s. A single acquisition was performed before contrast injection (to map the reference T1), and 8 consecutive acquisitions were performed 10 minutes after contrast injection – providing dynamic data over 40 minutes.

Injection of contrast agent into the cerebrospinal fluid

1 µl of 500 mM DOTA-Gd (Dotarem®, Guerbet®, France) was injected over 1 minute into the CSF with a glass micropipette through the cisterna magna, as described previously (Gaberel et al., 2014). Briefly, the mice were anesthetized with isoflurane (induction: 5%, maintenance: 2-3%) in 70% N_2O/30% O_2. The neck was shaved, and lidocaine was sprayed on for local analgesia. A vertical incision was performed, and the muscle planes were separated vertically upon reaching the cisterna magna. A micropipette formed from an elongated capillary glass tube and filled with 1 µL of DOTA-Gd was inserted into the cisterna magna. Before and after injection, one-minute pauses enabled the CSF pressure to normalize. Before micropipette removal, a drop of superglue was added to form a seal and prevent subsequent leakage of CSF. The incision was cleaned and then closed with 5.0 gauge surgical silk thread.

Magnetic resonance imaging analyses

T1 values, quantitative contrast measurements and apparent diffusion coefficient maps were calculated with in-house MATLAB code (R2021a, Natick, Massachusetts: the MathWorks Inc; 2020). Regions of interest were determined using the FIJI image analysis suite (Schindelin et al., 2012).

T1 maps were computed from the FAIR RARE data. Briefly, T1 was extracted after fitting the signal recovery equation:

$$M_t = M_0 . \exp\left(^{-t}/_{T1}\right)$$

The contrast agent concentration [CA] was determined from the equation:

$$[CA].r1 = \frac{1}{T1_{post}} - \frac{1}{T1_{pre}}$$

where r1, $T1_{post}$ and $T1_{pre}$ were respectively the T1 relaxivity, the T1 value after contrast, and the T1 value before contrast. The apparent diffusion coefficient was calculated as the slope of the log of signal loss for the b-value, according to the following equation:

$$ADC = \frac{ln\left(\frac{S_0}{S_b}\right)}{b}$$

where b = 1000 $s.mm^{-2}$.

Tissue clearing and immunohistochemical staining

Mice were killed with pentobarbital (600 mg/kg, i.p.). Brains were removed and post-fixed in 4% paraformaldehyde (PFA) for 24 h at 4 °C and then assessed using the "immunolabeling-enabled three-dimensional imaging of solvent-cleared organs" technique (Renier et al., 2014). The samples were first dehydrated with increasingly concentrated aqueous methanol solutions (MetOH: 20%, 40%, 60%, 80%, and twice 100%, for 1 h each) at RT and then incubated in 66% dichloromethane (DCM, Sigma Aldrich)/33% MetOH overnight. After 2 washes in 100% MetOH, brains were incubated in 5% H_2O_2/MetOH overnight at RT, rehydrated with increasingly dilute aqueous methanol solutions (80%, 60%, 40%, and 20%; 1h each). Before immunostaining, brains were permeabilized first for 2 x 1h at RT in 0.2% Triton X-100/PBS, for 24 h at 37 °C in 0.16% Triton X-100/2.3% glycine/20% DMSO/PBS, and then for 2 days at 37 °C in 0.16% Triton X-100/6% donkey serum/10% DMSO/PBS. Brains were incubated for 3 days at 37 °C with primary antibody diluted in a 0.2 Tween/1% heparin/3% donkey serum/5% DMSO/PBS solution, washed 5 times during 24h at 37 °C in 0.2% Tween20/1% heparin/PBS solution, incubated for 3 days at 37 °C with secondary antibody diluted in a 0.2 Tween/1% heparin/3% donkey serum/PBS solution, and another washed five times. The brain samples were then dehydrated again with a MetOH/H_2O series (20%, 40%, 60%, 80% and 100% for 1h each, and then 100% overnight) at RT. On the following day, brains were incubated for 3h in 66% DCM/33% MetOH and then twice for 15 min at RT in 100% DCM and lastly cleared overnight in dibenzyl ether.

The cleared tissues were imaged using a light sheet microscope and Inspector pro software (Lavision Biotec GmbH, Bielefeld, Germany). 3D reconstructions of the somatosensory cortex (a 400 µm-thick column for Pecam-1 and 500 to 750 µm for SMA) were visualized with Imaris software (Bitplane). The length and number of branch points of Pecam-1- or SMA-immunolabeled brain vessels were quantified using the "Surface" and "Filament" tools in Imaris software (Oxford instruments, Oxford). Anastomoses were measured by eye.

Astrocyte morphology

Hippocampal slices were pictured using a 40X objective on a Zeiss Axio-observer Z1 with a motorized XYZ stage (Zeiss, Oberkochen, Germany). To analyze astrocyte ramifications, we adapted a previously described technique (Pannasch et al., 2014). Using ImageJ software, 7 concentric circles at 5 µm intervals were drawn around each astrocyte on confocal Z-stack images. The number of intersections of GFAP-positive astrocytic processes with each circle was counted.

We analyzed the astrocytes' orientation by adapting a previously described technique (Ghezali et al., 2018). Using ImageJ software, a grid delimitating 100 μm^2 squares was drawn on confocal Z-stack images oriented with the pyramidal cell layer or a vessel. The number of intersections of astrocytic GFAP positive processes with horizontal lines (i.e. processes perpendicular to the pyramidal layer or vessel, so-called axial processes) and vertical lines (i.e. processes parallel to the pyramidal layer or vessel, so-called lateral processes) were counted. The cell's polarity index was defined as the ratio between the axial processes and the lateral processes. A polarity index of 1 indicates no polarity, whereas a polarity index greater than 1 indicates preferentially perpendicular orientation toward the pyramidal layer or the vessel.

Electron microscopy

Mice were anesthetized with ketamine-xylazine (140 and 8 mg/kg, respectively, i.p.) and transcardially perfused with the fixative (2% paraformaldehyde, 3% glutaraldehyde, 3mM $CaCl_2$ in 0.1M cacodylate buffer pH 7.4) for 12 min. The brains were removed and left overnight at 4 °C in the same fixative. Brain fragments (0.3 x 1 x 1 mm^3) were postfixed first in 0.1M cacodylate buffer pH 7.4 + 1% OsO_4 for

1h at 4 °C and then in 1% aqueous uranyl acetate for 2h at RT. After dehydration in graded ethanol and then propylene oxide, the fragments were embedded in EPON resin (Electron Microscopy Sciences, Hatfield, PA). Ultrathin (80 nm) sections were prepared, stained with lead citrate and imaged in a Jeol 100S transmission electron microscope (Jeol, Croissy-sur-Seine, France) equipped with a 2k x 2k Orius 830 CCD camera (Roper Scientific, Evry, France). Cells and structures were identified as follows. Endothelial cells are thin, elongated cells lining the vessel lumen and which can be joined together by electron-dense tight junctions. The endothelial cells are surrounded by a continuous layer of acellular matrix (the basal lamina). In the normal adult brain, the vascular wall is totally surrounded by astrocyte perivascular processes, which can be recognized by the presence of thin intermediate filaments and by the absence of basal lamina on the parenchymal side. Neuronal structures are typically recognized by the presence of microtubules, vesicles in pre-synapses, and an electron-dense region between the pre- and post-synapses.

Human tissue immunohistochemistry

Our study included specimens obtained from the brain collection "Hôpitaux Universitaires de l'Est Parisien – Neuropathologie du développement" (Biobank identification number BB-0033-00082). Informed consent was obtained for autopsy of the brain and histological examination. Our study included fetal brains obtained from spontaneous or medical abortion that did not display any significant brain pathology. After removal, brains were fixed with formalin for 5–12 weeks. Macroscopic analysis was performed to select samples that where embedded in paraffin, sliced in 7 µm sections and stained with hematein for a first histological analysis. Immunohistochemical analyses were performed on coronal slices that included the temporal telencephalic parenchyma and hippocampus. They were dewaxed and rinsed before incubation in citrate buffer (pH 9.0). Expression of MLC1 on the sections was detected using the Bond Polymer Refine Detection Kit (Leica) with specific antibodies and an immunostaining system (Bond III, Leica). Images were acquired using a slide scanner (Lamina, Perkin Elmer). Staining was analyzed using QuPath (Bankhead et al., 2017). A QuPath pixel classifier was trained to discriminate between DAB-positive spots and background areas. We selected a pixel classifier

939 that used a random trees algorithm and four features: a Gaussian filter to select intensity, and the three
940 structure tensor eigenvalues to select thin elongated objects. The classifier was trained on manually
941 annotated MLC1 spots and the background area on one image per developmental stage. When the result
942 was satisfactory, the pixel classifier was used to detect MLC1 in selected regions of interest.

943

944 **Statistics**

945 For all variables, the normality of data distribution was probed with using the Shapiro-Wilk test before
946 the appropriate statistical test was chosen. Test names and sample sizes are indicated in the figure
947 legends. Detailed results are presented in the figure source data files.

948
949
950
951

952

953

954

955

956 **Supplemental information**

957

958 **Fig. 1-figure supplement 1 The absence of MLC1 causes overall swelling of the brain**

959 **A**. Schematic representation of a mouse brain. Blue areas indicate the ventricles, and black areas indicate
960 neuronal fiber tracts. **B.** Anatomical T2-weighted magnetic resonance images of WT and KO mice. **C.D.**
961 Quantification of the brain volume (**C**) and the ventricles' relative volume (**D**), based on magnetic
962 resonance images. **E-G.** The apparent diffusion coefficient was calculated for the midbrain (**E**), septal
963 area (**F**), and thalamus (G). Two-tailed Student's T test. The data are represented in a Tukey box plot
964 (n=7 mice per genotype) and are given in **Fig. 1-figure supplement 1- source data 1.** *, $p \leq 0.05$, **,
965 $p \leq 0.01$, ***, $p \leq 0.001$, and ns: not significant.

966

967 **Fig. 6-figure supplement 1 The absence of MLC1 alters the postnatal development of astrocyte**
968 **morphology and polarity**

969 **A.B.** Representative images from the Sholl analysis of astrocyte ramification in WT and *Mlc1* KO mice
970 on P10 (**A**) and P15 (**B**). The concentric circles start from the astrocyte's soma. Scale bar: 20 µm. **C. D.**
971 Representative images from the grid analysis of astrocyte polarity towards vessels in WT and *Mlc1* KO
972 on P10 (**C**) and P15 (**D**). Scale bar: 20 µm.

973

974 **Fig. 7-figure supplement 1 Examples of changes in the architecture of the gliovascular unit in**
975 ***Mlc1* KO mice**

976 **A. B.** Representative transmission electron microscopy images of the gliovascular unit in the cortex of
977 P10 (**A**) and P15 (**B**) WT mice and *Mlc1* KO mice. On P10, the astrocytic perivascular coverage is
978 incomplete in WT and *Mlc1* KO mice. On P15, more neuronal fibers contact endothelial cells in *Mlc1*
979 KO mice (see quantifications in **Fig. 7** and **Figure 7-source data 1**). **C-F.** Representative transmission
980 electron microscopy images of the gliovascular unit in the cortex of 2-month-old P60 WT mice (C) and
981 *Mlc1* KO mice (**D-F**). A WT sample showing continuous coverage by perivascular astrocytic processes
982 around an endothelial cell (C). The perivascular astrocytic processes are linked by gap junctions. In
983 *Mlc1* KO mice, a synapse contacts the endothelial basal lamina (red arrowhead) (**D**), a perivascular

984 astrocytic process interdigitates into another perivascular astrocytic process and forms a large annular
985 gap junction (red arrowhead) (**E**), stacked perivascular astrocytic processes surrounded by basal lamina
986 (arrowhead) (**F**). Images are presented in pairs, with artificial colors in the lower panel: perivascular
987 astrocytic processes are shown in yellow, with gap junctions in green, synapses in orange, endothelial
988 cells in dark blue, mural cells in light blue, and tight junctions in purple.
989
990 **Fig. 7-figure supplement 2. Astrocytic perivascular endfeet are swollen in 1-year-old *Mlc1* KO**
991 **mice**
992 **A.** Representative transmission electron microscopy images of the gliovascular unit in the cortex of 1-
993 year-old *Mlc1* KO mice (n=3 mice per genotype). Three phenotypes are observed: normal perivascular
994 astrocytic process (swelling = 0); moderately swollen perivascular astrocytic process (swelling = 1);
995 edematous perivascular astrocytic process (swelling = 2). Images are presented in pairs, with
996 perivascular astrocytic process' swollen areas in red **B.** Comparative quantification in *Mlc1* KO mice.
997 Two-tailed Mann-Whitney test. The data are represented in a Tukey box plot (n=314 *Mlc1* KO cortical
998 vessels; n=328 WT cortical vessels; n=3 mice per genotype) and given in **Fig. 7-figure supplement 2-**
999 **source data 1**. *, p = 0.05.
1000
1001 **Source data Files**
1002
1003 **Figure 1-source data 1 The absence of MLC1 has no effect on blood brain barrier integrity or**
1004 **the organization of the endothelial network.**
1005
1006 **Figure 2-source data 1 MLC1 is crucial for the molecular maturation of vascular smooth muscle**
1007 **cell contractility**
1008
1009 **Figure 3-source data 1 MLC1 is crucial for the postnatal acquisition of vascular smooth muscle**
1010 **cell contractility, arterial diameter, and neurovascular coupling**
1011

Figure 4-source data 1 The absence of MLC1 alters the molecular maturation of the perivascular astrocytic processes

Figure 5-source data 1 The absence of MLC1 alters the perivascular cohesiveness of astrocytic processes

Figure 6-source data 1 The absence of MLC1 alters the postnatal development and maintenance of astrocyte morphology and polarity

Figure 7-source data 1 The absence of MLC1 impacts the organization and development of the gliovascular unit

Figure 8-source data 1 Contrast-enhanced magnetic resonance imaging reveals a low level of tracer dispersion

Figure 9-source data 1 Developmental perivascular expression of MLC1 in the human cortex

Figure 1 supplement 1-source data 1 The absence of MLC1 causes overall swelling of the brain

Figure 7 supplement 2-source data 1 Astrocytic perivascular endfeet are swollen in 1-year-old *Mlc1* KO mice

1037 **References**

1038

1039 Abbott NJ, Pizzo ME, Preston JE, Janigro D, and Thorne RG. 2018. The role of brain barriers in fluid
1040 movement in the CNS: is there a 'glymphatic' system? *Acta Neuropathol 135*: 387-407.10.1007/s00401-
1041 018-1812-4.
1042 Abbott NJ, Ronnback L, and Hansson E. 2006. Astrocyte-endothelial interactions at the blood-brain
1043 barrier. *Nat Rev Neurosci 7*: 41-53
1044 Alvarez JI, Katayama T, and Prat A. 2013. Glial influence on the blood brain barrier.
1045 *Glia*.10.1002/glia.22575.
1046 Anfray A, Drieu A, Hingot V, Hommet Y, Yetim M, Rubio M, Deffieux T, Tanter M, Orset C, and
1047 Vivien D. 2019. Circulating tPA contributes to neurovascular coupling by a mechanism involving the
1048 endothelial NMDA receptors. *J Cereb Blood Flow Metab*:
1049 271678X19883599.10.1177/0271678X19883599.
1050 Baldwin KT, Tan CX, Strader ST, Jiang C, Savage JT, Elorza-Vidal X, Contreras X, Rulicke T,
1051 Hippenmeyer S, Estevez R, *et al.* 2021. HepaCAM controls astrocyte self-organization and coupling.
1052 *Neuron 109*: 2427-2442 e2410.10.1016/j.neuron.2021.05.025.
1053 Bankhead P, Loughrey MB, Fernandez JA, Dombrowski Y, McArt DG, Dunne PD, McQuaid S, Gray
1054 RT, Murray LJ, Coleman HG, *et al.* 2017. QuPath: Open source software for digital pathology image
1055 analysis. *Sci Rep 7*: 16878.10.1038/s41598-017-17204-5.
1056 Benesova J, Rusnakova V, Honsa P, Pivonkova H, Dzamba D, Kubista M, and Anderova M. 2012.
1057 Distinct expression/function of potassium and chloride channels contributes to the diverse volume
1058 regulation in cortical astrocytes of GFAP/EGFP mice. *PLoS One 7*:
1059 e29725.10.1371/journal.pone.0029725.
1060 Bertolo A, Nouhoum M, Cazzanelli S, Ferrier J, Mariani JC, Kliewer A, Belliard B, Osmanski BF,
1061 Deffieux T, Pezet S, *et al.* 2021. Whole-Brain 3D Activation and Functional Connectivity Mapping in
1062 Mice using Transcranial Functional Ultrasound Imaging. *J Vis Exp*.10.3791/62267.
1063 Boulay AC, Saubamea B, Decleves X, and Cohen-Salmon M. 2015. Purification of Mouse Brain
1064 Vessels. *J Vis Exp 105*.10.3791/53208.

1065 Bugiani M, Dubey M, Breur M, Postma NL, Dekker MP, Ter Braak T, Boschert U, Abbink TEM,
1066 Mansvelder HD, Min R, *et al.* 2017. Megalencephalic leukoencephalopathy with cysts: the Glialcam-
1067 null mouse model. *Ann Clin Transl Neurol 4*: 450-465.10.1002/acn3.405.
1068 Capdevila-Nortes X, Lopez-Hernandez T, Apaja PM, Lopez de Heredia M, Sirisi S, Callejo G, Arnedo
1069 T, Nunes V, Lukacs GL, Gasull X, *et al.* 2013. Insights into MLC pathogenesis: GlialCAM is an MLC1
1070 chaperone required for proper activation of volume-regulated anion currents. *Hum Mol Genet 22*: 4405-
1071 4416.ddt290 [pii]
1072 10.1093/hmg/ddt290.
1073 Castro Dias M, Mapunda JA, Vladymyrov M, and Engelhardt B. 2019. Structure and Junctional
1074 Complexes of Endothelial, Epithelial and Glial Brain Barriers. *Int J Mol Sci 20*.10.3390/ijms20215372.
1075 Chen ZL, Yao Y, Norris EH, Kruyer A, Jno-Charles O, Akhmerov A, and Strickland S. 2013. Ablation
1076 of astrocytic laminin impairs vascular smooth muscle cell function and leads to hemorrhagic stroke. *J*
1077 *Cell Biol 202*: 381-395.10.1083/jcb.201212032.
1078 Chung WS, Allen NJ, and Eroglu C. 2015. Astrocytes Control Synapse Formation, Function, and
1079 Elimination. *Cold Spring Harb Perspect Biol 7*: a020370.cshperspect.a020370 [pii]
1080 10.1101/cshperspect.a020370.
1081 Clavreul S, Abdeladim L, Hernandez-Garzon E, Niculescu D, Durand J, Ieng SH, Barry R, Bonvento
1082 G, Beaurepaire E, Livet J, *et al.* 2019. Cortical astrocytes develop in a plastic manner at both clonal and
1083 cellular levels. *Nat Commun 10*: 4884.10.1038/s41467-019-12791-5.
1084 Cohen-Salmon M, Slaoui L, Mazare N, Gilbert A, Oudart M, Alvear-Perez R, Elorza-Vidal X, Chever
1085 O, and Boulay AC. 2021. Astrocytes in the regulation of cerebrovascular functions. *Glia 69*: 817-
1086 841.10.1002/glia.23924.
1087 Dagenais C, Rousselle C, Pollack GM, and Scherrmann JM. 2000. Development of an in situ mouse
1088 brain perfusion model and its application to mdr1a P-glycoprotein-deficient mice. *J Cereb Blood Flow*
1089 *Metab 20*: 381-386.10.1097/00004647-200002000-00020.
1090 Duarri A, Lopez de Heredia M, Capdevila-Nortes X, Ridder MC, Montolio M, Lopez-Hernandez T,
1091 Boor I, Lien CF, Hagemann T, Messing A, *et al.* 2011. Knockdown of MLC1 in primary astrocytes

causes cell vacuolation: a MLC disease cell model. *Neurobiol Dis 43*: 228-238.10.1016/j.nbd.2011.03.015.

Duarri A, Teijido O, Lopez-Hernandez T, Scheper GC, Barriere H, Boor I, Aguado F, Zorzano A, Palacin M, Martinez A, *et al.* 2008. Molecular pathogenesis of megalencephalic leukoencephalopathy with subcortical cysts: mutations in MLC1 cause folding defects. *Hum Mol Genet 17*: 3728-3739.ddn269 [pii]
10.1093/hmg/ddn269.

Dubey M, Brouwers E, Hamilton EMC, Stiedl O, Bugiani M, Koch H, Kole MHP, Boschert U, Wykes RC, Mansvelder HD, *et al.* 2018. Seizures and disturbed brain potassium dynamics in the leukodystrophy megalencephalic leukoencephalopathy with subcortical cysts. *Ann Neurol 83*: 636-649.10.1002/ana.25190.

Dubey M, Bugiani M, Ridder MC, Postma NL, Brouwers E, Polder E, Jacobs JG, Baayen JC, Klooster J, Kamermans M, *et al.* 2015. Mice with megalencephalic leukoencephalopathy with cysts: a developmental angle. *Ann Neurol 77*: 114-131.10.1002/ana.24307.

El-Khoury N, Braun A, Hu F, Pandey M, Nedergaard M, Lagamma EF, and Ballabh P. 2006. Astrocyte end-feet in germinal matrix, cerebral cortex, and white matter in developing infants. *Pediatr Res 59*: 673-679.10.1203/01.pdr.0000214975.85311.9c.

Elorza-Vidal X, Sirisi S, Gaitan-Penas H, Perez-Rius C, Alonso-Gardon M, Armand-Ugon M, Lanciotti A, Brignone MS, Prat E, Nunes V, *et al.* 2018. GlialCAM/MLC1 modulates LRRC8/VRAC currents in an indirect manner: Implications for megalencephalic leukoencephalopathy. *Neurobiol Dis 119*: 88-99.10.1016/j.nbd.2018.07.031.

Estevez R, Elorza-Vidal X, Gaitan-Penas H, Perez-Rius C, Armand-Ugon M, Alonso-Gardon M, Xicoy-Espaulella E, Sirisi S, Arnedo T, Capdevila-Nortes X, *et al.* 2018. Megalencephalic leukoencephalopathy with subcortical cysts: A personal biochemical retrospective. *Eur J Med Genet 61*: 50-60.10.1016/j.ejmg.2017.10.013.

Ezan P, Andre P, Cisternino S, Saubamea B, Boulay AC, Doutremer S, Thomas MA, Quenech'du N, Giaume C, and Cohen-Salmon M. 2012. Deletion of astroglial connexins weakens the blood-brain barrier. *J Cereb Blood Flow Metab 32*: 1457-1467.jcbfm201245 [pii]

1120 10.1038/jcbfm.2012.45.
1121 Gaberel T, Gakuba C, Goulay R, Martinez De Lizarrondo S, Hanouz JL, Emery E, Touze E, Vivien D,
1122 and Gauberti M. 2014. Impaired glymphatic perfusion after strokes revealed by contrast-enhanced MRI:
1123 a new target for fibrinolysis? *Stroke 45*: 3092-3096.10.1161/STROKEAHA.114.006617.
1124 Ghezali G, Calvo CF, Pillet LE, Llense F, Ezan P, Pannasch U, Bemelmans AP, Etienne Manneville S,
1125 and Rouach N. 2018. Connexin 30 controls astroglial polarization during postnatal brain development.
1126 *Development 145*.10.1242/dev.155275.
1127 Gilbert A, Vidal XE, Estevez R, Cohen-Salmon M, and Boulay AC. 2019. Postnatal development of the
1128 astrocyte perivascular MLC1/GlialCAM complex defines a temporal window for the gliovascular unit
1129 maturation. *Brain Struct Funct 224*: 1267-1278.10.1007/s00429-019-01832-w.
1130 Haj-Yasein NN, Jensen V, Ostby I, Omholt SW, Voipio J, Kaila K, Ottersen OP, Hvalby O, and
1131 Nagelhus EA. 2012. Aquaporin-4 regulates extracellular space volume dynamics during high-frequency
1132 synaptic stimulation: a gene deletion study in mouse hippocampus. *Glia 60*: 867-
1133 874.10.1002/glia.22319.
1134 Harris JJ, and Attwell D. 2012. The energetics of CNS white matter. *J Neurosci 32*: 356-
1135 371.10.1523/JNEUROSCI.3430-11.2012.
1136 He L, Vanlandewijck M, Raschperger E, Andaloussi Mae M, Jung B, Lebouvier T, Ando K, Hofmann
1137 J, Keller A, and Betsholtz C. 2016. Analysis of the brain mural cell transcriptome. *Sci Rep 6*:
1138 35108.srep35108 [pii]
1139 10.1038/srep35108.
1140 Hingot V, Brodin C, Lebrun F, Heiles B, Chagnot A, Yetim M, Gauberti M, Orset C, Tanter M, Couture
1141 O, *et al.* 2020. Early Ultrafast Ultrasound Imaging of Cerebral Perfusion correlates with Ischemic Stroke
1142 outcomes and responses to treatment in Mice. *Theranostics 10*: 7480-7491.10.7150/thno.44233.
1143 Hoegg-Beiler MB, Sirisi S, Orozco IJ, Ferrer I, Hohensee S, Auberson M, Godde K, Vilches C, de
1144 Heredia ML, Nunes V, *et al.* 2014. Disrupting MLC1 and GlialCAM and ClC-2 interactions in
1145 leukodystrophy entails glial chloride channel dysfunction. *Nat Commun 5*: 3475.ncomms4475 [pii]
1146 10.1038/ncomms4475.

1147 Iadecola C. 2017. The Neurovascular Unit Coming of Age: A Journey through Neurovascular Coupling
1148 in Health and Disease. *Neuron 96*: 17-42.10.1016/j.neuron.2017.07.030.
1149 Iliff JJ, Lee H, Yu M, Feng T, Logan J, Nedergaard M, and Benveniste H. 2013. Brain-wide pathway
1150 for waste clearance captured by contrast-enhanced MRI. *Journal of Clinical Investigation 123*: 1299-
1151 1309.10.1172/jci67677.
1152 Iliff JJ, Wang M, Liao Y, Plogg BA, Peng W, Gundersen GA, Benveniste H, Vates GE, Deane R,
1153 Goldman SA, *et al.* 2012. A paravascular pathway facilitates CSF flow through the brain parenchyma
1154 and the clearance of interstitial solutes, including amyloid beta. *Sci Transl Med 4*:
1155 147ra111.10.1126/scitranslmed.3003748.
1156 Jeworutzki E, Lopez-Hernandez T, Capdevila-Nortes X, Sirisi S, Bengtsson L, Montolio M, Zifarelli G,
1157 Arnedo T, Muller CS, Schulte U, *et al.* 2012. GlialCAM, a protein defective in a leukodystrophy, serves
1158 as a ClC-2 Cl(-) channel auxiliary subunit. *Neuron 73*: 951-961.S0896-6273(12)00091-8 [pii]
1159 10.1016/j.neuron.2011.12.039.
1160 Karlsson M, and Nordell B. 1999. Phantom and in vivo study of the Look-Locher T1 mapping method.
1161 *Magn Reson Imaging 17*: 1481-1488.10.1016/s0730-725x(99)00078-8.
1162 Kress BT, Iliff JJ, Xia M, Wang M, Wei HS, Zeppenfeld D, Xie L, Kang H, Xu Q, Liew JA, *et al.* 2014.
1163 Impairment of paravascular clearance pathways in the aging brain. *Ann Neurol 76*: 845-
1164 861.10.1002/ana.24271.
1165 Lanciotti A, Brignone MS, Visentin S, De Nuccio C, Catacuzzeno L, Mallozzi C, Petrini S, Caramia M,
1166 Veroni C, Minnone G, *et al.* 2016. Megalencephalic leukoencephalopathy with subcortical cysts protein-
1167 1 regulates epidermal growth factor receptor signaling in astrocytes. *Hum Mol Genet 25*: 1543-
1168 1558.ddw032 [pii]
1169 10.1093/hmg/ddw032.
1170 Leegwater PA, Yuan BQ, van der Steen J, Mulders J, Konst AA, Boor PK, Mejaski-Bosnjak V, van der
1171 Maarel SM, Frants RR, Oudejans CB, *et al.* 2001. Mutations of MLC1 (KIAA0027), encoding a putative
1172 membrane protein, cause megalencephalic leukoencephalopathy with subcortical cysts. *Am J Hum*
1173 *Genet 68*: 831-838.10.1086/319519.

1174 Nixdorf-Bergweiler BE, Albrecht D, and Heinemann U. 1994. Developmental changes in the number,
1175 size, and orientation of GFAP-positive cells in the CA1 region of rat hippocampus. *Glia 12*: 180-
1176 195.10.1002/glia.440120304.
1177 Osmanski BF, Pezet S, Ricobaraza A, Lenkei Z, and Tanter M. 2014. Functional ultrasound imaging of
1178 intrinsic connectivity in the living rat brain with high spatiotemporal resolution. *Nat Commun 5*:
1179 5023.10.1038/ncomms6023.
1180 Owens GK. 1995. Regulation of differentiation of vascular smooth muscle cells. *Physiol Rev 75*: 487-
1181 517.10.1152/physrev.1995.75.3.487.
1182 Owens GK, Kumar MS, and Wamhoff BR. 2004. Molecular regulation of vascular smooth muscle cell
1183 differentiation in development and disease. *Physiol Rev 84*: 767-801.10.1152/physrev.00041.2003.
1184 Pannasch U, Freche D, Dallerac G, Ghezali G, Escartin C, Ezan P, Cohen-Salmon M, Benchenane K,
1185 Abudara V, Dufour A, *et al.* 2014. Connexin 30 sets synaptic strength by controlling astroglial synapse
1186 invasion. *Nat Neurosci 17*: 549-558.nn.3662 [pii]
1187 10.1038/nn.3662.
1188 Rasmussen MK, Mestre H, and Nedergaard M. 2018. The glymphatic pathway in neurological disorders.
1189 *Lancet Neurol 17*: 1016-1024.10.1016/S1474-4422(18)30318-1.
1190 Renier N, Wu Z, Simon DJ, Yang J, Ariel P, and Tessier-Lavigne M. 2014. iDISCO: a simple, rapid
1191 method to immunolabel large tissue samples for volume imaging. *Cell 159*: 896-
1192 910.10.1016/j.cell.2014.10.010.
1193 Ridder MC, Boor I, Lodder JC, Postma NL, Capdevila-Nortes X, Duarri A, Brussaard AB, Estevez R,
1194 Scheper GC, Mansvelder HD, *et al.* 2011. Megalencephalic leucoencephalopathy with cysts: defect in
1195 chloride currents and cell volume regulation. *Brain 134*: 3342-3354.awr255 [pii]
1196 10.1093/brain/awr255.
1197 Rosko L, Smith VN, Yamazaki R, and Huang JK. 2019. Oligodendrocyte Bioenergetics in Health and
1198 Disease. *Neuroscientist 25*: 334-343.10.1177/1073858418793077.
1199 Schindelin J, Arganda-Carreras I, Frise E, Kaynig V, Longair M, Pietzsch T, Preibisch S, Rueden C,
1200 Saalfeld S, Schmid B, *et al.* 2012. Fiji: an open-source platform for biological-image analysis. *Nat*
1201 *Methods 9*: 676-682.10.1038/nmeth.2019.

1202 Schneider CA, Rasband WS, and Eliceiri KW. 2012. NIH Image to ImageJ: 25 years of image analysis.
1203 *Nat Methods 9*: 671-675
1204 Sibille J, Pannasch U, and Rouach N. 2014. Astroglial potassium clearance contributes to short-term
1205 plasticity of synaptically evoked currents at the tripartite synapse. *J Physiol 592*: 87-
1206 102.jphysiol.2013.261735 [pii]
1207 10.1113/jphysiol.2013.261735.
1208 Slaoui L, Gilbert A, Federici L, Rancillac A, Gelot A, Favier M, Lefort G, Mailly P, Cisternino S, Cohen
1209 Salmon M, *et al.* 2021. In mice and humans, the brain's blood vessels mature postnatally to acquire
1210 barrier and contractile properties. *BioRXiv 444486; en revue dans ELife*
1211 Takasato Y, Rapoport SI, and Smith QR. 1984. An in situ brain perfusion technique to study
1212 cerebrovascular transport in the rat. *Am J Physiol 247*: H484-493
1213 Topcu M, Gartioux C, Ribierre F, Yalcinkaya C, Tokus E, Oztekin N, Beckmann JS, Ozguc M, and
1214 Seboun E. 2000. Vacuoliting megalencephalic leukoencephalopathy with subcortical cysts, mapped to
1215 chromosome 22qtel. *Am J Hum Genet 66*: 733-739.10.1086/302758.
1216 van der Knaap MS, Abbink TEM, and Min R (1993). Megalencephalic Leukoencephalopathy with
1217 Subcortical Cysts. In GeneReviews((R)), M.P. Adam, H.H. Ardinger, R.A. Pagon, S.E. Wallace, L.J.H.
1218 Bean, G. Mirzaa, and A. Amemiya, eds. (Seattle (WA)).
1219 van der Knaap MS, Boor I, and Estevez R. 2012. Megalencephalic leukoencephalopathy with
1220 subcortical cysts: chronic white matter oedema due to a defect in brain ion and water homoeostasis.
1221 *Lancet Neurol 11*: 973-985.10.1016/S1474-4422(12)70192-8.
1222 Vanlandewijck M, He L, Mae MA, Andrae J, Ando K, Del Gaudio F, Nahar K, Lebouvier T, Lavina B,
1223 Gouveia L, *et al.* 2018. A molecular atlas of cell types and zonation in the brain vasculature. *Nature*
1224 *554*: 475-480.10.1038/nature25739.
1225 Wang MX, Ray L, Tanaka KF, Iliff JJ, and Heys J. 2020. Varying perivascular astroglial endfoot
1226 dimensions along the vascular tree maintain perivascular-interstitial flux through the cortical mantle.
1227 *Glia*.10.1002/glia.23923.

1228 Yalcinkaya C, Yuksel A, Comu S, Kilic G, Cokar O, and Dervent A. 2003. Epilepsy in vacuolating
1229 megalencephalic leukoencephalopathy with subcortical cysts. *Seizure 12*: 388-396.10.1016/s1059-
1230 1311(02)00350-3.
1231 Yao LL, Hu JX, Li Q, Lee D, Ren X, Zhang JS, Sun D, Zhang HS, Wang YG, Mei L, *et al.* 2020.
1232 Astrocytic neogenin/netrin-1 pathway promotes blood vessel homeostasis and function in mouse cortex.
1233 *J Clin Invest 130*: 6490-6509.10.1172/JCI132372.
1234
1235
1236

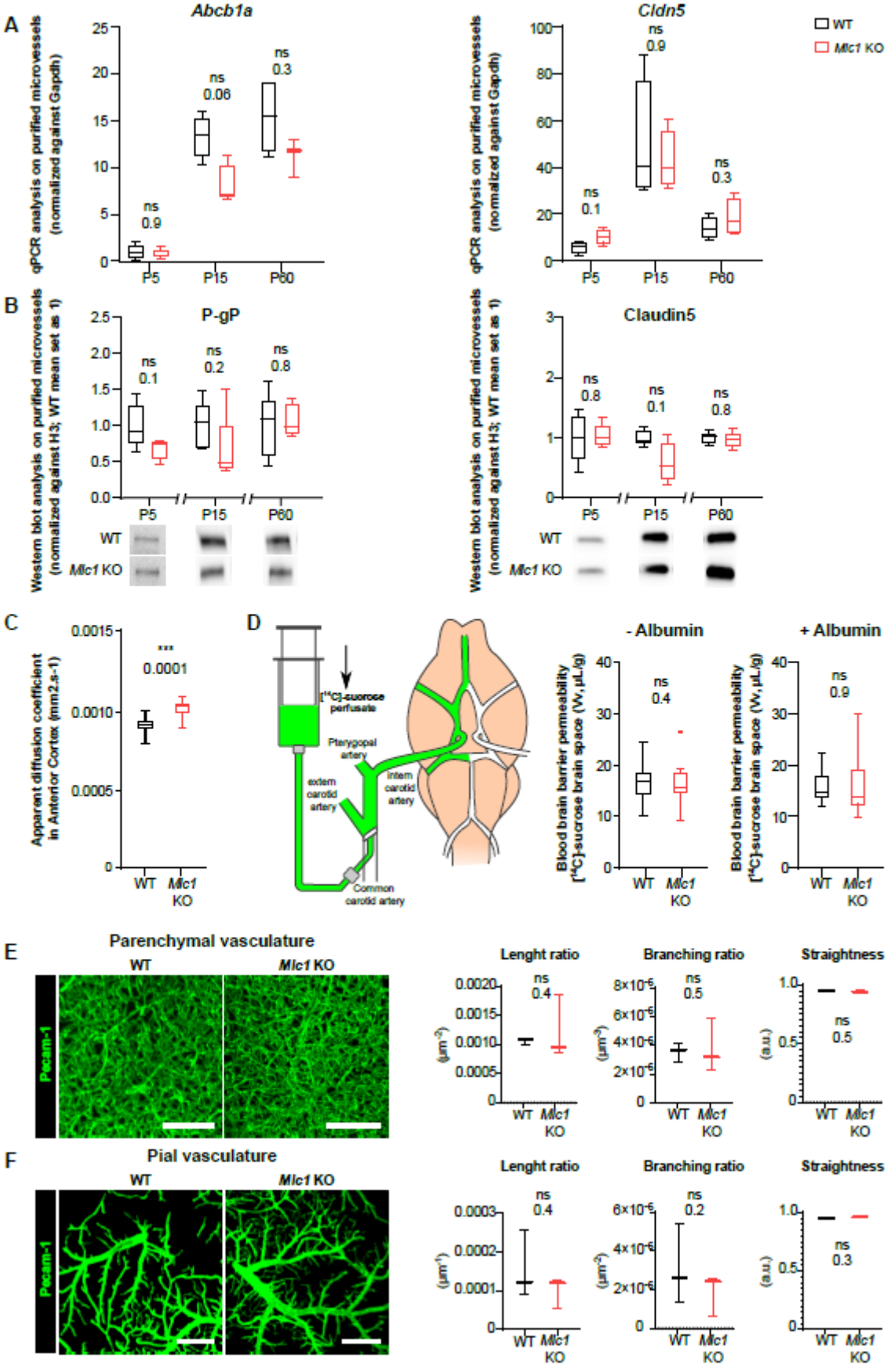
A
Abcb1a
Cldn5
qPCR analysis on purified microvessels (normalized against Gapdh)
WT
Mlc1 KO
ns 0.9
ns 0.06
ns 0.3
ns 0.1
ns 0.9
ns 0.3
P5
P15
P60
B
P-gP
Claudin5
Western blot analysis on purified microvessels (normalized against H3; WT mean set as 1)
ns 0.1
ns 0.2
ns 0.8
ns 0.8
ns 0.1
ns 0.8
C
Apparent diffusion coefficient in Anterior Cortex (mm2.s-1)
*** 0.0001
D
- Albumin
+ Albumin
Blood brain barrier permeability [14C]-sucrose brain space (Vv, µL/g)
ns 0.4
ns 0.9
[14C]-sucrose perfusate
Pterygopal artery
extern carotid artery
intern carotid artery
Common carotid artery
E
Parenchymal vasculature
Pecam-1
Lenght ratio
Branching ratio
Straightness
ns 0.4
ns 0.5
ns 0.5
F
Pial vasculature
ns 0.4
ns 0.2
ns 0.3

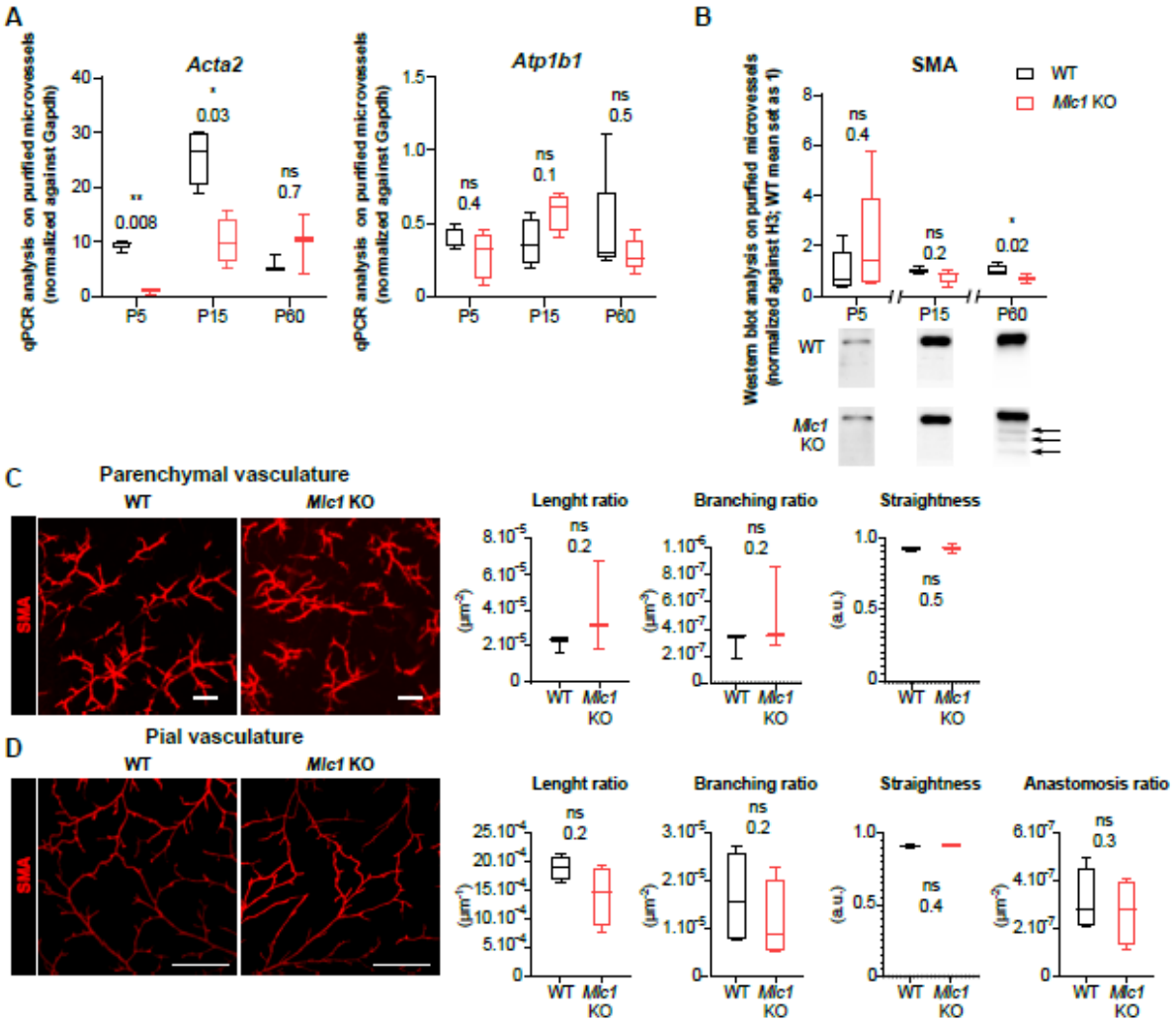
A
Acta2
qPCR analysis on purified microvessels (normalized against Gapdh)
0.008
0.03
0.7
P5
P15
P60
Atp1b1
0.4
0.1
0.5
B
SMA
WT
Mlc1 KO
Western blot analysis on purfied microvessels (normalized against H3; WT mean set as 1)
0.4
0.2
0.02
C
Parenchymal vasculature
WT
Mlc1 KO
SMA
Lenght ratio
Branching ratio
Straightness
0.2
0.5
D
Pial vasculature
Anastomosis ratio
0.4
0.3

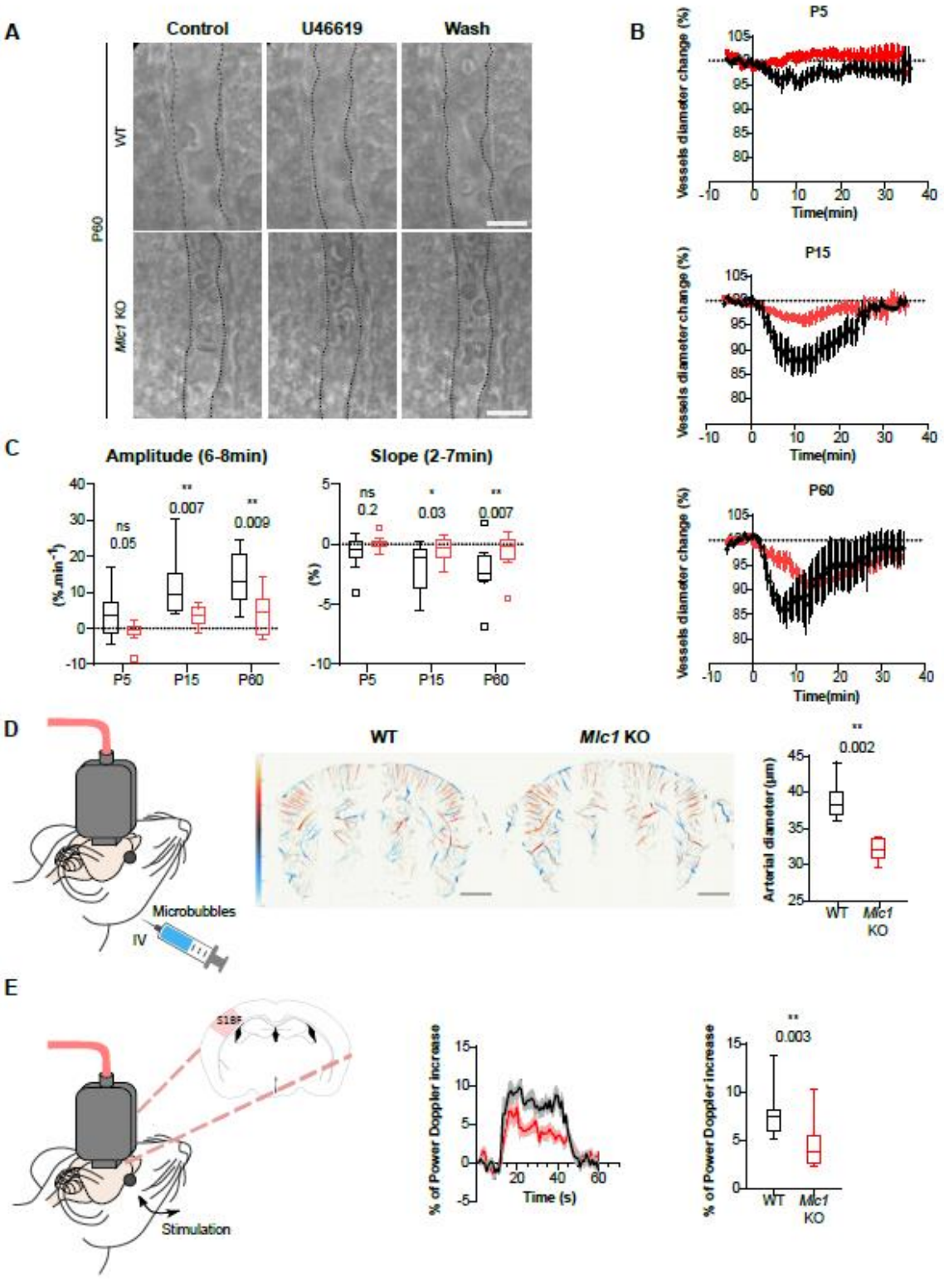
A
Control
U46619
Wash
P60
WT
Mlc1 KO
B
P5
P15
P60
Vessels diameter change (%)
Time(min)
C
Amplitude (6-8min)
Slope (2-7min)
(%.min-1)
(%)
ns
0.05
0.007
0.009
0.2
0.03
P5
P15
P60
D
WT
Mlc1 KO
Microbubbles
IV
Arterial diameter (µm)
0.002
E
S1BF
Stimulation
% of Power Doppler increase
Time (s)
0.003

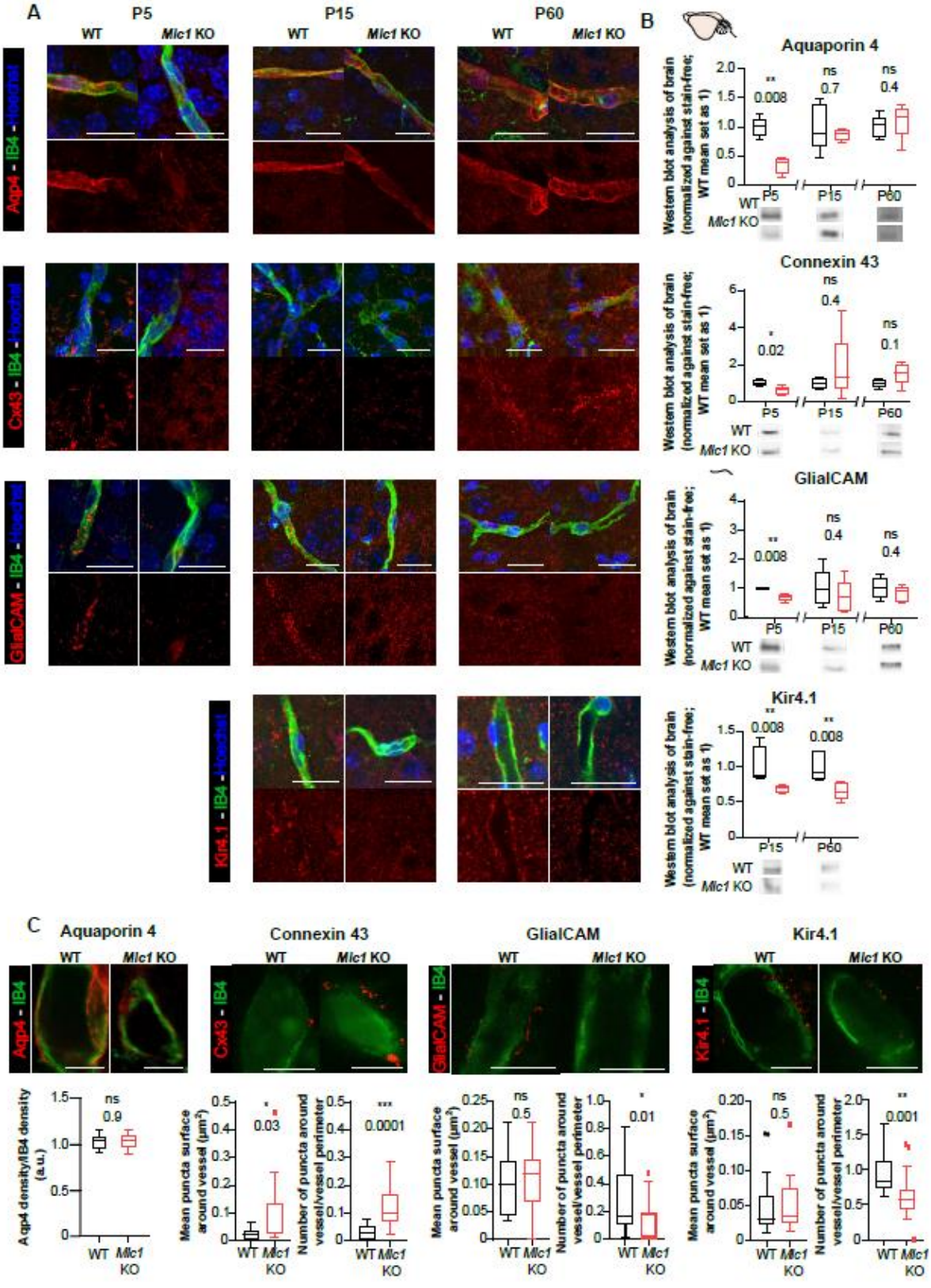
A
P5
P15
P60
WT
Mlc1 KO
Aqp4 - IB4 - Hoechst
Cx43 - IB4 - Hoechst
GlialCAM - IB4 - Hoechst
Kir4.1 - IB4 - Hoechst
B
Aquaporin 4
Connexin 43
GlialCAM
Kir4.1
Western blot analysis of brain (normalized against stain-free; WT mean set as 1)
C
Aquaporin 4
Connexin 43
GlialCAM
Kir4.1
Aqp4 - IB4
Cx43 - IB4
GlialCAM - IB4
Kir4.1 - IB4
Aqp4 density/IB4 density (a.u.)
Mean puncta surface around vessel (µm²)
Number of puncta around vessel/vessel perimeter
ns
0.9
0.03
0.0001
0.5
0.01
0.001

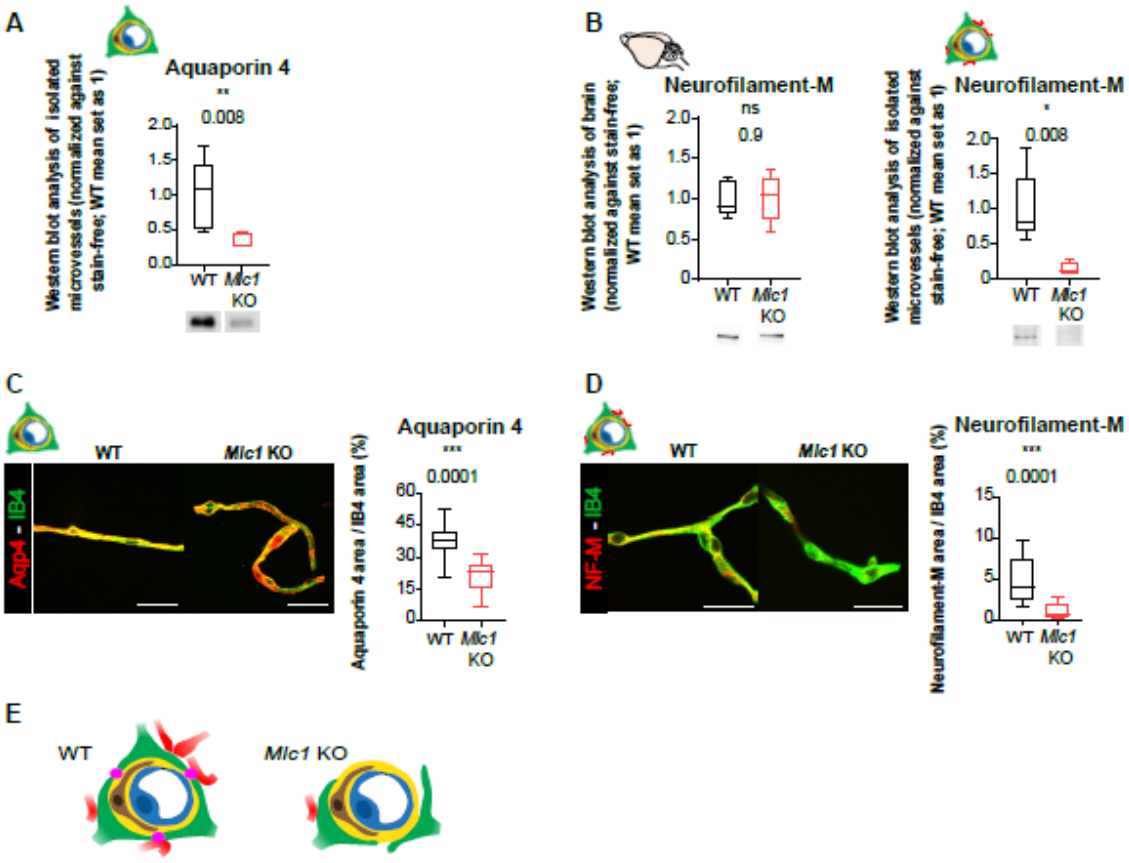
A
Aquaporin 4
**
0.008
Western blot analysis of isolated microvessels (normalized against stain-free; WT mean set as 1)
WT
Mlc1 KO
B
Neurofilament-M
ns
0.9
Western blot analysis of brain (normalized against stain-free; WT mean set as 1)
Neurofilament-M
*
0.008
Western blot analysis of isolated microvessels (normalized against stain-free; WT mean set as 1)
C
WT
Mlc1 KO
Aqp4 - IB4
Aquaporin 4
***
0.0001
Aquaporin 4 area / IB4 area (%)
D
WT
Mlc1 KO
NF-M - IB4
Neurofilament-M
***
0.0001
Neurofilament-M area / IB4 area (%)
E
WT
Mlc1 KO

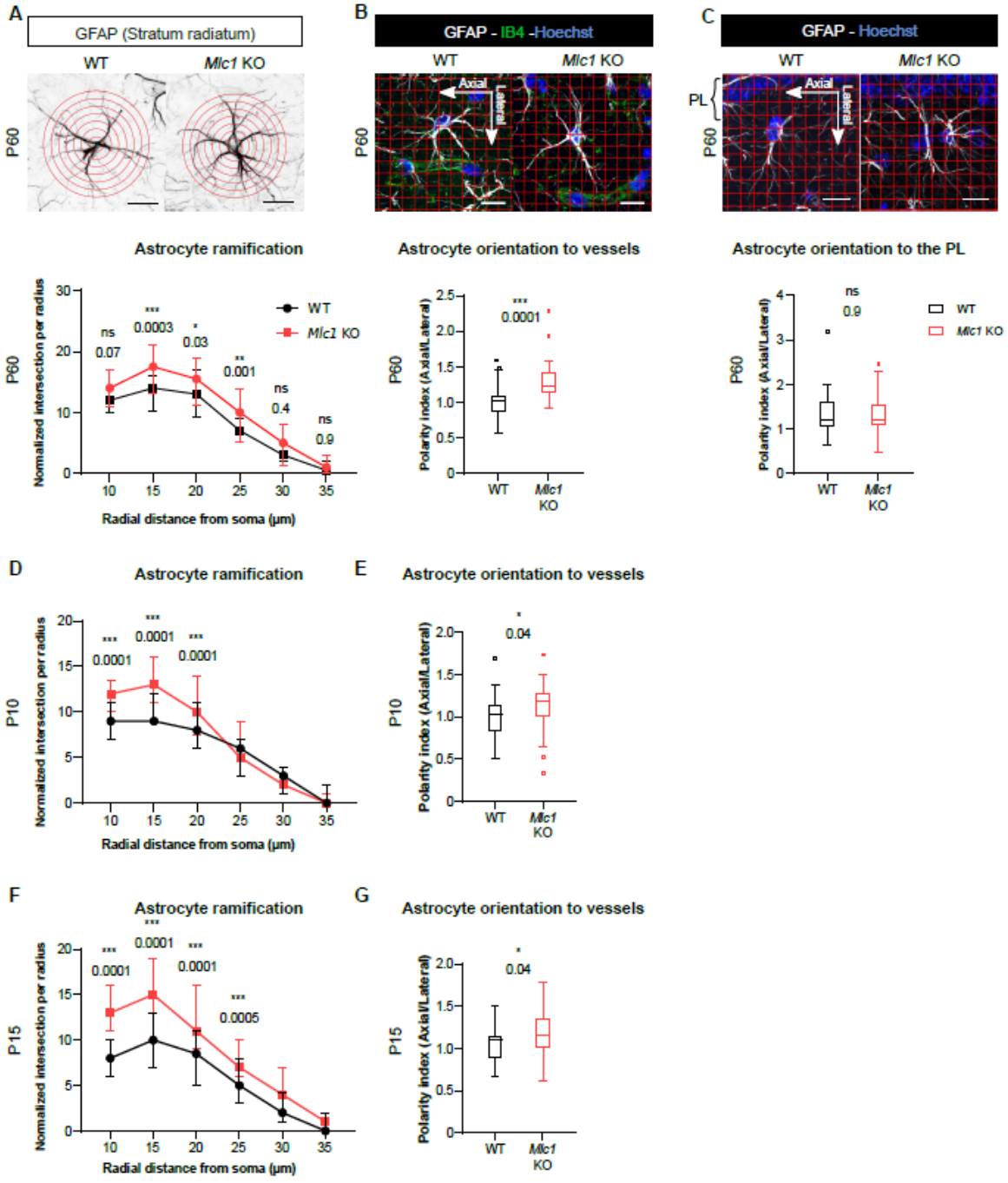
A
GFAP (Stratum radiatum)
WT
Mlc1 KO
P60
B
GFAP - IB4 -Hoechst
WT
Mlc1 KO
P60
Axial
Lateral
C
GFAP - Hoechst
WT
Mlc1 KO
PL
P60
Axial
Lateral
Astrocyte ramification
Normalized intersection per radius
Radial distance from soma (µm)
WT
Mlc1 KO
ns
0.07
***
0.0003
*
0.03
**
0.001
ns
0.4
ns
0.9
Astrocyte orientation to vessels
Polarity index (Axial/Lateral)
***
0.0001
WT
Mlc1 KO
Astrocyte orientation to the PL
Polarity index (Axial/Lateral)
ns
0.9
WT
Mlc1 KO
D
Astrocyte ramification
P10
Normalized intersection per radius
Radial distance from soma (µm)
***
0.0001
***
0.0001
***
0.0001
E
Astrocyte orientation to vessels
P10
Polarity index (Axial/Lateral)
*
0.04
WT
Mlc1 KO
F
Astrocyte ramification
P15
Normalized intersection per radius
Radial distance from soma (µm)
***
0.0001
***
0.0001
***
0.0001
***
0.0005
G
Astrocyte orientation to vessels
P15
Polarity index (Axial/Lateral)
*
0.04
WT
Mlc1 KO

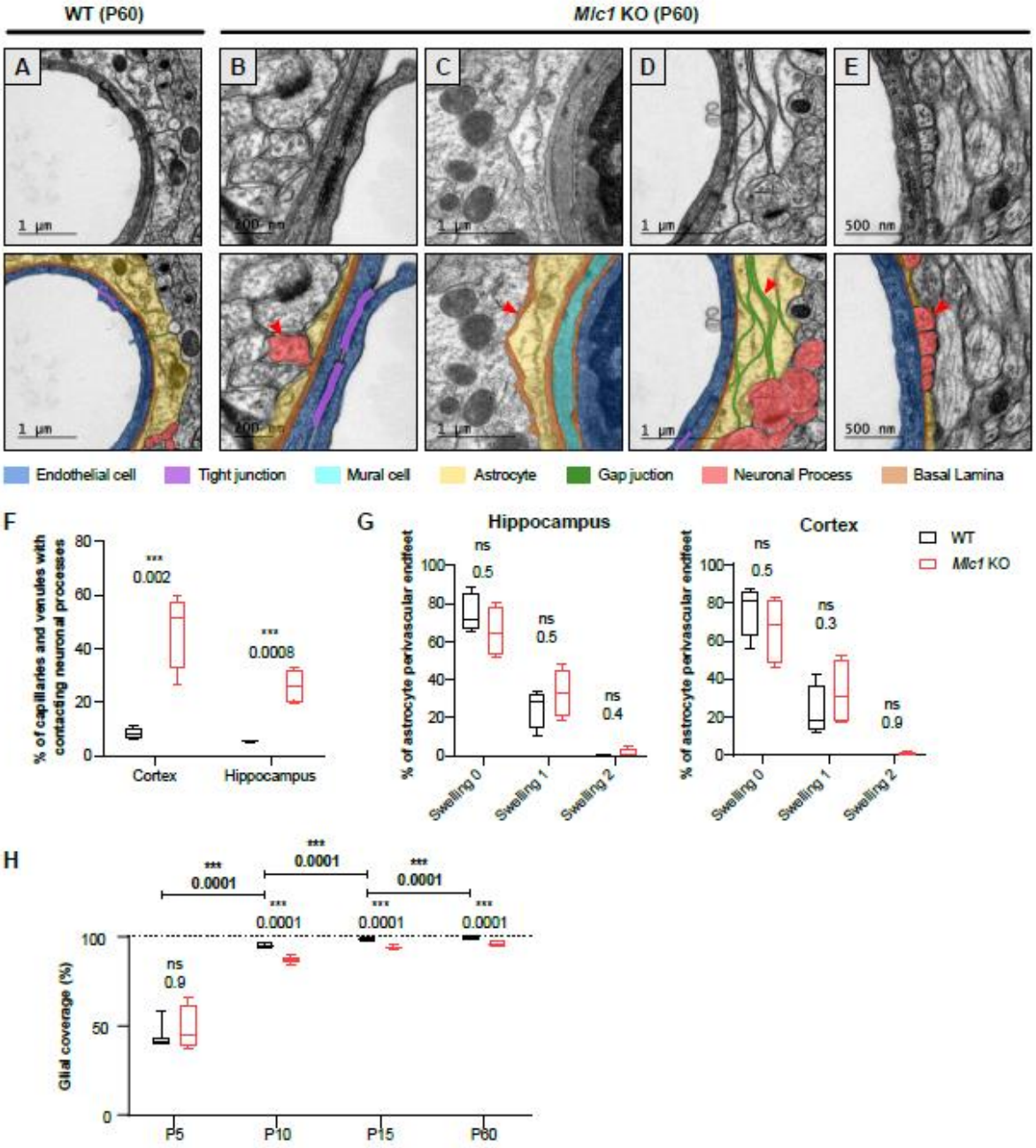
WT (P60)
Mlc1 KO (P60)
A
B
C
D
E
1 µm
200 nm
500 nm
Endothelial cell
Tight junction
Mural cell
Astrocyte
Gap junction
Neuronal Process
Basal Lamina
F
% of capillaries and venules with contacting neuronal processes
***
0.002
***
0.0008
Cortex
Hippocampus
G
Hippocampus
Cortex
% of astrocyte perivascular endfeet
ns
0.5
ns
0.5
ns
0.4
ns
0.5
ns
0.3
ns
0.9
Swelling 0
Swelling 1
Swelling 2
WT
Mlc1 KO
H
Glial coverage (%)
***
0.0001
***
0.0001
***
0.0001
***
0.0001
***
0.0001
***
0.0001
ns
0.9
P5
P10
P15
P60

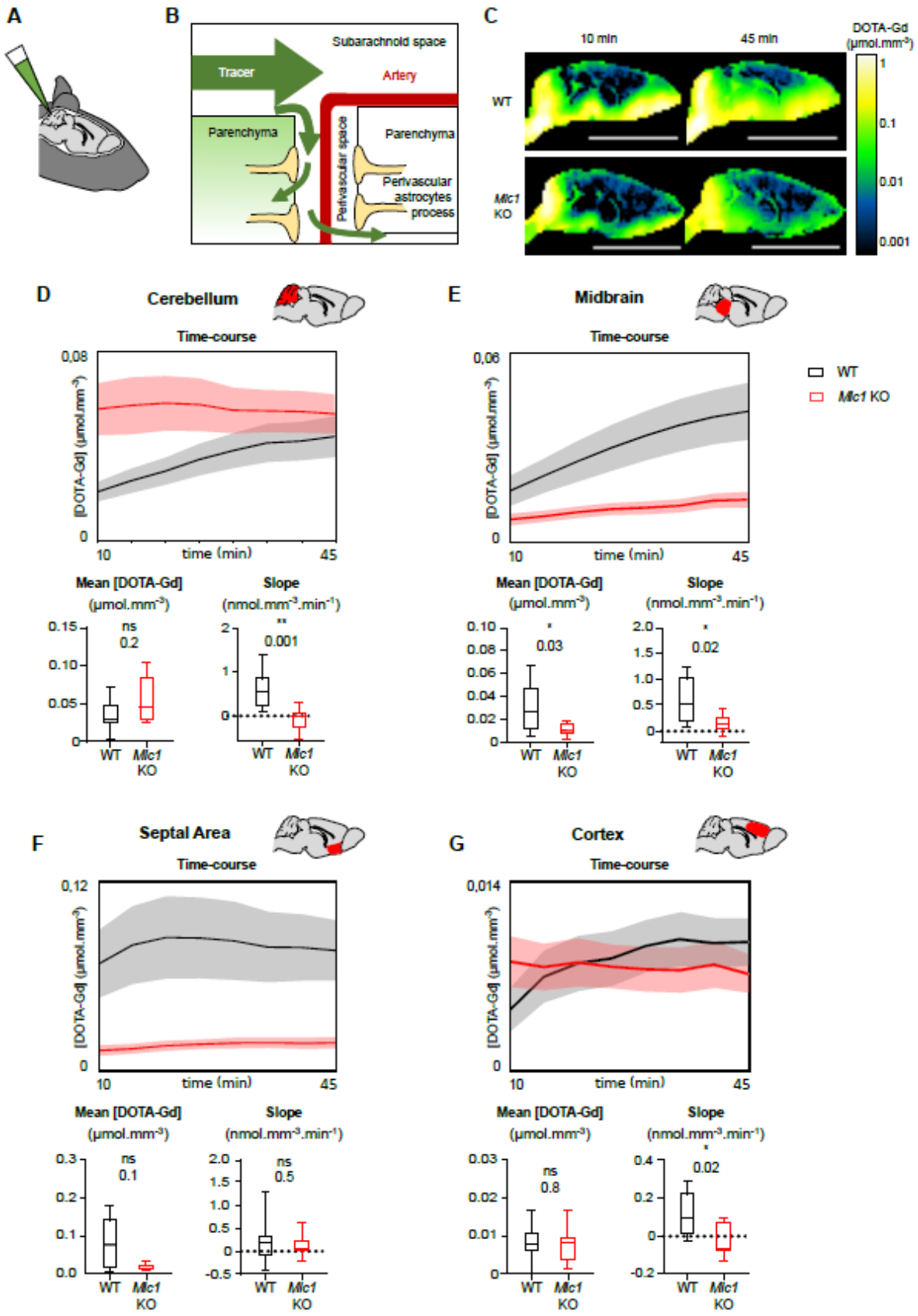
A
B
Subarachnoid space
Tracer
Artery
Parenchyma
Perivascular space
Parenchyma
Perivascular astrocytes process
C
10 min
45 min
DOTA-Gd (µmol.mm-3)
WT
Mlc1 KO
1
0.1
0.01
0.001
D
Cerebellum
Time-course
[DOTA-Gd] (µmol.mm-3)
time (min)
Mean [DOTA-Gd] (µmol.mm-3)
Slope (nmol.mm-3.min-1)
ns
0.2
**
0.001
E
Midbrain
WT
Mlc1 KO
*
0.03
*
0.02
F
Septal Area
ns
0.1
ns
0.5
G
Cortex
ns
0.8
*
0.02

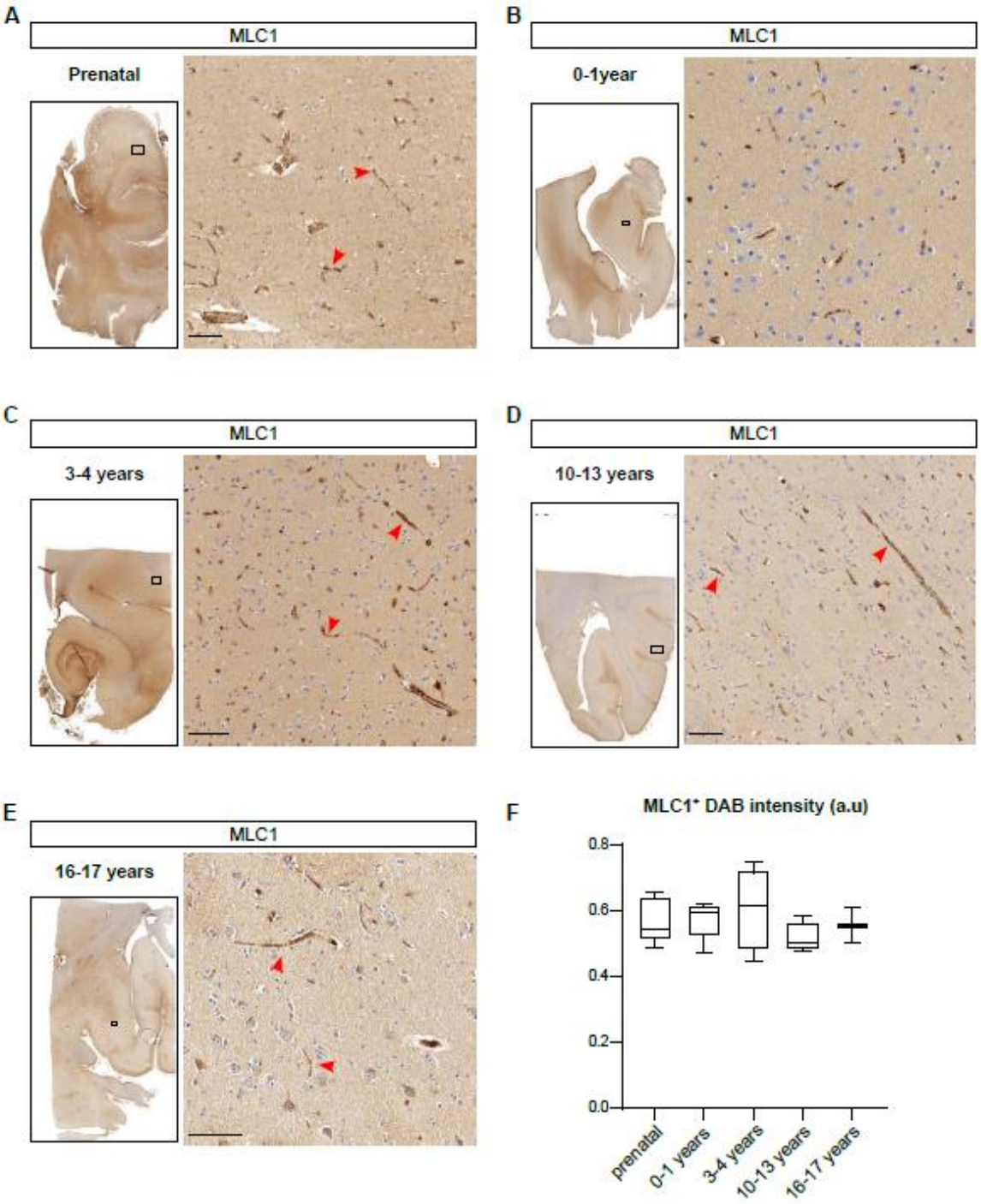
A
MLC1
Prenatal
B
MLC1
0-1year
C
MLC1
3-4 years
D
MLC1
10-13 years
E
MLC1
16-17 years
F
MLC1+ DAB intensity (a.u)
0.8
0.6
0.4
0.2
0.0
prenatal
0-1 years
3-4 years
10-13 years
16-17 years

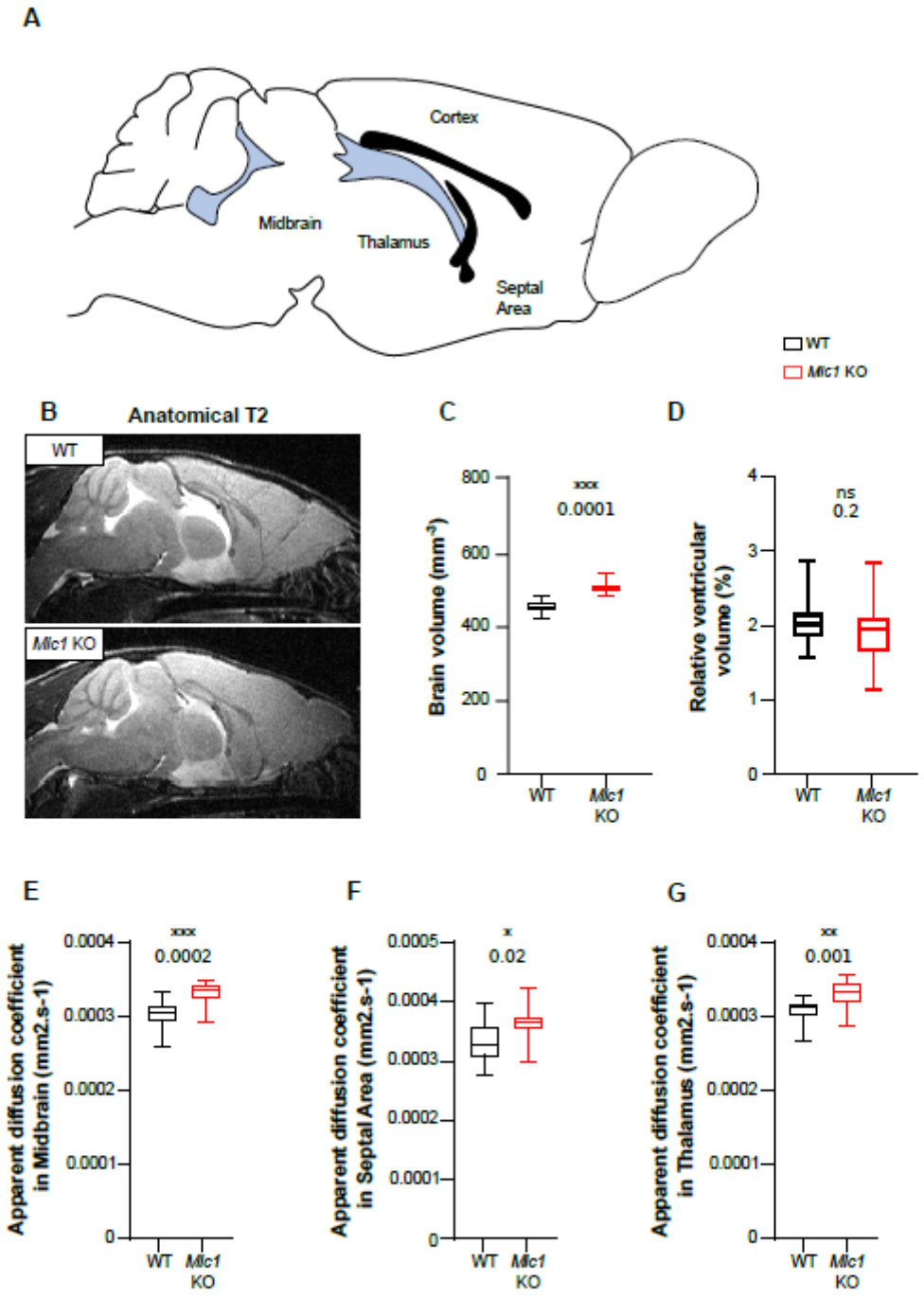
A
Cortex
Midbrain
Thalamus
Septal Area
WT
Mlc1 KO
B
Anatomical T2
WT
Mlc1 KO
C
Brain volume (mm-3)
xxx
0.0001
WT
Mlc1 KO
D
Relative ventricular volume (%)
ns
0.2
WT
Mlc1 KO
E
Apparent diffusion coefficient in Midbrain (mm2.s-1)
xxx
0.0002
WT
Mlc1 KO
F
Apparent diffusion coefficient in Septal Area (mm2.s-1)
x
0.02
WT
Mlc1 KO
G
Apparent diffusion coefficient in Thalamus (mm2.s-1)
xx
0.001
WT
Mlc1 KO

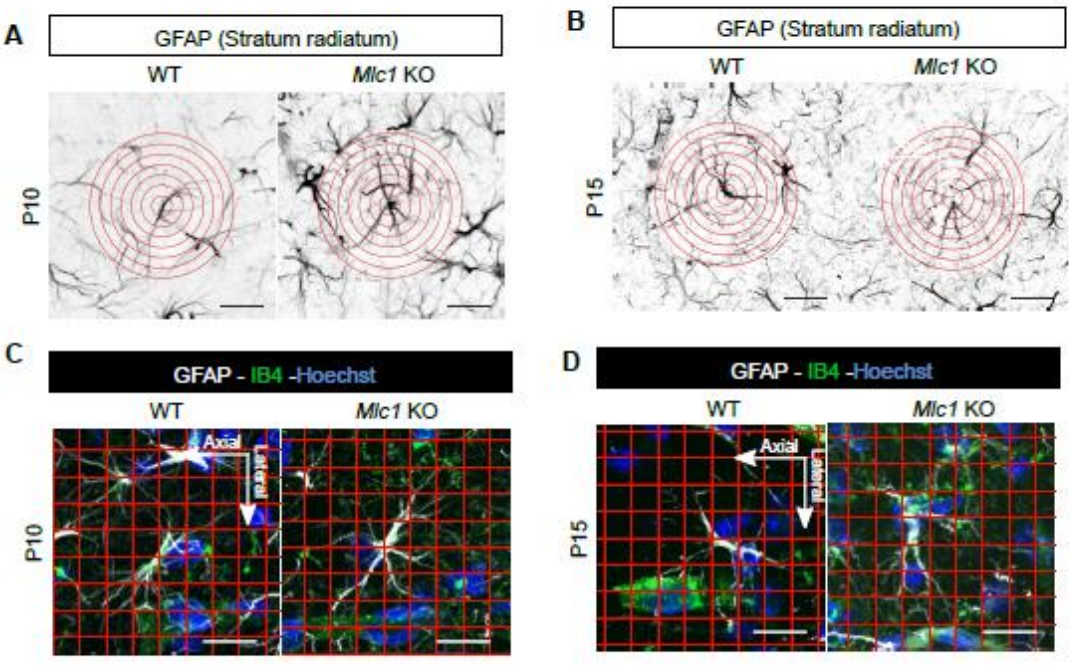
A
GFAP (Stratum radiatum)
WT
Mlc1 KO
P10
B
GFAP (Stratum radiatum)
WT
Mlc1 KO
P15
C
GFAP - IB4 -Hoechst
WT
Mlc1 KO
Axial
Lateral
P10
D
GFAP - IB4 -Hoechst
WT
Mlc1 KO
Axial
Lateral
P15

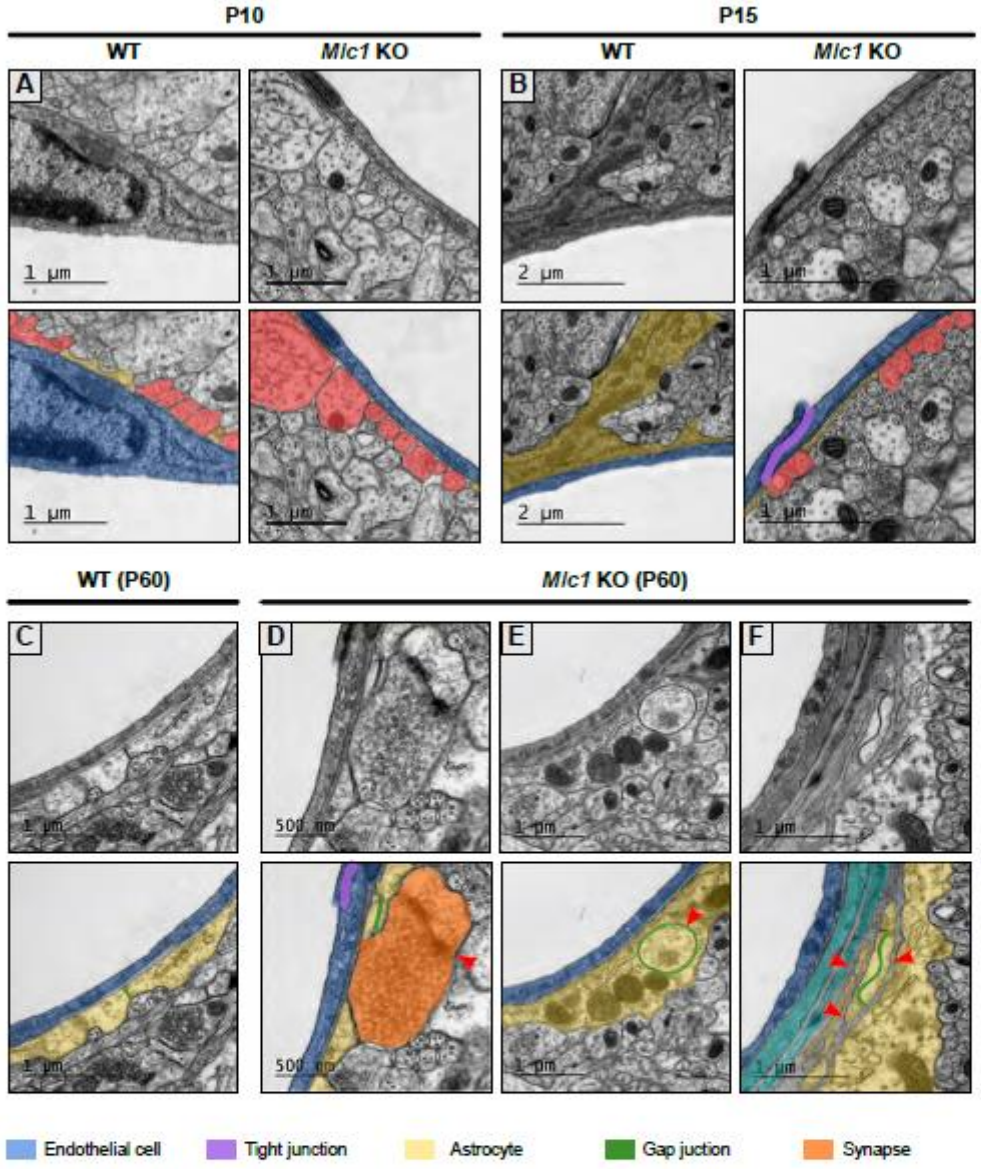
P10
P15
WT
Mlc1 KO
WT
Mlc1 KO
A
B
1 µm
2 µm
WT (P60)
Mlc1 KO (P60)
C
D
E
F
500 nm
Endothelial cell
Tight junction
Astrocyte
Gap junction
Synapse

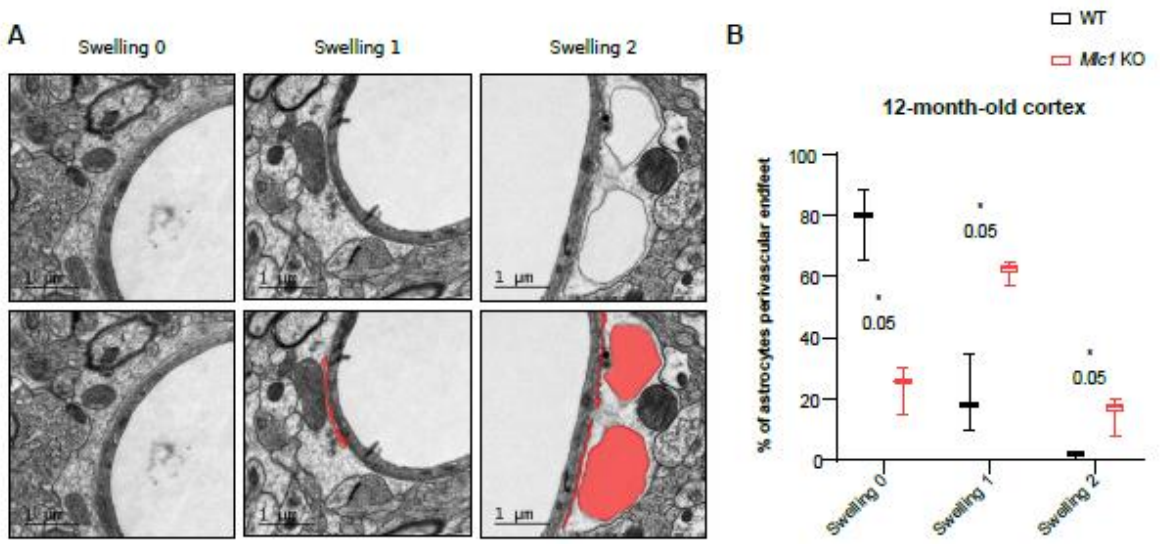
A
Swelling 0
Swelling 1
Swelling 2
1 µm
B
WT
Mlc1 KO
12-month-old cortex
% of astrocytes perivascular endfeet
100
80
60
40
20
0
0.05
0.05
0.05
Swelling 0
Swelling 1
Swelling 2

Bibliographie

A

Abbott, N. J., Rönnbäck, L., & Hansson, E. (2006). Astrocyte-endothelial interactions at the blood-brain barrier. In *Nature Reviews Neuroscience* (Vol. 7, Issue 1, pp. 41–53). https://doi.org/10.1038/nrn1824

Abelous, J. E., & Bardier, E. (1909). Les substances hypotensives de l'urine humaine normale. *C. R. Soc. Biol.*, *66*, 511–511.

Akazawa, C., Shigemoto, R., Bessho, Y., Nakanishi, S., & Mizuno, N. (1994). Differential Expression of Five N-Methyl-D-Aspartate Receptor Subunit mRNAs in the Cerebellum of Developing and Adult Rats. In *THE JOURNAL OF COMPARATIVE NEUROLOGY* (Vol. 347, Issue 150).

Albiston, A. L., McDowall, S. G., Matsacos, D., Sim, P., Clune, E., Mustafa, T., Lee, J., Mendelsohn, F. A. O., Simpson, R. J., Connolly, L. M., & Chai, S. Y. (2001). Evidence That the Angiotensin IV (AT4) Receptor Is the Enzyme Insulin-regulated Aminopeptidase. *Journal of Biological Chemistry*, *276*(52), 48623–48626. https://doi.org/10.1074/jbc.C100512200

Alfie, M. E., Slgmon, D. H., Pomposlello, S. I., & Carretero, O. A. (1996). *Effect of High Salt Intake in Mutant Mice Lacking Bradykinin-B2 Receptors*. http://ahajournals.org

Allen, A. M., Jancovski, N., Bassi, J. K., Carter, D. A., Choong, Y.-T., Connelly, A., Nguyen, T.-P., Chen, D., Lukoshkova, E. v, Menuet, C., & Head, G. A. (2013). *From the Department of Physiology (N Stimulation of Angiotensin Type 1A Receptors on Catecholaminergic Cells Contributes to Angiotensin-Dependent Hypertension Renin-Angiotensin System*. https://doi.org/10.1161/HYPERTENSIONAHA

Allen, R. A., Kluft, C., & Brommer, E. J. P. (1985). *Effect of Chronic Smoking on Fibrinolysis*. http://ahajournals.org

Alva, J. A., Zovein, A. C., Monvoisin, A., Murphy, T., Salazar, A., Harvey, N. L., Carmeliet, P., & Iruela-Arispe, M. L. (2006). VE-cadherin-cre-recombinase transgenic mouse: A tool for lineage analysis and gene deletion in endothelial cells. *Developmental Dynamics*, *235*(3), 759–767. https://doi.org/10.1002/dvdy.20643

Andral, G. (1843). Essai d'hématologie pathologique. *Fortin, Masson et Cie*.

Andreasen, P. A., Riccio, A., Welinder+, K. G., Douglas+, R., Sartorio*', R., Nielsen, L. S., Oppenheimer-T, C., Blasi, F., & Dan0, K. (1986). *Plasminogen activator inhibitor type-1: reactive center and amino-terminal heterogeneity determined by protein and cDNA sequencing* (Vol. 209, Issue 2).

Anfray, A., Drieu, A., Hingot, V., Hommet, Y., Yetim, M., Rubio, M., Deffieux, T., Tanter, M., Orset, C., & Vivien, D. (2020). Circulating tPA contributes to neurovascular coupling by a mechanism involving the endothelial NMDA receptors. *Journal of Cerebral Blood Flow and Metabolism*, *40*(10), 2038–2054. https://doi.org/10.1177/0271678X19883599

Angles-Cano, E., Balaton, A., le Bonniec, B., Genot, E., Elion, J., & Sultan, Y. (1985). Production of Monoclonal Antibodies to the High Fibrin-Affinity, Tissue-Type Plasminogen Activator of Human Plasma. Demonstration of Its Endothelial Origin by Immunolocalization. In *MATERIALS AND METHODS Blood* (Vol. 66, Issue 4).

Ardaillou, R., & Chansel, D. (1997). Synthesis and effects of active fragments of angiotensin II. *Kidney International*, *52*(6), 1458–1468. https://doi.org/10.1038/ki.1997.476

Arfors, K.-E., Arturson, G., & Malmberg, P. (1971). Effect of Prolonged Chloralose Anesthesia on Acid-Base Balance and Cardiovascular Functions in Dogs. *Acta Physiologica Scandinavica*, *81*(1). https://doi.org/10.1111/j.1748-1716.1971.tb04876.x

Armulik, A., Genové, G., & Betsholtz, C. (2011). Pericytes: Developmental, Physiological, and Pathological Perspectives, Problems, and Promises. In *Developmental Cell* (Vol. 21, Issue 2, pp. 193–215). https://doi.org/10.1016/j.devcel.2011.07.001

Ascular -b Ed -s Pecific H Emostasis, E. v, Ypercoagulable Tates R Obert D R Osenberg, H. S., & Illiam A Ird, W. C. (1999). *Mechanisms of Disease*.

Astrup, T. , & Stage, A. ,. (1952). Isolation of a soluble fibrinolytic activator from animal tissue. *Nature*, 929–929.

Attwell, D., Buchan, A. M., Charpak, S., Lauritzen, M., MacVicar, B. A., & Newman, E. A. (2010). Glial and neuronal control of brain blood flow. In *Nature* (Vol. 468, Issue 7321, pp. 232–243). https://doi.org/10.1038/nature09613

Attwell, D., & Iadecola, C. (2002). The neural basis of functional brain imaging signals. *Trends in Neurosciences*, *25*(12). https://doi.org/10.1016/s0166-2236(02)02264-6

Attwell, D., Mishra, A., Hall, C. N., O'Farrell, F. M., & Dalkara, T. (2016). What is a pericyte? *Journal of Cerebral Blood Flow and Metabolism*, *36*(2), 451–455. https://doi.org/10.1177/0271678X15610340

Audoly, L. P., Oliverio, M. I., Coffman, T. M., Audoly, L. P., Oliverio, M. I., & Coffman, T. M. (2000). *Insights into the Functions of Type 1 (AT 1) Angiotensin II Receptors Provided by Gene Targeting* (Vol. 11, Issue 7).

Augusto Souza dos Santos, R., Tomagnini Passaglio, K., Bosco Pesquero, J., Bader, M., & Cristina Simões Silva, A. (2001). *Interactions Between Angiotensin-(1-7), Kinins, and Angiotensin II in Kidney and Blood Vessels*. http://www.hypertensionaha.org

Auzan, C., & Clauser, É. (2010). Structure et fonctions des récepteurs AT1 de l'angiotensine II au cours de l'évolution. *Journal de La Societe de Biologie*, *203*(4), 295–302. https://doi.org/10.1051/jbio/2009033

B

Baranes, D., Lederfein, D., Huang, Y.-Y., Chen, M., Bailey, C. H., & Kandel, E. R. (1998). Tissue Plasminogen Activator Contributesto the Late Phase of LTP and to Synaptic Growthin the Hippocampal Mossy Fiber Pathway. In Neuron (Vol. 21). Moreover.

Baron, A., Montagne, A., Cassé, F., Launay, S., Maubert, E., Ali, C., & Vivien, D. (2010). NR2D-containing NMDA receptors mediate tissue plasminogen activator-promoted neuronal excitotoxicity. *Cell Death and Differentiation*, *17*(5), 860–871. https://doi.org/10.1038/cdd.2009.172

Bascands, J. L., Emond, C., Pecher, C., Regoli, D., & Girolami, J. P. (1991). Bradykinin stimulates production of inositol (1,4,5) trisphosphate in cultured mesangial cells of the rat via a BK2-kinin receptor. In *Br. J. Pharmacol* (Vol. 102).

Bashir, Z. I., Tam, B., & Collingridge, G. L. (1990). Activation of the glycine site in the NMDA receptor is necessary for the induction of LTP. In *Neuroscience Letters* (Vol. 108).

Benchenane, K., Castel, H., Boulouard, M., Bluthé, R., Fernandez-Monreal, M., Roussel, B. D., Lopez-Atalaya, J. P., Butt-Gueulle, S., Agin, V., Maubert, E., Dantzer, R., Touzani, O., Dauphin, F., Vivien, D., & Ali, C. (2007). Anti-NR1 N-terminal-domain vaccination unmasks the crucial action of tPA on NMDA-receptor-mediated toxicity and spatial memory. *Journal of Cell Science*, *120*(4), 578–585. https://doi.org/10.1242/jcs.03354

Bhattacharjee, P., & Bhattacharyy, D. (2014). An Insight into the Abnormal Fibrin Clots — Its Pathophysiological Roles. In *Fibrinolysis and Thrombolysis*. InTech. https://doi.org/10.5772/57335

Bicknell, G. R., & Cohen, G. M. (1995). Cleavage of DNA to large kilobase pair fragments occurs in some forms of necrosis as well as apoptosis. *Biochemical and Biophysical Research Communications*, *207*(1). https://doi.org/10.1006/bbrc.1995.1150

Binder, B. R., Spragg, J., & Austen, K. F. (1978). Purification and characterization of human vascular plasminogen activator derived from blood vessel perfusates. *The Journal of Biological Chemistry*, *254*(6).

Blais, C., Couture, R., Drapeau, G., Colman, R. W., Adam, A., Couture, R., & City, Q. (1997). Involvement Of Endogenous Kinins In The Pathogenesis Of Peptidoglycan-Induced Arthritis In The Lewis Rat. In *Arthritis & Rheumatism* (Vol. 40, Issue 7).

Blinder, P., Tsai, P. S., Kaufhold, J. P., Knutsen, P. M., Suhl, H., & Kleinfeld, D. (2013). The cortical angiome: An interconnected vascular network with noncolumnar patterns of blood flow. *Nature Neuroscience*, *16*(7), 889–897. https://doi.org/10.1038/nn.3426

Bliss, T. v, & Lomo, T. (1973). Long-lasting potentiation of synaptic transmission in the dentate area of the anaesthetized rabbit following stimulation of the perforant path. *The Journal of Physiology*, *232*(2). https://doi.org/10.1113/jphysiol.1973.sp010273

Bonvento, G., Charbonn6, R., Corr~ze, J.-L., Borredon, J., Seylaz, J., & Lacombe, P. (1994). Is a-chloralose plus halothane induction a suitable anesthetic regimen for cerebrovascular research? In *Brain Research* (Vol. 665).

Bonvento, G., Sibson, N., & Pellerin, L. (2002). Does glutamate image your thoughts? *Trends in Neurosciences*, *25*(7). https://doi.org/10.1016/s0166-2236(02)02168-9

Boulaftali, Y., Adam, F. R., Venisse, L., Ronique Ollivier, V., Richard, B., Taieb, S., Monard, D., Favier, R. M., Alessi, M.-C., Bryckaert, M., Ronique Arocas, V., Jandrot-Perrus, M., & Bouton, M.-C. (2010). *Anticoagulant and antithrombotic properties of platelet protease nexin-1*. https://doi.org/10.1182/blood-2009-04

Bouton, M.-C., Boulaftali, Y., Richard, B., Ronique Arocas, V., Michel, J.-B., & Jandrot-Perrus, M. (2012). *Emerging role of serpinE2/protease nexin-1 in hemostasis and vascular biology*. https://doi.org/10.1182/blood

Boyce, S., Rupniak, N. M. J., Carlson, E. J., Webb, J., Borkowski, J. A., Hess, F., Strader, C. D., & Hill, R. G. (1996). Immunopharmacol ogy Nociception and inflammatory hyperalgesia in B 2 bradykinin receptor knockout mice. In *Immunopharmacology* (Vol. 33). ELSEVIER.

Bozó, É., Éles, J., & Keser, G. M. (2012). Bradykinin B1 receptor antagonists: A patent update 2009 - 2012. In *Expert Opinion on Therapeutic Patents* (Vol. 22, Issue 12, pp. 1443–1452). https://doi.org/10.1517/13543776.2012.730521

Braaten, J. v, Handt, S., Jerome, W. G., Kirkpatrick, J., Lewis, J. C., & Hantgan, R. R. (n.d.). *Regulation of Fibrinolysis by Platelet-Released Plasminogen Activator Inhibitor 1: Light Scattering and Ultrastructural Examination of Lysis of a Model Platelet-Fibrin Thrombus*.

Braun-Dullaeus, R. C., Mann, M. J., Ziegler, A., von der Leyen, H. E., & Dzau, V. J. (1999). A novel role for the cyclin-dependent kinase inhibitor p27(Kip1) in angiotensin II-stimulated vascular smooth muscle cell hypertrophy. *The Journal of Clinical Investigation*, *104*(6). https://doi.org/10.1172/JCI5339

Braun-Menendez, E., Fasciolo, J. C., Leloir, L. F., & Munoz, J. M. (1940). THE SUBSTANCE CAUSING RENAL HYPERTENSION. In *J. Physiol* (Vol. 98).

Braun-Menendez, E., & Page, I. H. (1958). A Suggested Revision of Nomenclature—Angiotensin. *Nature*, *181*(4615). https://doi.org/10.1038/1811061b0

Brogren, H., Karlsson, L., Andersson, M., Wang, L., Erlinge, D., & Jern, S. (2004). Platelets synthesize large amounts of active plasminogen activator inhibitor 1. *Blood*, *104*(13), 3943–3948. https://doi.org/10.1182/blood-2004-04-1439

Brown, N. J., Gainer, J. v, Murphey, L. J., & Vaughan, D. E. (2000). *Bradykinin Stimulates Tissue Plasminogen Activator Release From Human Forearm Vasculature Through B 2 Receptor-Dependent, NO Synthase-Independent, and Cyclooxygenase-Independent Pathway*. http://www.circulationaha.org

Brown, N. J., Gainer, J. v, Stein, C. M., & Vaughan, D. E. (1999). *Bradykinin Stimulates Tissue Plasminogen Activator Release in Human Vasculature*. http://www.hypertensionaha.org

Brown, N. J., Nadeau, J. H., & Vaughan, D. E. (1997). Selective stimulation of tissue-type plasminogen activator (t-PA) in vivo by infusion of bradykinin. *Thrombosis and Haemostasis*, *77*(3).

Burgess, G. M., Mullaney, I., Mcneill, M., Dunn, P. M., & Rang, H. P. (1989). Second Messengers Involved in the Mechanism of Action of Bradykinin in Sensory Neurons in Culture. In *The Journal of Neuroscience* (Issue 9).

Busija, D. W., Bari, F., Domoki, F., & Louis, T. (2007). *Mechanisms Involved in the Cerebrovascular Dilator Effects of N-methyl-D-aspartate in Cerebral Cortex*.

Cacquevel, M., Launay, S., Castel, H., Benchenane, K., Chéenne, S., Buée, L., Moons, L., Delacourte, A., Carmeliet, P., & Vivien, D. (2007). Ageing and amyloid-beta peptide deposition contribute to an impaired brain tissue plasminogen activator activity by different mechanisms. *Neurobiology of Disease*, *27*(2), 164–173. https://doi.org/10.1016/j.nbd.2007.04.004

Calabresi, P., Napolitano, M., Centonze, D., Marfia, G. A., Gubellini, P., Teule, M. A., Berretta, N., Bernardi, G., Frati, L., Tolu, M., & Gulino, A. (2000). Tissue plasminogen activator controls multiple forms of synaptic plasticity and memory. *European Journal of Neuroscience*, *12*(3), 1002–1012. https://doi.org/10.1046/j.1460-9568.2000.00991.x

Carlson, K. S. B., Nguyen, L., Schwartz, K., Lawrence, D. A., & Schwartz, B. S. (2016). Neuroserpin differentiates between forms of tissue type plasminogen

activator via pH dependent deacylation. *Frontiers in Cellular Neuroscience*, *10*(JUN). https://doi.org/10.3389/fncel.2016.00154

Cassé, F., Bardou, I., Danglot, L., Briens, A., Montagne, A., Parcq, J., Alahari, A., Galli, T., Vivien, D., & Docagne, F. (2012). Glutamate controls tPA recycling by astrocytes, which in turn influences glutamatergic signals. *Journal of Neuroscience*, *32*(15), 5186–5199. https://doi.org/10.1523/JNEUROSCI.5296-11.2012

Caughey, G. H., Raymond, W. W., & Wolters, P. J. (2000). *Angiotensin II generation by mast cell K-and L-chymases*. www.elsevier.com/locate/bba

Cauli, B., & Hamel, E. (2010). Revisiting the role of neurons in neurovascular coupling. *Frontiers in Neuroenergetics*, *2*. https://doi.org/10.3389/fnene.2010.00009

Cauli, B., Tong, X. K., Rancillac, A., Serluca, N., Lambolez, B., Rossier, J., & Hamel, E. (2004). Cortical GABA interneurons in neurovascular coupling: Relays for subcortical vasoactive pathways. *Journal of Neuroscience*, *24*(41), 8940–8949. https://doi.org/10.1523/JNEUROSCI.3065-04.2004

Chaki, S., & Inagami, T. (1992). *Identification and characterization of a new binding site for angiotensin II in mouse neuroblastoma neuro-2a cells* (Vol. 182, Issue 1).

Chevilley, A., Lesept, F., Lenoir, S., Ali, C., Parcq, J., & Vivien, D. (2015). Impacts of tissue-type plasminogen activator(tPA) on neuronal survival. In *Frontiers in Cellular Neuroscience* (Vol. 9, Issue october). Frontiers Research Foundation. https://doi.org/10.3389/fncel.2015.00415

Choi, D. W., Koh, J.-Y., & Peters, S. (1988). Pharmacology of Glutamate Neurotoxicity in Cortical Cell Culture: Attenuation by NMDA Antagonists. In *The Journal of Neuroscience* (Vol. 8).

Citri, A., & Malenka, R. C. (2008). Synaptic plasticity: Multiple forms, functions, and mechanisms. In *Neuropsychopharmacology* (Vol. 33, Issue 1, pp. 18–41). https://doi.org/10.1038/sj.npp.1301559

Cline, H. T., Debski, E. A., & Constantine-Paton, M. (1987). N-Methyl-D-aspartate receptor antagonist desegregates eye-specific stripes (optic tectum/ocular dominance columns/correlated activity/aminophosphonovaleric acid/neural maps). In *Neurobiology* (Vol. 84).

Cohen, Z., Bonvento, G., Lacombe, P., & Hamel, E. (1996). Serotonin in the regulation of brain microcirculation. *Progress in Neurobiology*, *50*(4). https://doi.org/10.1016/s0301-0082(96)00033-0

Collen, D., & Lijnen, H. R. (1991). Basic and clinical aspects of fibrinolysis and thrombolysis. *Blood*, *78*(12).

Collen, D., & Lijnen, H. R. (2004). *Tissue-type plasminogen activator: a historical perspective and personal account*.

Collingridge, G. L., Kehl, S. J., Loo, R., & McLennan, H. (1983b). Effects of kainic and other amino acids on synaptic excitation in rat hippocampal slices: 1. Extracellular analysis. *Experimental Brain Research*, *52*(2). https://doi.org/10.1007/BF00236625

Collingridge, G. L., Kehl, S. J., & McLennan, H. (1983a). Excitatory amino acids in synaptic transmission in the Schaffer collateral-commissural pathway of the rat hippocampus. *The Journal of Physiology*, *334*. https://doi.org/10.1113/jphysiol.1983.sp014478

Corlew, R., Brasier, D. J., Feldman, D. E., & Philpot, B. D. (2008). Presynaptic NMDA receptors: Newly appreciated roles in cortical synaptic function and plasticity. In *Neuroscientist* (Vol. 14, Issue 6, pp. 609–625). https://doi.org/10.1177/1073858408322675

Correa, F., Gauberti, M., Parcq, J., Macrez, R., Hommet, Y., Obiang, P., Hernangómez, M., Montagne, A., Liot, G., Guaza, C., Maubert, E., Ali, C., Vivien, D., & Docagne, F. (2011). Tissue plasminogen activator prevents white matter damage following stroke. *Journal of Experimental Medicine*, *208*(6), 1229–1242. https://doi.org/10.1084/jem.20101880

Cortes-Canteli, M., & Iadecola, C. (2020). Alzheimer's Disease and Vascular Aging: JACC Focus Seminar. In *Journal of the American College of Cardiology* (Vol. 75, Issue 8, pp. 942–951). Elsevier USA. https://doi.org/10.1016/j.jacc.2019.10.062

Coulet, F., Gonzalez, W., Boixel, C., Meilhac, O., Pueyo, M. E., & Michel, J. B. (2001). Endothelium-independent conversion of angiotensin I by vascular smooth muscle cells. *Cell and Tissue Research*, *303*(2), 227–234. https://doi.org/10.1007/s004410000309

Cox, S. B., Woolsey, T. A., & Rovainen, M. (1993). *Journal of Cerebral Blood Flow and Metabolism Localized Dynamic Changes in Cortical Blood Flow With Whisker Stimulation Corresponds to Matched Vascular and Neuronal Architecture of Rat Barrels*.

Cull-Candy, S. G., & Leszkiewicz, D. N. (2004). Role of distinct NMDA receptor subtypes at central synapses. In *Science's STKE : signal transduction knowledge environment* (Vol. 2004, Issue 255). https://doi.org/10.1126/stke.2552004re16

Curtis, D. R., Phillis, J. W., & Watkins, J. C. (1961). Actions of amino-acids on the isolated hemisected spinal cord of the toad. In *J. Pharmacol* (Vol. 16).

Curtis, D. R., & Watkins, J. C. (1960). The excitation and depression of spinal neurones by structurally related amino acids. In *Journal of Neurochemistry* (Vol. 6).

D

da Costa, P. L. N., Sirois, P., Tannock, I. F., & Chammas, R. (2014). The role of kinin receptors in cancer and therapeutic opportunities. In *Cancer Letters* (Vol. 345, Issue 1, pp. 27–38). Elsevier Ireland Ltd. https://doi.org/10.1016/j.canlet.2013.12.009

Dahl, E. (1973). The Fine Structure of Intracerebral Vessels. In *Z. Zellforsch* (Vol. 145).

Dai, H. L., Hu, W. Y., Jiang, L. H., Li, L., Gaung, X. F., & Xiao, Z. C. (2016). p38 MAPK inhibition improves synaptic plasticity and memory in angiotensin II-dependent hypertensive mice. *Scientific Reports*, *6*. https://doi.org/10.1038/srep27600

Damisah, E. C., Hill, R. A., Tong, L., Murray, K. N., & Grutzendler, J. (2017). A fluoro-Nissl dye identifies pericytes as distinct vascular mural cells during in vivo brain imaging. *Nature Neuroscience*, *20*(7), 1023–1032. https://doi.org/10.1038/nn.4564

Darley-Usmar, V., Wiseman, H., & Halliwell, B. (1995). Nitric oxide and oxygen radicals: a question of balance. *FEBS Letters*, *369*(2–3). https://doi.org/10.1016/0014-5793(95)00764-z

Dastre, A. (1893). Fibrinolyse dans le sang. *Arch Norm Pathol*, *5*, 661–673.

Denys, J., & de Marbaix, H. (1889). Les peptonisations provoquees par le chloroforme. *Cellule*, *5*, 197–251.

Docagne, F., Nicole, O., Marti, H. H., Mackenzie, E. T., Buisson, A., & Vivien, D. (1999). *Transforming growth factor-1 as a regulator of the serpins/t-PA axis in cerebral ischemia*.

Dong, Z., Saikumar, P., Weinberg, J. M., & Venkatachalam, M. A. (1997). Technical Advance Internucleosomal DNA Cleavage Triggered by Plasma Membrane Damage during Necrotic Cell Death Involvement of Serine but Not Cysteine Proteases. In *American Journal ofPathology* (Vol. 151, Issue 5).

Drake, C. T., & Iadecola, C. (2007). The role of neuronal signaling in controlling cerebral blood flow. *Brain and Language*, *102*(2), 141–152. https://doi.org/10.1016/j.bandl.2006.08.002

Drapeau, G., Rhaleb, N.-E., Dion, S., Jukic, D., & Regoli, D. (1988). Rapid communication [Phes~(CH 2-NH) Arg 9]bradykinin, a B 2 receptor selective agonist which is not broken down by either kininase I or kininase II. In *European Journal of Pharmacology* (Vol. 155).

Dray, A., Patel, I. A., Perkins, M. N., & Rueff, A. (1992). Bradykinin-induced activation of nociceptors: receptor and mechanistic studies on the neonatal rat spinal cord-tail preparation in vitro. *British Journal of Pharmacology*, *107*(4), 1129–1134. https://doi.org/10.1111/j.1476-5381.1992.tb13418.x

Dray, A., & Perkins, M. (1993). *BradykMn and inflammatory pain*.

Drouin, J. N., St-Pierre, S. A., & Regoli, D. (1979). Receptors for bradykinin and kallidin. *Canadian Journal of Physiology and Pharmacology*, *57*(4). https://doi.org/10.1139/y79-056

Dudek, S. M., & Bear, M. F. (1992). Homosynaptic long-term depression in area CAl of hippocampus and effects of N-methyl-D-aspartate receptor blockade (long-term potentiation/hippocampal slice/synaptic plasticity/learning/memory). In *Neurobiology* (Vol. 89).

Duka, I., Kintsurashvili, E., Gavras, I., Johns, C., Bresnahan, M., & Gavras, H. (2001). *Vasoactive Potential of the B 1 Bradykinin Receptor in Normotension and Hypertension*. http://www.circresaha.org

Duling, B. R., & Berne, R. M. (1970). Propagated Vasodilation in the Microcirculation of the Hamster Cheek Pouch. *Circulation Research*, *26*(2). https://doi.org/10.1161/01.RES.26.2.163

Dzau, V. J. (2001). Tissue Angiotensin and Pathobiology of Vascular Disease A Unifying Hypothesis. http://www.hypertensionaha.org

E

Elliot, A. H., Nuzum, F. R., & Barbara, S. (1934). *The urinary excretion of a depressor substance (kallikrein of frey and kraut). In arterial hypertension**.

Emanueli, C., Maestri, R., Corradi, D., Marchione, R., Minasi, A., Tozzi, M. G., Salis, M. B., Straino, S., Capogrossi, M. C., Olivetti, G., & Madeddu, P. (1999). *Dilated and Failing Cardiomyopathy in Bradykinin B 2 Receptor Knockout Mice*. http://www.circulationaha.org

Emeis, J. J., van den Eijnden-Schrauwen, Y., van den Hoogen, C. M., de Priester, W., Westmuckett, A., & Lupu, F. (1997). An Endothelial Storage Granule for Tissue-Type Plasminogen Activator. In *The Journal of Cell Biology* (Vol. 139, Issue 1). http://www.jcb.org

Eugenie Lumbers, B. R., McCloskey, D. I., & Potter, E. K. (1979). Inhibition by angiotensin ii of baroreceptor-evoked activity in cardiac vagal efferent nerves in the dog. From the School of Physiology. In *J. Phy8iol* (Vol. 294).

Evans, R. H., Francis, A. A., Hunt, K., Oakes, D. J., & Watkins, J. C. (1979). Antagonism of excitatory amino acid-induced responses and of synaptic excitation in the isolated spinal cord of the frog. In *Br. J. Pliarmac* (Vol. 67).

F

Feldberg, W., & Lewis, G. P. (1964). The action of peptides on the adrenal medulla. release of adrenaline by bradykinin and angiotensin. In *J. Phy8iol* (Vol. 171).

Fernández-Monreal, M., López-Atalaya, J. P., Benchenane, K., Léveillé, F., Cacquevel, M., Plawinski, L., MacKenzie, E. T., Bu, G., Buisson, A., & Vivien, D. (2004). Is tissue-type plasminogen activator a neuromodulator? *Molecular and Cellular Neuroscience*, *25*(4), 594–601. https://doi.org/10.1016/j.mcn.2003.11.002

Fieldi, K. J., White, W. J., Lang, M., & Karl Field, lOr J. (1993). *Anaesthetic effects of chloral hydrate, pentobarbitone and urethane in adult male rats* (Vol. 27).

Filosa, J. A., Bonev, A. D., Straub, S. v., Meredith, A. L., Wilkerson, M. K., Aldrich, R. W., & Nelson, M. T. (2006). Local potassium signaling couples neuronal activity to vasodilation in the brain. *Nature Neuroscience*, *9*(11), 1397–1403. https://doi.org/10.1038/nn1779

Fredriksson, L., Li, H., Fieber, C., Li, X., & Eriksson, U. (2004). Tissue plasminogen activator is a potent activator of PDGF-CC. *EMBO Journal*, *23*(19), 3793–3802. https://doi.org/10.1038/sj.emboj.7600397

Freeman, R. D., & Li, B. (2016). Neural – Metabolic coupling in the central visual pathway. In *Philosophical Transactions of the Royal Society B: Biological Sciences* (Vol. 371, Issue 1705). Royal Society of London. https://doi.org/10.1098/rstb.2015.0357

Friedland, R. P., & Iadecola, C. (1991). Roy and Sherrington (1890): a centennial reexamination of “On the regulation of the blood-supply of the brain”. *Neurology*, *41*(1). https://doi.org/10.1212/wnl.41.1.10

Fulop, G. A., Ahire, C., Csipo, T., Tarantini, S., Kiss, T., Balasubramanian, P., Yabluchanskiy, A., Farkas, E., Toth, A., Nyúl-Tóth, Á., Toth, P., Csiszar, A., & Ungvari, Z. (2019). Cerebral venous congestion promotes blood-brain barrier disruption and neuroinflammation, impairing cognitive function in mice. *GeroScience*, *41*(5), 575–589. https://doi.org/10.1007/s11357-019-00110-1

Furukawa, H., Singh, S. K., Mancusso, R., & Gouaux, E. (2005). Subunit arrangement and function in NMDA receptors. *Nature*, *438*(7065), 185–192. https://doi.org/10.1038/nature04089

Gafford, J. T., Skidgel, R. A., Erdos, E. G., & Hersh, L. B. (1983). Human Kidney “Enkephalinase”, a Neutral Metalloendopeptidase That Cleaves Active Peptides? In *Biochemistry* (Vol. 22).

Ganju, P., Davis, A., Patel, S., Nunez, X., & Fox´˜, A. F. (2001). p38 stress-activated protein kinase inhibitor reverses bradykinin B 1 receptor-mediated component of inflammatory hyperalgesia. In *European Journal of Pharmacology* (Vol. 421). www.elsevier.nlrlocaterejphar

Garcia-Rocha, M., Avila, J., & Armas-Portela, R. (1994). Tissue-type plasminogen activator (tPA) is the main plasminogen activator associated with isolated rat nerve growth cones. In *Neuroscience Letters* (Vol. 180).

Girouard, H., & Iadecola, C. (2006a). Regulation of the Cerebral Circulation Neurovascular coupling in the normal brain and in hypertension, stroke, and Alzheimer disease. *J Appl Physiol*, *100*, 328–335. https://doi.org/10.1152/japplphysiol.00966.2005.-The

Girouard, H., & Iadecola, C. (2006b). Neurovascular coupling in the normal brain and in hypertension, stroke, and Alzheimer disease. In *Journal of Applied Physiology* (Vol. 100, Issue 1, pp. 328–335). https://doi.org/10.1152/japplphysiol.00966.2005

Girouard, H., Lessard, A., Capone, C., Milner, T. A., & Iadecola, C. (2008). The neurovascular dysfunction induced by angiotensin II in the mouse neocortex is sexually dimorphic. *Am J Physiol Heart Circ Phys-Iol*, *294*, 156–163. https://doi.org/10.1152/ajpheart.01137.2007.-Women

Goldblatt, H., Lynch, J., Hanzal, R. F., & Summerville, W. W. (1934). Studies on experimental hypertension: I. The production of persistent elevation of systolic blood pressure by means of renal ischemia. J Exp Med. 1934 Feb 28;59(3):347-79. doi: 10.1084/jem.59.3.347. PMID: 19870251; PMCID: PMC2132360.

Gonias, S. L. (2019). Hepatocyte tPA: where have you been hiding? *Blood*, *133*(7). https://doi.org/10.1182/blood-2018-12-891515

Gotthardt, M., Trommsdorff, M., Nevitt, M. F., Shelton, J., Richardson, J. A., Stockinger, W., Nimpf, J., & Herz, J. (2000). Interactions of the low density lipoprotein receptor gene family with cytosolic adaptor and scaffold proteins suggest diverse biological functions in cellular communication and signal transduction. *Journal of Biological Chemistry*, *275*(33), 25616–25624. https://doi.org/10.1074/jbc.M000955200

Grimwood, S., Kulagowski, J. J., Mawer, I. M., Rowley, M., Lee, P. D., & Foster, A. C. (1995). Allosteric modulation of the glutamate site on the NMDA receptor 1 four novel glycine site antagonists. In *European Journal of Pharmacology molecular pharm~ ELSEVIER Molecular Pharmacology Section* (Vol. 290).

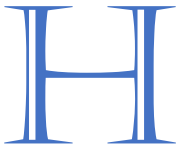

Haddad, E.-B., Fox, A. J., Rousell, J., Burgess, G., Mcintyre, P., Barnes, P. J., & Chung, K. F. (2000). *Post-Transcriptional Regulation of Bradykinin B1 and B2 Receptor Gene Expression in Human Lung Fibroblasts by Tumor Necrosis Factor-: Modulation by Dexamethasone*. http://www.molpharm.org

Hajjar, K. A., & Reynolds, C. M. (1994). α-Fucose-mediated binding and degradation of tissue-type plasminogen activator by HepG2 cells. *Journal of Clinical Investigation*, *93*(2), 703–710. https://doi.org/10.1172/JCI117023

Haley, J. E., Dickenson, A. H., & Schachter, M. (1989). *Electrophysiological evidence for a role of bradykinin in chemical nociception in the rat*.

Hamel, E. (2006). Perivascular nerves and the regulation of cerebrovascular tone. In *Journal of Applied Physiology* (Vol. 100, Issue 3, pp. 1059–1064). https://doi.org/10.1152/japplphysiol.00954.2005

Harding, J. W., Cook, V. I., Miller-Wing, A. v., Hanesworth, J. M., Sardinia, M. F., Hall, K. L., Stobb, J. W., Swanson, G. N., Coleman, J. K. M., Wright, J. W., & Harding, E. C. (1992). Identification of an AII(3–8) [AIV] binding site in guinea pig hippocampus. *Brain Research*, *583*(1–2), 340–343. https://doi.org/10.1016/S0006-8993(10)80047-2

Hardingham, G. E., & Bading, H. (2010). Synaptic versus extrasynaptic NMDA receptor signalling: Implications for neurodegenerative disorders. In *Nature Reviews Neuroscience* (Vol. 11, Issue 10, pp. 682–696). https://doi.org/10.1038/nrn2911

Hardingham, G. E., Fukunaga, Y., & Bading, H. (2002). Extrasynaptic NMDARs oppose synaptic NMDARs by triggering CREB shut-off and cell death pathways. *Nature Neuroscience*, *5*(5), 405–414. https://doi.org/10.1038/nn835

Harris, E. W., & Cotman, C. W. (1986). Long-term potentiation of guinea pig mossy fiber responses is not blocked by N-methyl D-aspartate antagonists. *Neuroscience Letters*, *70*(1). https://doi.org/10.1016/0304-3940(86)90451-9

Hartmann, D. A., Underly, R. G., Grant, R. I., Watson, A. N., Lindner, V., & Shih, A. Y. (2015). Pericyte structure and distribution in the cerebral cortex revealed by high-resolution imaging of transgenic mice. *Neurophotonics*, *2*(4), 041402. https://doi.org/10.1117/1.nph.2.4.041402

Harvey, A., Montezano, A. C., Lopes, R. A., Rios, F., & Touyz, R. M. (2016). Vascular Fibrosis in Aging and Hypertension: Molecular Mechanisms and Clinical Implications. In *Canadian Journal of Cardiology* (Vol. 32, Issue 5, pp. 659–668). Pulsus Group Inc. https://doi.org/10.1016/j.cjca.2016.02.070

Hassel, B., Paulsen, R. E., Johnsen, A., & Fonnum, F. (1992). Selective inhibition of glial cell metabolism in vivo by fluorocitrate. In *Brain Research* (Vol. 576).

Hatten, M. E. (1999). Central nervous system neuronal migration. In *Annu. Rev. Neurosci* (Vol. 22). www.annualreviews.org

Hayashi, T. (1954). Effects of sodium glutamate on the nervous system. In *Keio Journal of Medicine* (Vol. 3, Issue 4).

Hébert, M., Anfray, A., Chevilley, A., Martinez De Lizarrondo, S., Quenault, A., Louessard, M., Roussel, B. D., Obiang, P., Save, E., Orset, C., Maubert, E., Vivien, D., & Agin, V. (2017). Distant Space Processing is Controlled by tPA-dependent NMDA Receptor Signaling in the Entorhinal Cortex. *Cerebral Cortex*, *27*(10), 4783–4796. https://doi.org/10.1093/cercor/bhw275

Hedin, S. G. (1903). *On the presence of a proteolytic enzyme in the normal serum of the ox. BY*. https://doi.org/10.1113/jphysiol.1903.sp000989

Henry, V. J., Lecointre, M., Laudenbach, V., Ali, C., Macrez, R., Jullienne, A., Berezowski, V., Carmeliet, P., Vivien, D., Marret, S., Gonzalez, B. J., & Leroux, P. (2013). High t-PA release by neonate brain microvascular endothelial cells under glutamate exposure affects neuronal fate. *Neurobiology of Disease*, *50*(1), 201–208. https://doi.org/10.1016/j.nbd.2012.10.020

Herz, J., & Strickland, D. K. (2001). LRP: A multifunctional scavenger and signaling receptor. In *Journal of Clinical Investigation* (Vol. 108, Issue 6, pp. 779–784). https://doi.org/10.1172/JCI200113992

Holmes, W. E., Nelles, L., Lijnen, H. R., & Collen, D. (1987). Primary structure of human α2-antiplasmin, a serine protease inhibitor (serpin). *Journal of Biological Chemistry*, *262*(4), 1659–1664. https://doi.org/10.1016/s0021-9258(19)75687-7

Hori, T., Ohashi, N., Chen, F., Baine, A. M. T., Gardner, L. B., Hata, T., Uemoto, S., & Nguyen, J. H. (2012). Simple and reproducible hepatectomy in the mouse using the clip technique. *World Journal of Gastroenterology*, *18*(22), 2767–2774. https://doi.org/10.3748/wjg.v18.i22.2767

Hosomi, N., Lucero, J., Hoe Heo, J., Koziol, J. A., Copeland, B. R., & del Zoppo, G. J. (2001). *Rapid Differential Endogenous Plasminogen Activator Expression After Acute Middle Cerebral Artery Occlusion*. http://ahajournals.org

Houssay, B. A., & Fasciolo, J. C. (1937). *Demostración del mecanismo humoral de la hipertensión nefrógena*.

Hoylaerts, M., Rijken, D. C., Lijnen, H. R., & Collen, D. (1982). Kinetics of the activation of plasminogen by human tissue plasminogen activator. Role of fibrin.

Journal of Biological Chemistry, *257*(6), 2912–2919. https://doi.org/10.1016/s0021-9258(19)81051-7

Huber, D., Cramer, E. M., Kaufmann, J. E., Meda, P., Massé, J.-M., O Kruithof, E. K., & Vischer, U. M. (2002). *Tissue-type plasminogen activator (t-PA) is stored in Weibel-Palade bodies in human endothelial cells both in vitro and in vivo*. http://ashpublications.org/blood/article-pdf/99/10/3637/1685292/h81002003637.pdf

Hunyady, L., & Catt, K. J. (2006). Pleiotropic AT1 receptor signaling pathways mediating physiological and pathogenic actions of angiotensin II. In *Molecular Endocrinology* (Vol. 20, Issue 5, pp. 953–970). https://doi.org/10.1210/me.2004-0536

I

Iadecola, C. (1993). Regulation of the cerebral microcirculation during neural activity: is nitric oxide the missing link? *Trends in Neurosciences*, *16*(6). https://doi.org/10.1016/0166-2236(93)90156-g

Iadecola, C. (2004). Neurovascular regulation in the normal brain and in Alzheimer's disease. In *Nature Reviews Neuroscience* (Vol. 5, Issue 5, pp. 347–360). Nature Publishing Group. https://doi.org/10.1038/nrn1387

Iadecola, C. (2017). The Neurovascular Unit Coming of Age: A Journey through Neurovascular Coupling in Health and Disease. In *Neuron* (Vol. 96, Issue 1, pp. 17–42). Cell Press. https://doi.org/10.1016/j.neuron.2017.07.030

Ikeda, K., Nagasawa, M., Mori, H., Araki, K., Sakimura, K., Watanabe, M., Inoue, Y., & Mishina, M. (1992). Cloning and expression of the epsilon 4 subunit of the NMDA receptor channel. *FEBS Letters*, *313*(1). https://doi.org/10.1016/0014-5793(92)81178-o

Ikonomidou, C., Bosch, F., Miksa, M., Bittigau, P., Vöckler, J., Dikranian, K., Tenkova, T. I., Stefovska, V., Turski, L., & Olney, J. W. (1999). Blockade of NMDA receptors and apoptotic neurodegeneration in the developing brain. *Science (New York, N.Y.)*, *283*(5398). https://doi.org/10.1126/science.283.5398.70

Iliff, J. J., D'Ambrosio, R., Ngai, A. C., & Winn, H. R. (2003). Adenosine receptors mediate glutamate-evoked arteriolar dilation in the rat cerebral cortex. *American Journal of Physiology - Heart and Circulatory Physiology*, *284*(5 53-5). https://doi.org/10.1152/ajpheart.00909.2002

Inaba, S., Iwai, M., Furuno, M., Tomono, Y., Kanno, H., Senba, I., Okayama, H., Mogi, M., Higaki, J., & Horiuchi, M. (2009a). Continuous activation of renin-

angiotensin system impairs cognitive function in renin/angiotensinogen transgenic mice. *Hypertension*, *53*(2), 356–362. https://doi.org/10.1161/HYPERTENSIONAHA.108.123612

Inaba, S., Iwai, M., Tomono, Y., Senba, I., Furuno, M., Kanno, H., Okayama, H., Mogi, M., Higaki, J., & Horiuchi, M. (2009b). Exaggeration of focal cerebral ischemia in transgenic mice carrying human renin and human angiotensinogen genes. *Stroke*, *40*(2), 597–603. https://doi.org/10.1161/STROKEAHA.108.519801

Inagaki, N., Kuromi, H., Gonoi, T., Okamoto, Y., Ishida, H., Seino, Y., Kaneko, T., Iwanaga, T., & Seino, S. (1995). Expression and role of ionotropic glutamate receptors in pancreatic islet cells. *FASEB Journal : Official Publication of the Federation of American Societies for Experimental Biology*, *9*(8).

Inagami, T., Iwai, N., Sasaki, K., Guo, D. F., Furuta, H., Yamano, Y., Bardhan, S., Chaki, S., Makito, N., & Badr, K. (1993). Angiotensin II receptors: cloning and regulation. *Arzneimittel-Forschung*, *43*(2A).

Iriki, A., Pavlides, C., & Keller, A. (1988). 16. R. MacKinnon and C. Miller, unpublished observa-tion. 17. Biochemistry, in press. In *Methods Enzymol* (Vol. 105). CRC Press. www.sciencemag.org

Iturria-Medina, Y., Sotero, R. C., Toussaint, P. J., Mateos-Pérez, J. M., Evans, A. C., Weiner, M. W., Aisen, P., Petersen, R., Jack, C. R., Jagust, W., Trojanowki, J. Q., Toga, A. W., Beckett, L., Green, R. C., Saykin, A. J., Morris, J., Shaw, L. M., Khachaturian, Z., Sorensen, G., … Furst, A. J. (2016). Early role of vascular dysregulation on late-onset Alzheimer's disease based on multifactorial data-driven analysis. *Nature Communications*, *7*. https://doi.org/10.1038/ncomms11934

Iwasato, T., Datwani, A., Wolf, A. M., Nishiyama, H., Taguchi, Y., Tonegawa, S., Knöpfel, T., Erzurumlu, R. S., & Itohara, S. (2000). Cortex-restricted disruption of NMDAR1 impairs neuronal patterns in the barrel cortex. *Nature*, *406*(6797), 726–731. https://doi.org/10.1038/35021059

J

Jacobs, A., Schutte, A. E., Ricci, C., & Pieters, M. (2019). Plasminogen activator inhibitor-1 activity and the 4G/5G polymorphism are prospectively associated with blood pressure and hypertension status. *Journal of Hypertension*, *37*(12), 2361–2370. https://doi.org/10.1097/HJH.0000000000002204

Jacobsen, J. S., Comery, T. A., Martone, R. L., Elokdah, H., Crandall, D. L., Oganesian, A., Aschmies, S., Kirksey, Y., Gonzales, C., Xu, J., Zhou, H.,

Atchison, K., Wagner, E., Zaleska, M. M., Das, I., Arias, R. L., Bard, J., Riddell, D., Gardell, S. J., … Pangalos, M. N. (2008). *Enhanced clearance of A in brain by sustaining the plasmin proteolysis cascade*. www.pnas.org/cgi/content/full/

Jamieson, J. J., Searson, P. C., & Gerecht, S. (2017). Engineering the human blood-brain barrier in vitro. In *Journal of Biological Engineering* (Vol. 11, Issue 1). BioMed Central Ltd. https://doi.org/10.1186/s13036-017-0076-1

Johnson, J. W., & Ascher, P. (1987). Glycine potentiates the NMDA response in cultured mouse brain neurons. *Nature*, *325*(6104). https://doi.org/10.1038/325529a0

Jones, E. G. (1970). On the mode of entry of blood vessels into the cerebral cortex. In *J. Anat* (Vol. 106, Issue 3).

Jullienne, A., Montagne, A., Orset, C., Lesept, F., Jane, D. E., Monaghan, D. T., Maubert, E., Vivien, D., & Ali, C. (2011). Selective inhibition of GluN2D-containing N-methyl-D-aspartate receptors prevents tissue plasminogen activator-promoted neurotoxicity both in vitro and in vivo. *Molecular Neurodegeneration*, *6*(1). https://doi.org/10.1186/1750-1326-6-68

Jung, R. G., Simard, T., Labinaz, A., Ramirez, F. D., di Santo, P., Motazedian, P., Rochman, R., Gaudet, C., Faraz, M. A., Beanlands, R. S. B., & Hibbert, B. (2018). Role of plasminogen activator inhibitor-1 in coronary pathophysiology. In *Thrombosis Research* (Vol. 164, pp. 54–62). Elsevier Ltd. https://doi.org/10.1016/j.thromres.2018.02.135

Kagitani, H., Tagawa, M., Hatanaka, K., Ikari, T., Saito, A., Bando, H., Okada, K., & Matsuo, O. (1985). Expression in E. coli of finger-domain lacking tissue-type plasminogen activator with high fibrin affinity. FEBS letters, 189(1), 145–149. https://doi.org/10.1016/0014-5793(85)80860-7

Kamran, P., Sereti, K. I., Zhao, P., Ali, S. R., Weissman, I. L., & Ardehali, R. (2013). Parabiosis in mice: a detailed protocol. *Journal of Visualized Experiments : JoVE*, *80*. https://doi.org/10.3791/50556

Kaneko, M., Sakata, Y., Matsuda, M., & Mimuro, J. (1992). Interactions between the Finger and Kringle-2 Domains of Tissue-Type Plasminogen Activator and Plasminogen Activator Inhibitor-1 1. In *J. Biochem. Ill*. https://academic.oup.com/jb/article/111/2/244/874027

Kaplan, A. P., Joseph, K., Shibayama, Y., Nakazawa, Y., Ghebrehiwet, B., Reddigari, S., & Silverberg, M. (1998). *Bradykinin Formation Plasma and Tissue Pathways and Cellular Interactions*.

Kaplan, A. P., Joseph, K., & Silverberg, M. (2002). Pathways for bradykinin formation and inflammatory disease. *Journal of Allergy and Clinical Immunology*, *109*(2), 195–209. https://doi.org/10.1067/mai.2002.121316

Káradóttir, R., Cavelier, P., Bergersen, L. H., & Attwell, D. (2005). NMDA receptors are expressed in oligodendrocytes and activated in ischaemia. *Nature*, *438*(7071), 1162–1166. https://doi.org/10.1038/nature04302

Katada, J., & Majima, M. (2002). AT 2 receptor-dependent vasodilation is mediated by activation of vascular kinin generation under ¯ow conditions. In *British Journal of Pharmacology* (Vol. 136). www.nature.com/bjp

Kazama, K., Anrather, J., Zhou, P., Girouard, H., Frys, K., Milner, T. A., & Iadecola, C. (2004). Angiotensin II impairs neurovascular coupling in neocortex through NADPH oxidase-derived radicals. *Circulation Research*, *95*(10), 1019–1026. https://doi.org/10.1161/01.RES.0000148637.85595.c5

Keber, D. (1988). Mechanism of tissue plasminogen activator release during venous occlusion. *Fibrinolysis*, *2*, 96–103.

Kenny, A. J., & Maroux, S. (1982). Topo ogy of Microvillar Membrane Hydrolases of Kidney and Intestine Depal. In *REVIEWS* (Vol. 62, Issue 1). www.physiology.org/journal/physrev

Kerins, D. M., Hao, Q., & Vaughan, D. E. (1995). Angiotensin induction of PAI-1 expression in endothelial cells is mediated by the hexapeptide angiotensin IV. *Journal of Clinical Investigation*, *96*(5), 2515–2520. https://doi.org/10.1172/JCI118312

Kety, S. S. (1950). *Circulation and Metabolism of the Human Brain in Health and Disease**.

Kimura, M., Soeda, S., Oda, M., Ochiai, T., Kihara, T., Ono, N., & Shimeno, H. (2000). *Release of Plasminogen Activator Inhibitor-1 From Human Astrocytes Is Regulated by Intracellular Ceramide*.

Kisler, K., Nelson, A. R., Montagne, A., & Zlokovic, B. v. (2017). Cerebral blood flow regulation and neurovascular dysfunction in Alzheimer disease. In *Nature Reviews Neuroscience* (Vol. 18, Issue 7, pp. 419–434). Nature Publishing Group. https://doi.org/10.1038/nrn.2017.48

Kitamura, N., Kitagawa, H., Fukushima, D., Takagaki, Y., Miyata, T., & Nakanishi, S. (1985). Structural organization of the human kininogen gene and a model for its evolution. *Journal of Biological Chemistry*, *260*(14), 8610–8617. https://doi.org/10.1016/s0021-9258(17)39516-9

Kleckner, N. W., & Dingledine, R. (1988). Requirement for glycine in activation of NMDA-receptors expressed in Xenopus oocytes. *Science (New York, N.Y.)*, *241*(4867). https://doi.org/10.1126/science.2841759

Knape, J. T. A., & van Zwieten, P. A. (1988). Archivesof Pharmacology Positive chronotropic activity of angiotensin II in the pithed normotensive rat is primarily

due to activation of cardiac fll-adrenoceptors. In *Naunyn-Schmiedeberg's Arch Pharmacol* (Vol. 338).

Knipe, L., Meli, A., Hewlett, L., Bierings, R., Dempster, J., Skehel, P., Hannah, M. J., & Carter, T. (2010). A revised model for the secretion of tPA and cytokines from cultured endothelial cells. *Blood*, *116*(12), 2183–2191. https://doi.org/10.1182/blood-2010-03-276170

Knop, M., Aareskjold, E., Bode, G., & Gerke, V. (2004). Rab3D and annexin A2 play a role in regulated of vWF, but not tPA, from endothelial cells. *EMBO Journal*, *23*(15), 2982–2992. https://doi.org/10.1038/sj.emboj.7600319

Knop, M., & Gerke, V. (2002). *Ca 2+-regulated secretion of tissue-type plasminogen activator and von Willebrand factor in human endothelial cells*. www.bba-direct.com

Knot, H. J., Zimmermann, P. A., & Nelson, M. T. (1996). Extracellular K+-induced hyperpolarizations and dilatations of rat coronary and cerebral arteries involve inward rectifier K+ channels. In *Journal of Physiology* (Issue 2).

Ko, K. R., Ngai, A. C., Winn, H. R., Richard, H., & Roze, W. (1990). *Role of adenosine in regulation of regional cerebral blood flow in sensory cortex*. www.physiology.org/journal/ajpheart

Koide, M., Bonev, A. D., Nelson, M. T., & Wellman, G. C. (2012). Inversion of neurovascular coupling by subarachnoid blood depends on large-conductance Ca2+-activated K+(BK) channels. *Proceedings of the National Academy of Sciences of the United States of America*, *109*(21). https://doi.org/10.1073/pnas.1121359109

Korninger, C., Stassen, J. M., & Collen, D. (1981). Turnover of human extrinsic (tissue-type) plasminogen activator in rabbits. *Thrombosis and Haemostasis*, *46*(3).

Kraut, H., Frey EK, & Werle E. (1930). *Der Nachweis eines Kreislaufhormons in der Pankreasdrüse.(IV. Mitteilung über dieses Kreislaufhormon.)*.

Krebs, C., Fernandes, H. B., Sheldon, C., Raymond, L. A., & Baimbridge, K. G. (2003). *Functional NMDA Receptor Subtype 2B Is Expressed in Astrocytes after Ischemia In Vivo and Anoxia In Vitro*.

Krogsgaard-Larsen, P., Honore, T., Hansen, J. J., Curtis, D. R., & Lodge, D. (1980). *New class of glutamate agonist structurally related to ibotenic acid*.

Krystosek, A., & Seeds, N. W. (1981). Plasminogen activator secretion by granule neurons in cultures of developing cerebellum (protease/cell migration/tetanus toxin/histogenesis/fibrin slide assay). In *Neurobiology* (Vol. 78, Issue 12).

Kugler, P. (1982). Histochemistry of angiotensinase A in the glomerulus and the juxtaglomerular apparatus. *Kidney International. Supplement*, *12*.

Kuiper, J., Otter, M., Rijken, D. C., & van Berkel, T. J. C. (1988). Characterization of the interaction in vivo of tissue-type plasminogen activator with liver cells.

Journal of Biological Chemistry, *263*(34), 18220–18224. https://doi.org/10.1016/s0021-9258(19)81348-0

Kumar, R., & Boim, M. A. (2009). Diversity of pathways for intracellular angiotensin II synthesis. In *Current Opinion in Nephrology and Hypertension* (Vol. 18, Issue 1, pp. 33–39). https://doi.org/10.1097/MNH.0b013e32831a9e20

Kutsuwada, T., Sakimura, K., Katakura, N., Kushiya, E., & Natsume, R. (1996). Impairment of Suckling Response, Trigeminal Neuronal Pattern Formation, and Hippocampal LTD in NMDA Receptor 2 Subunit Mutant Mice The mutation hindered the formation of the whisker-related neuronal barrelette structure and the cluster-Toshiya Manabe, 3 Chitoshi Takayama, 4 ing of primary sensory afferent terminals in the brain. In *Neuron* (Vol. 16).

L

Lai, E. Y., Solis, G., Luo, Z., Carlstrom, M., Sandberg, K., Holland, S., Wellstein, A., Welch, W. J., & Wilcox, C. S. (2012). P47 phox is required for afferent arteriolar contractile responses to angiotensin II and perfusion pressure in mice. *Hypertension*, *59*(2 SUPPL. 1), 415–420. https://doi.org/10.1161/HYPERTENSIONAHA.111.184291

Lamba, D., Bauer, M., Huber, R., Fischer, S., Rudolph, R., Kohnert, U., & Bode, W. (1996). The 2.3 Å Crystal Structure of the Catalytic Domain of Recombinant Two-chain Human Tissue-type Plasminogen Activator. In *J. Mol. Biol* (Vol. 258).

Lassen, N. A. (1959). *Cerebral Blood Flow and Oxygen Consumption in Man*.

Lassen, N. A., Ingvar, D. H., & Skinhøj, E. (1978). Brain function and blood flow. *Scientific American*, *239*(4). https://doi.org/10.1038/scientificamerican1078-62

Lau, J., Rousseau, J., Kwon, D., Bénard, F., & Lin, K. S. (2020). A systematic review of molecular imaging agents targeting bradykinin B1 and B2 receptors. In *Pharmaceuticals* (Vol. 13, Issue 8, pp. 1–20). MDPI AG. https://doi.org/10.3390/ph13080199

le Meur, K., Galante, M., Angulo, M. C., & Audinat, E. (2007). Tonic activation of NMDA receptors by ambient glutamate of non-synaptic origin in the rat hippocampus. *Journal of Physiology*, *580*(2), 373–383. https://doi.org/10.1113/jphysiol.2006.123570

Lecrux, C., & Hamel, E. (2016). Neuronal networks and mediators of cortical neurovascular coupling responses in normal and altered brain states. In *Philosophical Transactions of the Royal Society B: Biological Sciences* (Vol. 371, Issue 1705). Royal Society of London. https://doi.org/10.1098/rstb.2015.0350

Lecrux, C., Toussay, X., Kocharyan, A., Fernandes, P., Neupane, S., Lévesque, M., Plaisier, F., Shmuel, A., Cauli, B., & Hamel, E. (2011). Pyramidal neurons are “neurogenic hubs” in the neurovascular coupling response to whisker stimulation. *Journal of Neuroscience*, *31*(27), 9836–9847. https://doi.org/10.1523/JNEUROSCI.4943-10.2011

Lee, H. Y., Hwang, I. Y., Im, H., Koh, J. Y., & Kim, Y. H. (2007). Non-proteolytic neurotrophic effects of tissue plasminogen activator on cultured mouse cerebrocortical neurons. *Journal of Neurochemistry*, *101*(5), 1236–1247. https://doi.org/10.1111/j.1471-4159.2007.04417.x

Lee, L. J., Lo, F. S., & Erzurumlu, R. S. (2005). NMDA receptor-dependent regulation of axonal and dendritic branching. *Journal of Neuroscience*, *25*(9), 2304–2311. https://doi.org/10.1523/JNEUROSCI.4902-04.2005

Leeb-Lundberg, L. M. F., Marceau, F., Müller-Esterl, W., Pettibone, D. J., & Zuraw, B. L. (2005). International union of pharmacology. XLV. Classification of the kinin receptor family: From molecular mechanisms to pathophysiological consequences. In *Pharmacological Reviews* (Vol. 57, Issue 1, pp. 27–77). https://doi.org/10.1124/pr.57.1.2

Lefferts, W. K., Deblois, J. P., Barreira, T. v, & Heffernan, K. S. (2018). Neurovascular coupling during cognitive activity in adults with controlled hypertension. *J Appl Physiol*, *125*, 1906–1916. https://doi.org/10.1152/japplphysiol.00100.2018.-Hypertension

Léger, C., Dupré, N., Aligny, C., Bénard, M., Lebon, A., Henry, V., Hauchecorne, M., Galas, L., Frebourg, T., Leroux, P., Vivien, D., Lecointre, M., Marret, S., & Gonzalez, B. J. (2020). Glutamate controls vessel-associated migration of GABA interneurons from the pial migratory route via NMDA receptors and endothelial protease activation. *Cellular and Molecular Life Sciences*, *77*(10), 1959–1986. https://doi.org/10.1007/s00018-019-03248-5

Leker, R. R., & Shohami, E. (2002). Cerebral ischemia and trauma-different etiologies yet similar mechanisms: neuroprotective opportunities. In *Brain Research Reviews* (Vol. 39). www.elsevier.com/locate/bres

Lemarchand, E., Maubert, E., Haelewyn, B., Ali, C., Rubio, M., & Vivien, D. (2016). Stressed neurons protect themselves by a tissue-type plasminogen activator-mediated EGFR-dependent mechanism. *Cell Death and Differentiation*, *23*(1), 123–131. https://doi.org/10.1038/cdd.2015.76

Leonetti, C., Macrez, R., Pruvost, M., Hommet, Y., Bronsard, J., Fournier, A., Perrigault, M., Machin, I., Vivien, D., Clemente, D., de Castro, F., Maubert, E., & Docagne, F. (2017). Tissue-type plasminogen activator exerts EGF-like chemokinetic effects on oligodendrocytes in white matter (re)myelination. *Molecular Neurodegeneration*, *12*(1). https://doi.org/10.1186/s13024-017-0160-5

Lesept, F., Chevilley, A., Jezequel, J., Ladépêche, L., Macrez, R., Aimable, M., Lenoir, S., Bertrand, T., Rubrecht, L., Galea, P., Lebouvier, L., Petersen, K. U., Hommet, Y., Maubert, E., Ali, C., Groc, L., & Vivien, D. (2016). Tissue-type

plasminogen activator controls neuronal death by raising surface dynamics of extrasynaptic NMDA receptors. *Cell Death and Disease*, *7*(11). https://doi.org/10.1038/cddis.2016.279

Leung, J. C., Travis, B. R., Verlander, J. W., Sandhu, S. K., Yang, S.-G., Zea, A. H., David Weiner, I., Silverstein, D. M., & Weiner, I. D. (2002). *Expression and developmental regulation of the NMDA receptor subunits in the kidney and cardiovascular system*. https://doi.org/10.1152/ajpregu.00629.2001.-An

Léveillé, F., Papadia, S., Fricker, M., Bell, K. F. S., Soriano, F. X., Martel, M. A., Puddifoot, C., Habel, M., Wyllie, D. J., Ikonomidou, C., Tolkovsky, A. M., & Hardingham, G. E. (2010). Suppression of the intrinsic apoptosis pathway by synaptic activity. *Journal of Neuroscience*, *30*(7), 2623–2635. https://doi.org/10.1523/JNEUROSCI.5115-09.2010

Levin, E. G., & Loskutofft, D. J. (1982). *Regulation of plasminogen activator production by cultured endothelial cells. Annals of the New York Academy of Sciences, 401, 184–194. https://doi.org/10.1111/j.1749-6632.1982.tb25717.x*

Levin, E. G., Marzec, U., Anderson, J., & Harker, L. A. (1984). Thrombin stimulates tissue plasminogen activator release from cultured human endothelial cells. *The Journal of Clinical Investigation*, *74*(6). https://doi.org/10.1172/JCI111620

Lian, X. Y., & Stringer, J. L. (2004). Astrocytes contribute to regulation of extracellular calcium and potassium in the rat cerebral cortex during spreading depression. *Brain Research*, *1012*(1–2), 177–184. https://doi.org/10.1016/j.brainres.2004.04.011

Lijnen, H. R. (2001). Plasmin and Matrix Metalloproteinases in Vascular Remodeling. In *Thromb Haemost* (Vol. 86).

Lin, H., Xu, L., Yu, S., Hong, W., Huang, M., & Xu, P. (2020). Therapeutics targeting the fibrinolytic system. In *Experimental and Molecular Medicine* (Vol. 52, Issue 3, pp. 367–379). Springer Nature. https://doi.org/10.1038/s12276-020-0397-x

Lindauer, U., Villringer, A., & Dirnagl, U. (1993). Characterization of CBF response to somatosensory stimulation: model and influence of anesthetics Characterization of CBF response to somatosensory stimula-tion: model and influence of anesthetics. In *Hecrrt Circ. Physiol* (Vol. 264). www.physiology.org/journal/ajpheart

Ling, Q., Jacovina, A. T., Deora, A., Febbraio, M., Simantov, R., Silverstein, R. L., Hempstead, B., Mark, W. H., & Hajjar, K. A. (2004). Annexin II regulates fibrin homeostasis and neoangiogenesis in vivo. *Journal of Clinical Investigation*, *113*(1), 38–48. https://doi.org/10.1172/jci200419684

Liot, G., Roussel, B. D., Lebeurrier, N., Benchenane, K., López-Atalaya, J. P., Vivien, D., & Ali, C. (2006). Tissue-type plasminogen activator rescues neurones from serum deprivation-induced apoptosis through a mechanism independent of its proteolytic activity. *Journal of Neurochemistry*, *98*(5), 1458–1464. https://doi.org/10.1111/j.1471-4159.2006.03982.x

Liu, D., Cheng, T., Guo, H., Fernández, J. A., Griffin, J. H., Song, X., & Zlokovic, B. v. (2004). Tissue plasminogen activator neurovascular toxicity is controlled by activated protein C. *Nature Medicine*, *10*(12), 1379–1383. https://doi.org/10.1038/nm1122

Liu, Y.-H., Yang, X.-P., Sharov, V. G., Nass, O., Sabbah, H. N., Peterson, E., & Carretero, O. A. (1997). Effects of Angiotensin-converting Enzyme Inhibitors and Angiotensin II Type 1 Receptor Antagonists in Rats with Heart Failure Role of Kinins and Angiotensin II Type 2 Receptors Key words: angiotensin-converting enzyme • angiotensin II type 1 and 2 receptors • kinins • kinin antagonist • chronic heart failure. In *J. Clin. Invest* (Vol. 99, Issue 8).

Lochner, J. E., Honigman, L. S., Grant, W. F., Gessford, S. K., Hansen, A. B., Silverman, M. A., & Scalettar, B. A. (2006). Activity-dependent release of tissue plasminogen activator from the dendritic spines of hippocampal neurons revealed by live-cell imaging. *Journal of Neurobiology*, *66*(6), 564–577. https://doi.org/10.1002/neu.20250

Lockwood, C. J., & Schatz, F. (1996). A Biological Model for the Regulation of Peri-Implantational Hemostasis and Menstruation. *Journal of the Society for Gynecologic Investigation*, *3*(4), 159–165. https://doi.org/10.1177/107155769600300401

Longden, T. A., Dabertrand, F., Koide, M., Gonzales, A. L., Tykocki, N. R., Brayden, J. E., Hill-Eubanks, D., & Nelson, M. T. (2017). Capillary K+-sensing initiates retrograde hyperpolarization to increase local cerebral blood flow. *Nature Neuroscience*, *20*(5), 717–726. https://doi.org/10.1038/nn.4533

Look, A. T., Ashmun, R. A., Shapiro, L. H., & Peiper, S. C. (1989). Human myeloid plasma membrane glycoprotein CD13 (gp150) is identical to aminopeptidase N. The Journal of clinical investigation, 83(4), 1299–1307. https://doi.org/10.1172/JCI114015

Lopez-Atalaya, J. P., Roussel, B. D., Levrat, D., Parcq, J., Nicole, O., Hommet, Y., Benchenane, K., Castel, H., Leprince, J., To Van, D., Bureau, R., Rault, S., Vaudry, H., Petersen, K. U., Santos, J. S. D. O., Ali, C., & Vivien, D. (2008). Toward safer thrombolytic agents in stroke: Molecular requirements for NMDA receptor-mediated neurotoxicity. *Journal of Cerebral Blood Flow and Metabolism*, *28*(6), 1212–1221. https://doi.org/10.1038/jcbfm.2008.14

Louessard, M., Lacroix, A., Martineau, M., Mondielli, G., Montagne, A., Lesept, F., Lambolez, B., Cauli, B., Mothet, J. P., Vivien, D., & Maubert, E. (2016). Tissue Plasminogen Activator Expression Is Restricted to Subsets of Excitatory Pyramidal Glutamatergic Neurons. *Molecular Neurobiology*, *53*(7), 5000–5012. https://doi.org/10.1007/s12035-015-9432-7

Low, C. M., & Wee, K. S. L. (2010). New insights into the not-so-new NR3 subunits of N-methyl-D-aspartate receptor: Localization, structure, and function. In *Molecular Pharmacology* (Vol. 78, Issue 1, pp. 1–11). https://doi.org/10.1124/mol.110.064006

Lu, H., Cassis, L. A., Kooi, C. W. V., & Daugherty, A. (2016). Structure and functions of angiotensinogen. In *Hypertension Research* (Vol. 39, Issue 7, pp. 492–500). Japanese Society of Hypertension. https://doi.org/10.1038/hr.2016.17

Ma, J., Ayata, C., Huang, P. L., Fishman, M. C., Moskowitz, M. A., Ma, C., Ayata, P. L., Huang, M. C., & Fishman, M. A. M. (1996). *Regional cerebral blood flow response to vibrissal stimulation in mice lacking type I NOS gene expression*. www.physiology.org/journal/ajpheart

Macdonald, M. E., van Zonneveld, A.-J., & Pannekoek, H. (1986). Functional analysis of the human tissue-type plasminogen activator protein: the light chain (Shuttle vector; recombinant DNA; transfection; S 1 mapping; chromogenic assay; functional domains; serine protease; fibrin). In *Gene* (Vol. 42).

Macrez, R., Obiang, P., Gauberti, M., Roussel, B., Baron, A., Parcq, J., Cassé, F., Hommet, Y., Orset, C., Agin, V., Bezin, L., Berrocoso, T. G., Petersen, K. U., Montaner, J., Maubert, E., Vivien, D., & Ali, C. (2011). Antibodies preventing the interaction of tissue-type plasminogen activator with N-methyl-D-aspartate receptors reduce stroke damages and extend the therapeutic window of thrombolysis. *Stroke*, *42*(8), 2315–2322. https://doi.org/10.1161/STROKEAHA.110.606293

Macrez, R., Ortega, M. C., Bardou, I., Mehra, A., Fournier, A., van der Pol, S. M. A., Haelewyn, B., Maubert, E., Lesept, F., Chevilley, A., de Castro, F., de Vries, H. E., Vivien, D., Clemente, D., & Docagne, F. (2016). Neuroendothelial NMDA receptors as therapeutic targets in experimental autoimmune encephalomyelitis. *Brain*, *139*(9), 2406–2419. https://doi.org/10.1093/brain/aww172

Madani, R., Hulo, S., Toni, N., Madani, H., Steimer, T., Muller, D., & Vassalli, J.-D. (1999). Enhanced hippocampal long-term potentiation and learning by increased neuronal expression of tissue-type plasminogen activator in transgenic mice. In *The EMBO Journal* (Vol. 18, Issue 11).

Mandle, R. J., Colmant, R. W., & Kaplan, A. P. (1976). *Identification of prekallikrein and high-molecular-weight kininogen as a complex in human plasma* (Vol. 73, Issue 11).

Mantuano, E., Lam, M. S., & Gonias, S. L. (2013). LRP1 assembles unique co-receptor systems to initiate cell signaling in response to tissue-type plasminogen activator and Myelin-associated glycoprotein. *Journal of Biological Chemistry*, *288*(47), 34009–34018. https://doi.org/10.1074/jbc.M113.509133

Mapelli, L., Gagliano, G., Soda, T., Laforenza, U., Moccia, F., & D'Angelo, E. U. (2017). Granular layer neurons control cerebellar neurovascular coupling through an NMDA receptor/NO-dependent system. *Journal of Neuroscience*, *37*(5), 1340–1351. https://doi.org/10.1523/JNEUROSCI.2025-16.2016

Marceau, F. O., Hess, J. F., & Bachvarov, D. R. (1998). *The B 1 Receptors for Kinins*. http://www.pharmrev.org

Marceau, F., & Regoli, D. (2004). Bradykinin receptor ligands: Therapeutic perspectives. In *Nature Reviews Drug Discovery* (Vol. 3, Issue 10, pp. 845–852). https://doi.org/10.1038/nrd1522

Marcic, B. M., Erd¨os, E. G., & Erd¨os, E. (1992). Gavras. In *The Journal Of Pharmacology And Experimental Therapeutics* (Vol. 294, Issue 2). Hope Study Investigators. http://www.jpet.org

Marcos-Contreras, O. A., Martinez De Lizarrondo, S., Bardou, I., Orset, C., Pruvost, M., Anfray, A., Frigout, Y., Hommet, Y., Lebouvier, L., Montaner, J., Vivien, D., & Gauberti, M. (2016). *Hyperfibrinolysis increases blood-brain barrier permeability by a plasmin-and bradykinin-dependent mechanism*. https://doi.org/10.1182/blood-2016-03

Martin, A. M., Kuhlmann, C., Trossbach, S., Jaeger, S., Waldron, E., Roebroek, A., Luhmann, H. J., Laatsch, A., Weggen, S., Lessmann, V., & Pietrzik, C. U. (2008). The functional role of the second NPXY motif of the LRP1 β-chain in tissue-type plasminogen activator-mediated activation of N-methyl-D-aspartate receptors. *Journal of Biological Chemistry*, *283*(18), 12004–12013. https://doi.org/10.1074/jbc.M707607200

Mashkina, A. P., Cizkova, D., Vanicky, I., & Boldyrev, A. A. (2010). NMDA receptors are expressed in lymphocytes activated both in vitro and in vivo. *Cellular and Molecular Neurobiology*, *30*(6), 901–907. https://doi.org/10.1007/s10571-010-9519-7

Mathis, S. A., Criscimagna, N. L., & Leeb-Lundberg, L. M. (1996). B1 and B2 kinin receptors mediate distinct patterns of intracellular Ca2+ signaling in single cultured vascular smooth muscle cells. *Molecular Pharmacology*, *50*(1).

Matys, T., Pawlak, R., Matys, E., Pavlides, C., Mcewen, B. S., & Strickland, S. (2004). *Tissue plasminogen activator promotes the effects of corticotropin-releasing factor on the amygdala and anxiety-like behavior*. www.pnas.orgcgidoi10.1073pnas.0407355101

May, P., Rohlmann, A., Bock, H. H., Zurhove, K., Marth, J. D., Schomburg, E. D., Noebels, J. L., Beffert, U., Sweatt, J. D., Weeber, E. J., & Herz, J. (2004). Neuronal LRP1 Functionally Associates with Postsynaptic Proteins and Is Required for Normal Motor Function in Mice. *Molecular and Cellular Biology*, *24*(20), 8872–8883. https://doi.org/10.1128/mcb.24.20.8872-8883.2004

Mayer, M. L. (2006). Glutamate receptors at atomic resolution. *Nature*, *440*(7083). https://doi.org/10.1038/nature04709

Mayer, M. L., Westbrook, G. L., & Guthrie, P. B. (1984). Voltage-dependent block by Mg2+ of NMDA responses in spinal cord neurones. *Nature*, *309*(5965). https://doi.org/10.1038/309261a0

McCulloch, R. M., Johnston, G. A. R., Gax~, J. A., & Curtis, D. R. (1974). The Differential Sensitivity of Spinal Interneurones and t/enshaw Cells to Kainate and N-Methyl-D-Aspartate. In *Brain Res* (Vol. 21). Springer-Verlag.

McEachern, A. E., Sheltont, E. R., Bhaktat, S., Obernoltet, R., Bacht, C., Zuppant, P., Fujisakit, J., Aldrich, R. W., & Jarnagint, K. (1991). Expression cloning of a rat B2 bradykinin receptor (oocyte expression/honnone receptor/pain/G protein-coupled receptor/rat uterus). In *Proc. Nati. Acad. Sci. USA* (Vol. 88).

McLennan, H., Huffman, R. D., & Marshall, K. C. (1968). Patterns of excitation of thalamic neurones by amino-acids and by acetylcholine. *Nature*, *219*(5152). https://doi.org/10.1038/219387a0

Medcalf, R. L. (2017). Fibrinolysis: from blood to the brain. *Journal of Thrombosis and Haemostasis*, *15*(11), 2089–2098. https://doi.org/10.1111/jth.13849

Mehra, A., Guérit, S., Macrez, R., Gosselet, F., Sevin, E., Lebas, H., Maubert, E., de Vries, H. E., Bardou, I., Vivien, D., & Docagne, F. (2020). Nonionotropic action of endothelial NMDA receptors on blood–brain barrier permeability via Rho/ROCK-mediated phosphorylation of myosin. *Journal of Neuroscience*, *40*(8), 1778–1787. https://doi.org/10.1523/JNEUROSCI.0969-19.2019

Mehta, A., Prabhakar, M., Kumar, P., Deshmukh, R., & Sharma, P. L. (2013). Excitotoxicity: Bridge to various triggers in neurodegenerative disorders. In *European Journal of Pharmacology* (Vol. 698, Issues 1–3, pp. 6–18). https://doi.org/10.1016/j.ejphar.2012.10.032

Menkes, J. G., Borkowskis, J. A., Bierilos, K. K., Macneils, T., Derrick$, A. W., Schneckg, K. A., Ransoms, R. W., Straders, C. D., Linemeyers, D. L., & Hesss, J. F. (1994). *THE JOURNAL OF BIOLOSICAL Expression Cloning of a Human B, Bradykinin Receptor** (Vol. 269, Issue 34).

Mennuni, S., Rubattu, S., Pierelli, G., Tocci, G., Fofi, C., & Volpe, M. (2014). Hypertension and kidneys: Unraveling complex molecular mechanisms underlying hypertensive renal damage. In *Journal of Human Hypertension* (Vol. 28, Issue 2, pp. 74–79). https://doi.org/10.1038/jhh.2013.55

Minai, K., Matsumoto, T., Horie, H., Ohira, N., Takashima, H., Yokohama, H., & Kinoshita, M. (2001). *Coronary Artery Disease Bradykinin Stimulates the Release of Tissue Plasminogen Activator in Human Coronary Circulation: Effects of Angiotensin-Converting Enzyme Inhibitors*.

Mishra, A. (2017). Binaural blood flow control by astrocytes: listening to synapses and the vasculature. *Journal of Physiology*, *595*(6), 1885–1902. https://doi.org/10.1113/JP270979

Molinaro, G., Gervais, N., & Adam, A. (2002). Biochemical basis of angioedema associated with recombinant tissue plasminogen activator treatment: An in vitro

experimental approach. *Stroke*, *33*(6), 1712–1716. https://doi.org/10.1161/01.STR.0000017284.77838.87

Mombouli, J.-V., Illiano, S., Nagao, T., Scott-Burden, T., & Vanhoutte, P. M. (1992). Potentiation of Endothelium-Dependent Relaxations to Bradykinin by Angiotensin I Converting Enzyme Inhibitors in Canine Coronary Artery Involves Both Endothelium-Derived Relaxing and Hyperpolarizing Factors144) KEY WORDS * bradykinin * endothelium-derived hyperpolarizing factor * nitric oxide-NG-nitro-L-arginine * angiotensin I converting enzyme * kininase II * kinin receptors. In *Circulation Research* (Vol. 71). http://ahajournals.org

Mombouli, J.-V., & Vanhoutte, P. M. (1995). KININS AND ENDOTHELIAL CONTROL OF VASCULAR SMOOTH MUSCLE. In *Annu. Rev. Pharmacol. Toxicol* (Vol. 35). www.annualreviews.org

Monyer, H., Sprengel, R., Schoepfer, R., Herb, A., Higuchi, M., Lomeli, H., Burnashev, N., Sakmann, B., & Seeburg, P. H. (1992). Heteromeric NMDA receptors: molecular and functional distinction of subtypes. *Science (New York, N.Y.)*, *256*(5060). https://doi.org/10.1126/science.256.5060.1217

Morgani, J. (1761). De sedibus et causis morborum per anatomen indagatis tomus primus. *Liber*.

Mori, H., & Mishina, M. (1995). *Review: Neurotransmitter Receptors VIII Structure and Function of the NMDA Receptor Channel* (Vol. 34, Issue 10).

Morishita, W., Marie, H., & Malenka, R. C. (2005). Distinct triggering and expression mechanisms underlie LTD of AMPA and NMDA synaptic responses. *Nature Neuroscience*, *8*(8), 1043–1050. https://doi.org/10.1038/nn1506

Mosso, A. (1880). Sulla circolazione del sangue nel cervello dell'uomo : ricerche sfigmografiche / del Angelo Mosso. *Royal College of Surgeons of England*.

Muldowney Iii, J. A. S., Vaughan, D. E., & Nashville, F. (2002). *Tissue-Type Plasminogen Activator Release New Frontiers in Endothelial Function**.

Müller-Esterl, W., Rauth, G., Lottspeich, F., Kellermann, J., & Henschen, A. (1985). Limited proteolysis of human low-molecular-mass kininogen by tissue kallikrein. Isolation and characterization of the heavy and the light chains. *European Journal of Biochemistry*, *149*(1). https://doi.org/10.1111/j.1432-1033.1985.tb08886.x

Nabavi, S., Fox, R., Alfonso, S., Aow, J., & Malinow, R. (2014). GluA1 trafficking and metabotropic NMDA: Addressing results from other laboratories inconsistent with

ours. *Philosophical Transactions of the Royal Society B: Biological Sciences*, *369*(1633). https://doi.org/10.1098/rstb.2013.0145

Nabavi, S., Kessels, H. W., Alfonso, S., Aow, J., Fox, R., & Malinow, R. (2013). Metabotropic NMDA receptor function is required for NMDA receptor-dependent long-term depression. *Proceedings of the National Academy of Sciences of the United States of America*, *110*(10), 4027–4032. https://doi.org/10.1073/pnas.1219454110

Nagaoka, M. R., Strital, E., Kouyoumdjian, M., & Borges, D. R. (2002). Participation of a galectin-dependent mechanism in the hepatic clearance of tissue-type plasminogen activator and plasma kallikrein. *Thrombosis Research*, *108*(4), 257–262. https://doi.org/10.1016/S0049-3848(02)00393-6

Nakahashi, Y., Shimamoto, K., Ura, N., Tanaka, S., Nishitani, T., Ishida, H., Yokoyama, T., Ando, T., & Iimura, O. (1986). Comprehensive studies on the renal kallikrein-kinin system in essential hypertension. *Advances in Experimental Medicine and Biology*, *198 Pt B*. https://doi.org/10.1007/978-1-4757-0154-8_44

Nakajima, C., Kulik, A., Frotscher, M., Herz, J., Schäfer, M., Bock, H. H., & May, P. (2013). Low density lipoprotein receptor-related protein 1 (LRP1) modulates N-methyl-D-aspartate (NMDA) receptor-dependent intracellular signaling and NMDA-induced regulation of postsynaptic protein complexes. *Journal of Biological Chemistry*, *288*(30), 21909–21923. https://doi.org/10.1074/jbc.M112.444364

Nakamura, S., Nakamura, I., Ma, L., Vaughan, D. E., & Fogo, A. B. (2000). Plasminogen activator inhibitor-1 expression is regulated by the angiotensin type 1 receptor in vivo1. *Kidney International*, *58*(1). https://doi.org/10.1046/j.1523-1755.2000.00160.x

Nakazawa, K., McHugh, T. J., Wilson, M. A., & Tonegawa, S. (2004). NMDA receptors, place cells and hippocampal spatial memory. In *Nature Reviews Neuroscience* (Vol. 5, Issue 5, pp. 361–372). Nature Publishing Group. https://doi.org/10.1038/nrn1385

Nassar, T., Akkawi, S., Shina, A., Haj-Yehia, A., Bdeir, K., Tarshis, M., Heyman, S. N., & Higazi, A. A. R. (2004). In vitro and in vivo effects of tPA and PAI-1 on blood vessel tone. *Blood*, *103*(3), 897–902. https://doi.org/10.1182/blood-2003-05-1685

Nassar, T., Yarovoi, S., Fanne, R. A., Akkawi, S., Jammal, M., Allen, T. C., Idell, S., Cines, D. B., & Higazi, A. A. R. (2010). Regulation of airway contractility by plasminogen activators through N-methyl-D-aspartate receptor-1. *American Journal of Respiratory Cell and Molecular Biology*, *43*(6), 703–711. https://doi.org/10.1165/rcmb.2009-0257OC

National Institute of Neurological Disorders and Stroke rt-PA Stroke Study Group. (1995). Tissue plasminogen activator for acute ischemic stroke. *The New England Journal of Medicine*, *333*(24). https://doi.org/10.1056/NEJM199512143332401

Neutel, J. M. (2004). Effect of the renin-angiotensin system on the vessel wall: Using ACE inhibition to improve endothelial function. In *Journal of Human Hypertension* (Vol. 18, Issue 9, pp. 599–606). https://doi.org/10.1038/sj.jhh.1001714

Neyses, L., & Vetter, H. (1989). Action of atrial natriuretic peptide and angiotensin II on the myocardium: studies in isolated rat ventricular cardiomyocytes. Biochemical and biophysical research communications, 163(3), 1435–1443. https://doi.org/10.1016/0006-291x(89)91139-x

Nicolakakis, N., Aboulkassim, T., Ongali, B., Lecrux, C., Fernandes, P., Rosa-Neto, P., Tong, X. K., & Hamel, E. (2008). Complete rescue of cerebrovascular function in aged Alzheimer's disease transgenic mice by antioxidants and pioglitazone, a peroxisome proliferator-activated receptor γ agonist. *Journal of Neuroscience*, *28*(37), 9287–9296. https://doi.org/10.1523/JNEUROSCI.3348-08.2008

Nicole, O., Ali, C., Docagne, F., Plawinski, L., Mackenzie, E. T., Vivien, D., & Buisson, A. (2001). *Neuroprotection Mediated by Glial Cell Line-Derived Neurotrophic Factor: Involvement of a Reduction of NMDA-Induced Calcium Influx by the Mitogen-Activated Protein Kinase Pathway*.

Nokkari, A., Abou-El-Hassan, H., Mechref, Y., Mondello, S., Kindy, M. S., Jaffa, A. A., & Kobeissy, F. (2018). Implication of the Kallikrein-Kinin system in neurological disorders: Quest for potential biomarkers and mechanisms. In *Progress in Neurobiology* (Vols. 165–167, pp. 26–50). Elsevier Ltd. https://doi.org/10.1016/j.pneurobio.2018.01.003

Norris, E. H., & Strickland, S. (2007). *Modulation of NR2B-regulated contextual fear in the hippocampus by the tissue plasminogen activator system*. www.pnas.orgcgidoi10.1073pnas.0705848104

Ny, T., Sawdey, M., Lawrence, D., Millant, J. L., & Loskutoff, D. J. (1986). Cloning and sequence of a cDNA coding for the human a-migrating endothelial-cell-type plasminogen activator inhibitor (vascular fibrinolysis/serine protease inhibitor/placental cDNA expression library/DNA sequence analysis). In *Proc. Nati. Acad. Sci. USA* (Vol. 83).

Odya, C. E., Dally, R. D., & Georgiadis, K. E. (1987). Specific, high-affinity bradykinin binding by purified porcine kidney post-proline cleaving enzyme. Biochemical pharmacology, 36(1), 39–49. https://doi.org/10.1016/0006-2952(87)90380-7

Ogawa, S., Lee, T. M., Kay, A. R., & Tank, D. W. (1990). Brain magnetic resonance imaging with contrast dependent on blood oxygenation (cerebral blood flow/brain metabolism/oxygenation). In *Proc. NatI. Acad. Sci. USA* (Vol. 87).

Oh, J., Lee, H. J., Song, J. H., Park, S. I., & Kim, H. (2014). Plasminogen activator inhibitor-1 as an early potential diagnostic marker for Alzheimer's disease. *Experimental Gerontology*, *60*, 87–91. https://doi.org/10.1016/j.exger.2014.10.004

Oikawa, T., Freeman, M., Lo, W., Vaughan, D. E., & Fogo, A. (1997). Modulation of plasminogen activator inhibitor-1 in vivo: a new mechanism for the anti-fibrotic effect of renin-angiotensin inhibition. *Kidney International*, *51*(1). https://doi.org/10.1038/ki.1997.20

Oliver, J. J., Webb, D. J., & Newby, D. E. (2005). Stimulated tissue plasminogen activator release as a marker of endothelial function in humans. In *Arteriosclerosis, Thrombosis, and Vascular Biology* (Vol. 25, Issue 12, pp. 2470–2479). https://doi.org/10.1161/01.ATV.0000189309.05924.88

Olney, J. W. (1978). *Neurotoxicity of excitatory amino acids. Kainic acid as a tool in neurobiology*.

Orth, K., Willnow, T., Herz, J., Gething, M. J., & Sambrook, J. (1994). Low density lipoprotein receptor-related protein is necessary for the internalization of both tissue-type plasminogen activator-inhibitor complexes and free tissue-type plasminogen activator. *Journal of Biological Chemistry*, *269*(33), 21117–21122. https://doi.org/10.1016/s0021-9258(17)31937-3

Osterwalder, T., Contartese, J., Stoeckli, E. T., Kuhn, T. B., & Sonderegger, P. (1996). Neuroserpin, an axonally secreted serine protease inhibitor. *EMBO Journal*, *15*(12), 2944–2953. https://doi.org/10.1002/j.1460-2075.1996.tb00657.x

Ozcan, L., Ghorpade, D. S., Zheng, Z., de Souza, J. C., Chen, K., Bessler, M., Bagloo, M., Schrope, B., Pestell, R., & Tabas, I. (2016). Hepatocyte DACH1 Is Increased in Obesity via Nuclear Exclusion of HDAC4 and Promotes Hepatic Insulin Resistance. Cell Reports, 15(10), 2214–2225. https://doi.org/10.1016/j.celrep.2016.05.006

Padró, T., Emeis, J. J., Steins, M., Schmid, K. W., & Kienast, J. (1995). Quantification of Plasminogen Activators and Their Inhibitors in the Aortic Vessel Wall in Relation to the Presence and Severity of Atherosclerotic Disease. *Arteriosclerosis, Thrombosis, and Vascular Biology*, *15*(7). https://doi.org/10.1161/01.ATV.15.7.893

Paoletti, P. (2011). Molecular basis of NMDA receptor functional diversity. In *European Journal of Neuroscience* (Vol. 33, Issue 8, pp. 1351–1365). Blackwell Publishing Ltd. https://doi.org/10.1111/j.1460-9568.2011.07628.x

Paoletti, P., Ascher, P., & Neyton, J. (1997). *High-Affinity Zinc Inhibition of NMDA NR1-NR2A Receptors*.

Paoletti, P., Bellone, C., & Zhou, Q. (2013). NMDA receptor subunit diversity: Impact on receptor properties, synaptic plasticity and disease. In *Nature Reviews Neuroscience* (Vol. 14, Issue 6, pp. 383–400). Nature Publishing Group. https://doi.org/10.1038/nrn3504

Paoletti, P., & Neyton, J. (2007). *NMDA receptor subunits: function and pharmacology. NMDA receptor subunits: function and pharmacology*. https://doi.org/10.1016/j.coph.2006.08.011ï

Parcq, J., Bertrand, T., Baron, A. F., Hommet, Y., Anglès-Cano, E., & Vivien, D. (2013). Molecular requirements for safer generation of thrombolytics by bioengineering the tissue-type plasminogen activator A chain. *Journal of Thrombosis and Haemostasis*, *11*(3), 539–546. https://doi.org/10.1111/jth.12128

Park, L., Gallo, E. F., Anrather, J., Wang, G., Norris, E. H., Paul, J., Strickland, S., & Iadecola, C. (2008). *Key role of tissue plasminogen activator in neurovascular coupling*. www.pnas.orgcgidoi10.1073pnas.0708823105

Park, L., Zhou, J., Koizumi, K., Wang, G., Anfray, A., Ahn, S. J., Seo, J., Zhou, P., Zhao, L., Paul, S., Anrather, J., & Iadecola, C. (2020). TPA deficiency underlies neurovascular coupling dysfunction by amyloid-b. *Journal of Neuroscience*, *40*(42), 8160–8173. https://doi.org/10.1523/JNEUROSCI.1140-20.2020

Parmer, R. J., Mahata, M., Mahata, S., Sebald, M. T., O'Connor, D. T., & Miles, L. A. (1997). Tissue plasminogen activator (t-PA) is targeted to the regulated secretory pathway: Catecholamine storage vesicles as a reservoir for the rapid release of t-PA. *Journal of Biological Chemistry*, *272*(3), 1976–1982. https://doi.org/10.1074/jbc.272.3.1976

Pasquet, N., Douceau, S., Naveau, M., Lesept, F., Louessard, M., Lebouvier, L., Hommet, Y., Vivien, D., & Bardou, I. (2019). Tissue-Type Plasminogen Activator Controlled Corticogenesis Through a Mechanism Dependent of NMDA Receptors Expressed on Radial Glial Cells. *Cerebral Cortex*, *29*(6), 2482–2498. https://doi.org/10.1093/cercor/bhy119

Paulsen, R. E., Contestabile, A., Villani, L., & Fonnum, F. (1987). An In Vivo Model for Studying Function of Brain Tissue Temporarily Devoid of Glial Cell Metabolism: The Use of Fluorocitrate. In *Journal ofNeurochemistry Raven Press*.

Paulson, O. B., & Newman, E. A. (1987). Does the release of potassium from astrocyte endfeet regulate cerebral blood flow? *Science (New York, N.Y.)*, *237*(4817). https://doi.org/10.1126/science.3616619

Pawela, C. P., Biswal, B. B., Hudetz, A. G., Schulte, M. L., Li, R., Jones, S. R., Cho, Y. R., Matloub, H. S., & Hyde, J. S. (2009). A protocol for use of medetomidine

anesthesia in rats for extended studies using task-induced BOLD contrast and resting-state functional connectivity. *NeuroImage*, *46*(4), 1137–1147. https://doi.org/10.1016/j.neuroimage.2009.03.004

Pawlak, R., Magarinos, A. M., Melchor, J., McEwen, B., & Strickland, S. (2003). Tissue plasminogen activator in the amygdala is critical for stress-induced anxiety-like behavior. *Nature Neuroscience*, *6*(2), 168–174. https://doi.org/10.1038/nn998

Pawlak, R., Nagai, N., Urano, T., Napiorkowska-Pawlak, D., Ihara, H., Takada, Y., Collen, D., & Takada, A. (2002). *Rapid, specific and active site-catalyzed effect of tissue-plasminogen activator on hippocampus-dependent learning in mice*. www.neuroscience-ibro.com

Pawlak, R., Shankaranarayana Rao, B. S., Melchor, J. P., Chattarji, S., Mcewen, B., & Strickland, S. (2005). Tissue plasminogen activator and plasminogen mediate stress-induced decline of neuronal and cognitive functions in the mouse hippocampus. In *PNAS December* (Vol. 13). www.pnas.orgcgidoi10.1073pnas.0509232102

Peach, M. J. (1977). Renin-Angiotensin System: Biochemistry and Mechanisms of Action. In *Reviews* (Vol. 57, Issue 2).

Pennica, D., Holmes, W. E., Kohr, W. J., Harkins, R. N., Vehar, G. A., Ward, C. A., Bennett, W. F., Yelverton, E., Seeburg, P. H., Heyneker, H. L., Goeddel, D. v., & Collen, D. (1983). Cloning and expression of human tissue-type plasminogen activator cDNA in E. coli. *Nature*, *301*(5897). https://doi.org/10.1038/301214a0

Perkins, M. N., Campbell, E., & Dray, A. (1993). Antinociceptive activity of the bradykinin B, and B, receptor antagonists, des-Arg', [Leu']-BK and HOE 140, in two models of persistent hyperalgesia in the rat. In *Pain* (Vol. 53).

Pesquero, J. B., Araujo, R. C., Heppenstall, P. A., Stucky, C. L., Silva, J. A., Walther, T., Oliveira, S. M., Pesquero, J. L., M Paiva, A. C., Calixto, J. B., Lewin, G. R., & Bader, M. (2000). *Hypoalgesia and altered inflammatory responses in mice lacking kinin B1 receptors* (Vol. 97, Issue 14). www.pnas.org

Petäjä, J. (1989). Fibrinolytic response to venous occlusion for 10 and 20 minutes in healthy subjects and in patients with deep vein thrombosis. *Thrombosis Research*, *56*(2). https://doi.org/10.1016/0049-3848(89)90167-9

Petersen, C. C. H. (2007). The functional organization of the barrel cortex. In *Neuron* (Vol. 56, Issue 2, pp. 339–355). https://doi.org/10.1016/j.neuron.2007.09.017

Pfeffer, J. M., Pfeffer, M. A., Mirsky, I., & Braunwald, E. (1982). Regression of left ventricular hypertrophy and prevention of left ventricular dysfunction by captopril in the spontaneously hypertensive rat (hemodynamics/pressure-volume relationship/ejection fraction-afterload relationship). In *Proc. NatL Acad. Sci. USA* (Vol. 79).

Piana, R. N., Wang, S. Y., Friedman, M., & Sellke, F. W. (1996). Angiotensin-converting enzyme inhibition preserves endothelium-dependent coronary

microvascular responses during short-term ischemia-reperfusion. *Circulation*, *93*(3). https://doi.org/10.1161/01.cir.93.3.544

Ping Zhang, L., Takahara, T., Yata, Y., Furui, K., Jin, B., Kawada, N., & Watanabe, A. (1999). Increased expression of phninogen activator and phsminogen activator inhibitor during liver fibrogenesis of ratx role of stellate cells. *Journal of Hepatology*, *31*, 703–711.

Pittman, R. N. (1985). Release of plasminogen activator and a calcium-dependent metalloprotease from cultured sympathetic and sensory neurons. *Developmental Biology*, *110*(1). https://doi.org/10.1016/0012-1606(85)90067-3

Popoli, M., Yan, Z., McEwen, B. S., & Sanacora, G. (2012). The stressed synapse: The impact of stress and glucocorticoids on glutamate transmission. In *Nature Reviews Neuroscience* (Vol. 13, Issue 1, pp. 22–37). https://doi.org/10.1038/nrn3138

Popov, V. M., Wu, K., Zhou, J., Powell, M. J., Mardon, G., Wang, C., & Pestell, R. G. (2010). The Dachshund gene in development and hormone-responsive tumorigenesis. In *Trends in Endocrinology and Metabolism* (Vol. 21, Issue 1, pp. 41–49). https://doi.org/10.1016/j.tem.2009.08.002

Porrello, E. R., Delbridge, L. M. D., & Thomas, W. G. (2009). The angiotensin II type 2 (AT 2) receptor: an enigmatic seven transmembrane receptor. In *Frontiers in Bioscience* (Vol. 14).

Porter, J. T., & Mccarthy, K. D. (1996). *Hippocampal Astrocytes In Situ Respond to Glutamate Released from Synaptic Terminals*.

Pruneau, D., Bélichard, P., Sahel, J.-A., & Combal, J.-P. (2010). Targeting the kallikrein-kinin system as a new therapeutic approach to diabetic retinopathy. *Current Opinion in Investigational Drugs (London, England : 2000)*, *11*(5).

Qian, Z., Gilbert, M. E., Colicos, M. A., Kandel, E. R., & Kuhl, D. (1993). Tissue-plasminogen activator is induced as an immediate-early gene during seizure, kindling and long-term potentiation. *Nature*, *361*(6411). https://doi.org/10.1038/361453a0

R

Rahman, A. M., Murrow, J. R., Ozkor, M. A., Kavtaradze, N., Lin, J., de Staercke, C., Hooper, W. C., Manatunga, A., Hayek, S., & Quyyumi, A. A. (2014). Endothelium-derived hyperpolarizing factor mediates bradykinin-stimulated tissue plasminogen activator release in humans. *Journal of Vascular Research*, *51*(3), 200–208. https://doi.org/10.1159/000362666

Raichle, M. E., & Gusnard, D. A. (2002). *Appraising the brain's energy budget*. www.pnas.orgcgidoi10.1073pnas.172399499

Raidoo, D. M., Ramsaroop, R., Naidoo, S., Muller-Esterl, W., & Bhoola, K. D. (1997). Kinin receptors in human vascular tissue: their role in atheromatous disease. In *Immunopharmacology* (Vol. 36).

Rakic, P. (1988). Defects of neuronal migration and the pathogenesis of cortical malformations. *Progress in Brain Research*, *73*. https://doi.org/10.1016/s0079-6123(08)60494-x

Ramoa, A. S., Mower, A. F., Liao, D., & Jafri, S. I. A. (2001). *Suppression of Cortical NMDA Receptor Function Prevents Development of Orientation Selectivity in the Primary Visual Cortex*.

Regoli, D., Barabé, J., & Park, W. K. (1977). Receptors for bradykinin in rabbit aortae. *Canadian Journal of Physiology and Pharmacology*, *55*(4). https://doi.org/10.1139/y77-115

Regoli, D., Marceau, F., & Barabé, J. (1978). De novo formation of vascular receptors for bradykinin. *Canadian Journal of Physiology and Pharmacology*, *56*(4). https://doi.org/10.1139/y78-109

Regolit, D., & Barabef, J. (1980). *Pharmacology of Bradykinin and Related Kinins** (Vol. 32, Issue 1).

Reijerkerk, A., Kooij, G., van der Pol, S. M. A., Leyen, T., Lakeman, K., van het Hof, B., Vivien, D., & de Vries, H. E. (2010). The NR1 subunit of NMDA receptor regulates monocyte transmigration through the brain endothelial cell barrier. *Journal of Neurochemistry*, *113*(2), 447–453. https://doi.org/10.1111/j.1471-4159.2010.06598.x

Rhaleb, N.-E., Yang, X.-P., Nanba, M., Shesely, E. G., & Carretero, O. A. (2001). *Effect of Chronic Blockade of the Kallikrein-Kinin System on the Development of Hypertension in Rats*. http://www.hypertensionaha.org

Ricagno, S., Caccia, S., Sorrentino, G., Antonini, G., & Bolognesi, M. (2009). Human Neuroserpin: Structure and Time-Dependent Inhibition. *Journal of Molecular Biology*, *388*(1), 109–121. https://doi.org/10.1016/j.jmb.2009.02.056

Rijken, D. C., & Collen, D. (1981). Purification and Characterization of the Plasminogen Activator Secreted by Human Melanoma Cells in Culture*. In *THE JOURNAL OF BIOLOGICAL CHEMISTVY* (Vol. 2, Issue 13).

Rijken, D. C., Hoylaerts, M., & Collen, D. (1982). Fibrinolytic properties of one-chain and two-chain human extrinsic (tissue-type) plasminogen activator. *Journal of Biological Chemistry*, *257*(6), 2920–2925. https://doi.org/10.1016/s0021-9258(19)81052-9

Rijken, D. C., & Lijnen, H. R. (2009). New insights into the molecular mechanisms of the fibrinolytic system. *Journal of Thrombosis and Haemostasis : JTH*, *7*(1). https://doi.org/10.1111/j.1538-7836.2008.03220.x

Rijken, D. C., Otter, M., Kuiper, J., & van Berkel, T. J. C. (1990). RECEPTOR-MEDIATED ENDOCYTOSIS OF TISSUE-TYPE PLASMINOGEN ACTIVATOR (t-PA) BY LIVER CELLS. In *THROMBOSIS RESEARCH Supplement*.

Robert Tigerstedt, V., & Bergman, P. G. (1898). *Niere und* Kreislauf. Skandinavisches Archiv Für Physiologie, 8: 223-271. https://doi.org/10.1111/j.1748-1716.1898.tb00272.x

Rocha, M., Silva, E., Beraldof, W. T., & Rosenfeld, G. (1949). *A HYPOTENSIVE AND SMOOTH MUSCLE STIMULATING FACTOR RELEASED FROM PLASMA GLOBULIN BY SNAKE VENOMS AND BY TRYPSIN*. www.physiology.org/journal/ajplegacy

Roggendorf, W., & Cerv6s-Navarro, J. (1977). Ultrastructure of Arterioles in the Cat Brain. In *Cell and Tissue Research* ~ (Vol. 178). Springer-Verlag.

Rogove, A. D., Siao, C., Keyt, B., Strickland, S., & Tsirka, S. E. (1999). Activation of microglia reveals a non-proteolytic cytokine function for tissue plasminogen activator in the central nervous system. *Journal of Cell Science*, *112 (Pt 22)*.

Rouf, S. A., Moo-Young, M., & Chisti, Y. (1996). TISSUE-TYPE PLASMINOGEN ACTIVATOR: CHARACTERISTICS, APPLICATIONS AND PRODUCTION TECHNOLOGY. In *Biotechnology Advances* (Vol. 14, Issue 3).

Roy, C. S., & Sherrington, C. S. (1890). On the Regulation of the Blood-supply of the Brain. *The Journal of Physiology*, *11*(1–2). https://doi.org/10.1113/jphysiol.1890.sp000321

Rubin, L. L., & Staddon, J. M. (1998). The cell biology of the blood-brain barrier. Annual review of neuroscience, 22, 11–28. https://doi.org/10.1146/annurev.neuro.22.1.11

Ruiz-Ortega, M., Lorenzo, O., Rupérez, M., Esteban, V., Suzuki, Y., Mezzano, S., Plaza, J. J., & Egido, J. (2001). *Role of the Renin-Angiotensin System in Vascular Diseases Expanding the Field*. http://www.hypertensionaha.org

S

Sabatini, F., Luppi, F., Petecchia, L., Stefano, A. di, Longo, A. M., Eva, A., Vanni, C., Hiemstra, P. S., Sterk, P. J., Sorbello, V., Fabbri, L. M., Rossi, G. A., & Ricciardolo, F. L. M. (2013). Bradykinin-induced asthmatic fibroblast/myofibroblast activities via bradykinin B2 receptor and different MAPK pathways. *European Journal of Pharmacology*, *710*(1–3), 100–109. https://doi.org/10.1016/j.ejphar.2013.03.048

Sadler, J. E. (1998). Biochemistry and genetics of von willebrand factor. In *Annu. Rev. Biochem* (Vol. 67). www.annualreviews.org

Sakai, K., Agassandian, K., Morimoto, S., Sinnayah, P., Cassell, M. D., Davisson, R. L., & Sigmund, C. D. (2007). Local production of angiotensin II in the subfornical organ causes elevated drinking. *Journal of Clinical Investigation*, *117*(4), 1088–1095. https://doi.org/10.1172/JCI31242

Salame, M. Y., Samani, N. J., Masood, I., & Debono, D. P. (2000). Expression of the plasminogen activator system in the human vascular wall. In *Atherosclerosis* (Vol. 152). www.elsevier.com/locate/atherosclerosis

Samad, F., Yamamoto, K., & Loskutoff, D. J. (1996). Distribution and regulation of plasminogen activator inhibitor-1 in murine adipose tissue in vivo: Induction by tumor necrosis factor-α and lipopolysaccharide. *Journal of Clinical Investigation*, *97*(1), 37–46. https://doi.org/10.1172/JCI118404

Samson, A. L., Nevin, S. T., Croucher, D., Niego, B., Daniel, P. B., Weiss, T. W., Moreno, E., Monard, D., Lawrence, D. A., & Medcalf, R. L. (2008). Tissue-type plasminogen activator requires a co-receptor to enhance NMDA receptor function. *Journal of Neurochemistry*, *107*(4), 1091–1101. https://doi.org/10.1111/j.1471-4159.2008.05687.x

Sappino, A.-P., Madani, R., Huarte, J., Belin, D., Jozsef, $, Kiss, Z., Wohlwend, A., & Vassalli, J.-D. (1993). *Extracellular Proteolysis in the Adult Murine Brain*.

Saxena, A., Little, J. T., Nedungadi, T. P., & Cunningham, J. T. (2015). Angiotensin II type 1a receptors in subfornical organ contribute towards chronic intermittent hypoxia-associated sustained increase in mean arterial pressure. *Am J Physiol Heart Circ Physiol*, *308*, 435–446. https://doi.org/10.1152/ajpheart.00747.2014.-Sleep

Schalekamp, M. A., & M Derkx, F. H. (1981). *Plasma kallikrein and plasmin as activators of prorenin: links between the renin-angiotensin system and other proteolytic systems in plasma* (Vol. 61).

Schieffer, B., Schieffer, E., Hilfiker-Kleiner, D., Hilfiker, A., Petri, ;, Kovanen, T., Kaartinen, M., Nussberger, J., Harringer, W., & Drexler, H. (2000). *Expression of Angiotensin II and Interleukin 6 in Human Coronary Atherosclerotic Plaques Potential Implications for Inflammation and Plaque Instability*. http://www.circulationaha.org

Schmidt, C. F., & Hendrix, J. P. (1938). The action of chemical substances on cerebral blood vessels. *Res Publ Assoc Res Nerv Ment Dis*, *18*, 229–276.

Schoepp, D. D., Jane, D. E., & Monn, J. A. (1999). Pharmacological agents acting at subtypes of metabotropic glutamate receptors. In *Neuropharmacology* (Vol. 38). www.elsevier.com/locate/neuropharm

Seeds, N. W., Basham, M. E., & Haffke, S. P. (1999). Neuronal migration is retarded in mice lacking the tissue plasminogen activator gene. *Proceedings of the National Academy of Sciences of the United States of America*, *96*(24). https://doi.org/10.1073/pnas.96.24.14118

Segal, S. S. (2015). Integration and modulation of intercellular signaling underlying blood flow control. In *Journal of Vascular Research* (Vol. 52, Issue 2, pp. 136–157). S. Karger AG. https://doi.org/10.1159/000439112

Sen, S., Tarazi, R. C., Khairallah, P. A., & Bumpus, F. M. (1974). *Cardiac Hypertrophy in Spontaneously Hypertensive Rats*. http://ahajournals.org

Sharp, C. D., Fowler, M., Iv, J., Houghton, J., Warren, A., Nanda, A., Chandler, I., Cappell, B., Long, A., Minagar, A., & Alexander, J. S. (2003). *Human Neuroepithelial Cells Express NMDA Receptors*. http://www.biomedcentral.com/1471-2202/4/28

Sharp, C. D., Hines, I., Houghton, J., Warren, A., Jackson IV, T. H., Jawahar, A., Nanda, A., Elrod, J. W., Long, A., Chi, A., Minagar, A., & Alexander, J. S. (2003). Glutamate causes a loss in human cerebral endothelial barrier integrity through activation of NMDA receptor. *American Journal of Physiology - Heart and Circulatory Physiology*, *285*(6 54-6). https://doi.org/10.1152/ajpheart.00520.2003

Sheikh, I. A., & Kaplan, A. P. (1986a). Studies of the digestion of bradykinin, Lys-bradykinin, and des-Arg9-bradykinin by angiotensin converting enzyme. Biochemical pharmacology, 35(12), 1951–1956. https://doi.org/10.1016/0006-2952(86)90726-4

Sheikh, I. A., & Kaplan, A. P. (1989). Mechanism of digestion of bradykinin and lysylbradykinin (kallidin) in human serum. Role of carboxypeptidase, angiotensin-converting enzyme and determination of final degradation products. Biochemical pharmacology, 38(6), 993–1000. https://doi.org/10.1016/0006-2952(89)90290-6

Shi, K., Zou, M., Jia, D. M., Shi, S., Yang, X., Liu, Q., Dong, J. F., Sheth, K. N., Wang, X., & Shi, F. D. (2021). TPA Mobilizes Immune Cells That Exacerbate Hemorrhagic Transformation in Stroke. *Circulation Research*, 62–75. https://doi.org/10.1161/CIRCRESAHA.120.317596

Shibata, M., Yamada, S., Ram Kumar, S., Calero, M., Bading, J., Frangione, B., Holtzman, D. M., Miller, C. A., Strickland, D. K., Ghiso, J., & Zlokovic, B. v. (2000). Clearance of Alzheimer's amyloid-β1-40 peptide from brain by LDL receptor-related protein-1 at the blood-brain barrier. *Journal of Clinical Investigation*, *106*(12), 1489–1499. https://doi.org/10.1172/JCI10498

Shin, C. Y., Kundel, M., & Wells, D. G. (2004). Rapid, activity-induced increase in tissue plasminogen activator is mediated by metabotropic glutamate receptor-dependent mRNA translation. *Journal of Neuroscience*, *24*(42), 9425–9433. https://doi.org/10.1523/JNEUROSCI.2457-04.2004

Shinozaki, H., & Konishi, S. (1970). Actions of several anthelmintics and insecticides on rat cortical neurones. *Brain Research*, *24*(2). https://doi.org/10.1016/0006-8993(70)90122-8

Siao, C.-J., Fernandez, S. R., & Tsirka, S. E. (2003). *Cell Type-Specific Roles for Tissue Plasminogen Activator Released by Neurons or Microglia after Excitotoxic Injury*.

Siao, C.-J., & Tsirka, S. E. (2002). *Tissue Plasminogen Activator Mediates Microglial Activation via Its Finger Domain through Annexin II*.

Sibony, M., Gasc, J.-M., Soubrier, F., Alhenc-Gelas, F., & Corvol, P. (1993). *Gene Expression and Tissue Localization of the Two Isoforms of Angiotensin I Converting Enzyme*. http://ahajournals.org

Silva, A. C., & Koretsky, A. P. (2002). Laminar specificity of functional MRI onset times during somatosensory stimulation in rat. In *National Institutes of Health*. www.pnas.orgcgidoi10.1073pnas.222561899

Sinclair, M. D. (2003). A review of the physiological effects of □ 2-agonists related to the clinical use of medetomidine in small animal practice. In *Can Vet J* (Vol. 44).

Sokoloff, L. (1996). Circulation in the Central Nervous System. In U. Greger Rainer and Windhorst (Ed.), *Comprehensive Human Physiology: From Cellular Mechanisms to Integration* (pp. 561–578). Springer Berlin Heidelberg. https://doi.org/10.1007/978-3-642-60946-6_29

Sokoloff, L., Mangold, R., Wechsler, R. L., Kenney, C., & Kety, S. S. (1955). The effect of mental arithmetic on cerebral circulation and metabolism. *The Journal of Clinical Investigation*, *34*(7, Part 1), 1101–1108. https://doi.org/10.1172/jci103159

Song, Y., Nagaoka, T., Yoshioka, T., Nakabayashi, S., Tani, T., & Yoshida, A. (2015). Role of glial cells in regulating retinal blood flow during flicker-induced hyperemia in cats. *Investigative Ophthalmology and Visual Science*, *56*(12), 7551–7559. https://doi.org/10.1167/iovs.15-17676

Soreq, H., & Miskin, R. (1983). Plasminogen Activator in the Developing Rat Cerebellum: Biosynthesis and Localization in Granular Neurons. In *Developmental Brain Research* (Vol. 11).

Soubrier, F., Alhenc-Gelas, F., Hubert, C., Allegrini, J., John, M., Tregear, G., & Corvol, P. (1988). Two putative active centers in human angiotensin I-converting enzyme revealed by molecular cloning. Proceedings of the National Academy of Sciences of the United States of America, 85(24), 9386–9390. https://doi.org/10.1073/pnas.85.24.9386

Sparks, M. A., Crowley, S. D., Gurley, S. B., Mirotsou, M., & Coffman, T. M. (2014). Classical renin-angiotensin system in kidney physiology. *Comprehensive Physiology*, *4*(3), 1201–1228. https://doi.org/10.1002/cphy.c130040

Sparks, M. A., Stegbauer, J., Chen, D., Gomez, J. A., Griffiths, R. C., Azad, H. A., Herrera, M., Gurley, S. B., & Coffman, T. M. (2015). Vascular type 1A angiotensin II receptors control BP by regulating renal blood flow and urinary sodium excretion. *Journal of the American Society of Nephrology*, *26*(12), 2953–2962. https://doi.org/10.1681/ASN.2014080816

Sprengers, E. D., & Kluft, C. (1987). Plasminogen activator inhibitors. *Blood*, *69*(2).

Starkopf, J., Bugge, E., & Ytrehus, K. (1997). Preischaemic bradykinin and ischaemic preconditioning in functional recovery of the globally ischaemic rat heart. In *Research Cardiovascular Research* (Vol. 33). https://academic.oup.com/cardiovascres/article/33/1/63/297279

Steins, M. B., Padró, T., Li, C.-X., Mesters, R. M., Ostermann, H., Hammel, D., Scheld, H. H., Berdel, W. E., & Kienast, J. (1999). Overexpression of tissue-type plasminogen activator in atherosclerotic human coronary arteries. In *Atherosclerosis* (Vol. 145).

Steranka, L. R., Manningt, D. C., Dehaas, C. J., Ferkany, J. W., Borosky, S. A., Connor, J. R., Vavrekt, R. J., Stewartt, J. M., & Snydert, S. H. (1988). Bradykinin as a pain mediator: Receptors are localized to sensory neurons, and antagonists have analgesic actions (spinal cord-dorsal horn/inflammatory pain/hyperalgesia/nociceptors/primary afferents). In *Proc. Nati. Acad. Sci. USA* (Vol. 85).

Storck, S. E., & Pietrzik, C. U. (2017). Endothelial LRP1 – A Potential Target for the Treatment of Alzheimer's Disease: Theme: Drug Discovery, Development and Delivery in Alzheimer's Disease Guest Editor: Davide Brambilla. In *Pharmaceutical Research* (Vol. 34, Issue 12, pp. 2637–2651). Springer New York LLC. https://doi.org/10.1007/s11095-017-2267-3

Stringer, J. L., & Aribi, A. M. (2003). Effects of glial toxins on extracellular acidification in the hippocampal CA1 region in vivo. *Epilepsy Research*, *54*(2–3), 163–170. https://doi.org/10.1016/S0920-1211(03)00064-0

Su, E. J., Cao, C., Fredriksson, L., Nilsson, I., Stefanitsch, C., Stevenson, T. K., Zhao, J., Ragsdale, M., Sun, Y. Y., Yepes, M., Kuan, C. Y., Eriksson, U., Strickland, D. K., Lawrence, D. A., & Zhang, L. (2017). Microglial-mediated PDGF-CC activation increases cerebrovascular permeability during ischemic stroke. *Acta Neuropathologica*, *134*(4), 585–604. https://doi.org/10.1007/s00401-017-1749-z

Su, E. J., Fredriksson, L., Geyer, M., Folestad, E., Cale, J., Andrae, J., Gao, Y., Pietras, K., Mann, K., Yepes, M., Strickland, D. K., Betsholtz, C., Eriksson, U., & Lawrence, D. A. (2008). Activation of PDGF-CC by tissue plasminogen activator impairs blood-brain barrier integrity during ischemic stroke. *Nature Medicine*, *14*(7), 731–737. https://doi.org/10.1038/nm1787

Suzuki, Y., Mogami, H., Ihara, H., & Urano, T. (2009). *Unique secretory dynamics of tissue plasminogen activator and its modulation by plasminogen activator inhibitor-1 in vascular endothelial cells*. *113*, 470–478. https://doi.org/10.1182/blood-2008-03

Sweeney, M. D., Kisler, K., Montagne, A., Toga, A. W., & Zlokovic, B. v. (2018). The role of brain vasculature in neurodegenerative disorders. In *Nature Neuroscience* (Vol. 21, Issue 10, pp. 1318–1331). Nature Publishing Group. https://doi.org/10.1038/s41593-018-0234-x

Szabo, R., Samson, A. L., Lawrence, D. A., Medcalf, R. L., & Bugge, T. H. (2016). Passenger mutations and aberrant gene expression in congenic tissue plasminogen activator-deficient mouse strains. *Journal of Thrombosis and Haemostasis*, *14*(8), 1618–1628. https://doi.org/10.1111/jth.13338

Tachias, K., & Madison, E. L. (1997). Converting tissue type plasminogen activator into a zymogen: Important role of Lys156. *Journal of Biological Chemistry*, *272*(1), 28–31. https://doi.org/10.1074/jbc.272.1.28

Takagaki, Y., Kitamura, N., & Nakanishi, S. (1985). Cloning and sequence analysis of cDNAs for human high molecular weight and low molecular weight prekininogens: Primary structures of two human prekininogens. *Journal of Biological Chemistry*, *260*(14), 8601–8609. https://doi.org/10.1016/s0021-9258(17)39515-7

Tallini, Y. N., Brekke, J. F., Shui, B., Doran, R., Hwang, S. M., Nakai, J., Salama, G., Segal, S. S., & Kotlikoff, M. I. (2007). Propagated endothelial Ca2+ waves and arteriolar dilation in vivo: Measurements in Cx40BAC-GCaMP2 transgenic mice. *Circulation Research*, *101*(12), 1300–1309. https://doi.org/10.1161/CIRCRESAHA.107.149484

Tang, C.-M., Dichter, M., & Morad, M. (1990). Modulation of the N-methyl-D-aspartate channel by extracellular H'. In *Proc. Natl. Acad. Sci. USA* (Vol. 87).

Tanner, F. C., Noll, G., Boulanger, C. M., & Liischer, T. F. (1991). *Oxidized Low Densit Lipoproteins Inhibit Relaxations of Porcine Coronary Arteries Role of*

Scavenger Receptor and Endothelium-Derived Nitric Oxide. http://ahajournals.org

Tarantini, S., Tran, C. H. T., Gordon, G. R., Ungvari, Z., & Csiszar, A. (2017). Impaired neurovascular coupling in aging and Alzheimer's disease: Contribution of astrocyte dysfunction and endothelial impairment to cognitive decline. In *Experimental Gerontology* (Vol. 94, pp. 52–58). Elsevier Inc. https://doi.org/10.1016/j.exger.2016.11.004

Teesalu, T., Kulla, A., Simisker, A., Sirén, V., Lawrence, D. A., Asser, T., & Vaheri, A. (2004). Tissue plasminogen activator and neuroserpin are widely expressed in the human central nervous system. *Thrombosis and Haemostasis*, *92*(2), 358–368. https://doi.org/10.1160/th02-12-0310

Thiebaut, A. M., Gauberti, M., Phd, A., Martinez, S., Lizarrondo, D., Phd, V., Roussel, B. D., Thiebaut, A. M., Gauberti, M., Ali, C., Martinez, S., Vivien, D., Yepes, M., & Roussel, B. D. (2018). The role of plasminogen activators in stroke treatment: fibrinolysis and beyond. In *Lancet Neurol* (Vol. 17). www.thelancet.com/neurology

Thompson, R. E., Mandle, R., & Kaplan, A. P. (1977). Association of factor XI and high molecular weight kininogen in human plasma. *Journal of Clinical Investigation*, *60*(6), 1376–1380. https://doi.org/10.1172/JCI108898

Thors, B., Halldórsson, H., Jónsdóttir, G., & Thorgeirsson, G. (2008). Mechanism of thrombin mediated eNOS phosphorylation in endothelial cells is dependent on ATP levels after stimulation. *Biochimica et Biophysica Acta - Molecular Cell Research*, *1783*(10), 1893–1902. https://doi.org/10.1016/j.bbamcr.2008.07.003

Tom, B., Dendorfer, A., & Danser, A. H. J. (2003). Molecules in focus Bradykinin, angiotensin-(1-7), and ACE inhibitors: how do they interact? In *The International Journal of Biochemistry & Cell Biology* (Vol. 35).

Toussay, X., Basu, K., Lacoste, B., & Hamel, E. (2013). Locus coeruleus stimulation recruits a broad cortical neuronal network and increases cortical perfusion. *Journal of Neuroscience*, *33*(8), 3390–3401. https://doi.org/10.1523/JNEUROSCI.3346-12.2013

Trotter, J. H., Lussier, A. L., Psilos, K. E., Mahoney, H. L., Sponaugle, A. E., Hoe, H. S., Rebeck, G. W., & Weeber, E. J. (2014). Extracellular proteolysis of reelin by tissue plasminogen activator following synaptic potentiation. *Neuroscience*, *274*, 299–307. https://doi.org/10.1016/j.neuroscience.2014.05.046

Troyanovskaya, M., Song, L., Jayaraman, G., & Healy, D. P. (1996). Expression of aminopeptidase A, an angiotensinase, in glomerular mesangial cells. *Hypertension (Dallas, Tex. : 1979)*, *27*(3 Pt 2). https://doi.org/10.1161/01.hyp.27.3.518

Tsirka, S. E., Gualandris, A., Amaral, D. G., & Strickland, S. (1995). Excitotoxin-induced neuronal degeneration and seizure are mediated by tissue plasminogen activator. *Nature*, *377*(6547). https://doi.org/10.1038/377340a0

Tuneva, E. O., Bychkova, O. N., & Boldyrev, A. A. (2003). Effect of NMDA on Production of Reactive Oxygen Species by Human Lymphocytes. In *Bulletin of Experimental Biology and Medicine* (Vol. 136, Issue 8).

Tymianski, M., Charlton, M. P., Carlen, P. L., & Tator, C. H. (1993). Source specificity of early calcium neurotoxicity in cultured embryonic spinal neurons. *The Journal of Neuroscience : The Official Journal of the Society for Neuroscience*, *13*(5).

U

Ueki, M., Mies, G., & Hossmann, K.-A. (1992). Effect of alpha-chloralose, halothane, pentobarbital and nitrous oxide anesthesia on metabolic coupling in somatosensory cortex of rat. In *Acta Anaesthesiol Scand* (Vol. 36).

Uhlirova, H., Kılıç, K., Tian, P., Thunemann, M., le Desjardins, M., Saisan, P. A., Mateo, C., Cheng, Q., Weldy, K. L., Razoux, F., Vandenberghe, M., Cremonesi, J. A., Ferri, C. G., Nizar, K., Sridhar, V. B., Steed, T. C., Abashin, M., Fainman, Y., Masliah, E., … Devor, A. (2016). *Cell type specificity of neurovascular coupling in cerebral cortex*. https://doi.org/10.7554/eLife.14315.001

Ulbrich, M. H., & Isacoff, E. Y. (2008). Rules of engagement for NMDA receptor subunits. In *PNAS September* (Vol. 16).

Unger, T., de Gasparo, M., Catt, K. J., Inagami, T., Wright, J. W., & Unger, T. H. (2000). *International Union of Pharmacology. XXIII. The Angiotensin II Receptors*. http://www.pharmrev.org

Uno, M., & Ozawa, N. (1991). Long-term potentiation of the amygdalo-striatal synaptic transmission in the course of development of amygdaloid kindling in cats. In *Neuroscience Research* (Vol. 12).

Urata, H., Healy, B., Stewart, R. W., Merlin Bumpus, F., Husain, A., & Surgery, C. (1990). Original Contributions Angiotensin II-Forming Pathways in Normal and Failing Human Hearts In addition to its vasoconstrictor effect and its stimulatory effects on aldosterone secretion,' the octapeptide hormone angiotensin II (Ang II) has a positive inotropic and chronotropic effect on the heart.1'2 High affinity membrane Ang II receptor From the Departments of Heart and Hypertension Research. In *Circulation Research* (Vol. 66). http://ahajournals.org

Vaccari, C. S., Lerakis, S., Hammoud, R., & Khan, B. v. (2008). Mechanisms of benefit of angiotensin receptor blockers in coronary atherosclerosis. *American Journal of the Medical Sciences*, *336*(3), 270–277. https://doi.org/10.1097/MAJ.0b013e31816d1dc5

van Aken, H., & van Hemelrijck, J. (1991). Influence of anesthesia on cerebral blood flow and cerebral metabolism: an overview. *Agressologie: Revue Internationale de Physio-Biologie et de Pharmacologie Appliquees Aux Effets de l'agression*, *32*(6–7).

van de Werf, F., Vanhaecke, J., de Geest, H., Verstraete, M., & Collen, D. (1986). THERAPY AND PREVENTION CORONARY TILROMBOLYSIS Coronary thrombolysis with recombinant single-chain urokinase-type plasminogen activator in patients with acute myocardial infarction. In *Circulation* (Vol. 74, Issue 5). http://ahajournals.org

van den Eijnden-Schrauwen, Y., Atsma, D. E., Lupu, F., de Vries, R. E. M., Kooistra, T., & Emeis, J. J. (1997). *Involvement of Calcium and G Proteins in the Acute Release of Tissue-Type Plasminogen Activator and von WiUebrand Factor From Cultured Human Endothelial Cells*. http://ahajournals.org

van Guilder, G. P., Pretorius, M., Luther, J. M., Byrd, J. B., Hill, K., Gainer, J. v., & Brown, N. J. (2008). Bradykinin type 2 receptor BE1 genotype influences bradykinin-dependent vasodilation during angiotensin-converting enzyme inhibition. *Hypertension*, *51*(2 PART 2), 454–459. https://doi.org/10.1161/HYPERTENSIONAHA.107.102574

van Hinsbergh, V. W., Sprengers, E. D., & Kooistra, T. (1987). Effect of thrombin on the production of plasminogen activators and PA inhibitor-1 by human foreskin microvascular endothelial cells. *Thrombosis and Haemostasis*, *57*(2).

van Leeuwen, R. T., Kol, A., Andreotti, F., Kluft, C., Maseri, A., & Sperti, G. (1994). *Basic Science Reports Angiotensin II Increases Plasminogen Activator Inhibitor Type 1 and Tissue-Type Plasminogen Activator Messenger RNA in Cultured Rat Aortic Smooth Muscle Cells*. http://ahajournals.org

van Zonneveld, A. J., Veerman, H., & Pannekoek, H. (1986). On the interaction of the finger and the kringle-2 domain of tissue-type plasminogen activator with fibrin. Inhibition of kringle-2 binding to fibrin by ε-amino caproic acid. *Journal of Biological Chemistry*, *261*(30), 14214–14218. https://doi.org/10.1016/s0021-9258(18)67006-1

Vaughan, D. E., Lazos, S. A., & Tong, K. (1995). Angiotensin II Regulates the Expression of Plasminogen Activator Inhibitor-1 in Cultured Endothelial Cells: A Potential Link between the Renin-Angiotensin System and Thrombosis. *Journal of Clinical Investigation*, *95*(3), 995–1001. https://doi.org/10.1172/JCI117809

Vavrek, R. J., & Stewart, J. M. (1985). Competitive Antagonists of Bradykinin. In *Peptides* (Vol. 6).

Vivien, D., Gauberti, M., Montagne, A., Defer, G., & Touzé, E. (2011). Impact of tissue plasminogen activator on the neurovascular unit: From clinical data to experimental evidence. In *Journal of Cerebral Blood Flow and Metabolism* (Vol. 31, Issue 11, pp. 2119–2134). https://doi.org/10.1038/jcbfm.2011.127

Wang, H., Hitron, I. M., Iadecola, C., & Pickel, V. M. (2005). Synaptic and vascular associations of neurons containing cyclooxygenase-2 and nitric oxide synthase in rat somatosensory cortex. *Cerebral Cortex*, *15*(8), 1250–1260. https://doi.org/10.1093/cercor/bhi008

Wang, X., Lee, S. R., Arai, K., Lee, S. R., Tsuji, K., Rebeck, G. W., & Lo, E. H. (2003). Lipoprotein receptor-mediated induction of matrix metalloproteinase by tissue plasminogen activator. *Nature Medicine*, *9*(10), 1313–1317. https://doi.org/10.1038/nm926

Wang, Y. F., Tsirka, S. E., Strickland, S., Stieg, P. E., Soriano, S. G., & Lipton, S. A. (1998). Tissue plasminogen activator (tPA) increases neuronal damage after focal cerebral ischemia in wild-type and tPA-deficient mice. *Nature Medicine*, *4*(2). https://doi.org/10.1038/nm0298-228

Wardlaw, J. M., Doubal, F. N., Valdes-Hernandez, M., Wang, X., Chappell, F. M., Shuler, K., Armitage, P. A., Carpenter, T. C., & Dennis, M. S. (2013). Blood-brain barrier permeability and long-term clinical and imaging outcomes in cerebral small vessel disease. *Stroke*, *44*(2), 525–527. https://doi.org/10.1161/STROKEAHA.112.669994

Watkins, J. C. (1972). Metabolic regulation in the release and action of excitatory and inhibitory amino acids in the central nervous system. *Biochemical Society Symposium*, *36*.

Weber, R., Ramos-Cabrer, P., Wiedermann, D., van Camp, N., & Hoehn, M. (2006). A fully noninvasive and robust experimental protocol for longitudinal fMRI studies in the rat. *NeuroImage*, *29*(4), 1303–1310. https://doi.org/10.1016/j.neuroimage.2005.08.028

Weimar, W., Stibbe, J., van Seyen, A. J., Billiau, A., de Somer, P., & Collen, D. (1981). Specific lysis of an iliofemoral thrombus by administration of extrinsic (tissue-type) plasminogen activator. *Lancet (London, England)*, *2*(8254). https://doi.org/10.1016/s0140-6736(81)91217-4

Wu, F., Echeverry, R., Wu, J., An, J., Haile, W. B., Cooper, D. S., Catano, M., & Yepes, M. (2013). Tissue-type plasminogen activator protects neurons from excitotoxin-induced cell death via activation of the ERK1/2-CREB-ATF3 signaling pathway. *Molecular and Cellular Neuroscience*, *52*, 9–19. https://doi.org/10.1016/j.mcn.2012.10.001

Wu, Q., Li, L., Cooper, M. D., Pierres, M., & Gorvel, J. P. (1991). Aminopeptidase A activity of the murine B-lymphocyte differentiation antigen BP-1/6C3 (ectopeptldases/angiotensins/B-lymphocyte development). In *Proc. Nati. Acad. Sci. USA* (Vol. 88).

Wyss-Coray, T. (2016). Ageing, neurodegeneration and brain rejuvenation. In *Nature* (Vol. 539, Issue 7628, pp. 180–186). Nature Publishing Group. https://doi.org/10.1038/nature20411

Y

Yamazaki, M., Mori, H., Araki, K., Mori, K. J., & Mishina, M. (1992). Cloning, expression and modulation of a mouse NMDA receptor subunit. *FEBS Letters*, *300*(1). https://doi.org/10.1016/0014-5793(92)80160-i

Yang, H. Y., Erdös, E. G., & Levin, Y. (1970). A dipeptidyl carboxypeptidase that converts angiotensin I and inactivates bradykinin. *Biochimica et Biophysica Acta*, *214*(2). https://doi.org/10.1016/0005-2795(70)90017-6

Yang-Feng, T. L., Opdenakker, G., Volckaert, G., & Francke' Summary, U. (1986). Human Tissue-Type Plasminogen Activator Gene Located Near Chromosomal Breakpoint in Myeloproliferative Disorder. In *Am J Hum Genet* (Vol. 39).

Yepes, M., Sandkvist, M., Moore, E. G., Bugge, T. H., Strickland, D. K., & Lawrence, D. A. (2003). Tissue-type plasminogen activator induces opening of the blood-brain barrier via the LDL receptor-related protein. *Journal of Clinical Investigation*, *112*(10), 1533–1540. https://doi.org/10.1172/JCI200319212

Young, C. N., Morgan, D. A., Butler, S. D., Rahmouni, K., Gurley, S. B., Coffman, T. M., Mark, A. L., & Davisson, R. L. (2015). Angiotensin type 1a receptors in the forebrain subfornical organ facilitate leptin-induced weight loss through brown adipose tissue thermogenesis. *Molecular Metabolism*, *4*(4). https://doi.org/10.1016/j.molmet.2015.01.007

Yu, B. Y., Subudeng, G., Du, C. G., Liu, Z. H., Zhao, Y. F., Namei, E., Bai, Y., Yang, B. X., & Li, H. J. (2019). Plasminogen activator, tissue type regulates germinal vesicle breakdown and cumulus expansion of bovine cumulus-oocyte complex in vitro. *Biology of Reproduction*, *100*(6), 1473–1481. https://doi.org/10.1093/biolre/ioz049

Z

Zhang, C., An, J., Strickland, D. K., & Yepes, M. (2009). The low-density lipoprotein receptor-related protein 1 mediates tissue-type plasminogen activator-induced microglial activation in the ischemic brain. *American Journal of Pathology*, *174*(2), 586–594. https://doi.org/10.2353/ajpath.2009.080661

Zhang, E. T., Inmant, C. B. E., & Wellert, R. 0. (1990). Interrelationships of the pia mater and the perivascular (Virchow-Robin) spaces in the human cerebrum*. In *J. Anat* (Vol. 170).

Zhang, F., Xu, S., & Iadecola, C. (1995). Role of nitric oxide and acetylcholine in neocortical hyperemia elicited by basal forebrain stimulation: evidence for an involvement of endothelial nitric oxide. In *Pergamon Neuroscience* (Vol. 69, Issue 4).

Zhang, W., Qu, J., Liu, G. H., & Belmonte, J. C. I. (2020). The ageing epigenome and its rejuvenation. In *Nature Reviews Molecular Cell Biology* (Vol. 21, Issue 3, pp. 137–150). Nature Research. https://doi.org/10.1038/s41580-019-0204-5

Zheng, Z., Nakamura, K., Gershbaum, S., Wang, X., Thomas, S., Bessler, M., Schrope, B., Krikhely, A., Liu, R. M., Ozcan, L., López, J. A., & Tabas, I. (2020). Interacting hepatic PAI-1/tPA gene regulatory pathways influence impaired fibrinolysis severity in obesity. *Journal of Clinical Investigation*, *140*(8), 4348–4359. https://doi.org/10.1172/JCI135919

Zheng, Z., Nayak, L., Wang, W., Yurdagul, A., Wang, X., Cai, B., Lapping, S., Ozcan, L., Ramakrishnan, R., Pestell, R. G., Jain, M. K., & Tabas, I. (2019). *An ATF6-tPA pathway in hepatocytes contributes to systemic fibrinolysis and is repressed by DACH1*. http://ashpublications.org/blood/article-pdf/133/7/743/1552523/blood864843.pdf

Zhou, A., Carrell, R. W., & Huntington, J. A. (2001). The Serpin Inhibitory Mechanism Is Critically Dependent on the Length of the Reactive Center Loop. *Journal of Biological Chemistry*, *276*(29), 27541–27547. https://doi.org/10.1074/jbc.M102594200

Zhuo, M., Holtzman, D. M., Li, Y., Osaka, H., Demaro, J., Jacquin, M., & Bu, G. (2000). *Role of Tissue Plasminogen Activator Receptor LRP in Hippocampal Long-Term Potentiation*.

Zonta, M., Angulo, M. C., Gobbo, S., Rosengarten, B., Hossmann, K. A., Pozzan, T., & Carmignoto, G. (2003). Neuron-to-astrocyte signaling is central to the dynamic control of brain microcirculation. *Nature Neuroscience*, *6*(1), 43–50. https://doi.org/10.1038/nn980

Résumé

La régulation du débit sanguin cérébral (DSC) implique des mécanismes complexes ayant des influences directes sur les fonctionnements et les dysfonctionnements du cerveau. Parmi ces mécanismes, il a été proposé que l'activateur tissulaire du plasminogène (tPA) de la famille des sérines protéases, pourrait jouer un rôle dans la modulation du couplage neurovasculaire (CNV) induit par la stimulation des vibrisses chez le rongeur, par son mécanisme d'action sur les récepteurs N-Méthyl-D-Aspartate (NMDA). Dans cette étude, via l'utilisation de souris tPA^{Null}, des délétions conditionnelles du tPA endothélial ou de la sous-unité GluN1 des récepteurs NMDA endothéliaux, des parabioses entre des souris tPA^{WT} et tPA^{Null}, des délétions induites par des transfections hydrodynamiques du tPA hépatique, une hépatectomie partielle et des approches pharmacologiques chez la souris, nous avons pu dévoiler ce mécanisme. Nous démontrons ainsi que les concentrations physiologiques de tPA vasculaire, principalement produit et libéré par les cellules endothéliales hépatiques de manière dépendante des récepteurs de la bradykinine de type 2, favorisent le CNV, par un mécanisme dépendant des récepteurs NMDA endothéliaux du cerveau. Ces données mettent en évidence un nouveau mécanisme de régulation du CNV, impliquant à la fois les récepteurs NMDA et le tPA endothéliaux.

Mots clés : tPA, récepteur NMDA, CNV, bradykinine, cellule endothéliale, hepatocyte, cerveau, foie.

Abstract

Regulation of the cerebral blood flow (CBF) involves complex mechanisms with direct influences on brain functions and dysfunctions. Among these mechanisms it was proposed that the serine protease tissue-type plasminogen activator (tPA) could play a role in the control of neurovascular coupling (NVC) induced by whiskers stimulation in rodents through its action on N-methyl-D-Aspartate receptors (NMDARs). In the present study, using tPA^{Null} mice, conditional deletions of either endothelial tPA or endothelial NMDARs, parabioses between wild-type and tPA^{Null} mice, hydrodynamic transfections-induced deletion of hepatic tPA, hepatectomy and pharmacological approaches in mice, we have unveiled this mechanism in detail. We thus demonstrate, that physiological concentrations of vascular tPA, mainly produced and released by the liver endothelial cells in a bradykinin type 2 receptors-dependent manner, promotes NVC, by a mechanism dependent of brain endothelial NMDA receptors. These data highlight a new mechanism of the regulation of NVC involving both endothelial tPA and NMDA receptors.

Key words: tPA, NMDA receptor, NVC, bradykinin, endothelial cell, hepatocyte, brain, liver.